Modelling of fuel fragmentation, relocation and dispersal during Loss-of-Coolant Accident in Light Water Reactor

THÈSE N^{O} 8018 (2017)

PRÉSENTÉE LE 27 OCTOBRE 2017
À LA FACULTÉ DES SCIENCES DE BASE
LABORATOIRE DE PHYSIQUE DES RÉACTEURS ET DE COMPORTEMENT DES SYSTÈMES
PROGRAMME DOCTORAL EN PHYSIQUE

ÉCOLE POLYTECHNIQUE FÉDÉRALE DE LAUSANNE

POUR L'OBTENTION DU GRADE DE DOCTEUR ÈS SCIENCES

PAR

Vladimir Vladimirov BRANKOV

acceptée sur proposition du jury:

Prof. N. Grandjean, président du jury
Prof. A. Pautz, Dr K. Mikityuk, directeurs de thèse
Dr W. Wiesenack, rapporteur
Prof. T. Haste, rapporteur
Prof. H.-M. Prasser, rapporteur

ÉCOLE POLYTECHNIQUE
FÉDÉRALE DE LAUSANNE
Suisse
2017

On a personal note, I would like to dedicate this work to the memory of my grandparents, Boris Brankov, who was the lead designer of the largest thermal power plant on the Balkan Peninsula at the time, Liliana Andreeva, Stoyka Ivanova and Stoyan Ivanov. I owe my success to my father, Vladimir Borisov Brankov, who supported me in various ways throughout my 11 years of study and helped me to reach this milestone. Also, I'd like to thank my mother, Krasimira Ivanova, and my sister, Liliana Brankova, for their support and encouragement.

Contents

List of Abbreviations i
Abstract iii
Zusammenfassung v
1 Chapter 1: Introduction 1
1.1 Introduction to nuclear fuel 1
1.2 The fission process 3
1.3 Fuel microstructure transformation under irradiation 5
1.4 Fission gas release in LWR fuel 7
1.5 Fuel Fragmentation 8
1.6 Fuel relocation 11
1.7 Fuel dispersal 15
1.8 General description of a Loss-of-Coolant Accident (LOCA) 16
1.9 LOCA Safety Criteria 17
1.10 The economic benefit of going to higher burnup 18
1.11 Goals and Structure of the thesis 19
2 Chapter 2: Introduction of the Computational Tools 21
2.1 Introduction to FALCON Fuel Performance Code 21
2.1.1 History 21
2.1.2 Finite Element Method 21
2.1.3 Finite Element Method in FALCON 23
2.1.4 Modelling capabilities of FALCON 24
2.1.5 Use of FALCON in the current doctoral work 25
2.2 GRSW-A: Gas Release and Swelling Advanced model 25
2.3 FRELAX: model for axial fuel relocation 27
2.4 Serpent Monte-Carlo code 29
2.4.1 Introduction into the Monte Carlo method 29
2.4.2 Modelling capabilities of Serpent 30
2.4.3 An example with Serpent: two-dimensional fuel pin 30
2.5 Brief introduction of TRACE 32
3 Chapter 3: OECD Halden Reactor Project and its LOCA Test Program 35
3.1 Introduction 35
3.2 General description of the Halden LOCA test program 36
3.3 LOCA test rig 38
3.4 Brief description of the LOCA tests 41

3.4.1 Halden LOCA test 3 41
3.4.2 Halden LOCA test 4 42
3.4.3 Halden LOCA test 5 44
3.4.4 Halden LOCA test 6 45
3.4.5 Halden LOCA test 7 46
3.4.6 Halden LOCA test 8 47
3.4.7 Halden LOCA test 9 48
3.4.8 Halden LOCA test 10 49
3.4.9 Halden LOCA test 11 50
3.4.10 Halden LOCA test 12 51
3.4.11 Halden LOCA test 13 52
3.4.12 Halden LOCA test 14 53
3.5 Data collected during the test 54
3.5.1 Gross gamma monitor in the blowdown line 54
3.5.2 Plenum pressure transducer 56
3.5.3 Thermocouple measurements 59
3.6 Post-irradiation examination after the LOCA test 61
3.6.1 Axial cladding profilometry 61
3.6.2 Gamma scanning 62
3.6.3 Cladding rupture size measurements 63
3.6.4 Approximation to the axial fill factor 64
3.6.5 Current enhancements of the gamma scanning at OECD Halden Reactor Project 65
3.6.6 Steps for improving the quality of the gamma scan data 66
4 Chapter 4: Base Irradiation 69
4.1 Description of the base irradiation fuel rod database 69
4.2 Fast neutron flux input 71
4.3 Fission gas trapping during base irradiation 74
4.4 Serpent Monte Carlo model for approximation of the burnup asymmetry 78
4.5 Fission gas trapping model 80
4.6 Best fit of calculated and measured fission gas release 82
4.7 Trapped fission gas release during the LOCA 83
4.8 Calculation of the trapped gas in the fuel rod segments used in Halden LOCA tests 12, 13 and 14 85
4.9 Conclusion 87
5 Chapter 5: Models for fuel fragmentation, relocation and dispersal 89
5.1 Fuel fragmentation model 89
5.1.1 Fuel pulverization model 90

5.2 Fuel relocation model 91
5.2.1 Introduction 91
5.2.2 Model parameters and assumptions 93
5.2.3 Calculation of relative change in LHGR 95
5.2.4 Preparing fuel fragment size input for the relocation model 96
5.2.5 Comparison with the fuel relocation model of FRELAX 98
5.2.6 TRACE model for sub-channel LOCA simulation 100
5.2.7 Coupling between TRACE – FALCON – MATLAB 101
5.3 Fuel dispersal modelling approach 103
5.3.1 Model outline 104
5.3.2 Model equations 105
5.3.3 Calibration using Studsvik LOCA tests with high burnup fuel 110
5.3.4 Application to Halden LOCA tests 115
5.4 Application of fuel relocation and dispersal to full-length fuel rod 122
5.4.1 Initialization of the transient calculation 122
5.4.2 Evaluation of the fraction of pulverized fuel 122
5.4.3 Input parameters to the fuel dispersal model 124
5.4.4 Calculation of the Equivalent-Cladding Reacted (ECR) 126
5.5 Conclusion 128
6 Chapter 6: Conclusions and recommendations 131
6.1 Executive summary 131
6.2 Main achievements 133
6.3 Recommendations for future work 134
6.3.1 Fuel fragmentation model 134
6.3.2 Fuel relocation model 134
6.3.3 Fission gas trapping model 135
6.3.4 Fuel dispersal model 135
6.3.5 Non-nuclear tests for gathering validation data 136
Acknowledgements 139
References 141
Appendix A: Other uses of the gamma scan data 147
Appendix B: Model for fast neutron flux calculation 149
Appendix C: Brief introduction to MATLAB 151

List of Abbreviations

BI – Base Irradiation

BWR – Boiling Water Reactor

BDBA – Beyond Design Base Accident

DBA – Design Base Accident

ECR – Equivalent Cladding Reacted

EPMA – Electron Probe Micro Analysis

FA – fuel assembly

FFBT – Fuel Fragmentation Burnup Threshold

FFRD – Fuel Fragmentation, Relocation and Dispersal

FGR – Fission Gas Release

FP – Fission Products

FRELAX – Fuel RELocation Axial

GRSW-A – Gas Release and Swelling – Advanced

HBS – High Burnup Structure

HRP – Halden Reactor Project

Kr – Krypton

KKG – Kernkraftwerk Goesgen

KKL – Kernkraftwerk Leibstadt

LOCA – Loss of Coolant Accident

MOX – Mixed OXide

MPa – Mega Pascal

ODE – Ordinary differential equations

OECD – Organisation for Economic Cooperation and Development

PCI – Pellet-cladding interaction

PCMI – Pellet Cladding Mechanical Interaction

PIE – Post Irradiation Examination

PSI – Paul Scherrer Institute

PWR – Pressurized Water Reactor

SEM – Scanning Electron Microscopy

U.S.NRC – United States Nuclear Regulatory Commission

Xe – Xenon

Abstract

Recent LOCA tests with **high burnup fuel** at the OECD Halden Reactor Project and at Studsvik demonstrated the susceptibility of the fuel to fragment to small pieces, to relocate and possibly cause a 'hot-spot' effect and to be dispersed in the event of cladding rupture. However, the LOCA safety criteria defined by the US NRC are still based on fuel tests with fresh and low burnup fuel and therefore require revision for high burnup fuel.

In this context a PhD project with the goal of developing new models for high burnup fuel fragmentation, relocation and dispersal during Loss of Coolant Accident in Light Water Reactors was launched at Paul Scherrer Institute in June 2013 with a financial support from *swiss*nuclear.

The PhD project included a three-month technical visit at the OECD Halden Reactor Project in Norway. The goal was to study the Halden LOCA tests and gather **experimental data** that can be used in the modelling work. After the data analysis, a journal paper proposing to use the gamma scanning measurements of Halden LOCA tests for predicting fuel relocation and dispersal was published.

The work continued with **base irradiation** simulation with a closer look at the fission gas release measurements of high burnup BWR fuel rods. It is important for the LOCA modelling to account for the trapped fission gas, because the fuel-cladding bonding layer can be broken early into the transient and the additional fission gas release will raise the gas pressure in the fuel rod which in turn may affect the cladding rupture and fuel dispersal. The data showed significant scatter for fuel rods at the same average burnup, originating from the same fuel assembly and having almost the same enrichment. The scatter was explained with a BWR-specific mechanism for fission gas trapping. It was motivated with Scanning Electron Microscopy images at the pellet-cladding interface that showed very strong fuel-cladding bonding layer on one side of the fuel rod. Base irradiation with the EPRI's FALCON code coupled with an in-house advanced fission gas release and gaseous swelling model GRSW-A was done for selected high burnup BWR fuel rods. The calculated fission gas release was overestimated in all cases. This was expected, because at the time the modelling did not account for fission gas trapping. From the available modelling and experimental data, a model for fission gas trapping was proposed. After calibration, the agreement between calculated and measured fission gas release was significantly improved. The main findings were published in the journal.

Fuel fragmentation modelling was focused on fuel pulverization. This is a high burnup fuel-specific phenomenon, in which the fuel pellet periphery may fragment to sizes less than 100 μm. Such fragments are very mobile and can be easily relocated and dispersed in the event of cladding rupture regardless of the rupture opening size. Therefore, the fuel fragmentation model addresses the potentially most important mode of fragmentation – fuel pulverization.

Fuel relocation inside fuel rod is simulated during cladding ballooning and until cladding failure. The model takes as input the time-dependent cladding deformation supplied by FALCON and the fragment size distribution either provided directly by experimental data or by the fuel fragmentation model. Fuel relocation was modelled under the specific assumption that outermost fragments (e.g. pulverized fuel) relocate first, resulting in a large packing factor and local cladding temperature increase at the balloon (i.e. hot-spot effect) and, as a consequence, in enhanced cladding oxidation at the balloon.

Fuel dispersal is modelled by solving the mass, energy and momentum conservation equations for two phases – the gas inside the fuel rod and the fraction of fuel which is "movable". Although the model uses simplified geometrical representation of the fuel rod and some other simplifying assumptions, the

underlying reason for fuel dispersal (namely the interfacial friction between the gas outflow and the solid) is explicitly simulated. The model for fuel dispersal is calibrated using Halden and Studsvik LOCA tests.

Fuel fragmentation, relocation and dispersal are complicated phenomena to model, mainly because of many uncertainties. The developed models provide a complete overall framework for simulating the mutual effects of FFRD during the LOCA. Recommendations for the next steps of the development are made together with a proposal of the new non-nuclear tests to gather experimental data for validation purposes.

Keywords: FFRD Modelling, nuclear power, nuclear fuel, high burnup, fuel fragmentation, fuel relocation, fuel dispersal, LOCA, Halden LOCA tests, FALCON

Zusammenfassung

Aktuelle Teststörfälle mit Kühlmittelverlust und **Brennstoffen mit hohem Abbrand**, die am OECD Halden Reaktor Projekt und an Studsvik durchgeführt wurden, haben die Anfälligkeit der Fragmentierung der Brennstoffstäbe in kleinere Stücke aufgezeigt. Diese kleineren Fragmente laufen Gefahr, sich zu verlagern, nach dem Hüllrohrbruch auszuweiten und möglicherweise Hot-Spot-Effekt an der aufgeblähten Stelle auszulösen. Allerdings sind die festgelegten Sicherheitskriterien für einen Kühlmittelverluststörfall bei der US NRC auf Kernbrennstofftests mit frischem, oder schwach abgebranntem Kernbrennstoff basiert und erfordern deswegen eine Revision, um die heutige Situation abzubilden.

In diesem Kontext wurde im Juni 2013 mit finanzieller Unterstützung von *swiss*nuclear ein Doktorat am Paul Scherrer Institut erstellt, das sich die Modellentwicklung für Kernbrennstofffragmentierung, Kernbrennstoffverlagerung und Kernbrennstoffausbreitung während eines Kühlmittelverluststörfalls in einem Leichtwasserreaktor zum Ziel gesetzt hat.

Als Teil des Projektes war ein drei monatiger technischer Besuch am OECD Halden Reaktor Projekt in Norwegen. Das Ziel war das Studieren des Halden Kühlmittelverluststörfalltests und die Ansammlung von **experimentellen Daten**, die für die Modellierungsarbeit nützlich werden würden. Nach der Datenanalyse konnte ein Artikel über die Gamma Scanning Daten nach den Halden Kühlmittelverluststörfalltests in einem wissenschaftlichen Journal publiziert werden.

Die Arbeit wurde mit der **Base Irradiation** Simulation mit Fokus auf die transienten Spaltgasfreisetzungsmessungen von hochabgebrannten BWR Kernbrennstäbe fortgesetzt. Die Menge der Spaltgasfreisetzung ist wichtig für die Modellierung von Kühlmittelverluststörfällen, da die Brennstoff-Hüllrohr Verbindung früh aufgebrochen werden kann. Infolgedessen führt dies zu einer weiteren Freisetzung von Spaltgasen, welche den Druck im Hüllrohr zusätzlich ansteigen lässt. Der Druckanstieg kann die Bruchgrösse und die Streuung des Brennstoffs erheblich beeinflussen. Die Daten haben eine signifikante Streuung für Stäbe mit dem gleichen durchschnittlichen Abbrand und bei ähnlicher Brennstoffanreicherung gezeigt. Dieses Ergebnis konnte mit BWR-spezifischen Auffangmechanismen des Spaltgases erklärt werden. Dies wurde mit Daten aus dem Rasterelektronenmikroskop verstärkt, die sehr starke Verbindungen zwischen dem Hüllrohr und dem Kernbrennstoff gezeigt haben. Base Irradiation Simulationen mit EPRI's FALCON Code, gekoppelt mit dem hauseigenen, fortgeschrittenen Spaltgasfreisetzungscode GRSW-A, wurde im Anschluss für ausgewählte BWR Kernbrennstäbe mit hohem Abbrand durchgeführt. Die berechnete Spaltgasfreisetzung wurde in allen Fällen überschätzt. Dies stimmte mit den Erwartungen überein, da die Modellierung noch kein Modell für die Auffangmechanismen des Spaltgases implementiert hatte. Aus den Unterschieden zwischen der Modellierung und den verfügbaren experimentellen Daten konnte schliesslich ein Modell für das Auffangen des Spaltgases entwickelt werden. Nach der Anpassung konnte die Übereinstimmung zwischen berechneten und gemessenen Spaltgasfreisetzungen bedeutsam verbessert werden. Die Hauptbefunde dieser Modellierung wurden in einem wissenschaftlichen Journal publiziert.

Kernbrennstofffragmentierung legte den Fokus auf die Kernbrennstoffpulverisierung. Sie ist ein spezifisches Phänomen für Kernbrennstoff mit hohem Abbrand, in welchem die Kernbrennstoffperipherie in bis zu 100 μm grosse Fragmente aufbrechen könnte. Solche Fragmente sind sehr beweglich und könnten sich problemlos verlagern und unabhängig der Bruchgrösse des Hüllrohrs. Deswegen behandelt das Kernbrennstofffragmentierungsmodell möglicherweise die wichtigste Form der Fragmentierung – nämlich Kernbrennstoffpulverisierung.

Die Kernbrennstoffverlagerung innerhalb des Brennstabes wurde von der Hüllrohraufblähung bis zum Versagen des Hüllrohrs simuliert. Das Modell benötigt als Eingabe die zeitabhängige Hüllrohrdeformation, die von FALCON berechnet wird und die Fragmentgrössenverteilung, die aus experimentellen Daten oder aus dem Kernbrennstofffragmentierungsmodell stammen kann. Die Kernbrennstoffverlagerung wurde mit der Annahme modelliert, dass sich die äussersten Fragmente zuerst verlagern. Das Ergebnis ist ein grösserer Verdichtungsfaktor und höhere Temperaturen an der Hüllrohraufblähung (i.e. Hot-Spot-Effekt) und demzufolge eine verstärkte Hüllrohroxidation.

Die Kernbrennstoffausbreitung wurde mithilfe der Auflösung des Energieerhaltungssatzes, der Kontinuitätsgleichung und des Impulserhaltungssatzes für zwei Aggregatzustände, das Gas innerhalb des Hüllrohrs und der Anteil der beweglichen Kernbrennstofffragmente, modelliert. Obwohl das Modell ein vereinfachtes geometrisches Konzept des Kernbrennstoffstabes nutzt, wurden Simulationen zur Bestimmung des grundsätzlichen Verhaltens der Kernbrennstoffausbreitung (nämlich die Grenzflächenreibkraft zwischen dem Gasausfluss und der Kernbrennstofffragmente) durchgeführt. Das Kernbrennstoffausbreitungsmodell wurde mit den Daten aus den Halden und Studsvik Kühlmittelverluststörfalltests kalibriert.

Kernbrennstofffragmentierung, Verlagerung und Ausbreitung sind komplizierte Phänomene und aufgrund vieler Ungewissheiten schwierig zu modellieren. Die entwickelten Modelle bieten ein komplettes Rahmenkonzept für die Simulierung den gemeinsamen Effekten zwischen Kernbrennstofffragmentierung, Verlagerung und Ausbreitung während eines Kühlmittelverluststörfalls. Die nächsten Schritte in der Entwicklung werden im Zusammenhang mit möglichen nicht-nuklearen Tests, die Validierungsdaten generieren könnten, mit entsprechenden Empfehlungen am Ende diskutiert.

Stichwörter: FFRD Modellierung, Kernenergie, Kernbrennstoff, hoch Abbrand, Halden LOCA Tests, LOCA Kernbrennstofffragmentierung, Kernbrennstoffverlagerung, Kernbrennstoffausbreitung, FALCON

1
Chapter 1:
Introduction

Nuclear fuel is likely the most complicated part in a fission reactor, because it requires both, microscopic and macroscopic understanding of its behaviour over long period of time. A typical fuel rod remains in the reactor for at least five years during which time it is exposed to corrosive environment, irradiation and mechanical and thermal loads during normal operation and power changes. Due to the difficulty in dealing with radioactive materials and the associated financial costs, experimental programs on irradiated fuel are limited, yet today's computing power enables the modelling of virtually all of the phenomena that may occur, but those models still need adequate experiments for code validation and verification. Nuclear power plants are very expensive installations that require highly skilled staff, regular maintenance and high-quality materials. At the same time, they produce reliable and clean electricity at competitive prices. The reason behind this is the enormous energy density of the nuclear fuel, but also improvements in fuel manufacturing. For the sake of an example, the thermal energy released from the fission of 1 kg of U-235 is equivalent to the thermal energy released by burning roughly 2,500,000 kg of coal. In addition, small optimization of the fuel cycle, via core loading patterns, may also lead to significant economic benefit for the operator. Furthermore, longer operation of the fuel is also economically motivating and more sustainable, which brings us to the notion of high burnup fuel. Despite the obvious advantages, there are also additional challenges. It is a well-established fact that the longer the fuel stays in the reactor the more susceptible to failure it becomes – a fact that may challenge the safety measures that were established in the 1970s based on experiments mostly with fresh and low burnup fuel (see section 1.9).

This chapter is meant to introduce the reader into the PhD project on Fuel Fragmentation, Relocation and Dispersal (FFRD) during the Loss of Coolant Accident (LOCA). The discussion begins with a general description of nuclear fuel and the fission process, followed by an explanation of what is meant by FFRD and why it is important and the phenomena leading to it with the focus being on LOCA. The LOCA safety criteria currently in use are briefly discussed and the chapter is concluded with a basic discussion on the economic benefit of high burnup fuel.

Good understanding of fuel behaviour at high burnup and the mechanisms leading to its performance degradation is necessary for advanced fuel and cladding designs that will allow the safe operation at higher burnup.

1.1 Introduction to nuclear fuel

Nuclear fuel is the end product that goes into the reactor. It begins with the mining of the uranium ore, its refinement and enrichment and finally its manufacture into a so-called fuel pellet. The fuel pellet is typically made of uranium dioxide (UO_2) ceramic and shaped into a cylinder of approximately 1 cm in diameter and height although other designs exist. The fuel pellets are arranged in a cladding tube of approximately 4 meters in length, made typically from Zirconium based alloys (e.g. Zircaloy-2 or Zircaloy-4). The tubes are sealed and filled with Helium up to specific pressure and

arranged in a regular grid, whether rectangular or hexagonal to make a fuel assembly (FA). The collection of all fuel assemblies in a reactor is referred to as the reactor core. The FA provides mechanical stability of the fuel rods via spacer grids that are placed along its length which also enhance the heat transfer from the fuel to the coolant [1] via mechanical structures called mixing vanes.

The design of the fuel pellet underwent improvements in its geometry such as the addition of dishing at the pellet ends in order to accommodate fuel swelling and chamfers to reduce the fuel pellet chipping – measures which reduced the mechanical load at the cladding and the frequency of cladding failure during normal operation. Understanding the behaviour of the fuel pellets during normal and transient conditions allows making predictions on the behaviour of the fuel rod, the fuel assembly and ultimately the reactor core as a whole. The topic of this PhD aims to understand the behaviour of high burnup fuel during LOCA and will not go into core-wide analysis, which can be a topic for another PhD project. Understanding the behaviour of a single fuel rod is pre-condition to understanding the behaviour of a fuel assembly and ultimately the whole core.

The most general features of a PWR fuel assembly are illustrated on Figure 1 and are briefly introduced.

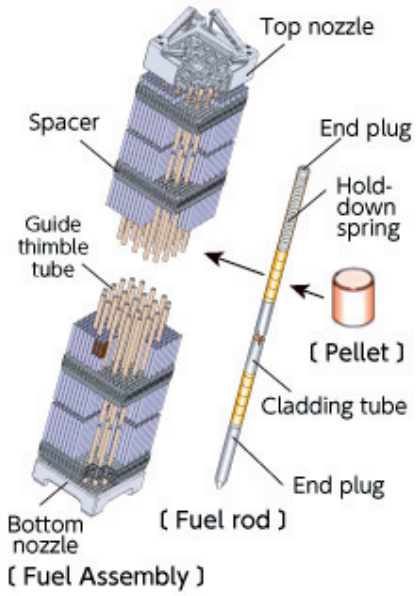

Figure 1: Scheme of a fuel rod and a 17x17 PWR fuel assembly[2]

- Top and bottom nozzles – they ensure the mechanical rigidity of the fuel assembly. The fuel rod ends are inserted into the bottom nozzle and everything is "clamped" by the top nozzle.
- Spacers – the spacers are mainly used for mechanical support of the approximately 4 meter long fuel rods and also to increase mixing and heat transfer from the fuel to the coolant as the spacers in the GAIA fuel assembly designed by AREVA claims to do [3]. Without spacers, the fuel rods will quickly deform under the action of the forced flow.
- Guide thimble tube – these are guiding tubes through which control rods are inserted. The purpose of the control rods is to increase (when withdrawn) or decrease (when inserted) the thermal neutron flux and thereby control the power of the reactor. The control rods are regularly dispersed in the fuel assembly (e.g. there is not a single guide thimble in the centre) in order to achieve more uniform control of the neutron flux and temperature.

- Cladding end plug – the end plug is inserted into the bottom nozzle and secures the fuel rod in its place.
- Hold-down spring – this spring is located inside the top of the rod and it applies compressive force on the fuel pellets stack. The spring will also respond to fuel expansion and contraction.
- Upper plenum – it provides room for the containment of fission gases as they are released from the fuel.
- Cladding tube – the first barrier against radioactive material release in the defence-in-depth concept. Ensuring integrity of the cladding ensures the containment of the radioactive species. Cladding tubes are typically manufactured from Zircaloy, but other materials used in commercial operation exist as well (e.g. stainless steel, and possibly in the future – silicon carbide). The choice of Zirconium-based alloys is based on three important properties: low neutron capture, good corrosion resistance in high-temperature water and high mechanical strength. Some alloying elements are added to enhance a particular feature. For example, addition of oxygen increases twice the yield strength at room temperature and addition of Niobium improves corrosion resistance

Due to the design of Boiling Water Reactors (BWR), the coolant evaporates inside the reactor which creates two-phase flow conditions. The fuel assembly design for BWR is more complicated in order to address this. For example, a central moderator channel (e.g. Figure 35) is added inside the fuel assembly in order to improve the neutron moderation in the upper parts of the core where the void fraction is high. Burnable absorbers and part-length rods are other features in a BWR fuel assembly design that are not part of the PWR FA design.

Improvement of nuclear fuel is on-going and some nuclear power plants irradiate in their cores so-called Lead Test Assemblies (LTAs) in order to test new FA designs in operating conditions.

1.2 The fission process

The process which produces heat in the nuclear fuel is fission which is the splitting of a U-233/U-235/Pu-239 (the last two are specific to LWR) atom most of the time into two atoms, called fission fragments, and 2-3 neutrons, which continue the chain reaction. To sustain the chain reaction and at the same time keep it under control, power reactors use neutron absorbers which basically ensure that on average the neutrons emitted from each fission event create only one fission event. Of the three fissile isotopes just mentioned, only U-235 occurs in nature. The others are produced via neutron capture in U-238 leading to Pu-239 and Th-232 leading to U-233. Thorium is an element which is about three times more abundant than natural uranium (0.7% U-235 and 99.3% U-238). The fission fragments are heavy atoms that are ejected with very high kinetic energy which is quickly dissipated as heat in the dense UO_2 lattice and causes the fuel to heat-up. The heat from the fuel is transferred to the coolant and then utilized in the steam generator (PWR) to make steam, or it is converted directly to steam inside the reactor (BWR). The steam then passes through a turbine connected to a generator to make electricity. Depending on the neutron energy and the fission material, the fission process follows a particular fission yield curve as seen on Figure 2 which gives the fraction of fission products with given mass number.

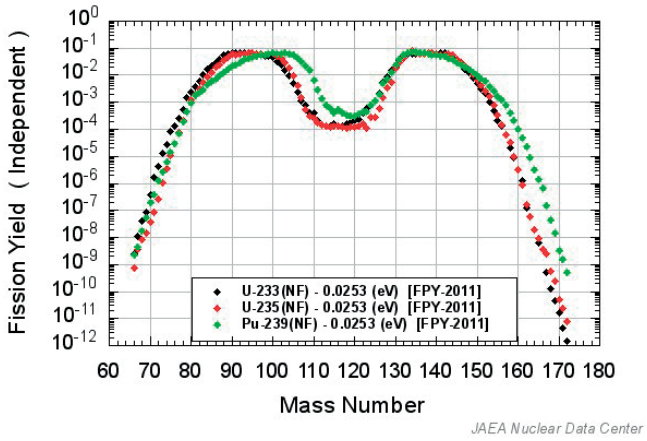

Figure 2: Fission product yield curves for the most common fission atoms: U-233, U-235 and Pu-239 in the thermal neutron spectrum.

The plot also shows, that the most of the time, the fission fragments are made up by a lighter (mass number around 90) and a heavier (mass number around 140) atom. For this reason, Xe-137 and Kr-85 - two of the most common gaseous fission products, have large fission yield. The fission gases are fuel performance limiting factors, because they significantly contribute to fuel swelling, increase pressure in the fuel rod and decrease pellet-cladding gap conductance. Fission products can be grouped roughly into two categories: solid and gaseous. The former are relatively immobile and remain near the location where they were created. The latter are highly mobile and play a key role in the fuel fragmentation process in the event of a LOCA, which directly has an impact on the fuel relocation and dispersal.

The fission products are typically radioactive and this requires the fuel to be cooled even when the reactor is not operational. During the first second after reactor shutdown, the decay heat is approximately 7% of the reactor thermal power and after 1 day it is about 0.6%, which means for a standard 3000MW thermal power reactor, this is equal to 18 MW thermal power – a substantial amount. Failure to remove the decay heat will result in the melting of the fuel. For a period of few years, spent nuclear fuel stays in so-called spent nuclear fuel pools, which are filled with water and are cooled continuously. When the radioactivity decreases sufficiently, cooling can be maintained by natural convection and the fuel can be stored in special steel casks, which are cooled by air.

The fission process produces virtually all elements in the periodic table with the likelihood governed by the fission yield curve (Figure 2). While the fission fragments are simply leftovers for a commercial nuclear power plant, some of them are considered extremely valuable in nuclear medicine (e.g. technetium 99-m) and are produced from research reactors (e.g. NRU reactor in Canada). Others find application in industry, such as for non-destructive testing and screening. The unit which is used to characterize the amount of energy generated by the fuel per unit mass is the burnup, typically expressed in MWd/kgU or GWd/tU. The energy released per fission is about 200 MeV, which means 1 MWd of energy requires approximately $2.7 \cdot 10^{21}$ fissions. Fission of 1kg of U-235 produces about as much thermal energy as the burning of 2.5 million kg of coal – a fact which shows an advantage of nuclear power.

1.3 Fuel microstructure transformation under irradiation

Unirradiated fuel matrix consists of pure UO_2 with a grain size of approximately 10μm, but larger grain fuels were purposefully manufactured to understand the effect of grain size on fuel matrix restructuring under irradiation [4, 5] and fission gas retention [6]. It is observed, that large grain fuel undergoes matrix restructuring at a later stage (Figure 3) and performs better in terms of fission gas retention. As the fuel is irradiated, its structure and chemistry is continuously modified, which in turn modifies properties like thermal conductivity, density, hardness and toughness.

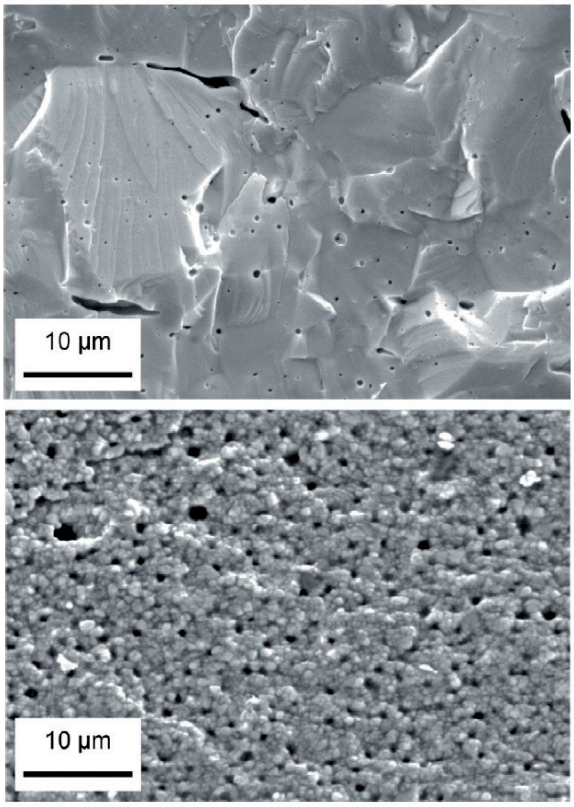

Figure 3: Scanning Electron Microscopy micrographs of unirradiated UO_2 fuel and fuel with local burnup of ~75 MWd/kgU [7].

When first put in the reactor, the pores resulting from the manufacturing process, which are visible on the left image on Figure 3, are removed, thereby leading to pellet densification, but with time due to the fission products and gas precipitation the density decreases thereby reversing the effect. According to [8], fission products contribute to fuel swelling at a rate of apparently 0.77% per 10MWd/kgU during normal steady-state irradiation at a relatively low temperature.

Initially, the fuel matrix contains grains of approximately the same size. Over time, the fuel matrix undergoes restructuring. The high temperature around the pellet centre may result in aggregation of grains [9], but the much lower temperature at the pellet rim experiences subdivision (polygonization) of the grains into sub-micron sizes after long irradiation [9] resulting in the so-called "High Burnup Structure" (HBS). In [10] grain sizes in the range of 20-30 nm are reported which is consistent with the results shown in [11] where the original grain size of 10-15 μm subdivides into 10^4 to 10^5 sub grains. The HBS is formed due to irradiation damage in combination with precipitation of fission gas at the grain boundaries and it extends towards the pellet centre with irradiation [5]. The High Burnup

Rim Project (HBRP) performed by Kinoshita et.al [12] established, that condition for HBS formation is local burnup greater than 70 MWd/kgU and local temperature less than 1000℃.

The fuel restructuring causes depletion of fission gas from the grains and accumulation in specific, relatively large pores that may reach sizes of about 7 μm [13], which is at least one order of magnitude larger than the fuel grain size at the HBS. If the temperature increases above its value at normal operation, so does the pressure in the pores in the HBS, which eventually may reach a so-called dislocation punching pressure [14] and cause decohesion (in the absence of hydrostatic pressure) of the fuel matrix along the grain boundaries, or in simpler words – fuel pulverization. Owing to the very small grains at the HBS, the fragments may also be very small, which makes them very mobile, that is, they can easily move to other parts of the fuel rod, and this movement of fuel fragments under the force of gravity is hereafter referred to as axial fuel relocation.

With the goal to understand the UO_2 polygonization, laboratory tests were performed by bombarding the fuel with heavy ions in order to simulate the fission process [15]. The irradiation damage level was varied from 1 displacement-per-atom (dpa) to 100 dpa and it was found, that displaced U atoms quickly returned to a vacant U-position in the UO_2 lattice. However, implanting non-soluble fission products, such as Xenon [16] and Iodine, resulted in polygonization. To simulate this effect, a certain dose needed to be implanted, which corresponds to the notion, that certain level of fission product concentration in the fuel needs to be surpassed, or equivalently – a certain level of burnup. This suggests that irradiation damage is not the only driver of polygonization, but also the presence of certain elements.

The fuel microstructure transformation first appears at the fuel periphery, where burnup is significantly higher owing to the transmutation of U-238 to Pu-239 and the subsequent fission of the latter. This transformation continues towards the fuel interior, but at the same time the fuel temperature also increases. Eventually thermal annealing overwhelms the subdivision of grains and the transformation is halted. The distance at which this happens is conservatively estimated to be 1500 μm [5], for the pellet-average burnup range of 75-100 MWd/kgU. Currently, all of the commercial nuclear power plants operate to average burnups well below 75 MWd/kgU, although some fuel rods are irradiated to higher burnup for research purposes.

The fuel's hardness and toughness are also modified by the restructuring. Hardness is shown to decrease towards the pellet periphery and this is easy to visualize. If we take two cubes of the same material, but one with lower density due to porosity and apply compressive force, the cube with the lower density will deform first. The toughness, on the other hand is reported to be two-times higher at the rim [15] compared with the rest of the fuel. In the absence of voids, cracks propagate by breaking the atomic bonds between parallel atomic planes. However, in the highly porous pellet rim, the crack, loosely speaking, has to go around the pore in order to progress.

Fuel microstructure changes also affect the thermal conductivity of the fuel. Changes in density due to porosity and fission gas precipitation, formation of cracks and changes in the composition due to fission products all have negative impact on the thermal conductivity. Heat transport through solids is achieved via lattice vibrations (phonons) and electronic conduction. For temperatures lower than 1600℃, which is the operating range of nuclear fuel, the main contributor is the lattice vibration [17]. Any irregularities in the lattice, due to interstitials (fission products), dislocation, voids (porosity and fission gas bubbles) results in scattering of the phonons and therefore decrease in conductivity and leads to higher temperatures. This is especially true at the HBS due to the high porosity and concentration of fission products. In the event of fuel fragmentation during LOCA, heat removal from the fuel fragments becomes even more difficult, because most of them are not in direct contact with

the cladding and instead the heat transfer must happen through the inner rod gas that likely contains large quantity of Xenon which has two orders of magnitude lower thermal conductivity than Helium.

1.4 Fission gas release in LWR fuel

The fission process produces isotopes of two main fission gas elements: Xenon (Xe) and Krypton (Kr). An estimated volume of 31 cm^3 of fission gas, at standard pressure and temperature, is generated for every MWd of energy liberated by the fuel. Fission gas atoms are created inside the fuel grain and diffuse towards the grain boundaries where they are trapped into already existing bubbles or initiate the nucleation of new ones. With the influx of new gas atoms, those bubbles grow and coalesce, thereby contributing to gas retention and fuel swelling. Eventually the interconnection creates a tunnel network through which fission gas is released to the rod free volume [18]. This causes the rod inner pressure to increase and the thermal conductivity through the pellet-cladding gap to decrease. Assuming the fuel swelling rate of 0.77% per 10 MWd/kgU, fuel pellet diameter of 8.19 mm and cladding inner diameter of 8.36 mm – values representative of LWR fuel, it can be calculated that after burnup of 50 MWd/kgU the gap will be closed solely by the fuel swelling. However, cladding creep, due to compressive pressure in the reactor, and thermal expansion of the fuel may close the gap much earlier. Therefore, the thermal conductivity through the gas gap is only important up to the first 2-3 one-year cycles.

Two types of fission gas release (FGR) mechanisms should be distinguished: during normal operation and during transients. With respect to the first, fission gas release can be further categorized as thermal and a-thermal. Thermal FGR during normal operation is achieved via diffusion of fission gas driven by temperature, from the grain to the grain boundaries. The grain boundaries can be visualized as a complicated network of paths, which eventually lead out of the fuel matrix into the rod free volume (represented by the fission gas plenum, pellet-cladding gap, dishes, cracks, etc.). A-thermal FGR occurs when high energetic fission product fragments drive fission gas atoms outside the fuel matrix. This mechanism occurs at the fuel periphery, which is shown to contain large quantity of fission gas, especially at high burnup. Fission rate at the periphery is considerably higher, due to the production and fission of Pu-239, and as such the a-thermal mechanism increases with burnup. Fission gas release during transients (e.g. LOCA) is mostly attributed to the fragmentation of the fuel. It is a well-established fact that large quantity of fission gas is stored at the high burnup structure at the fuel periphery. During LOCA, the fuel fragments and the gas are released. An additional mechanism of transient fission gas release during LOCA is discussed in Chapter 4 section 4.7 which is associated with the breaking of the fuel-cladding bonding layer.

Measurement of the ratio of Xe to Kr is an indication on where the FGR came from (centre or periphery). This is possible, owing to the fact, that with increasing burnup, Pu-239 fissions at the fuel periphery become significant and the fission product yields of Xe and Kr are different from those of U-235. This methodology, for example, has been used in the work of [8, 19, 20]. The paper by Serna et. al. [8] investigates FGR as function of burnup. They used the Xe/Kr isotopic ratio and observed that at lower burnup fission gas is released from the periphery, via the a-thermal mechanism. Their observations also show that thermal release from the pellet centre becomes predominant for higher burnup towards end of life. Such observation was also made by J. Noirot et. al. in the paper "Contribution of the Rim to the Overall Fission Gas Release" published in OECD/NEA report [21]. Zwicky et. al. also reported predominant FGR from the pellet interior [19] in high burnup PWR rods. This is a confirmation of already known fact, that fission gas retention in the pellet periphery is significant, because release is lower and generation is higher due to the higher burnup. These observations do not mean that thermal release cannot occur at lower burnup. Researchers at the Halden Reactor Project (HRP) in Norway, derived threshold for fission gas release based on measurements of

the fuel centreline temperature. This is known as the Vitanza curve [22] named after Carlo Vitanza from the HRP and it is presented on Figure 4.

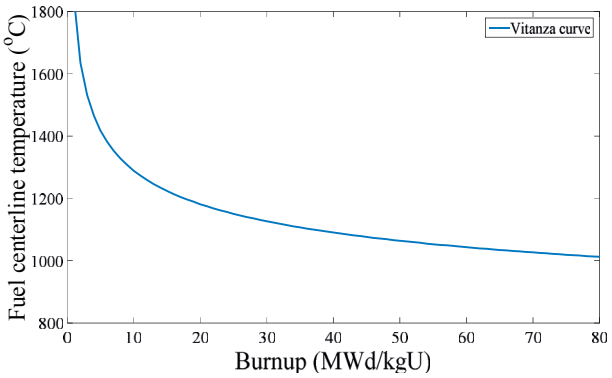

Figure 4: Vitanza curve for thermal fission gas release.

High centreline temperature exceeding the threshold can be achieved at low burnup, provided the linear heat generation rate (LHGR) of the fuel rod is high enough. According to the paper by J.A. Turnbull et.al. [23], the Vitanza curve has been shown to work for different fuel manufacturers and designs, including MOX fuel, and it has been used as benchmark in FGR models. For high burnup, the LHGR is significantly reduced, but also so does the fuel thermal conductivity, which could lead to high temperatures at the centre and therefore to thermal FGR.

The stored fission gas in the high burnup structure can be released via fuel fragmentation during a LOCA, and this is referred to as burst fission gas release. In recent Halden LOCA test [24], the FGR could be precisely measured, because the rod did not rupture. Post-irradiation examination revealed ~19% FGR and high isotopic ratio of Xe/Kr which suggests large FGR from the HBS. Transient FGR is strongly correlated with the degree of fuel fragmentation because the smaller the fragments the more gas is liberated from the matrix. High burnup fuel is particularly susceptible to fuel fragmentation, because the HBS occupies larger area and therefore more gas is stored inside the fuel matrix. Another mechanism of burst FGR is hypothesized for BWR fuel rods, in which fission gas is trapped in the pellet-cladding bond layer, which would be released at the moment the fuel-cladding bonding layer is broken. In the context of fuel modelling, this is the moment when the fuel and cladding begin to move relative to one another. This hypothesis is discussed in Chapter 4 section 4.3.

1.5 Fuel Fragmentation

Fuel fragmentation is the breaking up of the nuclear fuel pellets into smaller pieces. The reasons for this are several, but two mechanisms need to be distinguished: fragmentation during normal operation is shown on Figure 5 (left) and fragmentation after a LOCA test is shown on Figure 5 (right). Fuel fragmentation during LOCA has been known since earlier tests with low burnup nuclear fuel as summarized in NUREG-2121 [25], but it was made up mostly of large fragments and it was not of particular concern in the context of fuel relocation and dispersal. It is only since recently, that severe fuel fragmentation, relocation and dispersal was observed in very high burnup fuel rods (first in Halden LOCA test 4 [26] and later in Studsvik's LOCA tests 191-193[27]) and attracted the attention of the community back to this phenomenon. Although the level of burnup in the said LOCA tests was higher than present operating limits, understanding the phenomena leading to it is important to industry and interesting for research. First order parameters responsible for fuel fragmentation are given in [28] as burnup, cladding deformation and rod internal pressure at burst.

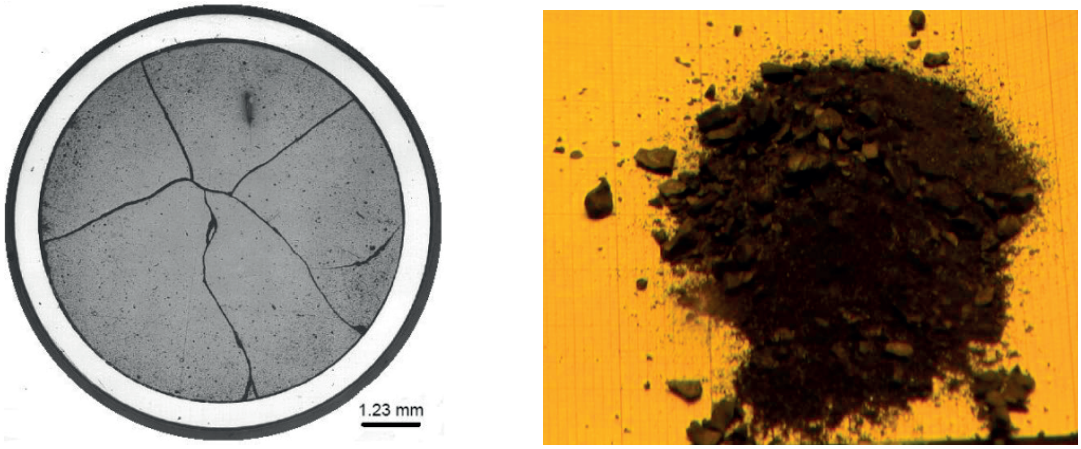

Figure 5: Fuel fragmentation during normal operation [26] and fuel fragmentation in Studsvik's LOCA test 193 [29].

During normal operation, the fuel is subjected to mechanical loads such as expansion and contraction during reactor operation and refuelling respectively. The UO_2 is a ceramic material and therefore it has low potential for plastic deformation and typically responds to such loads by cracking. The cracking is limited, because eventually the fuel-cladding gap is closed (due to formation of cracks, thermal expansion and fuel swelling due to fission product build-up) and no further cracking can develop.

Fine fuel fragmentation, such as the one shown on Figure 5, is shown to depend on the level of burnup [26, 27] and temperature [12, 27, 30, 31], but also on the cladding distention. In fact, high burnup fuel samples used in separate-effect tests fragmented more in the absence of cladding restraint compared to those with cladding restraint [30]. Fuel fragmentation necessarily leads to expansion due to the formation of cracks and it logically follows, that if fuel is restrained, then it cannot also fragment. In her work on a model for fuel fragmentation [14], Kulacsy writes, that for fuel fragmentation in the HBS to occur, a so-called dislocation punching pressure inside the HBS pores needs to be exceeded. The hydrostatic pressure, provided by the cladding or inner rod pressure and acts as a restraint to fuel fragmentation, is taken into account in her analysis.

In the search to explain fuel fragmentation, different mechanisms and factors are being proposed and discussed. A question was posed by the research community, whether fuel fragmentation required rod burst. This is a valid question, because before the rod ruptures the pressure inside is quite high which applies compressive pressure on the fuel, especially during the ballooning, when the fuel is separated from the cladding. The back-pressure would act against the mechanical stresses within the fuel pellet. Evidence against this hypothesis is presented by Post-Irradiation Examination on the 12^{th}, 13^{th} and 14^{th} Halden LOCA tests. Fuel fragment size distribution was performed by Kjeller hot laboratory in Norway and is shown on Table 1.

Table 1: Fragment size distribution obtained by ASTM sifting system for 12th, 13th and 14th Halden LOCA tests [32].

Particle size mm	Fuel weight (g)			Normalised weight fraction (%)		
	650.12	650.13	650.14	650.12	650.13	650.14
>4	139.26	172.405	133.246	97.78	99.18	98.03
4 – 2	2.68	0.017	1.486	1.88	0.01	1.09
2 – 1	0.19	0.028	0.047	0.13	0.02	0.03
1 – 0.5	0.16	0.233	0.164	0.11	0.13	0.12
0.5 – 0.24	0.08	0.239	0.199	0.06	0.14	0.15
0.25 – 0.125	0.04	0.211	0.160	0.03	0.12	0.12
<0.125	0.01	0.695	0.628	0.01	0.40	0.46
total sieved	142.42	173.828	135.930	100.00	100.00	100.00
blocked fuel	n/a	18.972	45.570			
total weight	n/a	192.800	181.500			

The 12th and 13th test rods were manufactured from the same mother rod, while test 14 came from a different rod but at the same level of burnup. The mother rods were irradiated in the Swiss NPP Leibstadt. The 14th LOCA test was designed to avoid rupture [33], which it did, and therefore rod burst could not have been the driving force behind fuel fragmentation. Looking at the fragment size distribution, all three tests experienced rather coarse fragmentation and there is no significant difference between the burst and non-burst test. It can be concluded, that while rod burst may be influential on fuel fragmentation, it is not the driving force behind it.

A. Bianco et. al [28] performed separate effect tests on small fuel rods prepared from a mother rod irradiated to an average burnup of 52 MWd/kgU in order to determine the impact on fuel fragmentation in three cases: when the cladding balloons but does not burst, when it balloons and bursts and when it does not balloon and does not burst. He identified as first order parameters for fragmentation burnup, cladding deformation and rod internal pressure and concluded that ballooning and burst had an effect on fuel fragmentation, although putting more emphasis on the loss of pressure rather than the fuel temperature as the main driver.

Ken Yueh et. al. [30] set out to determine a parameter called Fuel Fragmentation Burnup Threshold (FFBT) by conducting separate effect tests on small fuel specimens. This parameter is, loosely speaking, a level of burnup below which the fuel will fragment to medium (2 mm) and large (4 mm) pieces and above which – to fine fragments (bulk of fuel fragments below 1 mm). The tests were done by heating small fuel samples, of approximately 2 cm in length and at different burnup, to about 1000℃ and at atmospheric pressure. It was observed, that fuel fragmentation was very limited. On another set of samples, the cladding was cut open; thereby significantly reducing any restraint on the fuel to fragment. It was observed, that fragmentation was significant. This only confirmed existing observations on the suppressive effect of cladding on fuel fragmentation, which makes logical sense without necessity for experiments. If there is no room, fuel simply cannot fragment, because any fragmentation requires expansion in surface area and therefore reduction of effective density. In his paper, Ken Yueh also suggests influence on fragmentation by the last cycle power. Higher last cycle power means the fuel had higher temperature difference between centre and periphery than the same fuel operating at lower cycle power. This means higher internal stresses due to the difference in thermal expansion across the fuel pellet diameter. Such observation can be made when comparing the fragmentation in Halden LOCA test 12 and Studsvik's LOCA test 193. The average fuel burnup was about the same, cladding deformation was significant in both tests but the last cycle power was 7

kW/m and 15 kW/m respectively. Studsvik's test experienced much more fuel fragmentation. In addition, higher last cycle power may cause redistribution of fission gas, and in particular by "pushing" more gas from the interior to the periphery, which is highly susceptible to fragmentation. The collected data from their tests, suggest FFBT of 70-75 MWd/kgU. The FFBT may also be dependent on the fuel grain size, because as already discussed in section 1.3 large grained fuel has smaller HBS at a given burnup level and therefore more fission gas is contained in the grain rather than at the grain boundaries. Effect of the grain size was not examined in their separate effect tests, but it may suggest higher FFBT for large grain fuel.

In the Nuclear Fuels Industry Research (NFIR) program coordinated by the Electrical Power Research Institute (EPRI), separate effect tests with high burnup fuel samples of dimensions 1.5x1.5x1.0 mm were conducted to determine the effect of hydrostatic (restraint) pressure and temperature on fuel fragmentation [31]. In their tests, the restraint pressure was supplied by the test chamber and not by the cladding. The tests showed that for restraint pressure above 40-60 MPa fission gas release and fragmentation are impeded. Raising the temperature above the irradiation temperature resulted in fine fuel fragmentation and fission gas release. Local burnup of at least 71 MWd/kgU and temperature of 645 ℃ are given as the necessary conditions for fuel pulverization (fragment size < 0.2 mm). These conditions are used in the model for fuel pulverization discussed in Chapter 5 section 5.1.1.

The effect of temperature is easy to understand. At high temperatures and pressure the cladding begins to creep out thereby opening room for fragmentation. In terms of restraint (or hydrostatic) pressure, it does not matter if it is supplied by the cladding wall or the gas pressure inside the rod. The cladding creep-out will create local pressure drop and allow for some fragmentation to occur before the pressure is equalized, which may take some time depending on the fuel-clad bonding state. Also, the higher the temperature, the higher the pressure in the grain boundary pores and therefore the stress within the fuel matrix. In summary, the main drivers for fuel fragmentation are burnup, temperature, last cycle power and cladding restraint/hydrostatic pressure.

1.6 Fuel relocation

Fuel relocation in general describes any sort of fuel movement. This can be axial or lateral. For example, fuel cracking during normal operation is an example of lateral relocation. In a LOCA transient, fuel relocation takes on a different meaning. If it continues sufficiently long, then the fuel cladding will begin to deform and balloon. This will create additional space for fuel to relocate and will also unlock the mechanism for fuel fragmentation. Therefore, small fuel fragments will be able to relocate axially. Fine fuel fragmentation (or pulverization), together with large balloon volume may create the conditions for a cladding hot-spot, where the additionally relocated fuel causes higher local cladding temperature. Good definition of the hot-spot effect can be referenced to [34] where "fuel relocation may localize the heat load to "ballooned" parts of the rod, thereby increasing the risk for cladding failure and aggravating local oxidation". One of the goals of OECD Halden Reactor Project's LOCA tests series (discussed at length in Chapter 3) is also to investigate fuel relocation into the balloon and its effect on the cladding temperature [26]. This could be important, because at the ballooned location the cladding is already weakened by the deformation and it may lead to faster fuel rod failure. An example of fuel relocation and of hot-spot effect, whose impact on rod failure could not be evaluated, is shown on the gamma count intensity plot on Figure 6 of the 9th Halden LOCA test [26]. The gamma count intensity is proportional to the fission product concentration, which in turn is directly proportional to the amount of fuel. Decay heat, which is due to alpha, beta and gamma radiation, is proportional to the amount of fuel. Axial fuel relocation clearly occurred in the upper part of the rod, because there are almost no gamma counts. The faint signal could be coming from dust-like fuel fragments which were likely stuck to the inside of the cladding wall, or it could just be noise.

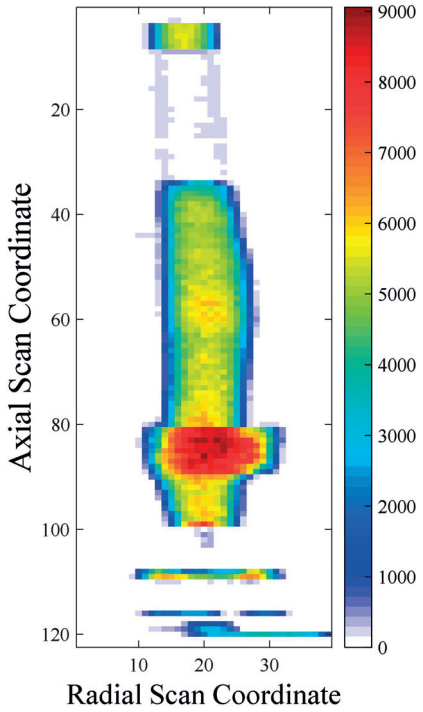

Figure 6: Gamma count intensity plot of Halden LOCA test 9.

The hot-spot effect is a logical hypothesis of what may happen during fuel relocation and it remains to demonstrate its real effect by means of experiments. Such experiments only need a heat source which can provide more heating at the level of balloon. This can be achieved by specially designed electrical heaters which deliver higher heat flux at a particular cladding elevation (e.g. where the balloon is). A simple evaluation of the hot-spot would be to consider two identical claddings with pre-manufactured balloon. In one, the cladding is heated uniformly along the length and in the other more heating is applied at the balloon. The experiments can be performed in steam environment and they can measure cladding oxidation and evaluate impact on cladding rupture (if any). In a fuel assembly, formation of a balloon and subsequent hot-spot may impact the temperature of neighbouring rods as well, because ballooning and fuel relocation essentially moves heat source closer to neighbour rods. This is just a hypothesis, which can be confirmed by experiments.

More detailed discussion of the Halden LOCA tests is found in Chapter 3, but the online temperature measurements demonstrated clear evidence of fuel relocation and its effect. Figure 7 shows on-line measurements from Halden LOCA test 4 of the temperature at different axial elevations of the cladding and the heater.

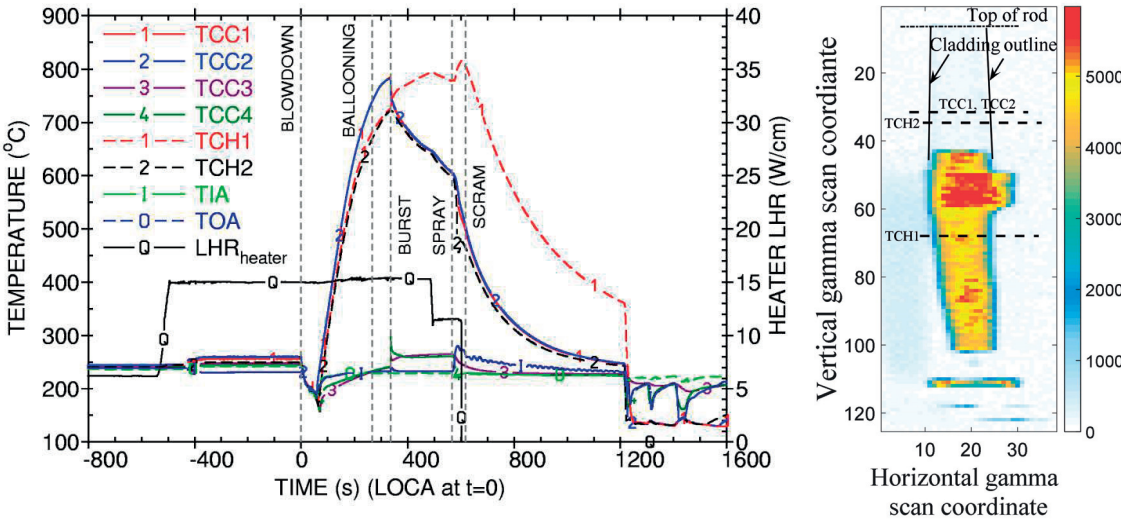

Figure 7: On the left: temperature signals recorded during the 4th Halden LOCA test [26]. On the right: gamma scanning count intensity plot of the fuel rod.

The heater thermocouples are labelled TCH1 and TCH2, which are located near the bottom and above the middle of the fuel rod respectively. Cladding thermocouples TCC1 and TCC2 were installed slightly above TCH2. At the moment of burst, the temperatures of TCH1 and TCH2 begin to diverge and reach a ΔT of 200℃ in approximately 200 seconds after the burst. Looking at the axial position of the thermocouples, the explanation is clear: heat source relocated below the thermocouple level. The two temperature measurements continue to diverge until the reactor is scrammed and the fission process is terminated, then the temperature gradually decreased. Decrease of heat source density via fuel relocation in one part of the rod means increase in another part, for example the balloon, which is none other than the hot-spot effect mentioned earlier. Fuel relocation was registered by the heater thermocouples which are about 1 cm from the fuel rod. The rod-pitch in a fuel assembly is about the same distance, which means neighbour rods in a fuel assembly could in principle "detect" the fuel relocation. The different phases of the LOCA test are clearly labelled on the figure. For a full description of Halden LOCA test series, please refer to Chapter 3.

The cladding ballooning during LOCA was considered a concern that may lead to fuel channel blockage in a fuel assembly and thereby challenge the coolability of neighbour rods. Fuel bundle tests were executed to address this concern, and it was found out, that even at 90% channel blockage [35], the coolability could be maintained. In an unpublished work by the UKAEA Winfrith 30 years ago it was shown that coolability could be maintained under similar blockage conditions including fuel relocation. Furthermore, in the modelling work discussed in [36] the simulated levels of blockage due to clad ballooning also did not impair coolability. On the other hand, Halden LOCA test 4 (Figure 7) demonstrated, that fuel got stuck between the cladding and the heater thereby creating conditions of blockage. It can be argued, that in reactor conditions with re-established cooling any blocked fuel could be carried away by the coolant, yet it is possible that these fuel fragments find another place to get stuck.

The Halden LOCA tests 4 and 9 just discussed were prepared from mother rod irradiated to very high burnup. Yet, extensive fuel fragmentation and relocation was observed even for fuel at low burnup, as demonstrated in the Power Burst Facility at Idaho National Labs in the 1980s [25]. The FR-2 program at Karlsruhe also in the early 1980s conducted 39 tests on very low to medium burnup fuel rods. They observed that fuel fragmentation and relocation increased with burnup. Tests at the NRU reactor in

Canada used full-length fresh PWR fuel rods to study deformation and flow blockage in a fuel bundle. The grid spacers, as anticipated, were acting as choke points for fuel relocation and rod deformation. Such effect is absent for short-length rods such as those in the Halden LOCA test program. The PHEBUS LOCA test program of IRSN also performed fuel bundle tests with low burnup fuel. They also confirmed that fragmentation and relocation is unlikely, even at high cladding deformation [25]. Present LOCA test programs (e.g. Halden and Studsvik) have been focusing on single rod tests of length less than half-meter. They demonstrated severe fuel relocation for high burnup fuel, but the role of spacer grids in limiting fuel relocation in full-length rods is not clear.

Due to only the recent interest in the FFRD phenomena during LOCA, there are no commercially available relocation models yet that are integrated into fuel performance codes such as FALCON, FRAPTRAN and others. Some researchers did develop in-house models [34, 37], that is, models which are not part of the official released versions of the codes, with the purpose of investigating the effect of fuel relocation on the cladding temperature. The approach is logical: extract the cladding strain dynamics, impose a fragment size distribution (taken from post-irradiation examination or calculation) and relocate fragments downwards provided there is sufficient cladding deformation (e.g. 5% cladding strain in Halden LOCA tests [26]). In UKAEA Windscale ballooning tests [38], with low rod-average burnup fuel of about 20 GWd/tU, it was shown that below hoop strain of 50% only limited fuel relocation occurred. Owing to the large fuel fragments, below 36% strain there was no fuel relocation. Additionally, it was found that vibrations may induce fuel relocation during core re-flood [39]. Similar approach to the above referenced fuel relocation models is undertaken in this PhD project (see section 5.2) with the addition of considering the heat source density of fuel fragments as function of radial distance from the fuel pellet centre. This is necessary, because burnup at the periphery could be two times higher than burnup at the centre, which means decay heat is also higher.

A numerical simulation approach using the discrete element method (DEM) based on the representation of fuel as granular material is described by [40]. The authors reported qualitative and quantitative agreement with experimental data such as the packing factors in the balloon. Motivated by experimental data on fuel fragmentation, the authors represented the fragmented fuel pellet interior based on distribution of radial and circumferential cracks, as agglomeration of spheres where each agglomeration, or fragment, is tracked separately. The presence of small fuel fragments in the pellet periphery of high burnup fuel was modelled by spheres with a diameter of 0.5 mm. This approach allowed for visualization of the fuel relocation with limited cladding deformation. The authors could not simulate fuel relocation of pulverized fuel within a cladding with large balloon due to time constrains of the DEM, but succeeded in simulating relocation for medium burnup fuels where small fragments are absent and concluded good agreement with experimental data. Ultimately, the effect of the relocated fuel on cladding temperature is important and not so much the individual motion of fragments. The report by Jernkvist et.al [34] reported reduction in the time to cladding rupture by 17 s when thermal feedback effect from fuel relocation is considered. The approach to modelling fuel relocation presented in this dissertation will focus on evaluating the thermal feedback effect on the cladding oxidation.

1.7 Fuel dispersal

Fuel dispersal in a LOCA may occur after the cladding ruptures. In a prolonged LOCA transient, the cladding temperature and inner rod pressure will increase while the pressure on the other side of the 0.7 mm thin cladding wall can reach atmospheric level. After some minutes the cladding begins to deform, the fuel begins to fragment and relocate and eventually the cladding ruptures. The pressure difference between inside the fuel rod and outside will drive gas outflow, which in turn will interact with fuel fragments and try to drive them outside the rod (see Chapter 5 section 5.3). Several parameters can be identified as being important. First of all, if the cladding rupture is too small (e.g. pin-hole rupture), then only limited amount of fuel can be dispersed and this is only a possibility if the fuel was high burnup and the periphery pulverized. At lower burnup, most of the fuel fragments are large and will have no chance of escaping. On the other hand, large rupture openings, which were observed in Halden's 4th and 9th LOCA tests [26] and Studsvik's 191 and 193 LOCA tests [41], would allow virtually all fuel fragment sizes to pass through. Fission gas release during the LOCA is also important, because larger gas quantity will take longer time for the rod to depressurize and it may also cause stronger interfacial friction with the fuel and therefore impact fuel dispersal. Distance between cladding rupture and gas plenum is also important. If the rupture is close to the plenum, then there will be less resistance to the gas outflow and the dispersal can be larger. On the other hand, if the rupture is far away from the plenum and the cladding deformation is small, then gas flow will experience significant resistance from the fuel stack above the rupture and may lead to limited gas-solid interaction and therefore less fuel dispersal. In full-length rods, spacer grids will limit the cladding deformation and this may also increase resistance to gas outflow. Burnup level plays a role in fuel fragmentation and therefore also has an effect on dispersal.

It is hypothesized, that fuel dispersal from ruptured fuel rods may challenge the integrity of neighbour rods in a fuel assembly. That direction of thinking leads to chain of fuel rod failures. Another potential problem could be the interactions of the hot fuel fragments with the coolant during core re-flood. Heat transfer from the fuel fragments could be very high and lead to small steam explosions, whose possible effect on neighbour rods is not clear. In any case, fuel dispersal would require great effort to clean up the primary circuit, which would imply extended period of outage and significant financial losses for the operator and it should be avoided. There are just a few experimental programs that perform single rod LOCA tests (Halden and Studsvik for example) for the purpose of exploring fuel relocation and ejection, but none of them evaluate fuel balloon and rupture in a fuel bundle and how the failure of one rod could affect the neighbour ones.

Clear limitation in the prediction of fuel dispersal is the uncertainty on cladding rupture size. Pressure, temperature, hydrogen uptake in the cladding, oxidation and rate of rod inner pressure increase all may have influence on the rupture size. This is a parameter that is very difficult to predict and in the core-wide estimates [42] on fuel dispersal done by the US Nuclear Regulatory Commission, it was assumed, that only powder-like fuel fragments (pulverized fuel) could escape.

Despite the evidence of severe fuel dispersal during recent LOCA tests, the working group on fuel safety (WGFS) wrote in 2015, that **"**Fuel relocation within the cladding tube and its impact on local power and ECR are deemed more important than fuel dispersal." [43]. This is likely because the current burnup level is below the fuel fragmentation burnup threshold discussed in section 1.5 and therefore the bulk of fuel fragments below 1 mm are not anticipated.

As with the case with fuel relocation, there are no comprehensive fuel dispersal models that are available with fuel performance codes. One reason for this is probably the recent interest towards this phenomenon (i.e. current efforts are made without having fully validated models that are integrated

into existing fuel performance codes). Another reason can be attributed to the large uncertainties associated with modelling of fuel dispersal. In particular, determining fuel cladding rupture shape and size remains a challenge. More generally, understanding of solid-gas interactions is mostly at the level of fluidized beds, but the conditions inside a fuel rod are much different. For example, in the former case there is counter-current gas-solid flow whereas in the latter the motion of both phases is in the same direction. Fluidization is achieved with continuous injection of gas whereas the gas quantity in a ruptured rod continuously decreases. Fluidization implies that the solid particles are separated from one another, whereas in a fuel rod such separation is unthinkable owing to the much tighter packing and the fact that gravity and gas flow act in the same direction which would result in packing and not in separation.

Some authors hypothesize that fuel dispersal may lead to coolant channel blockage [40]. For such occurrences, relatively large fuel fragments would be needed which consequently requires large rupture opening. Within the same reference, adequate simulation of fuel dispersal was achieved with discrete element method, but it required large computational time.

1.8 General description of a Loss-of-Coolant Accident (LOCA)

Together with Reactivity-Initiated Accidents (RIA), a LOCA is a design-base accident (DBA), which is a postulated accident that a nuclear power plant must be designed to withstand "without loss to the systems, structures, and components necessary to assure public health and safety" as per the definition of the U.S.NRC. The definition of a LOCA is for any accident that results in coolant loss that is higher than the reactor cooling make-up systems to cope with. Typically, a LOCA can be assigned into one of three categories: small (SBLOCA), medium (MBLOCA) and large (LBLOCA) break LOCA. They are distinguished by the break size and the rate of loss of the coolant and hence the rate of depressurization of the core. The most severe case is a double-ended guillotine break of a main coolant line, in which the depressurization is fast and causes the coolant to flash to steam, because BWR operates at 70 bars and a PWR at 150 bars. Emergency core cooling systems (ECCS) are part of the design of nuclear power plants and should handle such transients. A comprehensive state-of-the-art report on LOCA, including all related phenomena to the fuel and cladding, experimental programs and available simulation tools, was prepared by the Nuclear Energy Agency (NEA) Working Group on Fuel Safety [44].

During a LOCA transient, the pressure applied on the cladding from the outside is lost due to depressurization of the reactor, which results in large pressure difference across the fuel cladding wall. In combination with high temperature, the cladding begins to deform (balloon) and once that happens fuel rod ruptures are almost guaranteed. A prolonged LOCA may move from a DBA to Beyond Design Base Accident (BDBA) as was the case in Three Mile Island. LOCA is a challenging situation for the fuel, because prolonged interrupted cooling results in increase of the fuel temperature and unlocks mechanisms such as cladding plastic deformation and rupture, runaway cladding oxidation and even fuel melting. In order to ensure the safety of the fuel, so-called LOCA Safety Criteria are put in place; they are summarized in the next section.

1.9 LOCA Safety Criteria

The U.S.NRC defined in the 1970s a set of criteria [45] that will ensure the mitigation of a LOCA scenario. Their goal is to guarantee, that the cladding integrity is not compromised. These LOCA safety criteria were derived primarily from data analysis on tests with fresh fuel and at a time when fuel burnup at discharge was significantly lower than todays. With this in mind, these guidelines are still in use in most of the nuclear power plant operating countries and are listed below.

1. **Peak Cladding Temperature (PCT)**. The maximum cladding temperature of the hottest fuel rod should not exceed 1204℃. Keeping the cladding temperature below this threshold should eliminate the possibility for runaway cladding oxidation which is an exothermic process.
2. **Maximum cladding oxidation limit**. During operation, the outer cladding wall picks up oxygen, which leads to the formation of ZrO_2 which is a brittle material with low mechanical properties. During transients, the cladding is exposed to high temperature and steam and as such the oxidation rate is increased. The term which quantifies the cladding oxidation is Equivalent Cladding Reacted (ECR). During LOCA, the ECR is limited to 0.17, which means that at most 17% of the initial cladding wall thickness is "allowed" to transform to ZrO_2. In essence, it is the oxygen content within the load-bearing β phase, below the oxide and the oxygen-stabilized α-phase, which determines the residual ductility in the cladding. By the time 17% of the initial cladding wall oxidizes, it is deemed that enough oxygen had diffused to the β phase to embrittle it [44]. Some fuel rod claddings, such as Areva's M5® have higher tolerance to oxidation. Research on cladding embrittlement has determined, that increased hydrogen uptake lowers the embrittlement limit of the cladding based on ECR [35]. The current limit of 17% ECR, also termed "zero-ductility limit" does not take the effect of hydrogen, which is shown to increase the embrittlement as the hydrogen content increases [46]. Because the concentration of hydrogen in the cladding increases with time, the 17% ECR may not be adequate for high burnup fuel. This criterion is under review.
3. **Limit on the generated Hydrogen.** The calculated total amount of hydrogen generated from the chemical reaction of the cladding with water or steam shall not exceed 0.01 times the hypothetical amount that would be generated if all of the metal in the cladding cylinders surrounding the fuel, excluding the cladding surrounding the plenum volume, were to react [47].
4. **Maintain coolable geometry.** This is essential for the reactor core recovery after a LOCA. If for whatever reason, there is a local blockage of the cooling channels, then some fuel rods will not receive adequate cooling and will overheat and eventually fail. Coolable geometry will be ensured if the fuel rod and assembly deformation is avoided altogether.
5. **Guarantee the long term cooling of the core.** Establishing core re-flood via the ECCS is necessary for the mitigation of a LOCA, but the decay heat removal must be ensured by continuous coolant circulation.

At the time these criteria were put in place, fuel burnup at discharge was about 35 MWd/kgU and fuel tests were done on fresh or low burnup fuel at best. Effect of fission gas release on rod internal pressure and conductivity was limited. It was discussed in section 1.3 that with burnup fuel microstructure changes dramatically, resulting in drop of thermal conductivity. The cladding experiences radiation creep, oxide layer build up and hydrogen pick-up which weakens its mechanical strength. The longer a fuel stays in the reactor, the more "fragile" it becomes. Naturally, this calls for a limitation on its use in the reactor. Review of the LOCA safety criteria is underway.

1.10 The economic benefit of going to higher burnup

Over the years, the nuclear industry continuously increased the fuel burnup limit at discharge and the driver for this is mostly economical. Forty years ago, typical burnup at discharge were around 30 MWd/kgU. Currently, most countries operate up to an average burnup around 55 MWd/kgU, but Switzerland operates to an average burnup of around 65 MWd/kgU. In the end, it is the regulator which determines the limit, however improvement in fuel manufacturing and core management also play an important role. As with most industries, maximizing profit and minimizing expenses is a necessary requirement to stay competitive. Energy production is no different, because there is competition from fossil fuel power plants as well as from hydro and increasingly wind and solar installations. An example of a cost breakdown of a nuclear fuel assembly is presented in Table 2.

Table 2: Approximate fuel assembly costs presented in [48].

Approximate Cost of One PWR 17×17 Fuel Assembly (450 kg of Uranium)

	Fuel Assembly Cost	Cost per kg of Fuel	
Cost of raw material, U_3O_8	$386,000	$860	30%
Cost of enrichment	$480,000	$1,067	37%
Cost of conversion to UF_6 and then to UO_2	$42,000	$93	3%
Cost of manufacture of the assembly	$400,000	$890	30%
Total cost of the assembly	$1,308,000	$2,910	100%

There is a strong economic incentive to increase the discharge burnup of fuel. A typical power reactor core has around 300 fuel assemblies, where the price of a fuel assembly as reported in Table 2 is about 1,308,000$. Therefore, the whole core costs 300·1,308,000 = 392,400,000$. Assuming each fuel assembly stays in the core for 5 cycles (5 years), then the cost per year is 392,400,000$ / 5 = 78,480,000$ / year. One operational year has about 330 days (the other 35 days are reserved for maintenance and refuelling). Therefore, the cost per day is 237,800$. In other words, even increase of 10 days of the operation of the fuel would save the power plant close to 2.5 million dollars. If the fuel remains in the core for one full cycle longer, then that translates to savings of 78,480,000$ in fuel costs. Clearly, the increase of the burnup limit at discharge has strong economical motivation for a nuclear power plant. However, there is another cost – that of the spent fuel handling. The increase in burnup limit would mean that over the life-time of the power plant, the total amount of spent fuel will be reduced. Yet, it can be argued, that economic benefit from reduced volume of spent fuel is diminished by the more difficult handling, storage and reprocessing of high burnup fuel [49], necessity to update infrastructure such as transport casks and perform more research to verify that safety is not compromised.

Some power plants operate on 18 month cycles, which means every three years they work 35 days more than plants operating on 12 month cycles, which by the rough analysis just presented, means savings of 8,323,000 $ every three years. Of course, the drawback is requirement for higher enriched fuel, in order to sustain criticality between the cycles when fresh fuel is inserted and the fuel assemblies are reshuffled. Increasing the enrichment will increase the fuel cost. Although going to higher discharge burnup and longer operating cycles has economic benefits, there are also drawbacks such as, but not limited to, requirement of higher enriched fuel.

Estimating the potential savings is beyond the scope of this section, but it is clear, that operating nuclear fuel to high burnup is well-motivated. From resource sustainability point of view, higher burnup is also advantageous, because less spent fuel will be discharged over the lifetime of a power plant and therefore less uranium needs to be mined, enriched and manufactured as nuclear fuel. On the

other side, there is cost increase due to fuel handling, longer cooling times and more research is necessary on the applicability of current licensing basis. Nevertheless, the industry has been continuously increasing the burnup at discharge over the years, which means there is economic benefit.

1.11 Goals and Structure of the thesis

The thesis is structured in such a way as to represent the logical and chronological order of the different aspects in this research project. The next chapter discusses the different computational tools that were used throughout the modelling work followed by special chapter introducing the Halden LOCA tests and focusing on the available experimental data and its uses for the modelling work discussed afterwards. The last chapter summarizes the work and discusses recommendations for further improvement of the presented models and few ideas for gathering experimental data. Each of the chapters is described in more detail below.

Chapter 2. This chapter introduces briefly the various computational tools that were used. Fuel modelling was performed with FALCON coupled with in-house advanced model for fission gas release and gaseous swelling GRSW-A. Calculations with Serpent Monte Carlo code was used to formulate a model for fission gas trapping in Chapter 4 and TRACE thermal-hydraulic system code was used to supply boundary conditions for the simulation of a LOCA of a full-length fuel rod.

Chapter 3. This chapter is especially dedicated to the OECD Halden Reactor Project LOCA test series. During a three-month technical visit, the LOCA tests were studied and experimental data was gathered and some of it - analysed. Chapter 3 starts with a general introduction of the LOCA tests, followed by focused discussion of the available post-irradiation examination data and how it can be used to reveal useful information regarding fuel relocation and dispersal. The findings were published in a journal paper that can be found as an attachment in Appendix A.

Chapter 4. The focus is on base irradiation and fission gas release of high burnup BWR fuel rods. The main goal is to explain the scatter between measured and calculated fission gas release. A hypothesis for fission gas trapping is motivated with the help of available post-irradiation examination data and a model is suggested that can be incorporated within the scope of base irradiation modelling. In particular, the hypothesized fission gas trapping is a BWR fuel specific phenomenon which is explained with the appearance of partial fuel-cladding bonding layer due to the non-uniform azimuthal burnup, which in turn is caused by the design features of the BWR fuel assembly. The significance of the trapped fission gas during LOCA is put in the proper context. The main results were published in a journal paper.

Chapter 5. This chapter presents the models for fuel fragmentation, relocation and dispersal in the chronological order in which these phenomena occur. The model on fuel fragmentation focuses at the moment only on fuel pulverization for reasons explained in the chapter. Fuel relocation is modelled from the onset of clad ballooning until cladding rupture with the implicit driving force being gravity. An approach is taken that the outermost fuel fragments, namely the pulverized fuel, relocate first which allow simulating hot-spot effect. The model for fuel dispersal, although highly simplified, manages to capture the driving force behind dispersal, namely the interfacial friction between the gas outflow and the fragmented fuel. The model is calibrated with experimental data from Halden and Studsvik LOCA tests.

Chapter 6. The last chapter begins with executive summary of the whole PhD project on fuel fragmentation, relocation and dispersal and focuses on what was accomplished and discusses

recommendations for further improvements for the presented models. At the end it introduces few ideas for possible non-nuclear tests that can be useful for further model development and validation.

2
Chapter 2:
Introduction of the Computational Tools

This chapter provides an overview of all the tools used in the present doctoral work. Modelling work is based on the calculations of EPRI's fuel performance code FALCON coupled with an in-house model for fission gas release and swelling GRSW-A. Data processing and model development for fuel fragmentation, relocation and dispersal is mostly performed in MATLAB. Some specific tasks were completed with the Monte-Carlo code for reactor physics burnup calculations, Serpent, and the reactor system thermal-hydraulics code TRACE. The tools are briefly introduced with a focus on specific features pertaining to this doctoral project.

2.1 Introduction to FALCON Fuel Performance Code

The PhD project on fuel fragmentation, relocation and dispersal uses EPRI's fuel performance code (FPC) FALCON [50]. It is a 2-dimensional code, whose solution processor is based on the Finite Element Method, which is briefly introduced in section 2.1.2. FALCON is capable to model fuel rod behaviour in both steady state and transient situations. The modelled geometries are R-Z, which are used for base-irradiation simulation and transients such as LOCA and RIA and R-Θ, which are used for simulation of Pellet Cladding Interaction (PCI) in cases dealing with some sort of asymmetry such as Missing Pellet Surface [51].

2.1.1 History

FALCON is abbreviation from Fuel Analysis and Licensing COde New and it came as a combination of a steady-state code ESCORE and transient analysis code FREY under ownership of the Electric Power Research Institute (EPRI) in the U.S. The first version is called FALCON MOD 01 [50] and it was released in 2004 and it is written entirely in FORTRAN 77. In 2012, EPRI released the first version of a so-called redesigned version of FALCON whose source code is updated to FORTRAN 95 and comes with graphical user interface for input and post-processing based on the Hierarchical Data Format (HDF) file structure developed and maintained by the HDF Group. The current version is FALCON 1.3 with the near release of the 1.4 version which includes the advanced fission gas release and swelling code developed by G. Khvostov [52] and coupled into the FALCON code at PSI [9] which is briefly introduced in section 2.2 of this chapter.

2.1.2 Finite Element Method

In this method, an object is divided into very small but finite size elements (hence, finite element method). Regions where geometry is complex (curves, notches, holes, etc.) require increased number of elements to accurately represent the shape; whereas, the regions with simple geometry can be represented by coarser mesh (or fewer elements).

Simply speaking, the Finite Element Method (FEM) approximates an object of any shape by simple geometrical objects, such as lines or beams in 1D, triangles and rectangles in 2D modelling, or tetrahedrons, hexahedrons in 3D. If more accurate approximation to the object is needed, then the number of elements is increased and their size is decreased. The larger the number of elements is the

better the approximation, which also leads to more accurate modelling results. Beyond certain mesh size, the improvement in accuracy is negligible and it can be said that convergence to the most-optimal mesh size is reached – e.g. there is no more advantage to make the mesh finer, because there is no gain and only increase in computational power. Each of these elements can deform their shape based on the displacement of nodes and the deformation of all elements leads to deformation of the whole object.

Creating a mesh to represent the object which will be subjected to Finite Element Analysis can be done in two ways: 1) the user creates the mesh by drawing all elements and nodes and 2) the user makes a CAD model of the object and lets the software automatically generate the mesh. The first way is the old approach and requires solid experience with meshing and the FEM whereas the second way gives control to the software and leaves the user with the mesh refinement at locations such as holes, joints, corners and such places where stresses may concentrate, or smaller elements are simply needed in order to get better surface approximation.

On each side of an element there can be two or three nodes, which are located at the two ends and the middle. Applied forces on the object are focused at the nodes and they give rise to displacements (or strains). Figure 8 shows simple object modelled with triangular elements and a single element whose nodes are displaced.

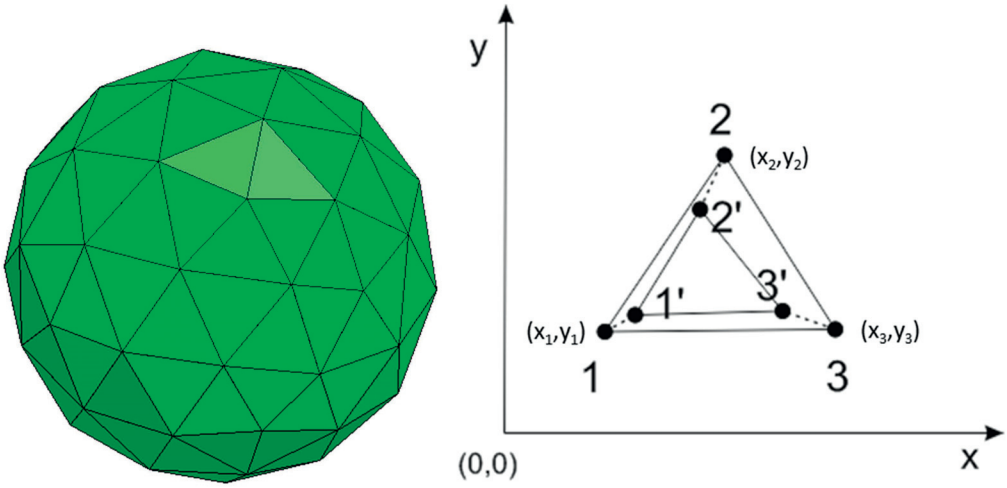

Figure 8: Sphere whose surface is represented by triangular elements (left) and example of triangular element nodal displacement (right).

All elements share nodes with the neighbour elements (sphere in Figure 8) and therefore a force exerted at one element may be experienced by an element located far away. This fact allows modelling of mechanical and thermal stresses of any object and owing to today's computational power the FEM is used virtually in every industry. There is one shortcoming of the FEM, which is the inability to model a crack because this causes discontinuity in the mesh that the method cannot deal with. In reality, all materials have some sort of cracks and these cracks act as localized stress concentrators. This means once a crack initiates, stress will preferentially focus at the crack location. Understanding the progression of cracks and to find a way to reduce the speed of crack progression through the material is important, because they determine the lifetime of an object. To address this shortcoming, the FEM was extended to the EXtended Finite Element Mesh (XFEM).

2.1.3 Finite Element Method in FALCON

FALCON is a single rod fuel performance code and uses the FEM to represent the fuel rod geometry which consists of fuel, cladding, and top and bottom end plugs (e.g. Figure 1) in R-Z geometry, or fuel and cladding in R-Θ geometry (Figure 9). The fuel and cladding elements are assigned the physical properties e.g. density, yield stress, heat capacity, thermal conductivity of the fuel and cladding material respectively. With reference to Figure 9 the fuel and cladding gap is modelled by so-called gap elements, which is a line element connecting fuel outer surface with cladding inner surface and whose initial length (unirradiated fuel at room temperature) is equal to the as-manufactured gap. The gap elements facilitate the heat transfer and stresses (if contact exists) between the fuel and the cladding.

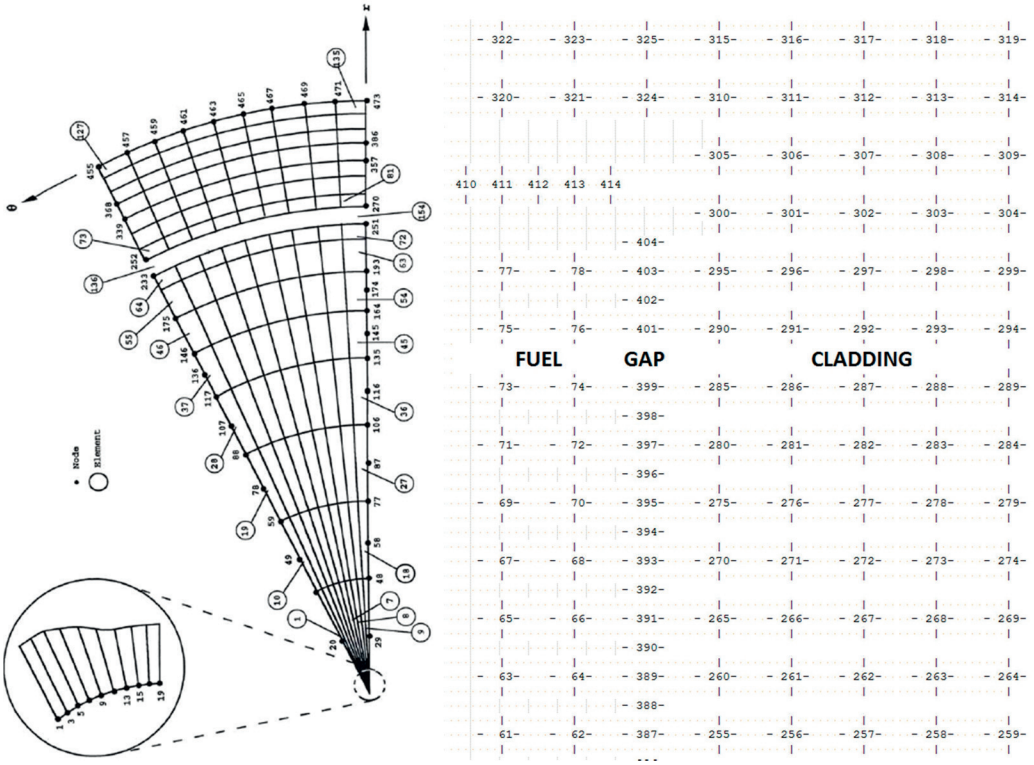

Figure 9: On the left: example of fuel-cladding mesh geometry in R-Θ [50]. On the right: Part of the fuel rod mesh in R-Z coordinates, which consists of elements describing the fuel, fuel-cladding gap and the cladding.

Typically, the use of R-Θ geometry is focused on such issues as PCMI, which arises when fuel is brought up to power after refuelling or there is a part of the fuel pellet periphery which is chipped (due to manufacturing reason, for example) or so-called Missing Pellet Surface (MPS), with the particular focus on simulating cladding hoop stresses. The R-Z geometry is used for Base Irradiation (BI) and Transient Analysis (TA) such as Loss-of-Coolant Accidents (LOCA) or Reactivity-Initiated Accidents (RIA).

The chosen mesh should be tailored to the modelled phenomena. In BI calculation where cladding failure is not expected the cladding can be modelled with only a few elements. On the other hand, TA would require finer meshing of the cladding because it may be subjected to significant deformation.

Since FALCON uses FEM and not XFEM cladding failure is not modelled as a progression of a crack through the mesh, but rather when cladding inner node occupies the same position as a cladding outer

node, which in a physical sense means the cladding wall has very small thickness which would occur during plastic rupture of material.

2.1.4 Modelling capabilities of FALCON

In the context of fuel modelling, the main materials of concern are the fuel, the cladding, the cladding oxide, the coolant and the gas mixture inside the rod (fill gas and fission gas release). Each of these is discussed further.

- **The fuel.** At this time, FALCON models are validated only for UO_2. For some physical properties such as fuel density, thermal conductivity and radial power distribution models are available for gadolinium-doped and MOX fuel, too.
- **The coolant.** It facilitates the heat removal from the fuel rod and it determines the cladding outer temperatures. During base irradiation, the cladding-coolant heat transfer is calculated internally using an enthalpy rise model taking into account the input for mass flow rate, temperature and pressure provided by the user. In the case of a transient such as a LOCA, the outer cladding temperatures can be provided by a thermal-hydraulic code such as TRACE, because the models in FALCON are not adequate for accurate modelling of the thermal-hydraulic part of a LOCA.
- **The cladding.** FALCON can model Zr-2, Zr-4, ZIRLO, stainless steel and barrier claddings. Current efforts exist to provide models for accident tolerant fuel claddings such as SiC-SiC and to incorporate hydrogen cladding uptake models. Concerning the latter, it is recognized that hydrogen uptake has detrimental consequences on the cladding mechanical properties.
- **Cladding oxidation.** During base irradiation (i.e. normal operation), thin layer of the outer cladding surface becomes oxidized with time. This oxide layer prevents further cladding oxidation but it also deteriorates the heat transfer through the cladding and therefore has a feedback on the fuel rod temperature. Cladding oxidation in FALCON is treated depending on the temperature, cladding material and coolant conditions (e.g. void-fraction). During base irradiation, low temperatures oxidation models, such as the CORROS model described in the Material Properties library MATPRO is used [53]. For LOCA transient simulation, it is envisaged that the cladding temperature can become much larger and a high-temperature model is used, such as one of Baker and Just [54] for licensing analysis or Cathcart model [55] for best-estimate analysis. The change from low to high temperature oxidation model occurs at 1083K.
- **Clad failure models.** To adequately model ballooning which can occur quickly and lead to large displacements of the element nodes, a so-called large strain formulation is adopted. The clad failure modes in FALCON are three. The first is concerned with cladding failure during normal operation due to intergranular stress corrosion cracking (IGSCC). The second model is based on the concept of cumulative damage and is used during LOCA transient simulations. In this mode, as the ballooning grows so does the cumulative damage and once a critical value (e.g. 1) is reached the cladding is assumed to rupture. The third one is based on the Strain Energy Density (SED) approach and it is used for PCMI simulation.
- **Coolant channel thermal-hydraulic model in FALCON.** The coolant channel model is based on a homogeneous closed channel flow model with thermal equilibrium between the vapour and liquid phases. Mass**,** energy and momentum transfer with neighbouring channels is not modelled which is a limitation. The coolant channel is subdivided axially to match the finite element mesh of the fuel rod. To initialize the model, the mass flow rate, fluid temperature and pressure are specified at the lower plenum through the FALCON input file. These parameters are used to initialize the inlet conditions at the lower boundary of the first

control volume, which are then used to obtain the conditions at the outlet. Then those conditions are the initial conditions for the next control volume. In such a way, the temperature, pressure and mass flow rate are solved at all axial elevations of the fuel rod.

On a final note, FALCON allows the users to provide their own models for fission gas release (e.g. GRSW-A described in section 2), new cladding type, gap conductance, low and high temperature cladding oxidation, critical heat flux, steady-state and transient creep, cladding irradiation axial growth and others.

2.1.5 Use of FALCON in the current doctoral work

The phenomena considered in this work, namely fuel fragmentation, relocation and dispersal (FFRD), are deemed particularly important for high burnup fuels. Base Irradiation (BI) simulation is the first step which is necessary to calculate parameters such as characteristics of fission gas release and retention, axial and radial burnup distribution, oxide layer thickness and others. Base Irradiation of BWR fuel rods in the nuclear power plant Leibstadt (KKL) is simulated with FALCON by providing power plant data such as the power production as function of time and elevation of the fuel rod (known as the linear heat generation rate) and fuel vendor data for the rod design (geometry, initial filler gas pressure and composition, material properties, etc.). An outcome of the BI calculations was the formulation of a model for fission gas trapping, which is discussed in section 4.3.

LOCA Transient calculations are started with calculated parameters from the BI simulation with the aim to determine how the fuel fragmentation and relocation affects the local cladding temperature; what will be the effect of burst fission gas release on the rod inner pressure; what is the effect on local cladding oxidation due to fuel relocation into the balloon and ultimately how these phenomena affect the cladding failure. Most of the analysis is done in an iterative way e.g. to evaluate the effect from fuel relocation on the cladding temperature during LOCA, at least two FALCON calculations need to be done. The first calculates the ballooning and provides the necessary input for the fuel relocation model. The fuel relocation model evaluates changes in the axial power distribution and provides input to TRACE which re-calculates the cladding temperature which is then input back to FALCON (see section 5.2.7).

2.2 GRSW-A: Gas Release and Swelling Advanced model

Fission gas products are continuously being generated by the fission process. In fact, for every MWd of energy released by the fission process, about 31 cm^3 at standard temperature and pressure of stable isotopes of fission gases (Xe and Kr) are generated. Fission gas release refers to the transport of fission gases out of the fuel matrix and to the rod free volume which is mostly the fuel cladding gap and the rod plenum. This has two effects: reduction of the thermal conductivity through the fuel-cladding gap and increase of the inner rod gas pressure. The latter has potential negative effect during a Loss-of-Coolant Accident by raising the pressure difference through the cladding wall when the reactor is depressurized. Fission gas release during normal operation is driven by thermal and a-thermal mechanisms. The thermal mechanism is particularly pronounced in the pellet centre because the temperature can be high and consequently the diffusion processes - more intensive. With the formation of the HBS at the pellet periphery, more and more fission gas begins to accumulate and the a-thermal mechanism becomes important where fission gas atoms are literally driven out of the fuel by high energy fission fragments. It is also relevant to mention that fission at the pellet periphery occurs more often than at the centre because of the formation of Pu-239 due to epithermal neutron captures by U-238 [56]. Both fission gas release mechanisms and fuel restructuring (including formation of HBS) are addressed in the GRSW-A model [9]. Furthermore, the model also considers fuel swelling.

During normal operation in a reactor, the fuel swells with burnup at the rate of ~1% per 10 MWd/kgU for burnups ≤ 60 MWd/kgU and somewhat higher than that that at extended burnup [57] due to accumulation of the specific porosity in the HBS at the pellet rim. Swelling is also important because it may lead to very high cladding hoop stress and challenge the integrity of the cladding which would limit the lifetime of the fuel rod, particularly during thermal transients such as power ramps.

The fuel grains are modelled as spheres whose surface is approximated by 14 round faces. The fuel matrix undergoes different type of restructuring depending on the temperature. At low temperature and long irradiation time, grain sub-division (or polygonization) takes place. This is in-line with experimental observations at the pellet periphery, where the temperature is lowest and the appearance of HBS is documented. At the HBS, the fuel matrix is characterized by sub-micron sized grains surrounded by gas pores. In the high temperature region of the fuel pellet (around the centre), the model simulates aggregation of grains.

The modelled processes by GRSW-A are divided into microscopic and mesoscopic. The former are further divided into intra-granular (within the fuel grain) and inter-granular (at the grain surface) processes.

The intra-granular processes consist of the following:

- Generation (due to the fission process) and dissolution of fission gas mono-atoms
- Diffusion of the gas mono-atoms inside the grain
- Creation of diatomic bubbles – when two fission gas atoms get close enough they coalesce and form a bubble which can further attract other gas mono-atoms and grow in size
- Growth of the bubbles due to trapping additional gas mono-atoms, coalescence with other bubbles or trapping of vacancies and interstitials
- Arrival of the remaining gas at the grain boundary

The inter-granular processes deal with the arrival of the gas flux from the grain bulk and consist of the following:

- Formation of gas clusters on the grain surface
- Evolution of the gas clusters into closed gas pores
- Eventual evolution of closed gas pores into vented pores - a gas pore will continue to grow until it becomes large enough and touches a grain boundary. As soon as this happens the gas is considered released and the pores become open

The mesoscopic and macroscopic processes stem from the microscopic ones and they deal with:

- Changes to porosity – during polygonization more grains appear which creates more surface area for intergranular pores and it is one of the reasons why high amount of fission gas is stored at the periphery – the most porous region of the fuel pellet at high burnup. Furthermore, porosity affects the thermal conductivity which ultimately raises the fuel temperature. This in turn has an effect on the thermal diffusion of fission gases.
- Swelling – the rise in porosity causes the fuel pellet to swell. This in turn has an impact on the closure of the pellet-cladding gap.
- Fission gas release – it rises the pressure of the fuel rod and lowers the thermal conductivity through the gas gap (Xenon has approximately 100 times lower thermal conductivity than Helium)

GRSW-A is explicitly coupled with FALCON, which means that at each time step of the simulation there is a mutual feedback between the two codes. In particular, the FGR model receives temperature, temperature gradient, fission rate and either hydrostatic pressure or gas pressure in the rod free volume from FALCON. In return, GRSW-A feeds back to FALCON the fuel porosity distribution (which affects the thermal conductivity), the state of the fuel pellet swelling due to the solid and gaseous fission products and the reduction of thermal conductivity and pressure increase due to FGR into the rod free volume. In essence, "a new mechanisms of the pellet swelling have been included into the FALCON code, which are caused by the build-up of fission products and the evolution of gaseous and as-fabricated porosity"[9].

The GRSW-A model has been validated against wide range of data from both separate-effect tests and integral experiments. Although the model is integrated into FALCON, it can also function as a standalone module. Verification and validation (V&V) of the model is described in [9], and also discussed in [58]. The advanced FALCON code has been used in different projects with experiment planning, data interpretation, as well as fuel reliability and safety justification ([59, 60]). The code improvement and V&V is ongoing.

2.3 FRELAX: model for axial fuel relocation

FRELAX is a Halden-specific model for axial fuel relocation developed at the Paul Scherrer Institute by Grigori Khvostov [37, 61], which is used in conjunction with FALCON for pre-test calculations and post-test analysis of Halden LOCA tests. It considers the Halden LOCA test section geometry (see section 3.3) and its main purpose is calculation of the axial distribution of cladding temperature, taking into account axial change in local Linear Heat Generation Rate (LHGR) due to fuel relocation [61]. A scheme of the model, together with the modelled parameters is shown on Figure 10.

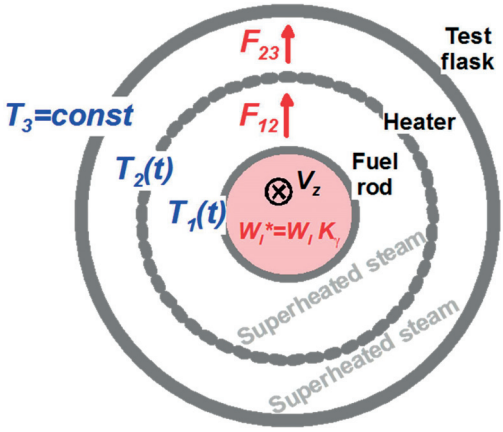

Figure 10: Model outline of FRELAX [37].

Located in the centre is the fuel rod, whose LHGR for each axial layer is expressed as the product of the initial LHGR and a weight factor which changes during the transient. It is equal to 1 if there is no change in the initial fuel quantity, greater than 1 if there is more fuel and less than 1 if there is less fuel due to fuel relocation. The cladding temperature is labelled as T_1 and is impacted by the LHGR and the heat flux going from the rod to the heater (F_{12}). The heater temperature, T_2 is affected by the incoming heat flux from the fuel, F_{12}, and the outgoing heat flux to the test flask, F_{23}. The test flask is cooled by the boiling water and acts as a heat sink and it is modelled at constant temperature. The axial fuel relocation, which is the reason for the changing LHGR, is modelled as a uniform slumping

of the fuel stack as more space is created by the ballooning of the cladding. This was roughly the case for Halden LOCA tests 4 and 9, which were performed with very high burnup fuel and the fuel fragmented to small pieces. For the LOCA tests 12, 13 and 14 with high burnup BWR fuel, relocation from the upper part of the rod may have been prevented by the insufficient local hoop strain. Gamma scanning revealed presence of large fuel fragments all along the height, which suggests overall preservation of the fuel stack which implies that relocation into the balloon, could be coming from the fuel periphery. The aim of the fuel relocation model described in this dissertation (see section 5.2) is to consider the scenario when the fuel relocation starts at the periphery. The implications could be significant, because the fuel pellet periphery is at approximately two-times higher burnup than the fuel pellet centre. This means the decay heat power density will also be larger. Predominant relocation from the periphery will lead to higher decay heat generation than predominant relocation from the fuel centre or the uniform fuel relocation approach currently used in FRELAX.

The modelled phenomena by FRELAX are as follows:

1) Heat transfer from the fuel rod to the heater and from the heater to the test flask, which acts as a heat sink.
2) Axial fuel relocation as a result of cladding deformation and evaluation of the impact on the cladding temperatures.
3) Axial gas flow between the plenum and balloon driven by the pressure difference caused by the ballooning and taking into consideration the resistance by the fuel stack length connecting the plenum and the balloon

One of the main goals behind FRELAX is to model non-equilibrium pressure between the balloon and plenum. Fuel performance codes, including FALCON, consider inner rod pressure to be uniform along the whole length of the fuel rod. This, however, is not always adequate, because as the clad balloons, there is a local pressure drop and this may cause a delay in axial gas flow from the plenum, particularly in the presence of pellet-cladding bonding somewhere above the balloon. Although in Halden LOCA tests the time to equilibrate pressures may be insignificant due to the short length of the test rods (40-50 cm), in full-length rods (about 4m) the time may be non-negligible. Still, some tests from the Halden LOCA test program (test 5 and 9) did exhibit slow depressurization which suggests that there was a high resistance to axial gas flow and possibly the balloon was at lower pressure than the plenum. In full length fuel rods, the presence of spacer grids could limit the extent of cladding deformation and therefore reduce the gas permeability through the fuel stack. Possible delayed gas redistribution has a positive impact on the cladding rupture time as it was shown in [37].

Besides application of FRELAX to the post-test analysis of Halden LOCA tests, it was successfully used for the pre-test calculations of the 14^{th} test – a non-burst LOCA test [32, 62]. The model in conjunction with FALCON and measured parameters from the 12^{th} Halden LOCA test was successfully used to pre-calculate the test parameters for LOCA test 14. The main outcome of this test was a credible measurement of the FGR during LOCA: about 20 % of total generation in the tested sample [24].

2.4 Serpent Monte-Carlo code

The involvement of the Serpent Monte-Carlo code in this PhD project is very limited. It was used in the formulation of a model for fission gas trapping (see section 4.3), and more specifically to model the azimuthal burnup asymmetry (see section 4.4) of the fuel pellets within a BWR fuel assembly. This section begins with a brief introduction into the Monte Carlo method and then presents some of the modelling capabilities of Serpent.

2.4.1 Introduction into the Monte Carlo method

To begin with, a Monte-Carlo code is a computer package which uses Monte-Carlo method to solve a given problem. Monte-Carlo methods can vary, but typically they follow the pattern:

1) Define a domain of possible inputs
2) Generate inputs randomly over the domain from a probability distribution
3) Perform a deterministic computation of the input
4) Aggregate the results

A simple example is throwing a 6-sided fair die. The domain of possible inputs is having a number from 1 to 6. A die is tossed randomly N times (N being a multiple of 6) and the ratio of the number of times each number shows up over the N tosses is evaluated. The theoretical probability of tossing any of the six sides of a fair die is 1/6. Finally, the ratio of the number of occurrences of each number over the N tosses is calculated and compared with the theoretical probability.

The Monte-Carlo method can be used to solve a mathematical problem, such as estimating the value of π. As an example, an approximation to the value of π by using a square of side 2 cm and a nested circle with radius of 1 cm can be done. In a random way, as many crosses with a pen as possible are drawn inside the square. The ratio, R, of the number of crosses inside the circle over the total number of crosses is approximately equal to the ratio of the area of the circle and the square, which gives approximation of π as ~4R.

One last example concerns application of MC codes in the nuclear industry for neutron transport calculations. The geometry of interest is defined, which could be a fuel assembly or a full 3D reactor core. Each object in the geometry provides a given probability that the neutron will interact with it. The probabilities on a microscopic level are presented as cross-sections, which are made available in so-called nuclear data libraries. A neutron is randomly released into the geometry and its interaction with the objects is tracked. Depending on the boundary conditions, the neutron can definitely be absorbed (reflective boundary conditions in which when the neutron reaches the boundary it is simply sent back) or it can leak out (which is more realistic considering reactor pressure vessels undergo irradiation damage due to leaked neutrons).

On average, the approximation will get better as the number of events (tossing a die, drawing crosses, releasing neutron in the domain) increases. For MC simulations in which interactions become complicated, such as releasing a neutron in a reactor and following its path until it leaks out or gets absorbed, the computational time may become significant.

Unlike deterministic calculations, such as finding the roots of a quadratic function which produces always the same result, in stochastic calculations two simulations done with the same input are never the same. Then, how can one be sure, that the results of a MC calculation are realistic? This requires running MC simulations with different number of events and analysing the output. The results will not change appreciably after sufficiently large number of events and then it can be concluded that the

average state, or the most-likely end state of the problem, is simulated. Increasing the number of events past this point will only increase the computation time.

2.4.2 Modelling capabilities of Serpent

Serpent is a three-dimensional continuous-energy Monte Carlo reactor physics burnup calculation code developed at the Technical Research Centre in Finland (VTT). From its first release in 2004 until now, Serpent is used in research and industry throughout the world. In Switzerland alone, the code is used at Paul Scherrer Institute, Axpo AG, and the Swiss Federal Institute of Technology Lausanne to name just a few examples. Serpent is free to use, but it is not open-source. License can be obtained from the OECD Nuclear Energy Agency (NEA) databank.

Building the geometry. The basic building blocks in Serpent are geometrical objects, called surfaces, such as cylinders, squares, planes and hexagons. Some of them are infinite such as the planes or cylinders in the axial direction and others are finite such as the cube, sphere and cone. Combination of these geometrical objects can generate virtually any geometry (an example is given in section 2.4.3). This procedure is based on the constructive solid geometry (CSG) model, which is a typical choice for other MC particle transport codes [63]. Optimization of the particle tracking in Serpent helps to speed up calculations in Light Water Reactors by a factor of 2. Serpent switches from the delta-tracking to surface tracking when the particle enters a region with heavy absorbers [63].

Burnup calculation option. Serpent does not require external coupling with other codes, because it has built-in subroutines to perform burnup calculations. To form the Bateman equation, one-group cross sections are calculated during the neutron transport calculation and decay and transmutation paths are created automatically. Necessary data is read from the ENDF data libraries [63]. "Irradiation history can be divided into multiple intervals with different normalization, defined by power, power density, or total flux, fission or source rate."[63]

Coupling with other codes. Serpent facilitates the coupling with CFD, thermal-hydraulics and fuel performance codes in order to perform multi-physics calculations via two coupling schemes: "(1) internal light-weight solvers for fuel behaviour and thermal hydraulics and (2) external coupling via a universal multi-physics interface"[63]. Coupling with the fuel performance code ENIGMA has been established, and Serpent is included into the High Performance Monte Carlo Reactor Core Analysis project aimed at coupling of high-fidelity neutronics and thermal hydraulics [63].

Core design analysis. Due to the fact that Serpent can model any geometry without major approximation, it draws interest in full-scale reactor physics simulations, but the size of this task requires too much computational time. Although at this time modelling of full-scale Light Water Reactor is not possible, Serpent has been successfully tested in the modelling of small research reactors such as the VTT's TRIGA Mark II type FiR reactor, the Advanced Test Reactor at Idaho National Laboratory and the High-temperature Engineering Test Reactor operated by the Japan Atomic Energy Agency [63]. Additionally, Serpent is used for modelling of fast spectrum systems such as the European Lead-Cooled Training Reactor (ELECTRA) and the Molten Salt Reactor (MSR).

2.4.3 An example with Serpent: two-dimensional fuel pin

In Serpent geometry, a two-dimensional fuel pin is built from three nested concentric cylinders; the inner-most defines the boundaries of the fuel pellet, the outer-most the cladding outer wall and the middle cylinder defines the cladding inner wall and the cladding gap. By defining a square or hexagon (VVER fuel geometry) around the outermost cylinder and "filling" it with water

creates in essence the building block for a fuel assembly (see Figure 11) and then the whole core with all the fuel assemblies and their differences (enrichment, part-length rods, etc.) can be defined.

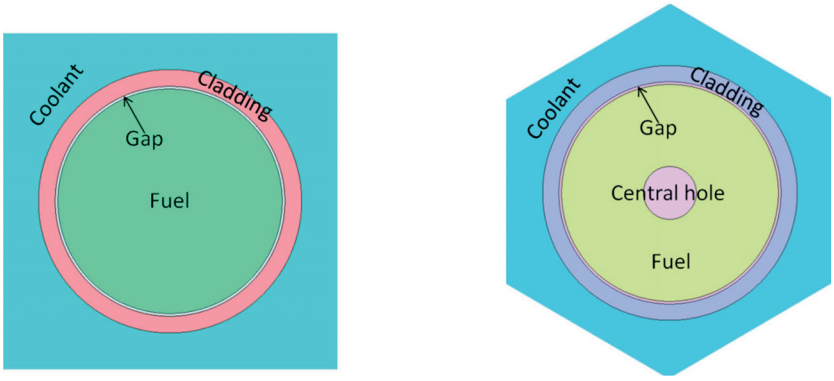

Figure 11: Two-dimensional geometry of a PWR and VVER fuel pin in Serpent

Part of the input file instructions are given below, with the purpose of illustrating the procedure. For complete examples please refer to the Serpent manual [64].

The focus of this example is the VVER fuel pin geometry. First, the surfaces need to be defined with reference to the surface definitions in the Serpent manual [64]. The building of the geometry starts from inside-out. Comments are added with % next to each line for explanation.

```
surf fuel_IR cyl 0.0  0.0  0.1 % definition of the central hole, or
fuel inner radius
surf fuel_OR cyl 0.0  0.0  0.4096 % fuel outer radius
surf clad_IR cyl 0.0  0.0  0.4196 % cladding inner radius
surf clad_OR cyl 0.0  0.0  0.4810 % cladding outer radius
surf hex_subchannel hexxc 0.0   0.0   0.62 % the boundary of the
hexagonal sub-channel
```

Next, the computational cells are defined by specifying the boundaries and material types of the central hole, fuel, fuel-cladding gap, cladding and sub-channel which are named gap_mat, fuel_mat, clad_mat and coolant_mat respectively. Each of the materials corresponds to a set of cross-sections which are invoked at run-time in order to evaluate the neutron interactions within each cell.

```
cell vver_pin_1 vver_pin gap_mat -fuel_IR % the boundary of the first
cell is the fuel inner radius
cell vver_pin_2 vver_pin fuel_mat fuel_IR -fuel_OR % inner boundary
of the fuel pellet is the fuel inner radius and outer boundary is the
fuel outer radius
cell vver_pin_3 vver_pin gap_mat fuel_OR -clad_IR % boundaries of the
fuel-cladding gap are fuel outer radius and cladding inner radius
cell vver_pin_4 vver_pin clad_mat clad_IR -clad_OR % boundaries of
the cladding are the cladding inner radius and cladding outer radius
cell vver_pin_5 vver_pin coolant_mat clad_OR -hex_subchannel % the
sub-channel is bounded by the cladding outer radius and the hexagonal
surface
```

The second string after the keyword ‘cell’ is the name of a so-called **universe**. The geometry in Serpent is built by cells which are combined into universes. All cells describing the same object, such

as fuel pin, will be assigned the same universe name. The minus sign before a surface's name declares the surface as **outer** boundary, otherwise it is **inner** boundary.

Some Serpent applications are:

1) Fuel cycle studies and detailed assembly burnup calculations
2) Full-core modelling of research reactors
3) Validation of deterministic lattice transport codes
4) Spatial homogenization and group constant generation for reactor simulator calculations

2.5 Brief introduction of TRACE

TRAC/RELAP Advanced Computational Engine, or better known as TRACE, is developed by the United States Nuclear Regulatory Commission (U.S.NRC). It is a merger of four other codes into a single entity. TRACE belongs to the family of so-called thermal hydraulic system codes. They solve the mass, momentum and energy conservation equations for the provided geometry. Owing to its modular structure, the entire primary and secondary circuit of a nuclear power plant can be modelled using simple structures connected to one-another with the necessary conservation equations and closure relations.

The code is characterized as "best-estimate", which means that it tries to calculate important parameters, such as temperature and pressure, as realistically as possible. This in turn requires that every model is validated against experimental data that represents given phenomenon as realistically as possible and furthermore the range of application of those models is properly defined. This gives rise to uncertainties and it follows that best-estimate calculation typically go hand in hand with uncertainty analyses [65]. This is in contrast with the conservative approach where, for example, the thickness of a material will be increased two-fold just to be sure that it can withstand the necessary mechanical stresses. This was necessary in the time before powerful computers, sophisticated software and lack of knowledge of the physical phenomena in question. Typically, conservative calculations result in an upper bound, for a given parameter (e.g. peak fuel temperature), that will not be exceeded. This suggests that a TRACE model for a nuclear power plant, or a component, in the best-estimate framework, should come as close as possible to reality. It is simply not enough to consider the average power of a fuel rod, but rather an axial division of the geometry into regions each of which with its own linear heat generation rate (LHGR) and burnup because local effects such as neutron flux and moderator void, in the case of Boiling Water Reactors, play significant role. A LOCA transient is characterized by depletion of the coolant, whose rate will depend on the type of LOCA, due to the evaporation caused by the depressurization of the reactor pressure vessel and the decay heat coming from the fuel rods. Eventually, the emergency core cooling systems (ECCS) are able to re-establish heat removal and terminate the transient. Fuel fragmentation, relocation and dispersal during LOCA in LWR have only recently been considered as a potential safety issue. So far there are no comprehensive models on these phenomena and the question on their impact on safety remains open.

The modelled system's (e.g. secondary circuit) thermal-hydraulic behaviour can be adequately represented, for the most part, as one-dimensional network of control volumes (e.g. pipes) where the pressure, temperature and mass flow are evaluated. For more complicated structures, where 3-dimensional effects, such as cross-flows, can occur (e.g. reactor pressure vessel) TRACE provides the VESSEL component.

Depending on what is being modelled, a selection of two-phase flow models that solve the mass, energy and momentum conservation equations can be used. For example, a three - equations two-phase flow model assumes that temperature of the two phases and their velocity is equal (no-slip) and

as such a single mass, momentum and energy conservation equation is solved. On the other hand, when velocity between the two phases is different and the temperatures are not necessarily equal (e.g. in a transient simulation such as LOCA), six-equations two-phase flow model is used which solves the mass, energy and momentum conservation equations for the two phases separately. Closure laws, such as heat transfer coefficients and friction factors between the two phases or with the wall and equations of state close the system of equations.

Special flow process models are included in TRACE that address specific phenomena such as critical flow model, counter-current flow limitation model, off-take model and form loss model. Each of these is briefly described below.

Critical (chocked) Flow Model. Such phenomenon occurs when the flow rate within a pipe, or through an orifice, cannot be further increased by increasing the pressure difference between the inlet and outlet. Such condition can occur during LOCA transient, especially in the primary circuit where the pressure can be as high as 15 MPa. The critical flow model in TRACE is made up of three models: a subcooled liquid choked-flow model, a two-phase two-component choked-flow model and a single phase vapour choked-flow model.

Counter-current flow limitation (CCFL). Under certain conditions and at different locations in the reactor system, single or two-phase flow streams may run against each other. For example, during Small Break LOCA, counter-current flow can occur when steam enters the U-tubes in the steam generator. Part of the condensed steam will enter the reactor through the cold leg, but the rest will flow back through the hot-leg and will run counter to the established natural circulation. For emergency core cooling systems that inject coolant at the upper part of the core, CCFL may occur at the tie plate when the coolant "collides" with the rising steam. TRACE allows the user to define CCFL correlations according to the geometry that is being modelled and apply it within the VESSEL component where this type of phenomenon is expected to occur.

Off-take model. This model predicts the flow discharged from a small break that is located in a large pipe containing horizontal stratified flow. This can occur in one of the large diameter pipes such as the cold or hot legs. The flow quality depends on whether the rupture is above or below the horizontal flow. If it is above, then most of the discharge will be steam, and if it is below – most of the discharge will be liquid. In transient simulations, this is important in order to accurately follow the progression of the transient and the system response.

Form Loss Model. This model deals with the components of the pressure gradient associated with single-phase pipe flow, namely the wall drag, gravity head, recoverable flow area loss/gain (e.g. flow to/from pipe with smaller/larger diameter) and irrecoverable loss. Examples of the latter occur for flow through pipe bends, orifices, T-junctions due to the creation of turbulence.

The involvement of the thermal-hydraulic system code TRACE in this doctoral work is very limited. It is used only to demonstrate a modelling approach to fuel relocation in reactor-case LOCA (see section 5.2) in effort to evaluate the hot-spot effect. Its particular use is to provide more realistic cladding temperature boundary conditions which are then given as input to FALCON.

3
Chapter 3:
OECD Halden Reactor Project and its LOCA Test Program

3.1 Introduction

OECD Halden Reactor Project is part of the Institute for Energy Technology, established in 1948. The main office is at IFE (Institutt for Energiteknikk) Kjeller located 20 km North-East from Oslo, Norway. The extensive test irradiation, including the Halden LOCA test program, has been conducted in the Halden Heavy Boiling Water Reactor (HBWR), in Halden, while the most of the fuel handling, preparation and post-irradiation examinations are performed at Kjeller Hot Laboratory.

The fuel rod is prepared for the reactor tests and examined after the reactor tests in the hot laboratory at Kjeller where various destructive and non-destructive examinations are performed, including visual inspection, cladding diameter profilometry, neutron radiography, measurement of hydrogen concentration in the cladding, fuel fragment analysis, fuel microscopy and others. The post-irradiation examination can be customized according to the needs of the particular experiment. This chapter discusses the Halden LOCA test program, the different experimental data and how some of it can be used in the modelling part of this PhD work.

Typically, after each test a so-called Halden Work Report (HWR) is completed, which includes, among others, rod geometry, test planning and execution and preliminary analysis. The analysis is typically derived from the on-line measurement signals, some of which are discussed in this chapter. In particular, a gamma scanning done after the LOCA test has the potential to reveal more information than just visual confirmation of the final state of the rod (see Appendix A).

The Halden Reactor is in operation since 1958. At the time of writing this chapter, the HRP is supported by 130 organizations worldwide in 19 countries. The current participating countries are: Belgium, Czech Republic, Denmark, Finland, France, Germany, Hungary, Italy, Japan, Kazakhstan, Norway, Republic of Korea, Russia, Slovak Republic, Spain, Sweden, Switzerland, United Kingdom and the United States of America. Of these, only Italy and Denmark are not operating nuclear power plants. The Halden reactor is a material testing reactor, of which there are only few in Europe with the newest one being the Jules Horowitz Reactor in France which is planned to commence operation in 2021.

3.2 General description of the Halden LOCA test program

The OECD HRP LOCA test program with designation IFA-650 commenced in 2003. In general, the tests are performed with high burnup fuel with the aim to address fuel behaviour during LOCA transient and initially the primary objectives of the LOCA test program are found in [26] as :

- "Measure the extent of fuel (fragment) relocation into the ballooned region and evaluate its possible effect on cladding temperature and oxidation"
- "Investigate the extent (if any) of "secondary transient hydriding" on the inner side of the cladding above and below the burst region"

At present, fifteen tests have been conducted where the first two were used to check the instrumentation and commission the LOCA testing procedure as discussed in [26]. In the official documents from the HRP, the tests are designated IFA-650.X, where X is the test number. In this text, they are sometimes simply referenced with their test number (e.g. test 4, test 12, etc.).

Switzerland is an active supporter of the LOCA test program and so far has provided PWR fuel, irradiated at Kernkraft Goesgen (KKG), for the tests 3, 4, 5 and 9 and BWR fuel irradiated at Kernkraft Leibstadt (KKL) for the tests 7, 12, 13 and 14. Furthermore, G. Khvostov at PSI had conducted pre-test calculations for tests IFA-650.7 [66], IFA-650.12 [67], IFA-650.13 [67] and IFA-650.14 [33]. Test 14 was designed to achieve sufficient cladding ballooning and relocation without rod burst. The test was successfully conducted according to the procedure outlined in the pre-test calculations and after the LOCA test the rod underwent extensive post-irradiation examination at Kjeller, including fragment size distribution and determination of the fission gas release (FGR) during the LOCA test (Chapter 4 section 4.3 discusses a BWR fuel - specific source of FGR during the LOCA, which is relevant to tests 12, 13 and 14). The main outcome was a credible measurement of the FGR during the LOCA: about 20 % of total generation in the tested sample [32], which is of great value for code validation and verification, as well as for the appropriate safety analysis.

The LOCA program at Halden is performed in-pile, whereas the ongoing LOCA test program at Studsvik, for example, is done out-of-pile by electrical heaters and a system of mirrors surrounding the fuel rod specimen. At Halden, low level of nuclear power generation is used to simulate decay heat, whereas electrical heater surrounding the rod is used to represent heat from neighbouring rods. The in-pile testing is more representative of the real situation in a LOCA, at least in terms of heat transport and temperature gradients (from inside-out versus from outside-in). At the moment it is unclear whether the external heating used in Studsvik's LOCA tests has any important effects on the test results.

Typically before LOCA test execution, the reactor is operated with the LOCA test rig inside for 7-8 hours at about 15 MW (fuel average linear heat rate about 85 W/cm). This pre-conditioning phase activates the fuel for post-irradiation gamma scanning. After power calibration, the LOCA test is performed at a reactor power of 4.0 MW and a low linear rod power of 10-30 W/cm depending on the target peak cladding temperature. The experiments are terminated by switching off the electrical heater and scramming the reactor, causing the fission heat generation in the fuel rod to cease.

Three Month Technical Visit

The Halden LOCA test program is the main source of experimental data for this doctoral project on fuel fragmentation, relocation and dispersal during the LOCA. With that in mind, a three month technical visit to the Halden Reactor Project was organised in order to gain familiarity with the LOCA test programme and to collect experimental data for further analysis.

Some of the tasks to be addressed during the visit were as follows:

- Study the details of the Halden LOCA experiments, particularly the principles of the system design, the thermal-hydraulic behaviour of the system during the tests, the system instrumentation, along with the structure and contents of the experimental information obtained.
- Collect and start analysis of the data from all the conducted LOCA tests.
- Study the results of analysis of the experimental data, and models implemented by HRP.
- Try to find out which data are already available and which are essentially missing, but may be needed for model parameterization and validation. For the latter, discuss with experts at HRP whether this absent data for the PhD project might be obtained from the Halden LOCA experiments to be conducted in the near future, or acquired from other open HRP programs, or sought among the results of the previous LOCA testing programs.
- Consider extension of the already established PSI methodology of the test analysis, with a view of further validation of the models, developed by the student, against the Halden data.

The data analysis began with a closer look on a gross-gamma dose rate measurement (discussed in section 3.5.1), which comes from a gamma detector (MON 40 on Figure 14) that is able to detect radiation but cannot measure the energy and therefore is not able to identify the source. It is indicative, however, of rod failure during the LOCA testing and it has been observed that each test with rupture produced a unique response. The goal was to look for a correlation between quantity of dispersed fuel and dose rate signal. Due to the difficulty in interpreting these measurements, focus was shifted towards gamma scanning of the fuel rod after the LOCA test (see section 3.6.2 and the discussion in Appendix A). The scanning is done with a High-Purity Germanium (HPGe) detector that records high-resolution gamma spectrum and allows identifying the individual gamma peaks. The balloon and dispersed fuel regions are clearly visible on the gamma scan data (e.g. Figure 6) and this motivated the time investment to study it in more detail. Soon it was discovered that much more, besides a visual image, can be learned from this data. An outcome is the formulation of a gamma transport model (see Appendix A) which has the potential to bring forward valuable information regarding fuel relocation and dispersal (see section 5.3.4) and motivate changes to the gamma scanning procedure in order to enhance the data analysis (see section 3.6.6).

3.3 LOCA test rig

Fuel rods subjected to LOCA testing are encapsulated in a so-called pressure flask, whose cross-section is shown on Figure 12a. It is a cylindrical tube of about 4 cm in diameter which houses the heater and the fuel rod. The fuel cladding during a LOCA test is heated by the nuclear fission in the fuel as well as by the decay heat of the fission products and an electrical heater whose purpose is to simulate heating by neighbouring rods in the fuel assembly in a reactor-case LOCA. The pressure flask is inserted in a shroud (Figure 12b). The flask can be pressurized to the desired level to simulate reactor operating conditions. The Halden reactor is a heavy water boiling reactor operating at ~ 34 bars. The pressure flask makes it possible to simulate both PWR and BWR conditions by adjusting the pressure to ~ 150 or 70 bars respectively

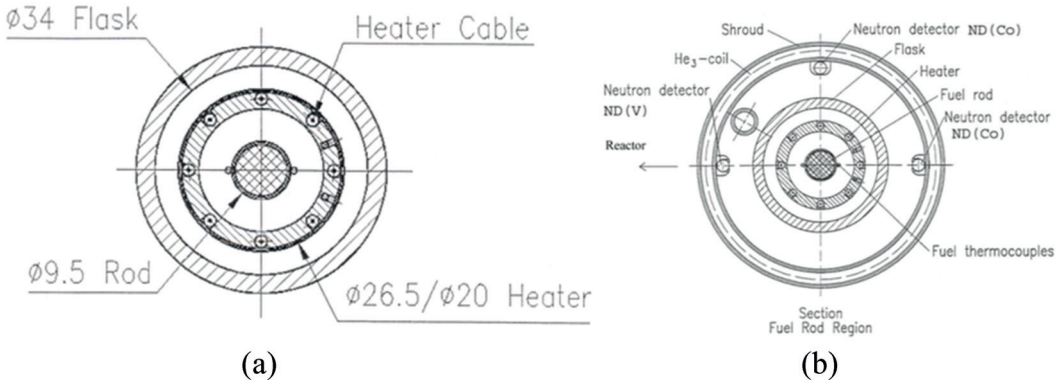

Figure 12: Cross-section of the pressure flask (a) and the shroud (b) showing dimensions (mm) and different instrumentation [68].

The cladding temperature can be controlled by the heat generation in the rod and the heater. Both, cladding and heater are equipped with thermocouples to provide on-line temperature measurements during the execution of the LOCA test. In this way, it can be controlled whether the desired peak cladding temperature, specified in the pre-test calculation, is reached. Additionally, the thermocouples could provide real-time information on fuel relocation as was the case during LOCA test 4 (see 1.6). The axial cross-section of the pressure flask together with all the standard instrumentation used in the Halden LOCA tests is shown on Figure 13. Neutron detectors are placed on the inside wall of the pressure flask in order to ensure the necessary fission power is provided by the Halden reactor. Three self-powered vanadium detectors and two fast response cobalt neutron detectors are placed within the shroud. Rapid power changes can be monitored with the cobalt detectors. The rod power can also be controlled via the He-3 coils located in the shroud, but in most LOCA tests, they were not utilized. Spray system is included to provide steam for two-side cladding oxidation after the cladding burst (Figure 13). The fuel rod elongation detector consists of an LVDT (Linear Variable Differential Transformer) and it is used to measure the changes of the fuel rod length during the LOCA test. Its data was not used in this project. The fuel rod pressure transducer measures the fuel rod gas pressure during the LOCA and can show clearly the onset of ballooning and rupture. Additionally, it can be used to approximate transient fission gas release as reported in Table 12 in [32] and in section 3.5.2.1.

The LOCA test loop is shown on Figure 14. The LOCA phase of the test begins with evacuation of the coolant by opening a drain pipe connected with a blowdown tank (opening of valves VA 6333 and VA 6334) on Figure 14). The path to the tank is equipped with a gross gamma monitor that detects gamma emitters as they pass by. These are represented by the volatiles (Iodine, Caesium, etc.) and the fission gas.

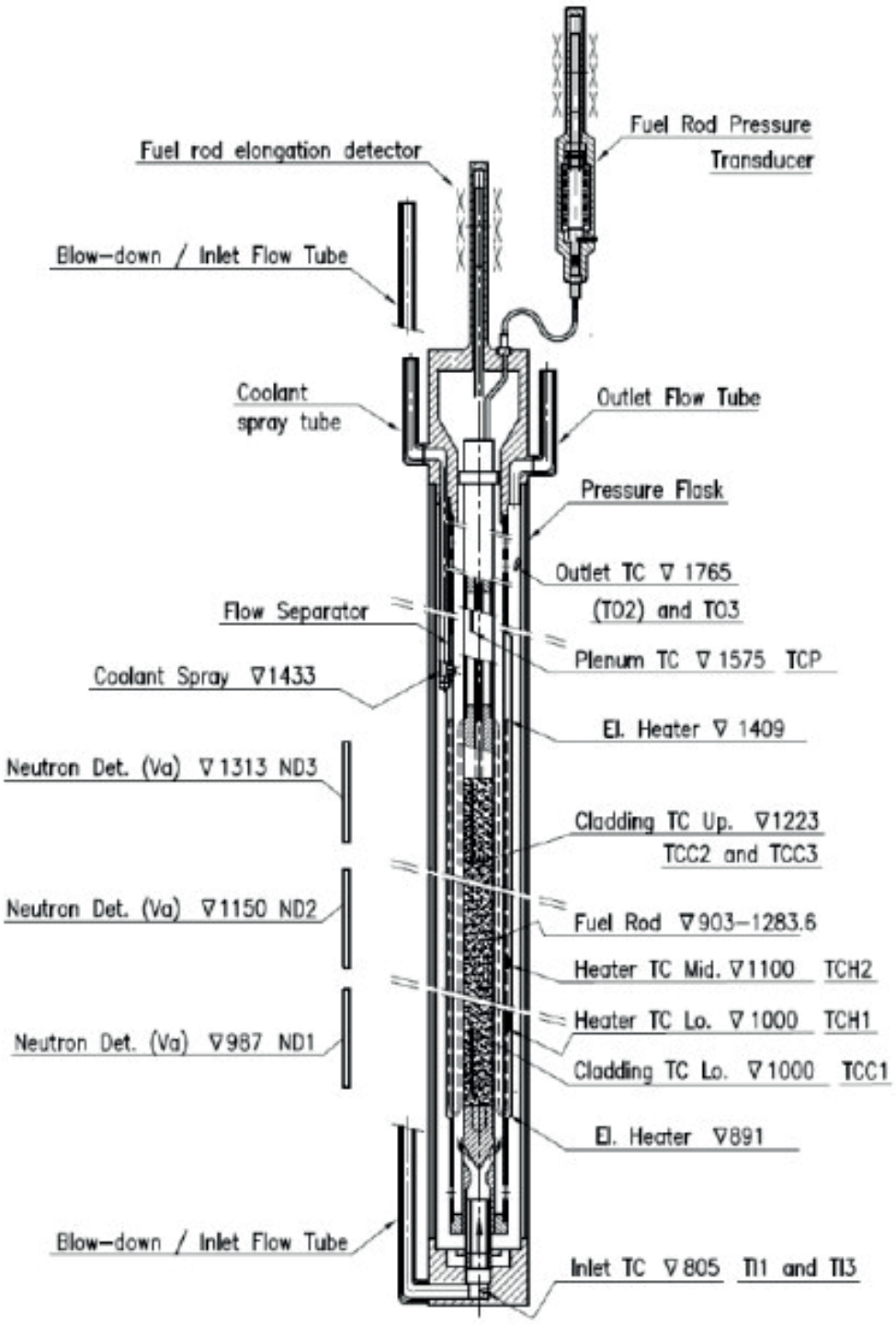

Figure 13: Axial cross-section and instrumentation of the LOCA test rig [26].

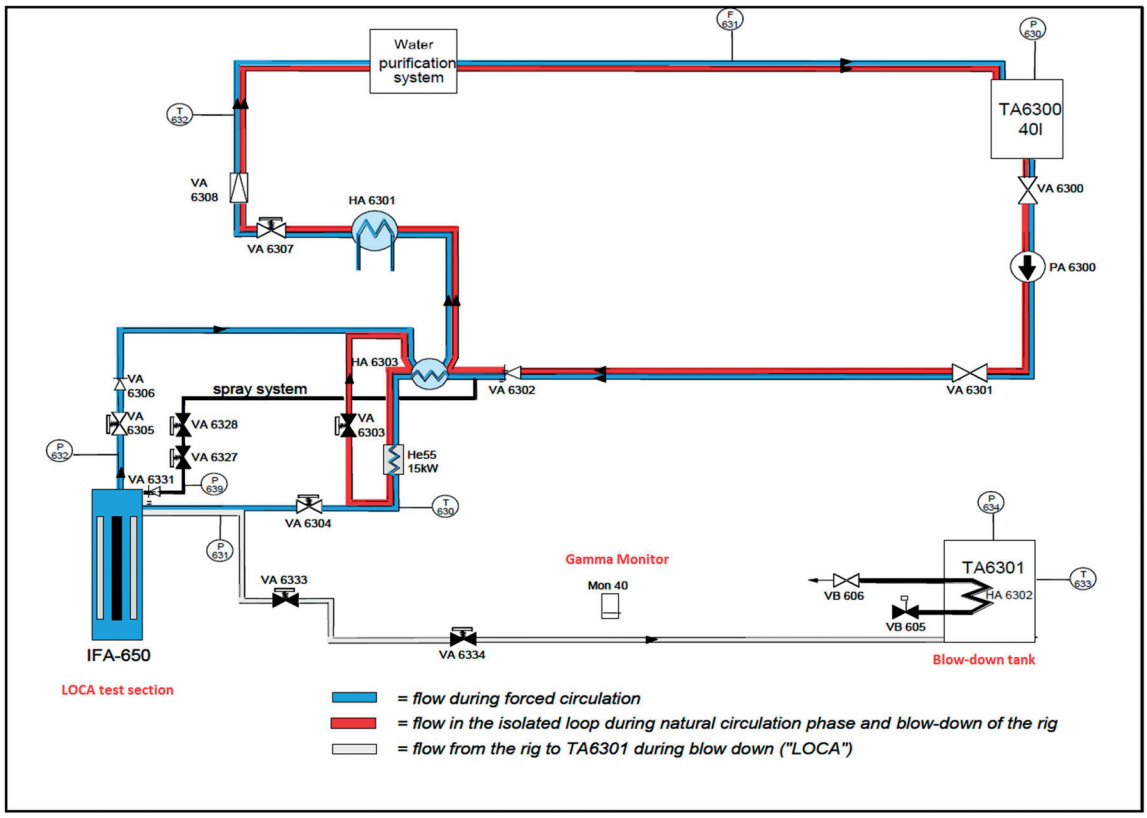

Figure 14: Simplified scheme of the thermal-hydraulic part of the LOCA test loop [26].

A brief description and summary of the test outcome for all LOCA tests is presented in the next section. The emphasis is put on the usefulness of the gathered experimental data for model validation in the framework of this doctoral work. In case a particular experiment presents no interest for validation within this project, reason will be given.

The first insight into the post-LOCA state of the fuel rod is provided by gamma scanning. So far it has been used only for visual confirmation of the fuel relocation and dispersal. In fact, it can be used to obtain other useful information, including more insight into the fuel relocation (see Appendix A) in the balloon by examining the ratio of gamma counts of different isotopes which are sensitive to Pu-239 fission, approximation to the quantity of dispersed fuel by using an isotope emitting high-energy gamma and an estimation of the axial void profile. The current quality of the gamma scan data does not actually allow precise estimation for several reasons which are discussed later in this chapter, but the methodology is nonetheless described and some recommendations on how to improve the quality of the data and recent advancements are discussed in sections 3.6.5 and 3.6.6. The next section begins with a presentation of the gamma count intensity plots for most Halden LOCA tests.

3.4 Brief description of the LOCA tests

The following section provides brief summary of most Halden LOCA tests with the focus being on how each test could be used with the fuel dispersal model discussed in Chapter 5. The tests are presented in chronological order and the discussion is aided with a gamma count intensity plot.

3.4.1 Halden LOCA test 3

This was the first test performed with a high burnup fuel. The mother rod, from which the test fuel rod was prepared, was irradiated in Kernkraftwerk Goesgen (PWR) to an average burnup of 81.9 MWd/kgU, which is considered very high burnup fuel and it is not representative of nuclear fuel in power reactors. Nevertheless, such burnup level should amplify the fuel fragmentation, relocation and dispersal (FFRD) phenomena and therefore it is appropriate for conservative analysis. Yet, the test rod failed with a maximum cladding strain of 7% and rather coarse fuel fragmentation. Neutron radiography of the fuel rod after the test presented in [26] showed no visible fuel relocation. Furthermore, the limited cladding deformation and small rupture opening also prolonged the rod depressurization, which took more than 1 minute to complete (as shown on Figure 28). The gamma count intensity plot shown on Figure 15 shows that the rod is bent and that there is no evidence of ballooning. There was also no evidence of fuel dispersal. The very limited cladding deformation likely was enough to preclude fuel fragmentation and relocation. The measured parameters (e.g. pressure) during this LOCA test were already used in the validation of FRELAX's model for axial gas flow in the case with a tight fuel column [37] and will be used in the validation of the fuel dispersal's model discussed in Chapter 5 section 5.3. Considering the coarse fuel fragments and small cladding strain, all fuel can be considered as immobile (definition of 'immobile' fuel is discussed in section 5.3).

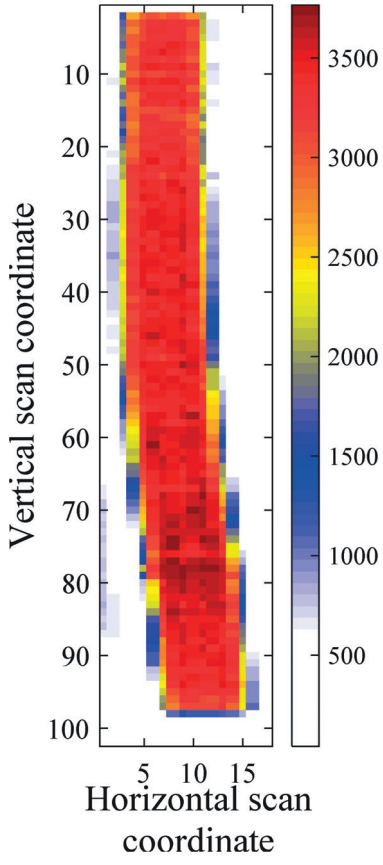

Figure 15: Test 3 gamma count intensity plot [69].

3.4.2 *Halden LOCA test 4*

The mother rod of the fourth LOCA test was also irradiated in KKG (PWR) but to an average burnup of 92 MWd/kgU. This test brought new light to the FFRD phenomena, because it demonstrated significant fuel dispersal and fragmentation - events that were previously only anticipated during Reactivity Initiated Accidents (RIA). Although commercial average fuel burnup at discharge barely exceeds 60 MWd/kgU, the tendency of increasing it requires that the LOCA safety criteria are revised in order to reflect the significant changes in fuel properties at high burnup. The cladding ballooned up-to the heater channel and a large fraction of the fuel fragmented to pieces with the size of few tens of microns which are commonly described as pulverized fuel particles [70]. Such powder-like fragments are highly mobile and can easily relocate into the balloon and therefore fulfil the first objective of Halden's LOCA test program. The gamma count intensity plot of test 4 is shown on Figure 16.

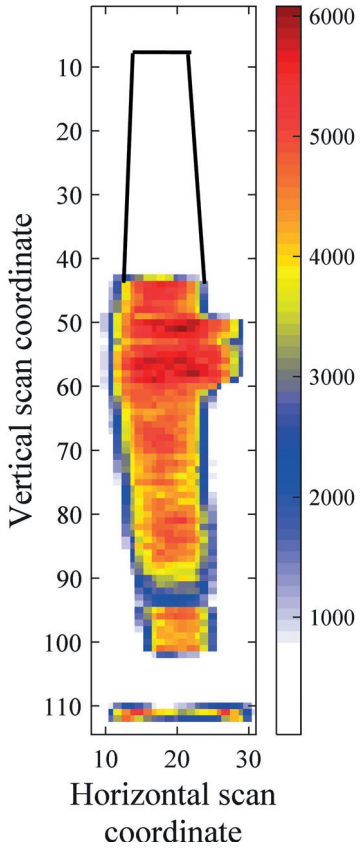

Figure 16: Test 4 gamma count intensity plot [71].

Due to fuel relocation and dispersal, the upper part of the cladding was emptied of fuel and because of that the cladding outline had to be added manually to the figure. The gamma count intensity below the rod signifies fuel dispersal. Some of the fuel was in fact stuck between the cladding and the heater, but it should be considered as dispersed. As much as 40% of the fuel may have been dispersed which is substantial. In this case, the whole fuel stack above the balloon can be considered mobile which will increase the solid-gas interaction and likely the fuel dispersal. This LOCA test is a rather an extreme case for several reasons. First of all, the rod's average burnup is very much higher than current average burnup at discharge from nuclear power plants (in United States, this is around 55 MWd/kgU and in Switzerland around 65 MWd/kgU). There was nothing to restrict ballooning in this LOCA test except the heater inner wall and this may be the reason for the large balloon. The regularly placed

spacer grids in a fuel assembly may impede cladding deformation as it was shown within the REBEKA program [72] and the multi-rod tests in the NRU reactor [44] and increase heat transfer due to creation of turbulence. Finally, the 50 cm test rod was filled with as much gas as a full-length 4 m fuel rod – thereby amplifying the solid-gas interaction. In conclusion, the large axial cladding strain, instantaneous depressurization through large rupture opening and small fuel fragments observed in test 4 are the exact opposite conditions compared with the third LOCA test and therefore provide the envelope case boundary conditions for the fuel dispersal model (see section 5.3).

3.4.3 Halden LOCA test 5

The mother rod (PWR) was supplied by Framatome ANP and also irradiated at KKG to an average burnup of 83.4 MWd/kgU. The peak cladding strain was about 15 % and overall the cladding deformation was limited. Rod depressurization took approximately 1 minute, similarly to test 3, but there was some fuel dispersal that could be seen on the gamma scan intensity plot shown on Figure 17. After the LOCA test, the rod was filled with epoxy in order to "freeze" in place the fuel fragments. It was then cut at several axial elevations, ranging from low to high cladding strain, and the cross sections showed fuel fragments ranging from large to small in-line with the increasing cladding distention. This test demonstrated clear correlation between cladding distention and fuel fragmentation. Logically, it is anticipated that for fuel fragmentation to occur there must be room for it. Further details can be seen in the report by W. Wiesenack [26].

From the point of view of the fuel dispersal model, due the limited cladding strain in the upper half of the rod, the fuel can be considered as immovable because the fragments could not relocate and the balloon was not large enough to promote fuel stack slumping. The conditions of this test allow checking the response of the fuel dispersal model when there is high resistance to the axial gas flow between the plenum and the balloon. The occurrence of the cladding rupture near the bottom of the rod and the slow de-pressurization (see Figure 28) in a sense may be representative to reactor-case scenario where axial cladding deformation is limited and the rupture is far away from the plenum. Like test 3, this test was also used for validation of the FRELAX model in the conditions of the high resistance to axial gas flow [37].

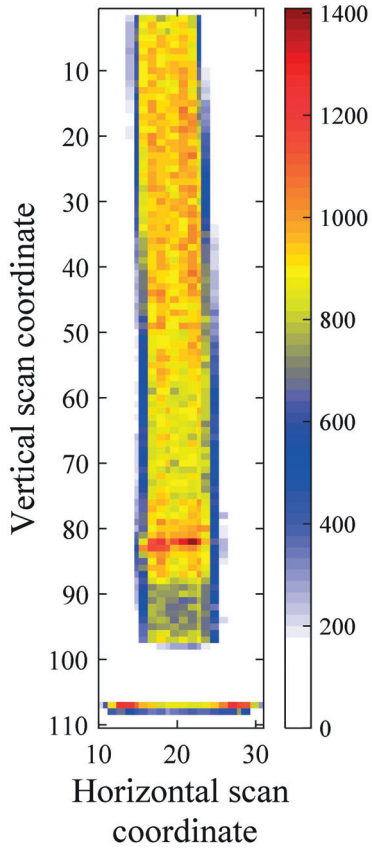

Figure 17: Test 5 gamma count intensity plot [73].

3.4.4 Halden LOCA test 6

The first test with VVER fuel was prepared from a mother rod irradiated in the Finnish nuclear plant of Loviisa to an average burnup of 55.5 MWd/kgU. The gamma scan intensity plot shown on Figure 18 does reveal signs of fuel relocation near the balloon in the bottom half of the rod. The top half experienced limited cladding distention but also some relocation judging by the axial gap whose height must be about 5 mm: the axial scanning step of the gamma scanning equipment. The bottom half shows jagged appearance which is clear sign of fuel relocation and large fragment sizes. There was no dispersed fuel because of the small cladding rupture opening and large fragment sizes. Unlike tests 3 and 5 where the top part of the fuel rod provided large resistance to axial gas flow, this was not the case here. Test 6 depressurized within 1 second of cladding failure (see Figure 28). The presence of the central hole in the VVER fuel pellets ensures direct communication with the rod plenum during normal operation, and may have also provided a direct path through the fragmented fuel stack between the plenum and balloon during this LOCA test. The data from this test can be used in the fuel dispersal model validation by considering the fuel to be immobile in the upper half of the rod with adjusted hydraulic diameter to account for the central hole. Owing to the design of VVER fuel, it could be argued that the gas can flow more freely, even when the fuel has fragmented and relocated, and thereby reduce the gas-solid interaction and consequently the fuel dispersal.

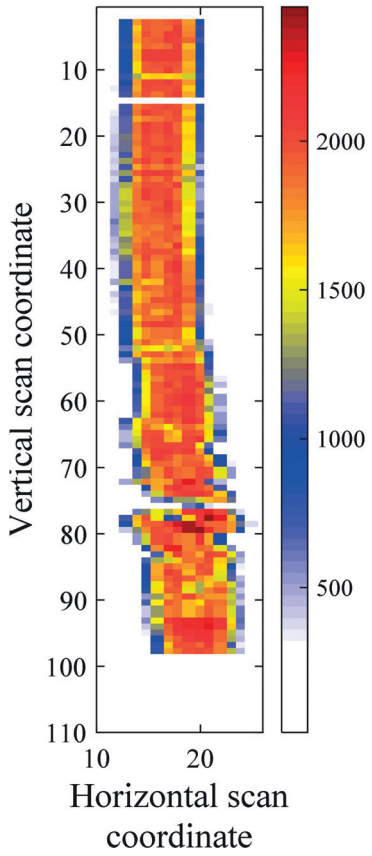

Figure 18: Test 6 gamma count intensity plot [74].

3.4.5 Halden LOCA test 7

This is the first test with Boiling Water Reactor (BWR) fuel. The mother rod was irradiated in KKL to an average burnup of 44.3 MWd/kgU. The maximum cladding strain was about 20%, but the fuel fragmented to large pieces and the overall fuel stack shape was preserved. The cladding rupture length and width are reported as 11 mm long and 1.5 mm respectively [26], but there was no evidence of dispersed fuel on the gamma count intensity plot shown on Figure 19. Considering the size of the rupture opening and the large fuel fragments (as evident on the neutron radiography in [32]) fuel dispersal can be ruled out. Rod de-pressurization was rather quick (see Figure 28), which implies there was little resistance to axial gas flow. Neutron radiography reported in [26] shows fuel fragments to be completely detached from the cladding wall. This is not surprising, because at this level of burnup fuel-cladding bonding layer (if any) was still too weak and likely broke early into the transient. The rate of gas outflow could be useful to check the adequacy of the calculated rod depressurization by the fuel dispersal model when the mass of relocatable fuel is set to zero.

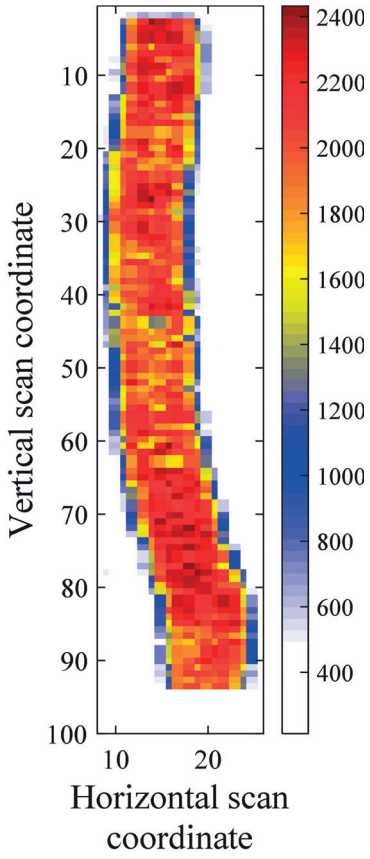

Figure 19: Test 7 gamma count intensity plot [75].

3.4.6 *Halden LOCA test 8*

This test was not a typical LOCA test and the usefulness of its data in the context of the present doctoral work is to make an argument for the gamma scanning facility at Halden, which could potentially reveal much more than just a visualization (see Appendix A). The test was conducted with fresh PWR fuel for the purpose of optimizing the blowdown and heat-up phase of the LOCA tests. The gamma count intensity plot on Figure 20 shows some noteworthy features. First of all, the horizontal stripes with reduced count intensity likely correspond to the interface between individual fuel pellets. The particularly high gamma counts reduce the statistical error, which would be beneficial with the applications of this data discussed in this chapter and in Appendix A. The increase of gamma counts around the middle is due to higher power production caused by the axial shape of the neutron flux in the Halden reactor. Using the neutron flux profile in the Halden reactor, correction can be made, but this only makes sense to cases where fuel relocation was very limited (e.g. test 3 and 5). In other words, when relocation happens, this bias in gamma counts can no longer be corrected.

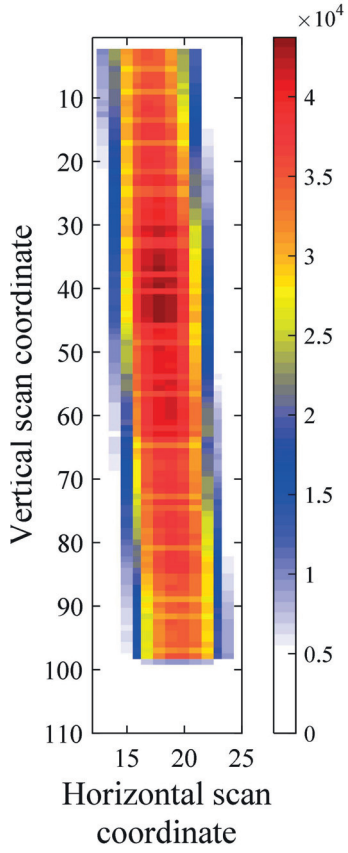

Figure 20: Test 8 gamma count intensity plot [76].

3.4.7 Halden LOCA test 9

The test rod in the ninth Halden LOCA test was prepared from a fuel rod irradiated in KKG (PWR) to an average burnup of 89.9 MWd/kgU. The rod experienced significant ballooning, fuel fragmentation, relocation and dispersal. There are many similarities with the 4th test which demonstrates a level of repeatability – a desirable requirement for the modelling of any process. The slower pressure decrease seen on Figure 28 could be caused by the fuel that remained stuck at the top of the rod, as evident on the gamma count intensity plot shown on Figure 21, thereby slowing down the rate of depressurization. The quantity of gas inside the test rod, relative to the fuel mass, was few times larger compared to that in a full-length rod (like in test 4). This should be kept in mind when making parallels between Halden LOCA tests and full-length rod LOCA analyses. Concerning validation of the model for fuel dispersal, test 9 provides conditions of highly mobile fuel, large balloon volume and high resistance to axial gas flow as complete depressurization took more than 200 seconds as shown on Figure 28. On one side there is repeatability of FFRD phenomena and cladding deformation, but on the other the outflow conditions are completely different and therefore this test is very valuable to the model validation.

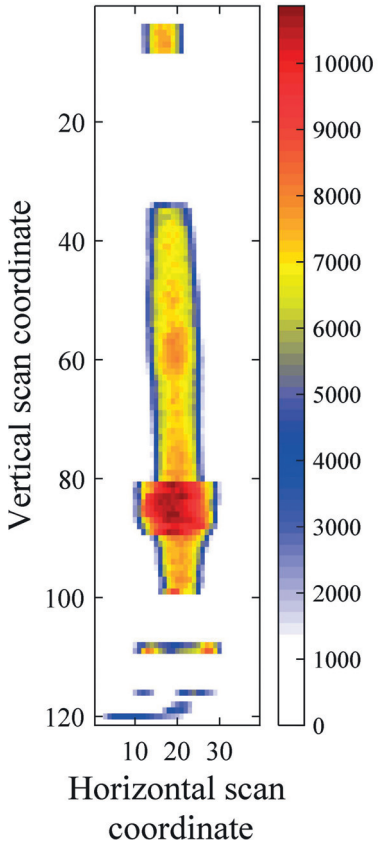

Figure 21: Test 9 gamma count intensity plot [77].

3.4.8 Halden LOCA test 10

The 10th LOCA test was also done with PWR fuel irradiated to an average burnup of 61 MWd/kgU [26].The fuel rod failed with modest cladding deformation as shown on the gamma count intensity plot on Figure 22. The rupture opening was relatively large, measuring 15 mm in length and 5 mm in width, and there was some dispersed fuel. Neutron radiography revealed limited fuel fragmentation and relocation into the balloon [26]. Despite the limited cladding deformation, axial gas transfer between the plenum and rupture appeared to be good, because the rod depressurized instantaneously (see Figure 28). On the other hand, the earlier PWR fuel rod tests 3 and 5 also showed modest cladding deformation but slow de-pressurization. The reason for the fast de-pressurization in test 10 can perhaps be explained with more limited fuel fragmentation that retained the original fuel geometry and absence of fuel-cladding bonding, which at this level of burnup is possible. To model this test with the fuel dispersal model (see section 5.3), the fraction of movable fuel located between the plenum and balloon will be reduced, which will also reduce the solid-gas interaction.

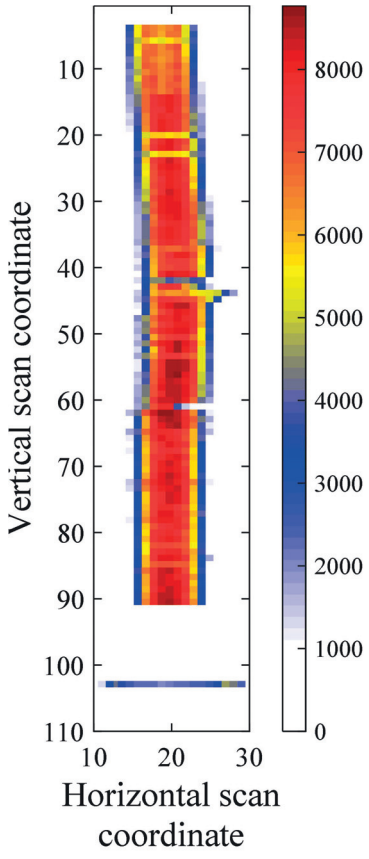

Figure 22: Test 10 gamma count intensity plot [78].

3.4.9 Halden LOCA test 11

This was the second LOCA test with VVER fuel. The test rod was cut from a mother rod irradiated to an average burnup of 55 MWd/kgU in the Finnish nuclear plant Loviisa. An immediate parallel between the gamma count intensity plots of this test (Figure 23) and test 6 (see Figure 18) can be made. First of all, both rods appear bent. Each has a gamma scan level voided of fuel. The cladding rupture occurs in the bottom half and the jagged appearance is a sign of coarse fuel fragmentation. Furthermore, both tests show no evidence of fuel dispersal. The pair of VVER tests provides another good example for repeatability. From validation point of view, there is nothing new to be added from this test. The conclusions drawn for test 6 apply here as well. Perhaps the only striking difference regarding the gamma scanning is that owing to the high number of counts it appears that test 11 was scanned shortly after the LOCA test compared to test 6. This has implications for the quality of the gamma scan data which is discussed in section 3.6.6.

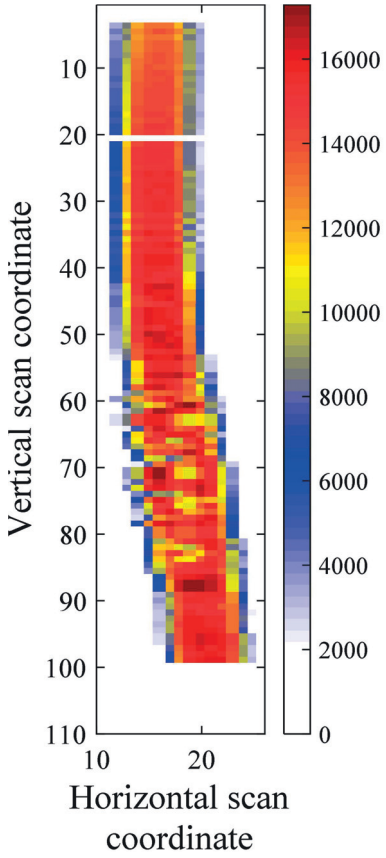

Figure 23: Test 11 gamma count intensity plot [79].

3.4.10 Halden LOCA test 12

The mother rod was irradiated at the Swiss nuclear power plant KKL (BWR) to an average burnup of 72 MWd/kgU. Since this is a high burnup fuel, the FFRD phenomena is expected to be pronounced. In reality, however, the average fuel fragment size was about 4 mm, which supports the notion that burnup is not the only driver for fragmentation. The goal of the test was to achieve sufficient cladding ballooning and fuel relocation, but to stop the LOCA transient before the cladding ruptured in order to measure exactly the transient fission gas release during the test. This required significant reduction of the plenum size in order to amplify the pressure reduction in the rod after ballooning starts [60]. The reactor was scrammed when the pressure inside the rod fell to 50% of the maximum, but 10 seconds later the cladding failed. Despite the large fragments, the gamma scan intensity plot shown on Figure 24 shows that the rod experienced significant fuel relocation as evidenced by the jagged appearance. The gamma scan intensity plot also shows some fuel dispersal and considering the 3 mm long by 0.5 mm wide rupture opening the dispersed fragments likely originated from the periphery. Rod depressurization was almost instantaneous, as seen on Figure 28, which is likely due to two reasons: (1) there was much less initial gas compared to other tests due to the small plenum size and (2) the axial cladding strain was large enough to ensure little resistance to the gas flow. For code validation, this test provides conditions of much lower quantity of inner gas, large fuel fragments, and little resistance to axial gas flow and by appearance - low quantity of dispersed fuel. The expectation is that fuel dispersal is related to the amount of gas, but in this case a limiting factor was also likely the small cladding rupture opening.

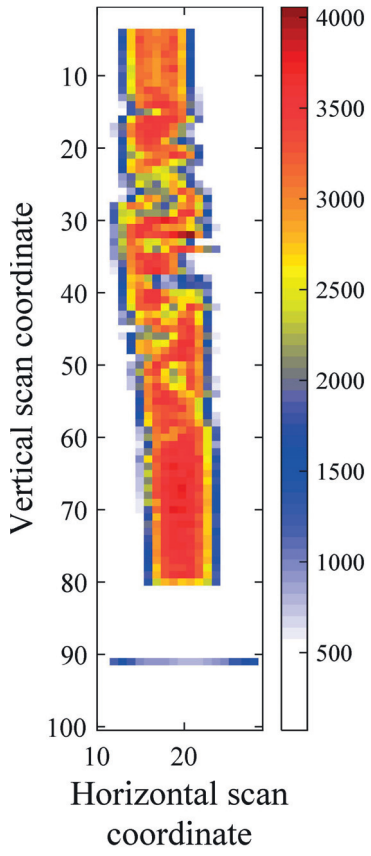

Figure 24: Test 12 gamma count intensity plot [80].

3.4.11 Halden LOCA test 13

The fuel segment for test 13 was cut from the same mother rod as test 12 (BWR). The goal was to obtain large balloon and rupture by increasing the initial gas pressure and it was achieved. The gamma count intensity plot shown on Figure 25 indicates, at least qualitatively, similar amount of dispersed fuel as in test 12. Post-irradiation examination revealed very similar fragment size distribution as test 12 and significantly larger cladding deformation which measured 8 mm in length and 2 mm in width. The initial quantity of gas was almost 10 times larger and this could suggest stronger gas-solid interaction. By appearance, it looks like the dispersed fuel is comparable to, or less than that in test 12 which seems a little counterintuitive. Confirmation of whether test 12 had more dispersed fuel is difficult, because the gamma scanning may have missed part of the dispersed fuel in test 13. This is possible, because the axial scanning is done every 5 mm with a collimator of 1.5 mm in diameter. What is seen on Figure 25 may well be the tip of the dispersed fuel pile. The same conclusion is of course valid for test 12. Again, the repeatability between tests (with test 12) must be noted. Fuel fragmentation, relocation and dispersal, and cladding deformation appear very similar for both test 12 and 13. Repeatability was already acknowledged for the VVER tests 6 and 11 and the PWR tests 4 and 9. As it happens, it is further demonstrated in the next test – LOCA test 14. Test 13 complements the validation efforts by providing virtually the same fuel fragmentation and relocation as test 12 but with larger rupture opening and much higher gas quantity.

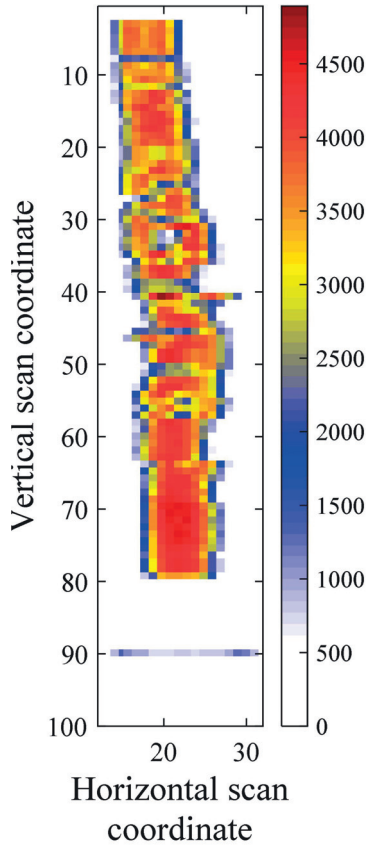

Figure 25: Test 13 gamma count intensity plot [81].

3.4.12 Halden LOCA test 14

This test was a repetition of the attempt to design a LOCA test which will be interrupted before cladding rupture (e.g. test 12) but after significant fuel fragmentation and relocation has taken place. After careful analysis of experimental data from test 12 and modelling with FALCON/GRSW-A by Grigori Khvostov at PSI, adjustments were made to the test execution procedure and in test 14 the Halden reactor was scrammed when the pressure dropped below 70% of the maximum (as opposed to 50%). The test was a complete success and it allowed the measurement of transient fission gas release during simulated LOCA transient. The PIE has shown a relative FGR during the test of about 20 % of total generation [32]. This is basically consistent with the estimates in [60] made from the calculated trapping of the fission gases (intergranular gas plus gas retained in a closed gap), as well as with the analysis of the measurement from the pressure transducer (see section 3.5.2). General conclusions cannot be drawn, because the LOCA specific fission gas release essentially depends on the conditions of the fuel after base irradiation (burnup, pellet-cladding bonding, inter-granular porosity, HBS pores in the pellet rim, etc.), but the data is nonetheless very valuable for code validation because it is a direct measure of transient FGR from high burnup fuel under specific test conditions. The test rod was prepared from a mother rod irradiated in KKL (BWR). The level of burnup was about the same as tests 12 and 13. The gamma count intensity plot shown on Figure 26 confirms significant fuel relocation and the coarse fuel fragmentation that was observed in the previous two tests, thereby emphasizing the repeatability. This test is not interesting from the point of view of validation for the fuel dispersal model.

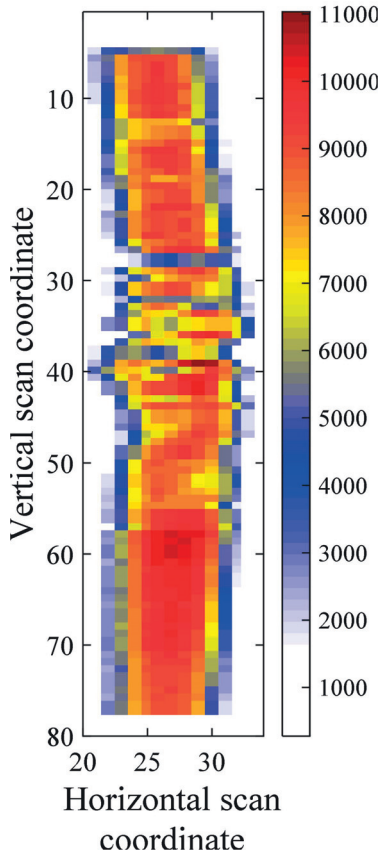

Figure 26: Test 14 gamma count intensity plot [82].

3.5 Data collected during the test

The discussion continues with brief introduction of some of the on-line measurement signals which could provide useful information on the FFRD phenomena. For example, in high burnup fuel, large quantity of fission gases is stored in the high burnup structure. During extensive fuel fragmentation, such as in tests 4 and 9, that gas is expected to be released. In principle, the pressure signal should be influenced by such release. In practice, such information can be obscured by the volume increase and subsequent pressure decrease due to ballooning. In any case, some approximations may be possible for selected cases which are discussed later.

3.5.1 Gross gamma monitor in the blowdown line

The gross gamma monitor is positioned in the blowdown line as shown on Figure 14 (Mon 40). Its purpose is to detect gamma emitting isotopes, but it does not have the capability to measure their energy and identify the source. The blowdown tank is at much lower pressure than the inside pressure of the LOCA test rig, and as the blowdown line is opened via the valves VA 6333 and VA 6334 shown on Figure 14 all the coolant is evacuated. The contents in the pressure flask (steam and gas from inside the rod if there is rod burst) are directed past the gamma monitor and towards the blowdown tank. This signal indicates with absolute certainty that the fuel rod had burst if gamma dose rate is registered. The pressure transducer measurement is also an indicator, but the possibility of a malfunction cannot be ruled out. The gross gamma monitor signals for all LOCA tests with rupture are shown on Figure 27 (left). The figure is plotted from the on-line measurement data collected during the three-month visit at the Halden Reactor. With reference to the gamma count intensity plots shown in the previous section, it appears that the larger the fuel dispersal the larger the gross gamma monitor signal. There are, however, other events that need to be considered. To begin with, any actuation of the spray system shortly after the LOCA test will produce steam which may carry volatile fission products towards the blowdown tank. Spray system is actuated with valves VA6327 and VA6328 shown on Figure 14. The first is always open and the second is a fast-response valve which allows the creation of pulses. This will cause a reading on the gross gamma monitor signal. Actuation of the spray system for few tests is shown on Figure 27 (right). The multiple peaks in the dose rate signal of test 3 shows abrupt increase and subsequent peaks after the 300^{th} second, which corresponds to the actuation of the spray system. A complete matching of the spray pulses and the response by the gross gamma monitor should not be expected, because with every pulse the finite amount of radioactivity that can be removed from the test flask is decreasing. The peaks after the 500^{th} second are almost 100 seconds apart although the spray is actuated every 20 seconds. It is possible that a single pulse and the subsequent conversion to steam is not sufficient to produce the necessary pressure increase to establish a driving force, but after some more water is converted to steam then the flow is strong enough. Without actuation of the spray system there are no additional pulses on the gross gamma monitor signal as evidenced by the data from tests 12 and 13.

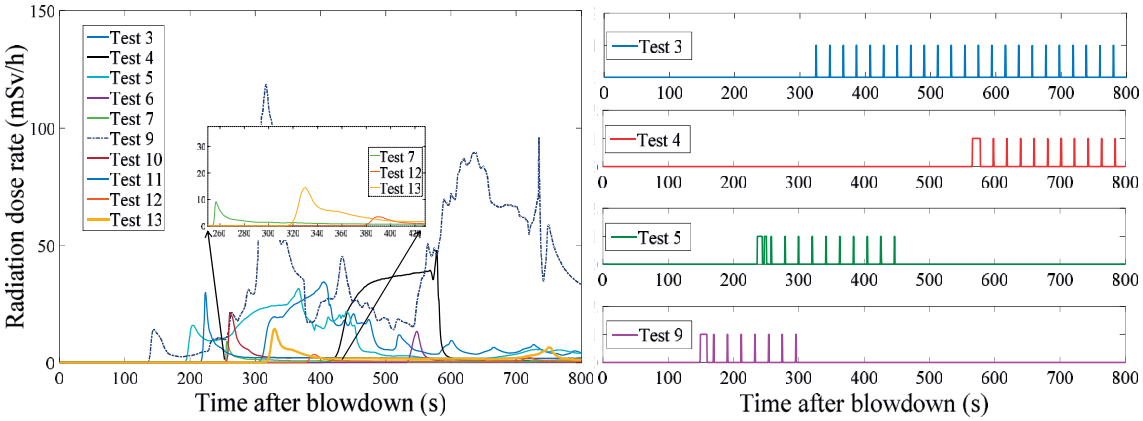

Figure 27: Blowdown line gross gamma monitor signal (MON-40) for LOCA tests with cladding failure (left) and actuation of the spray system for selected tests (right).

All signals share one thing in common – the first peak is always indicative of the cladding failure. Any subsequent peaks, such as those in the signal of test 9, are more difficult for interpretation. The large peak occurring after the 300th second can be attributed to the actuation of the spray system which is active between 150-300 seconds. The rest of the dose rate signal cannot be explained with it. Another property to be considered is the gas quantity put inside the test fuel rod during its manufacturing. It is logical to assume that the larger the gas quantity, the larger the interaction with the volatile fission products (such as Cs-137 and Iodine) and not surprisingly the larger the amount of radioactive elements passing by the gamma counter. The tests 7, 12 and 13 had considerably less fill gas than the rest as seen on Table 3.

Table 3: Initial gas quantity in Halden LOCA tests with cladding failure.

Test Number	Volume (cm^3)
3	830
4	849
5	592
6	503
7	104
9	750
10	651
11	488
12	34
13	292

The magnification on Figure 27 (left) shows that the amplitude of the peaks is clearly correlated with the amount of fill gas. Additionally, fission gas release occurs during the LOCA test and its quantity is non-negligible especially for the very high burnup fuel tests 4 and 9.

In conclusion, the magnitude of the gamma monitor signal does appear to be correlated with the amount of dispersed fuel at least from what is visible from the gamma scanning. For example, tests 4 and 9 showed significant quantity of dispersed fuel as shown on Figure 16 and Figure 21. On the other hand, test 12 and 13, judging by the gamma count intensity plots on Figure 24 and Figure 25 had considerably less dispersed fuel. Yet, if it is assumed that the signal is indicative of the quantity of dispersed fuel, then test 13 should have dispersed considerably more fuel compared to test 12.

3.5.2 Plenum pressure transducer

The pressure transducer is connected with the fuel rod plenum in order to measure the rod pressure during the test. This provides important information, such as the moment when cladding ballooning starts, the time of cladding failure and even carries information on the transient fission gas release – which is discussed further. The pressure signal is a complex function of the temperature of the gas, variable volume due to cladding distention and transient fission gas release. The pressure measurement may also carry information on the state of fuel-cladding bonding. Figure 28 shows the pressure measurements of all Halden LOCA tests (except the latest test 15).

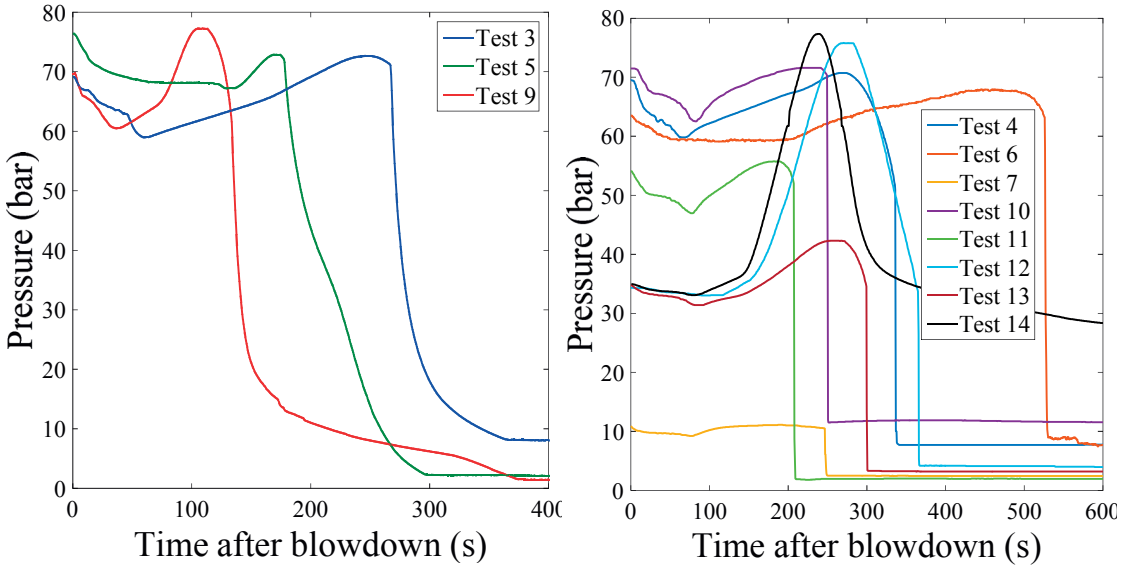

Figure 28: On the left: pressure measurement of the Halden LOCA tests that experienced resistance to the axial gas flow after rupture. On the right: pressure measurement of all other tests.

The observed resistance to gas outflow for test 3 is explained with the limited cladding deformation. In test 5, the cladding deformation was also limited, but additionally the rupture occurred near the bottom of the rod. This increased the distance that the gas must travel, and therefore the resistance. In the formulation of FRELAX [37], the resistance to axial gas flow is directly related with the distance between the plenum and balloon. The situation in test 9 was different. The cladding deformation was very large; however, some fuel, located at the top of the fuel stack and just below the plenum (Figure 21), remained stuck. The reason was most likely fuel-cladding bonding in combination with very low cladding deformation at this position. The pressure measurements for all other tests (shown on the right pane of Figure 28) suggest instantaneous depressurization, which is indicated with the sharp drop of the pressure. The moment when ballooning starts could be approximated by the inflection point in the pressure measurement curve. On a final note, the pressure and cladding deformation at cladding rupture are input parameters for the fuel dispersal model (see section 5.3.1 and Table 18).

3.5.2.1 Transient fission gas release during BWR Halden LOCA tests 12, 13 and 14

As already mentioned, the pressure measurement carries information on the transient fission gas release. In this subsection, a closer look is taken at the data from tests 12 and 13. Test 12 was planned as a non-burst test that will achieve significant fuel fragmentation and relocation and be interrupted before cladding rupture, in order to measure the exact volume of transient fission gas release. The design of the test included small plenum in order to amplify the pressure decrease inside the rod in response to the increase in free volume due to ballooning in order to be sure that sufficient

ballooning has been achieved as elaborated in [67]. The pressure measurement (Figure 28) showed unexpectedly high values which were attributed to higher-than-expected transient FGR [83]. The fuel for the two tests came from the same high burnup BWR fuel rod and a hypothesis for fission gas trapping, discussed in Chapter 4 section 4.3, may partly explain the experimental observations.

This section presents estimates for the transient fission gas release during these two tests. Towards the end of the test, when cladding has sufficiently ballooned, direct communication is established between plenum and the balloon and this is suggested by the quick pressure reduction shown on Figure 28. This means that with knowledge of the pressure and temperature at rupture, the cladding deformation and the initial quantity of gas, the amount of transient fission gas release gas could be approximated using the Ideal Gas Law. At the moment of peak pressure, pressure reduction due to volume expansion overwhelms the pressure increase due to heating up (and eventually FGR) and the pressure starts to decrease. From that point onwards, there is a short time until cladding failure will occur as evidenced from the measurement in test 13. In tests 12 and 14 the aim was to avoid cladding rupture and as such the Halden reactor was scrammed after the pressure reached 50% and 70% of the maximum pressure for tests 12 and 14 respectively with reference to [32] and [33]. Test 12 experienced cladding failure few seconds after the scram, while test 14 was left to gradually cool down without the spray system in order to avoid thermal stresses on the cladding. Since the cladding in test 14 did not rupture, direct measurement of the transient fission gas release was possible which amounted to 70 cm^3. The FGR approximations for tests 12 and 13 are calculated next.

The initial conditions for tests 12, 13 and 14, which are necessary for this calculation, are shown on Table 4. Using the fill temperature, pressure and volume, the number of helium gas atoms are calculated using the Ideal Gas Law. The last column shows the gas volume expressed at standard temperature and pressure.

Table 4: Relevant initial parameters for the calculation of initial gas quantity.

Test ID	Fill pressure	Fill temperature	Plenum volume	$N_{INITIAL}$	Fill gas volume at 1 bar and 0°
IFA650.12	$2 \cdot 10^6$ Pa	293K	1.8 cm^3	$8.9 \cdot 10^{20}$	34 cm^3
IFA650.13	$2 \cdot 10^6$ Pa	293K	15.9 cm^3	$7.86 \cdot 10^{21}$	292 cm^3
IFA650.14	$2 \cdot 10^6$ Pa	293K	1.9 cm^3	$9.39 \cdot 10^{20}$	35 cm^3

Precise knowledge of the total quantity of gas, both fill gas and transient fission gas release, inside the rod is desirable when initializing the model for fuel dispersal, because the higher the quantity of gas the larger the gas-solid interaction which may increase the fuel dispersal considering all other conditions such as geometry, fuel fragment sizes and cladding rupture opening are kept the same.

When cladding ballooning starts, the gas transfer between balloon and plenum can only improve and therefore the pressure measurement corresponds to the pressure inside the balloon as well. This was especially true for tests 12, 13 and 14 where the axial cladding deformation, shown on Figure 29, was large enough to ensure direct path for axial gas transfer. In this figure, the cladding diameter is obtained from digitizing figures taken from [32].

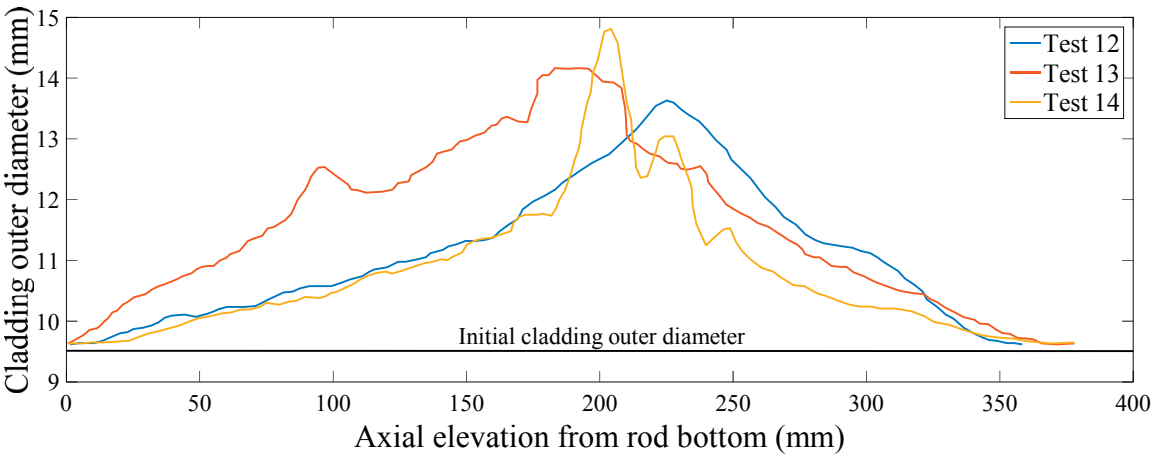

Figure 29: Axial profile of outer cladding diameter of fuel rods after Halden LOCA tests 12, 13 and 14.

In order to estimate the amount of transient fission gas release it is assumed that the entire gas quantity was distributed within the entire volume. Additionally, the knowledge of the rod free volume, gas temperature and pressure at a particular moment during the test is necessary. Such moment is the cladding rupture for tests 12 and 13 (after rupture it can be assumed that the rod will stop ballooning). For test 14, the reference pressure and temperature are taken at reactor SCRAM. These quantities are tabulated in Table 5 in which the total free volume, plenum volume and volume due to cladding deformation are presented. The number of gas atoms, both filler gas and transient FGR, is calculated and then the volume is expressed in the reference units.

Table 5: Relevant parameters for the calculation of final gas quantity.

Test ID	Ref. pressure	Ref. Temperature	Free volume	N_{FINAL}	Total gas volume at 1 bar and 0°C
IFA650.12	$3.8 \cdot 10^6$ Pa	1053K	11.06 cm^3	$3.387 \cdot 10^{21}$	126 cm^3
IFA650.13	$3.5 \cdot 10^6$ Pa	1093K	28.96 cm^3	$1.088 \cdot 10^{22}$	405 cm^3
IFA650.14	$5.7 \cdot 10^6$ Pa	1064K	10.208 cm^3	$3.96 \cdot 10^{21}$	149 cm^3

To obtain the volume of FGR, expressed at standard temperature and pressure, during the LOCA test, the two values are subtracted to obtain 92 cm^3, 113 cm^3 and 114 cm^3 respectively for test 12, 13 and 14. The calculated FGR for test 14 is clearly overestimated and the reason for this is most likely the choice for reference temperature and pressure. Although there are uncertainties with the temperature and pressure, the largest uncertainty in those estimates comes from the estimation of the free volume, which is based on the cladding strain profile on Figure 29. The actual measured fission gas release in test 14 is 70.88 cm^3 [32] , with Xe/Kr ratio of 11.36 which indicates primary release of transient fission gases near the pellet rim, because higher Xe/Kr ratio implies higher fraction of fissions coming from Pu-239.

Another source of error could potentially be the calculation of $N_{INITIAL}$ which requires precise knowledge of the rod free volume including voids in the fuel-cladding column. The calculation of $N_{INITIAL}$ only considers the plenum volume, which is known, and assumes that fuel and cladding is tightly bonded. For the sake of example, it can be assumed that half of the initial fuel-cladding gap still exists in test 12. The length of the fuel stack is 38 cm, cladding inner diameter is 8.36 mm and fuel outer diameter is 8.19 mm. Assuming half of the original pellet cladding gap is still open, the additional free volume is 0.42 cm^3. This means that:

$$N_{initial} = \frac{PV}{k_B T} = \frac{2 \cdot 10^6 \cdot 2.24 \cdot 10^{-6}}{1.3806 \cdot 10^{-23} \cdot 293} = 1.107 \cdot 10^{21}$$

$$N_{final} = \frac{PV}{k_B T} = \frac{3.8 \cdot 10^6 \cdot 11.48 \cdot 10^{-6}}{1.3806 \cdot 10^{-23} \cdot 1053} = 3.0 \cdot 10^{21}$$

$$N_{FGR} = N_{final} - N_{initial} = 1.893 \cdot 10^{21}$$

or, using the Ideal Gas Law with standard temperature and pressure, the volume of transient FGR for test 12 is 69 cm^3 instead of 92 cm^3.

In conclusion, the estimated FGR during the LOCA test is an important parameter for fuel dispersal and it needs to be approximated. An example of this is shown in Chapter 4 section 4.8.

3.5.3 Thermocouple measurements

In the design of the LOCA test rig (see Figure 13), thermocouples are placed at different elevations both on the heater and the cladding. Besides indicating the approximate rupture temperature, they are also used to confirm whether the rod heat-up is uniform axially. Typically two or three thermocouples attached at the same elevation and separated equidistant from each other, are found in the upper half. Their task is to confirm that the cladding temperature is azimuthally uniform (to be distinguished from the axial uniformity). There are also two thermocouples at the inner wall of the heater located near the bottom and the rod mid-height. Typically, there are cladding thermocouples at both the lower and the upper ends, but some tests such as test 4 only had thermocouples in the upper half of the cladding. The information delivered by the thermocouples is better explained with an example. For this purpose, the thermocouple readings of tests 3 and 4 are put next to each other on Figure 30.

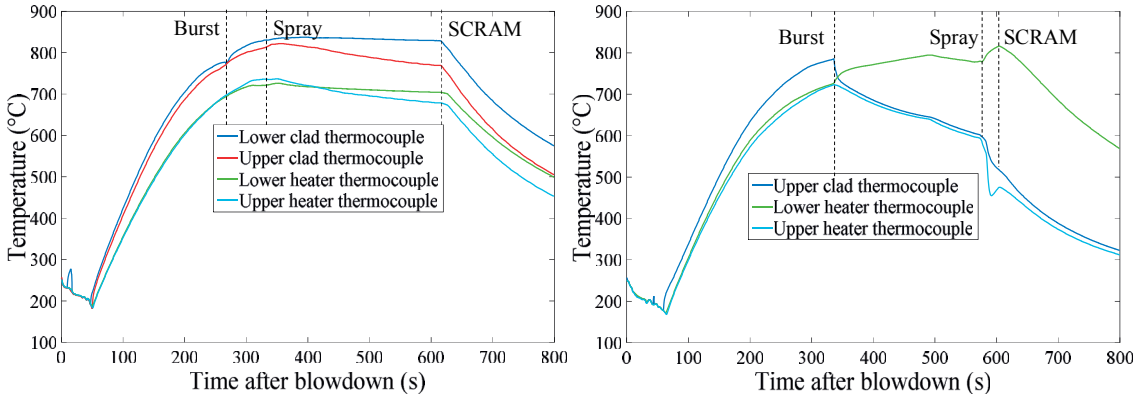

Figure 30: Thermocouple measurements during the execution of tests 3 (left) and 4 (right).

As already discussed in section 3.4.1, there was no fuel relocation in test 3 and the original cladding geometry was almost preserved. As such, the thermocouple readings are easier to interpret. All temperature measurements start to decrease at the time when SCRAM is initiated and the heater is switched off. The lower and upper cladding thermocouples begin to diverge at approximately 330 seconds. This is correlated with the actuation of the spray system as shown on Figure 27. The spray system injection is closer to the upper clad thermocouple as shown on Figure 13 and probably has a stronger effect on it. In contrast to test 3, there is more to say about the thermocouple measurements of test 4. During the LOCA test, both heater and cladding thermocouples were able to detect axial fuel relocation. As it is seen from the gamma count intensity plot on Figure 16, almost the entire upper half

of the fuel rod was emptied of fuel. This had an effect on both the thermocouples at the heater – located at rod mid-height and the cladding thermocouples at the upper end. The two thermocouples at the cladding registered a sharp drop at around 320 s (Figure 30, right). This was caused by the fuel relocation after the cladding burst. The lower heater thermocouple happened to be near the elevation with largest cladding strain and the temperature increase is caused by the relocated fuel (hot-spot effect). The upper heater thermocouple, on the other hand, steadily decreased. The temperature feedback due to fuel relocation on the thermocouples was likely delayed by few seconds due to thermal inertia of the relocated fuel.

The thermocouple readings may provide additional insight into the phenomena that takes place during LOCA. In the case of test 4, the upper heater thermocouple was able to capture the hot-spot effect. For complete presentation of the thermocouple measurements, please refer to the report by W. Wiesenack [26].

3.6 Post-irradiation examination after the LOCA test

After each LOCA test, different post-irradiation examinations are performed. Cladding profilometry, gamma scanning and cladding rupture size measurement are common to all tests. Additional PIE, such as fuel fragment size distribution, is performed for selected tests (e.g. tests 13 and 14). This section discusses some of the common PIE and what type of data for model validation can be obtained from them.

3.6.1 Axial cladding profilometry

The axial cladding profilometry can be done in different ways. When very high precision is needed, a device at Kjeller hot laboratory is used which basically consists of a needle that is moved axially on the surface of the cladding. Another way to get the shape of the cladding is by taking photographs and digitizing the image. Since this produces a 2-dimensional image, it must be assumed that the deformation is azimuthally uniform.

In the context of this dissertation, the axial cladding profile was already used in conjunction with the pressure transducer measurements for the LOCA tests 12, 13 and 14 (Figure 29) in order to estimate the released fission gas during the test. Furthermore, this information is necessary as input to the fuel dispersal model discussed in section 5.3. The axial cladding profile for the remaining LOCA tests are shown on Figure 31.

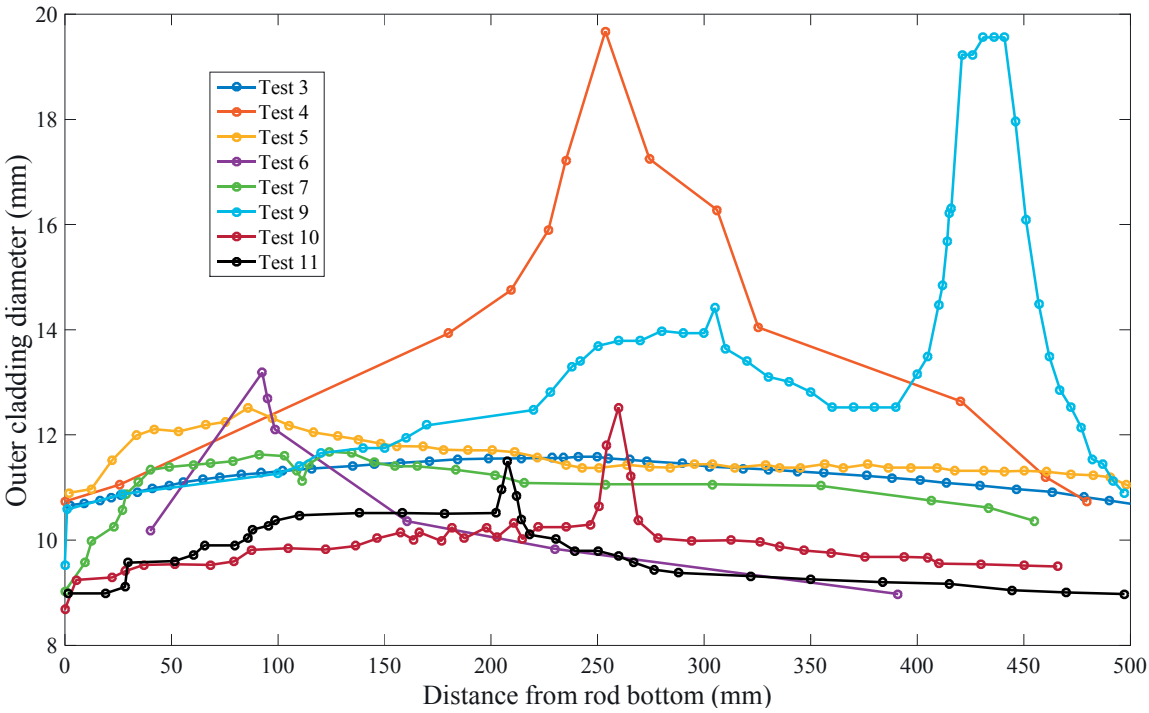

Figure 31: Axial cladding profile for all Halden LOCA tests except tests 12, 13 and 14. The data is taken from [26].

This data is used to calculate average values for the cladding strain in the balloon and the fuel stack as input to the fuel dispersal model (see Table 18). All of the above tests had cladding failure. The rupture occurs at the region of largest diameter.

3.6.2 Gamma scanning

Gamma scanning at Halden is a standard PIE procedure for the LOCA test program. Shortly after the test, the fuel rod is transported to the gamma scanning facility which is located at the premises of the Halden reactor. The facility is equipped with High-Purity Germanium (HPGe) detector connected with data acquisition system and cooled down to the necessary operating temperature (about 120 Kelvin). The scanning is performed by moving the pressure flask vertically in steps of 5 mm and horizontally in steps of 1 mm. The standard collimator size for this PIE is 1.5 mm in diameter, but sizes down to 0.1 mm are available. Horizontal scanning covers the entire rod radially with slight overlap between the scans whereas vertical scanning misses 3.5 mm of every 5 mm. Gamma scanning is typically taken at two azimuthal rod orientations.

The raw data can be read by Halden-developed software, called "Gamma Spectrum Reader". The data format can be visualized as a three-dimensional matrix with coordinates (**x**, **y**, **z**), where **x** is the radial coordinate, **y** is the axial coordinate, and **z** is the gamma spectrum. The gamma spectrum is a record of the number of gamma counts falling within certain energy range and an example is show on Figure 32.

To plot a gamma count intensity plot, such as those already shown for each LOCA test (section 3.4) an energy range from the spectrum should be selected. This corresponds to filtering the gamma counts of a particular gamma-emitting fission product. Then, the format of the data becomes a matrix of counts which when plotted produces image of the rod for the selected isotope/energy range. Typically, the fuel rod is about 480 mm long, which means there are 480/5 = 96 axial scans. Each axial scan comes with about 30 scans in the horizontal direction. Therefore, in total there are 96·30 = 2880 measurement points for the fuel rod alone. In total, there are over 5000 measurement points in order to be sure that the whole fuel rod, including the dispersed fuel, if any, is measured. Duration of a single measurement varies, but typically it is about 40 seconds. This means, that a full scan takes nearly three days to complete which is non-negligible time for short-lived isotopes such as Ba^{140} (half-life of 13 days). As a consequence, the gamma scan data must be decay corrected with reference to the first measurement point when using short-lived isotopes for any analysis.

The available gamma spectrum depends on how long after the LOCA test the measurement was taken. Two contrasting examples are shown on Figure 32. The presence of multiple gamma peaks is "ensured' if the gamma scan is taken shortly after the LOCA test. The gamma spectrum is entirely made up of short-lived fission products with the exception of the Cs isotopes. The latter are the only ones remaining if the gamma scan is taken several weeks after the LOCA test as shown on the right plot. Ideally, gamma scanning should be performed within the first two weeks after the LOCA test in order to capture more isotopes. From the point of view of further analysis using the gamma scan data, the short-lived isotopes are necessary.

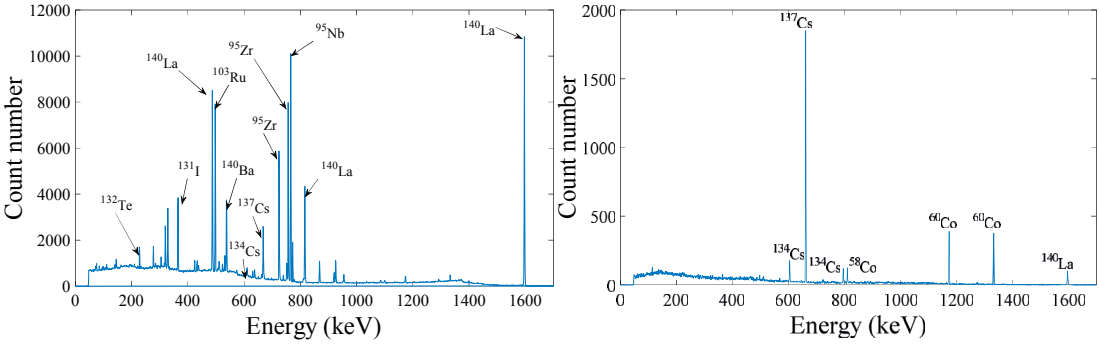

Figure 32: Gamma spectrum seen shortly after the LOCA test (left) and available gamma spectrum few weeks after (right).

Uses of the gamma scan data are several. Up until now, it has been used primarily as a visual confirmation of the test objectives – namely sufficient cladding ballooning and fuel relocation, and to show, at least qualitatively, the amount of dispersed fuel, although some things need to be considered when drawing conclusions. Other applications include usage of available fission product pairs to distinguish the origin of the relocated and dispersed fuel, estimation of quantity of dispersed fuel (see Appendix A) and axial void distribution of relocated fuel (section 3.6.4).

3.6.3 Cladding rupture size measurements

Cladding rupture size measurements were performed on all LOCA tests. They are done by taking a photograph of the rupture location and superimposing a ruler from which the rupture size can be judged. Table 6 presents a summary of the post-irradiation examination relating to cladding rupture. The table was adapted from Table 12 found in the report [26] and the missing data for Test 13 was taken from another report [32].

Evidently, the rupture sizes vary from small cracks all the way to 7 cm long ruptures. There does not appear to be a correlation between the burnup and the rupture size. It is interesting to note that most ruptures, with the exception of test 7 occurred at about the same temperatures. W. Wiesenack in his report [26] obtained a good correlation between the hydrogen content and the maximum ballooning strain. The higher the hydrogen content, the lower the maximum strain and this is explained with the negative effect of hydrogen uptake on the cladding ductility [84].

Table 6: Characteristics of the cladding failure for the Halden LOCA tests.

Test #	Visual	Burnup MWd/kg	Rupture strain (%)	Rupture length (mm)	Rupture width (mm)	T_{burst} °C (TCC1)
3		81.9	8	crack	crack	775
4	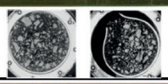	92	62	70	7	780
5		83	15	7	2	760
6		55.5	49	not seen	not seen	825
7		44.3	23	11	1.5	1100
9	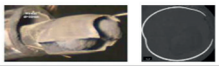	90	61	40	7	805
10		60	15	15	5	755
11		56	25	3	1	835
12		72.3	40	3	0.5	780
13	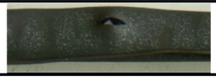	73.1	48	8	2	820

3.6.4 *Approximation to the axial fill factor*

An approximation to the axial fill factor is possible to obtain from the gamma scan data following the LOCA test. The gamma count intensity is proportional to the quantity of fuel at the scanned location. There are, however, things to be kept in mind, such as the number of gamma counts, gamma attenuation and even influence of the neutron flux distribution within the Halden reactor. The higher the number of gamma counts, the lower is the uncertainty which is given by $N \mp \sqrt{N}$, where N is the number of gamma counts. The number of gamma counts can be improved either by longer scanning time or if scanning is done as quickly as possible after the LOCA test. There are practical difficulties with both ways. Attenuation is a more serious problem mostly because the relocated fuel has unknown geometry and it is unclear how to account for it. This motivates the selection of the gamma with the highest energy from the gamma spectrum. With reference to Figure 32 this is the 1596 keV gamma of La-140. The source of La-140 is decay of Ba-140 as well as the fission itself. Considering the short half-life of 40 hours and the fact that scanning was taken more than one week after the fission process stopped, almost all of the La-140 originating from the fission process is gone. This means, the entire La-140 source is produced by the decay of Ba-140. As such, decay correction is done with the decay constant of the Barium. The use of La-140 for this task requires correction to be done with the neutron flux profile, because as described in [85], the La-140 distribution reflects the last days of irradiation. An approximation to the axial fill factor for test 14 is shown on Figure 33.

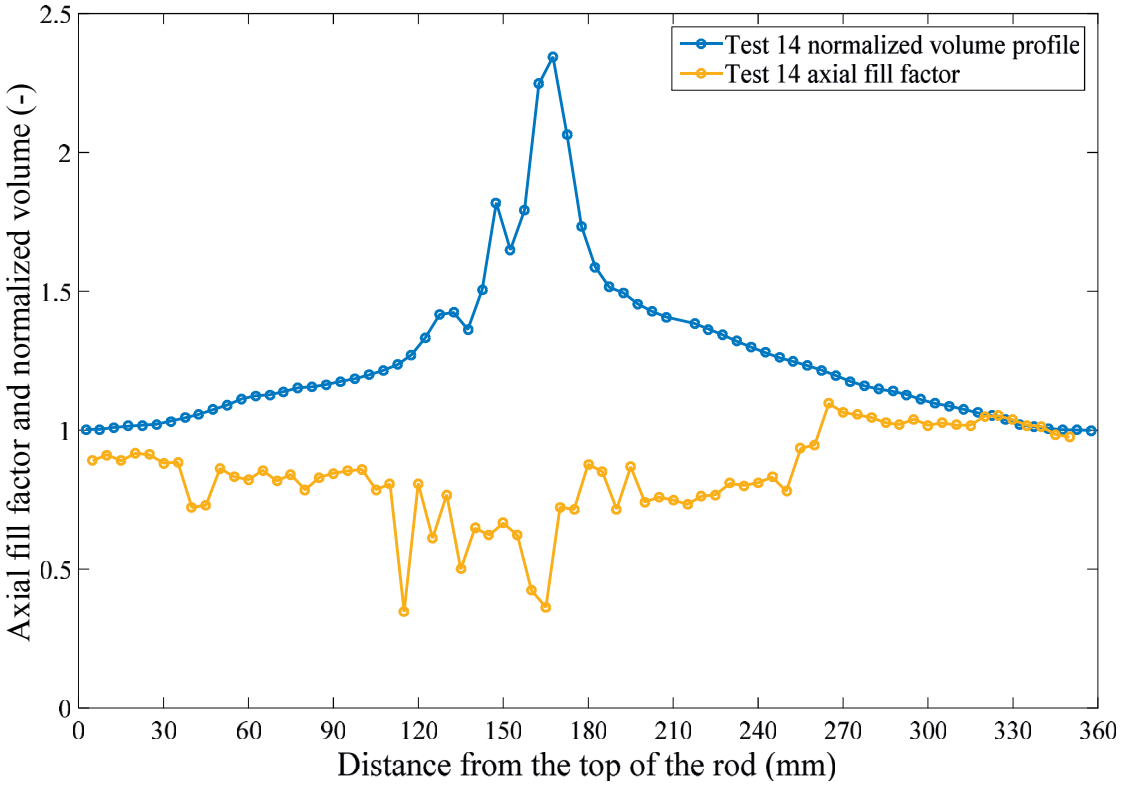

Figure 33: Axial fill factor distribution for test 14 based on the gamma scanning data.

The procedure to get the approximation to the axial fill factor is given below.

- Obtain the cladding strain profile. In this case, it was done by digitizing the photographs of the cladding in steps of 5 mm in order to match the axial gamma scanning resolution.
- Extract the gamma counts for La-140 at 1596 keV from the gamma spectrum. This is done with a Halden-developed software called “Gamma Spectrum Reader”

- Calculate the axial distribution of the volume within the cladding based on the cladding strain profile and normalize it with the volume of a cylinder with height 5 mm and diameter equal to the un-deformed cladding diameter
- Sum up all gamma counts for a particular axial elevation to obtain a 1-dimensional vector of total gamma counts
- Normalize that vector with the number of gamma counts found at the bottom. At this location the fuel geometry is most preserved.
- Finally, take the ratio of the normalized number of gamma counts with the normalized cladding volume

The axial fill factor can be useful parameter for the evaluation of the hot-spot effect and for the validation of a more sophisticated fuel fragmentation and relocation models. In this dissertation, the axial fill factor is not used, but this analysis was shown to emphasize that useful analyses can be done with the gamma count data.

3.6.5 Current enhancements of the gamma scanning at OECD Halden Reactor Project

A team of researchers currently working at OECD HRP are using a gamma tomography to enhance the information on fuel relocation after the LOCA test and before too much handling is introduced. This technique produces a 2D planar image of the relocation as opposed to a line image in the typical gamma scanning. A reconstructed image of the distribution of dispersed and relocated fuel in the balloon, where individual fragments can be discerned, is shown on Figure 34.

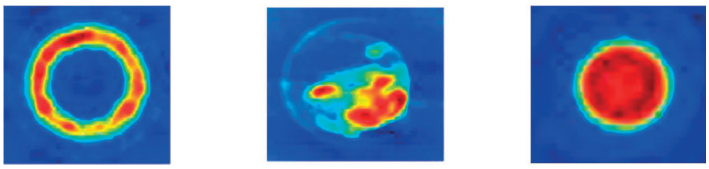

Figure 34: Gamma tomography of a Halden LOCA test in the dispersed fuel region (left), just above the balloon (middle) and at a location with relatively unchanged geometry (right). Source: HWR-1164 [86].

As the authors of the report stipulate, the new apparatus may be able to provide important information such as axial void fraction and together with precise knowledge of the fragment size distribution will provide data for validation of fuel relocation models. Additionally, determination of the packing fraction of the balloon will provide more accurate simulation of the hot-spot effect. Taking a second look at the first image on Figure 34, one could even try and determine the orientation of the cladding rupture. The darkest colour is oriented almost north, whereas the lightest – south. This may be an indication of the rupture orientation, because of the formation of a heap (higher count density) and at the same time lowest count intensity on the opposite side. Such information may be useful when looking at the tomographic reconstruction of the distribution of relocated fuel in the rupture region in the sense whether the gas forms clear path through the fragmented fuel and out of the rupture, therefore reducing the solid-gas flow interaction.

3.6.6 Steps for improving the quality of the gamma scan data

This section is largely taken from the presented paper in the Enlarged Halden Programme Group Meeting (EHPGM) 2014 [87]. The gamma scanning at Halden typically takes between two and three days to complete for one rod orientation. Table 7 presents some summary of the gamma scan data with focus on the number of scanned points, scanning time and approximation of the fraction of points within the balloon and dispersed fuel regions which are deemed regions of interest.

Table 7: Selected gamma scan data parameters for most of Halden's LOCA tests.

LOCA test number	Scan time per point (s)	Total points in the gamma scan	Total scan time (hrs.)	Number of points at balloon/rupture region	Number of points in dispersed fuel region	Total points outside fuel region	Fraction of points outside fuel region
Test 4	N/A	4749	N/A	180	87	3761	0.79
Test 5	N/A	4069	N/A	N/A	40	3092	0.76
Test 6	N/A	4442	N/A	70	Not clear	3618	0.81
Test 7	77	3189	68	Not clear	Not clear	2409	0.76
Test 9	37	4718	48	170	100	3673	0.78
Test 10	37	4484	46	50	19	3531	0.79
Test 11	47	3192	42	70	4	2193	0.69
Test 12	24	3192	21	Not clear	20	2416	0.76
Test 13	22	4016	25	80	19	3192	0.79
Test 14	55	4079	62	76	N/A	3329	0.82

Preferential scanning of selected coordinates and variable scanning time are parameters that are very dependent on the flexibility of the automatic scanning procedure. If there is possibility to program the scanning procedure, then some improvements can be achieved without relying too much on manual operation, which is a major point to consider.

Furthermore, the primary region of interest is the balloon and the dispersed fuel, which represent much smaller fraction considering the current scanning resolution. The number of scanning points within these regions is tabulated in Table 7, except tests 7 and 12 that showed extended balloon areas, which spread out over virtually the whole active length of the rods, so that it is difficult to identify on the gamma count intensity plots where the balloons are.

It is clear, that the detector cannot be positioned exactly on the fuel rod because it remains encased in the pressure flask and furthermore the thick glass window of the shielding compartment provides optical distortion. However, the possibility to do a quick scan to identify the coordinates of the fuel rod can then be followed by higher resolution scanning of selected locations.

There can be trouble to identify the exact location of the balloon, as in Test 7 and Test 12. In such cases, higher resolution scanning and longer counting time can be applied at least to the dispersed fuel region (if applicable).

In Summary:

1. Overlap between neighbouring scans can be most easily addressed by selecting a matching collimator size to the horizontal resolution.
2. Gamma scanning should not be delayed too much. Some of the LOCA tests (e.g. tests 8, 9, 10, 11) have very good gamma count statistics but also there are tests with low or no data on the short-lived isotopes altogether (e.g. tests 7, 12 and to some degree 13 and 14). Also, timely gamma scanning will capture the most geometrically transparent gamma of La-140 at 1596 keV.
3. Over 75% of the scanned points are outside the fuel rod region. The possibility to do a quick fast scan to find out the coordinates of the fuel rod and dispersed fuel may save valuable scanning time and could be discussed. If possible, then a more detailed scan can be launched for

selected coordinates only (balloon and dispersed fuel regions) with smaller collimator opening and higher resolution. In the end, there will be a fast full scan to get the overall "picture" and a more detailed scan for the regions of interest.

4. Most precise analysis can be done at the periphery, because the projection length is smallest. Scanning the fuel rod periphery should be given more time, whereas less time is needed for the fuel rod bulk due to the longer projection length (higher source of gammas).
5. The balloon and dispersed fuel regions make up a very small fraction of the total gamma counts and therefore higher resolution scanning can be done without compromising the current scanning time.
6. Two scanning angles are very limiting in drawing conclusions even if a higher resolution scanning is available. Four orientations, thereby completing the full rotation of the fuel rod, will still provide limited information but it will be more reliable.

Higher resolution scanning of the dispersed fuel region should be able to benefit from the lower fuel density and perhaps a more precise origin of the fuel can be assigned (pellet rim or bulk) based on the isotopes ^{103}Ru and ^{140}La (see more details in appendix A).

4
Chapter 4:
Base Irradiation

The base irradiation of a fuel rod to a large extent pre-determines the fuel behaviour during a LOCA transient. Fuel fragmentation and relocation of low and medium burnup fuel (shorter base irradiation) is not considered as problematic, because neither the hot-spot effect is a problem because the packing factor in the balloon is too low as elaborated in [88], nor could there be large fuel dispersal (if any) in the event of cladding failure, because the fragments are too large. In addition, the high burnup structure, which has high propensity to fragment, does not yet exist in medium burnup fuel. On the other hand, all of the above issues can be relevant for high burnup fuel (long base irradiation) as clearly demonstrated in Halden LOCA tests 4 [71] and Studsvik's tests 189, 191, 192 and 193 [27]. Finally, it has been demonstrated, that the last cycle power of the base irradiation also has an impact on the extent of fuel fragmentation, for example [30].

The first section in this chapter describes the database of high burnup BWR fuel rods which are subjected to numerical analysis of the fuel behaviour during base irradiation using EPRI's FALCON code [50] coupled to the GRSW-A - an advanced model for fuel swelling and fission gas release [9]. After that, post-irradiation examinations conducted at the Paul Scherrer Institute's (PSI) hot laboratory are used to formulate a hypothesis for fission gas trapping which addresses the scatter in fission gas release measurements of high burnup BWR fuel rods. In particular, it is hypothesized that the rod position within the BWR fuel assembly plays an important role. The hypothesis is then formulated as a fission gas trapping model in section 4.5 which is finally applied to the calculation of trapped fission gases in the fuel rods used in Halden LOCA tests 12, 13 and 14. Some of the contents in this chapter are published in [89].

4.1 Description of the base irradiation fuel rod database

In the framework of a fuel performance program (FPP) between PSI, Westinghouse and the Swiss power plant Leibstadt (KKL) the fission gas release for a few dozen BWR high burnup fuel rods, irradiated in KKL, has been measured at the end of life. Some of the data is already presented in [90] and [91]. From that database, 18 rods with comparable design were selected for base irradiation calculations with FALCON coupled with the in-house FGR model GRSW-A [9]. Most of them are seven cycle (1 cycle = 1 year) rods with an average burnup of over 60 MWd/kgU. Relevant information to the base-irradiation calculation is shown on Table 8.

The first six letters in the rod ID number designate the fuel assembly, while the last two – the position of the rod inside the assembly. For visualization purpose, those coordinates are arranged within the sketch of a BWR fuel assembly shown on Figure 35. Different colour scheme is applied in order to segregate the rods into three groups. The blue region corresponds to the fuel rods located around the moderator channel. The green region includes all fuel rods which are located in the interior of the fuel assembly. The red region represents all rods at the periphery. This grouping is important for the discussion that follows in sections 4.5 and 4.6.

Table 8: Fuel rod parameters relevant for the base irradiation simulation [89].

ROD ID	Enrichment (%)	Cycles
AEB067-E4	4.46	6
AEB068-E4	4.46	6
AEB069-E4	4.46	5
AEB071-E4	4.46	7
AEB072-E4	4.46	7
AEB072-J7	4.07	7
AEB072-J9	3.71	7
AEB071-D5	4.46	7
AEB071-F9	4.9	7
AEB071-H10	4.07	7
AEB071-I6	4.9	7
AEB071-J8	4.07	7
AEB072-D5	4.46	7
AEB072-F9	4.9	7
AEB072-I6	4.9	7
AGA002-F9	4.9	6
AGA002-H10	4.07	6
AGA002-I6	4.9	6

Common parameters	
Parameter (units)	Value
Fuel OD (mm)	8.19
Clad ID (mm)	8.36
Clad OD (mm)	9.62
Filler gas	He
Plenum length (mm)	259
Clad material	Zry-2
Zr-liner (µm)	70
Clad type	LK3/L
Fuel length (mm)	3810
Fuel density (g/cm^3)	10.5
Fuel mass (g)	2087
Assembly type	SVEA96+
Fuel pitch (mm)	12.4
Reactor type	BWR
Coolant pressure (bar)	75
Fuel grain size (µm)	10

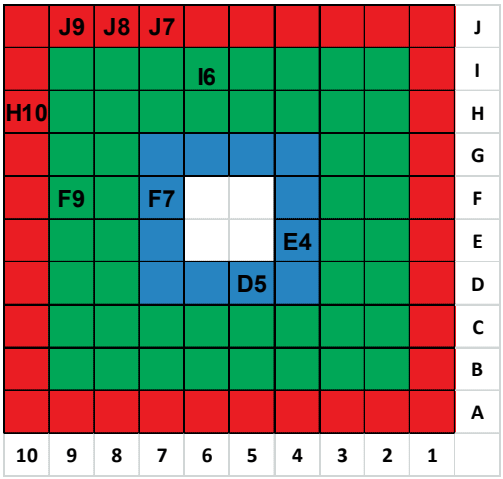

Figure 35: Fuel rod coordinates within a reference 10x10 BWR fuel assembly.

Measurements of the fission gas release were performed at the Hot Laboratory at the Paul Scherrer Institute and the results are tabulated in Table 9. Most of them were done by rod puncturing – a procedure during which all of the gas in the plenum is collected and the volume is precisely determined. The uncertainty of the measurements (in cm^3) by puncture is about 1%. For some of the rods, the FGR was determined by gamma measurement and those are marked with a *.

Table 9: BWR fuel database of measured fission gas in the rod plenum and calculated with FALCON/GRSW-A (reported at standard temperature and pressure). This table is taken from [89] and some of it can also be referenced to [90] and [91].

Rod ID	Burnup (MWd/kgU)	Measurement (%)	Measurement (cm^3)	Calculation (cm^3)
AEB067-E4	57	1.08	40	121
AEB068-E4	57	0.86	32	110
AEB069-E4	51	0.28	9	44
AEB071-E4	58	1.46	54	127
AEB072-E4	63	1.10	45	203
AEB072-J7	64	2.69	112	231
AEB072-J9	65	3.25	137	252
*AEB071-D5	58	2.06-2.75	77-103	132
*AEB071-F9	63	3.76-5.00	153-203	211
*AEB071-H10	62	2.05-2.73	83-110	205
AEB071-I6	62	5.35	214	193
*AEB071-J8	62	2.54-3.38	102-135	197
AEB072-D5	63	1.81	74	208
*AEB072-F9	66	4-5.31	171-228	269
AEB072-I6	66	3.79	161	259
*AGA002-F9	60	2.92-3.89	114-152	149
*AGA002-H10	60	3.18-4.23	123-164	143
*AGA002-I6	61	3.23-4.30	127-170	161

** Fission gas quantity in the rod plenum is determined by gamma measurement*

The measured FGR is reported both as % and as absolute quantity in cm^3 at standard temperature and pressure. The last column shows the calculated fission gas release with the coupled FALCON / GRSW-A model for fission gas release. The gamma measurements show a range of values which should include the uncertainty. As it is evident, the level of burnup is comparable (with the exception of rod AEB068-E4) and at the same time the measured FGR shows considerable scatter. Strong variation in measured FGR from BWR fuel is also mentioned in [85] although not much details about the fuel are given. Considering that the generated fission gas per MWd energy is about 31 cm^3 at standard temperature and pressure and looking at the measured FGR of the pair of fuel rods AEB072-E4 and AEB071-I6 the most logical conclusion is to hypothesize that there exists a mechanism for fission gas trapping that prevents fission gases to reach the plenum. This is discussed in section 4.3. On a final note, the necessary LHGR evolution during base irradiation is provided by the power plant. It contains few thousand points which makes it very detailed. The next section discusses the importance of providing an input of fast neutron flux for the base irradiation calculation of BWR fuel rods.

4.2 Fast neutron flux input

Fast neutron flux contributes to cladding creep [92, 93] which in turn plays a role on the fuel-cladding gap closure and mechanical contact pressure – both are necessary conditions for the creation of a pellet-cladding bonding layer. In-reactor cladding creep is composed of thermal creep, which is important for Zircaloy cladding for temperatures above 300-350 °C (i.e. during transients such as LOCA) and irradiation creep, which is the main contributor in the normal temperature operating range of light water reactors [94]. The creation of a pellet-cladding bonding layer is one hypothesis that could explain the discrepancies in the FGR measurements reported in Table 9. Therefore, properly accounting for the fast neutron flux is necessary for fuel modelling. The effect of the fast neutron

fluence, the time integral of the fast neutron flux, on the time of gap closure and on the magnitude of the pellet-cladding contact pressure should be evaluated.

FALCON allows the user to input time-dependent axial fast neutron flux. In a PWR, the fast neutron flux is directly correlated with the profile in the core. In a BWR, however, it is more complicated, because the void fraction increases with the axial elevation owing to the evaporation of the coolant. An increase in the coolant void fraction decreases the moderation and therefore the fraction of fast neutrons increases, but at the same time there are less thermal neutrons causing less fission and therefore resulting in lower count of neutrons, both thermal and fast. Open literature models for fast flux calculation in BWR are scarce. The fast flux input can be provided by a core physics code such as CASMO, but in the present BWR-specific analysis, the main equations are adopted from [95]. A full description of the equations can be found in Appendix B.

The axially varying void fraction, which is needed for the fast neutron flux calculation, can be extracted from the FALCON thermal-hydraulic model output, or provided by a stand-alone thermal-hydraulic code such as TRACE. In this discussion, it is taken from FALCON. This approach requires two base irradiation calculations. The first calculation generates the void fraction profile as function of time, which is then used to prepare the fast neutron flux input for the second calculation. In order to simplify the discussion, from now on the fast neutron flux dependent only on the LHGR (in other words, constant fast-to-thermal neutron flux ratio) will be referred to as the "PWR case" while the fast-neutron flux dependent on the LHGR and void fraction, i.e. an assumption that the fast-to-thermal neutron flux ration depends on the void fraction, will be called the "BWR case". The difference in the axial distribution of fast neutron fluence (time integral of the fast flux) between the two cases at the end of life is shown on the left pane of Figure 36.

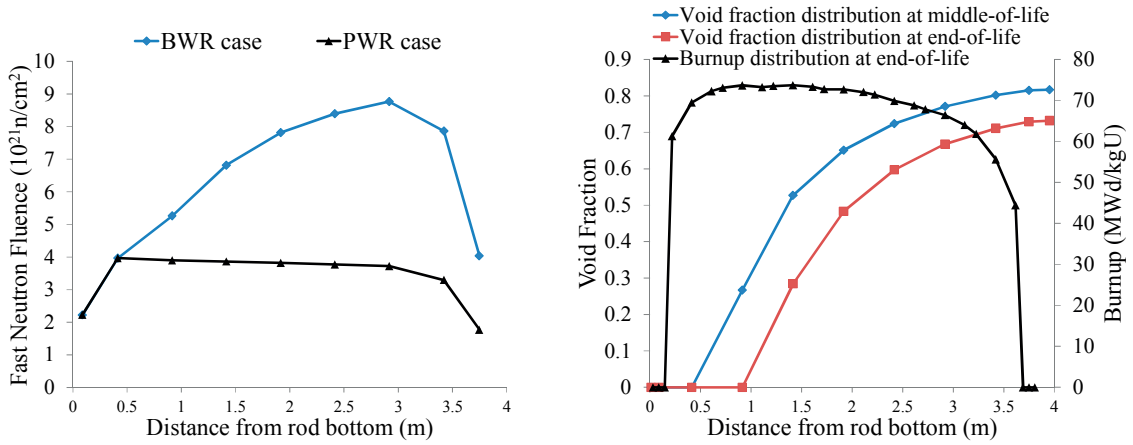

Figure 36: On the left: fast neutron fluence distribution at end-of-life calculated with constant and void-dependent fast to thermal neutron flux ratio. On the right: burnup profile at end-of-life and void fraction axial profile distribution at middle-of-life and end-of-life.

The fast neutron fluence is computed at different axial elevations of the fuel rod. Near the bottom, where the void fraction is zero, there is no difference between the PWR and BWR case. The two distributions begin to diverge at about 0.5 m from the fuel rod bottom owing to the increase of void fraction in the coolant. The axial fast neutron fluence profile for the PWR case is straightforward to explain. It is dictated by the axial power profile which is almost flat as evidenced by the end-of-life burnup profile shown on the right pane of Figure 36. On the other hand, the BWR case shows more interesting behaviour. There is a steady increase of the neutron fluence until about 2.6 m and then a sharp drop. Clearly, the distribution cannot be directly correlated with burnup because the changing

axial profile of the void fraction also plays a role. The impact of the different axial profile of the fast neutron fluence can be easily demonstrated by plotting the radii of the fuel outer surface and the cladding inner wall for different moments of the base irradiation. This is well visualized on Figure 37.

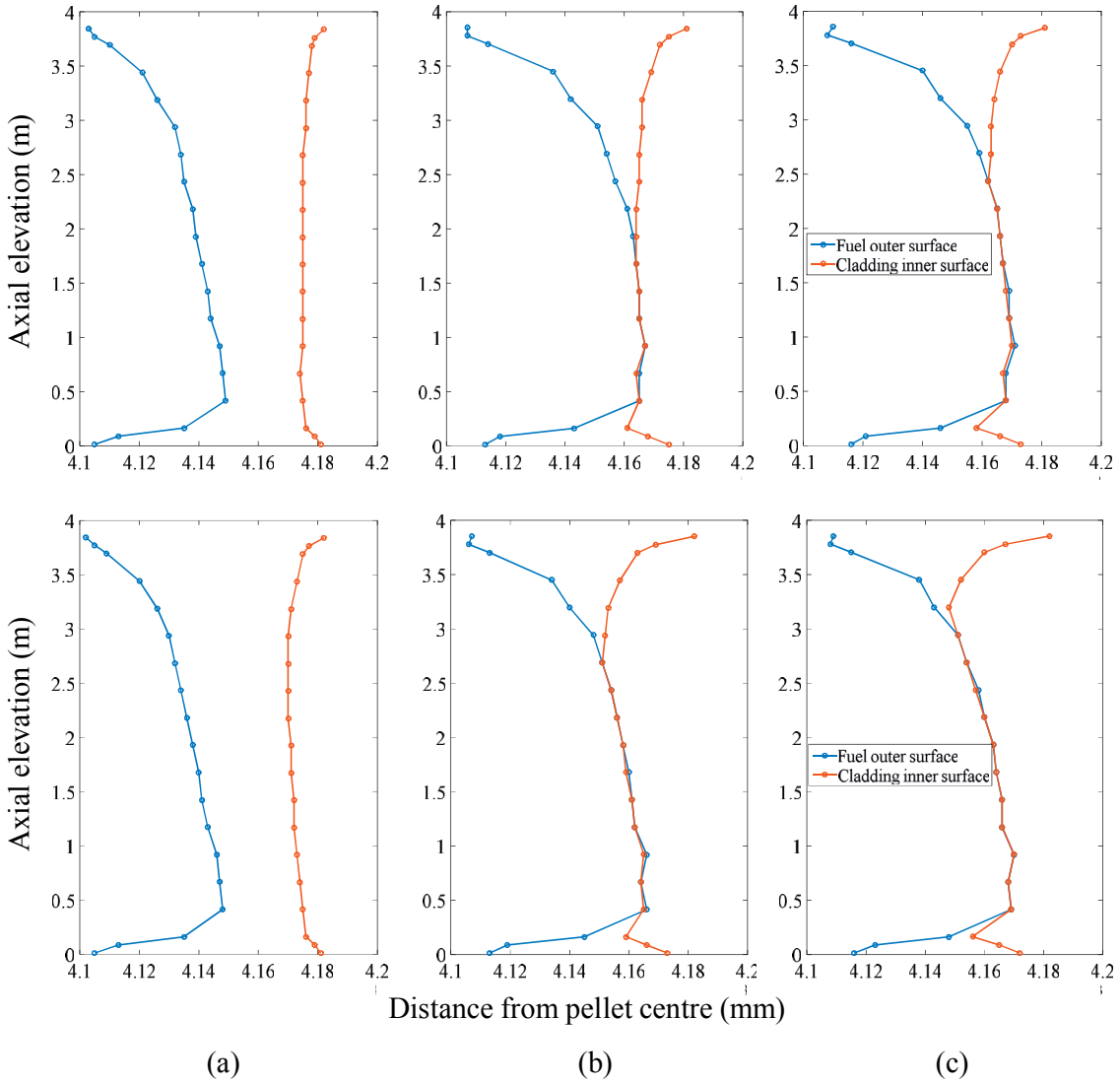

Figure 37: State of the fuel-cladding gap at the middle of the second cycle (a), beginning of the fifth cycle (b) and end of the fifth cycle (c). The top figures show the PWR case and the bottom – the BWR case.

At the beginning of the second cycle, the gap for both cases is open. Yet, even early into the base irradiation the larger cladding creep-down for the BWR case is evident in the upper half of the cladding. This is a confirmation, that the void-dependent fast neutron flux input does not introduce some unexpected effects. The situation is much different at the beginning of the fifth cycle where the region with a closed gap is almost 1 meter longer for the BWR case. The gap closure at the lower half of the fuel rod is reached at approximately the same time, because the void fraction does not have big impact and the fast neutron flux is dictated only by the LHGR. At the end of the fifth cycle, the gap is further reduced but still there is a notable difference between the two cases. The effect of the different input for fast flux on the pellet-cladding gap closure is evident in the upper half of the rod where the difference is more pronounced as the plot on the left pane of Figure 36 shows. At the lower half of the rod, there is not much difference, as it should not be, because the void fraction is not yet a big factor and the fast neutron flux correlates with the thermal neutron flux, which for both cases is derived from

the same LHGR input. Figure 38 provides another look at the different gap closure times between the PWR and BWR cases in the upper part of the rod. It shows a plot of the contact pressure at different elevations as function of burnup.

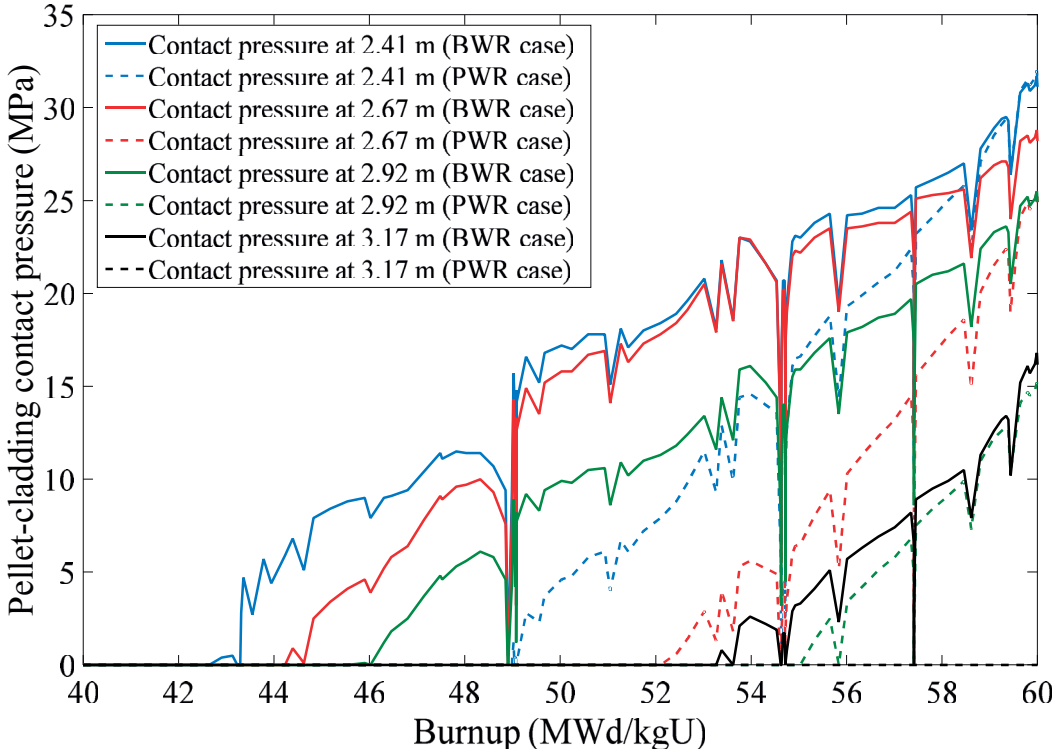

Figure 38: Effect of void-fraction dependent fast neutron flux on fuel-cladding contact pressure (CP) in the upper half of the fuel rod.

The gap closure and the contact pressure between the fuel and the cladding over time is a necessary condition for the creation of a pellet-cladding bonding layer and this is discussed in the next section. Additionally, the contact pressure is a necessary input parameter for the model of fission gas trapping discussed in section 4.5.

4.3 Fission gas trapping during base irradiation

Modelling of the fuel fragmentation, relocation and dispersal phenomena does not apply only to one type of reactors. However, BWR fuel presents additional challenges that should be considered, in particular, owing to heterogeneities in the fuel assembly design, such as presence of a central moderator channel, water wings and part-length rods. The topic of discussion in this section is a hypothesis for fission gas trapping in high burnup BWR fuel. The reason this is important is because trapped fission gasses will be released during a LOCA and will in turn modify the internal rod pressure and may even impact the quantity of dispersed fuel.

Additional post-irradiation examination was performed for some of the rods shown in Table 8. Of a particular interest are the Electron Probe Micro Analysis (EPMA) measurements which show the diametric distribution of different fission products. Additionally, Scanning Electron Microscopy (SEM) images reveal some interesting features at the fuel-cladding interface (e.g. Figure 41).

The as-manufactured pellet-cladding gap is about 100 microns. During reactor operation, the fuel thermal expansion and fission products build-up contributes to fuel swelling. Due to the pressure and

temperature inside the reactor pressure vessel, the cladding creeps down onto the pellet. Eventually, the gap closes and a pellet-cladding bonding layer is formed.

The fuel performance code FEMAXI-6 [96] uses a pellet-cladding bonding model based on the ratio of the time integral of contact pressure between the fuel and the cladding from the time of the first contact and an empirical parameter characterizing the formation of a bonding layer [97]. As soon as the ratio becomes unity, the bonding layer is assumed to be developed as stipulated in [97].

The paper by Yagnik, Machiels and Yang [98] reports that between 25-65% of the circumferential surface area of high burnup (~50 MWd/kgU) samples showed the presence of an interaction layer and strong bonding of the fuel to the cladding inner surface. TEM analysis discussed in [99] reports 20 μm thick bonding layer in BWR fuel irradiated to an average burnup of 49 MWd/kgU. On the other hand, such observation was absent in the lower burnup samples (< 40 MWd/kgU) of their study. From the cladding wall inward, the different phases encountered are pure Zr, ZrO_2, Zr-Cs-O, U-Cs-O and UO_2 [100]. This implies that sufficient time is needed in order for these species to migrate and interact. As the time progresses, and the burnup increases, the development of bonding layers becomes more likely.

Owing to the fact that in PWR fuel assembly there are no moderator channels, water wings and part-length rods, the thermal neutron flux reaching the fuel rod periphery is likely more azimuthally uniform. This implies that the burnup and the fuel swelling are also more azimuthally uniform. Given these assumptions, it can be hypothesized that the development of a bonding layer in PWR fuel likely proceeds more uniformly azimuthally compared to the one in BWR fuel. In the latter, due to the heterogeneous thermal neutron flux (owing to design features, in the fuel assembly, such as moderator channel, water wings, part-length rods and others) the burnup becomes azimuthally asymmetrical which is characterized by the appearance of “high” and “low” burnup sides. This suggests that the development of a bonding layer will begin sooner on the “high” burnup side, which also has implication on the relative strength of the bonding layer between the high and low burnup sides.

Let it be assumed that a pellet-cladding bonding layer is developed. During normal operation the temperature profile across the pellet diameter resembles inverted parabola with the highest temperature at the centre and lowest at the periphery. This means that different parts of the pellet have different thermal expansion. During refuelling, the temperature decreases and UO_2 cracks at the very beginning of power operations. This results in circumferential cracks and any existing pellet-cladding bonding layer is likely broken. Considering all of these assumptions, it can be hypothesized that a PWR fuel during power dips opens fully the pellet-cladding gap while BWR fuel - only partially. The discussed asymmetry in the latter suggests that the pellet-cladding gap at the low burnup side may open during power dips, such as refuelling, in order to account for the differential thermal contraction between cladding and pellet, while at the same time keeping the high burnup side bonding layer intact and the adjacent fuel area non-cracked. It is hypothesized that the permanent existence of a bonding layer in BWR fuel may cause the trapping of fission gases. This behaviour is illustrated in Figure 39. The colour gradient from red to green represents the asymmetrical burnup in the fuel pellet.

The fuel rods from Table 8 were installed in a BWR fuel assembly design SVEA96+. As a design feature, there is a moderator channel located in the centre of the fuel assembly as shown on Figure 35. The fuel rods situated around the moderator channel will experience higher thermal flux on the side oriented towards the channel. This is confirmed by an EPMA analysis of the radial burnup profile on fuel cross section of fuel rod AEB072-E4 (see Table 8) as shown on Figure 40.

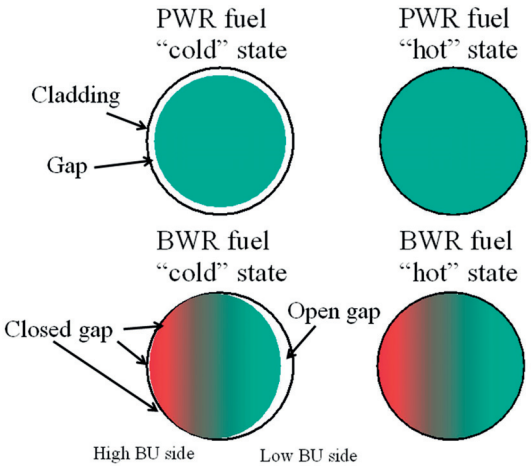

Figure 39: Hypothetical behaviour of PWR and BWR fuel during refuelling or other power dips (colour illustrates burnup).

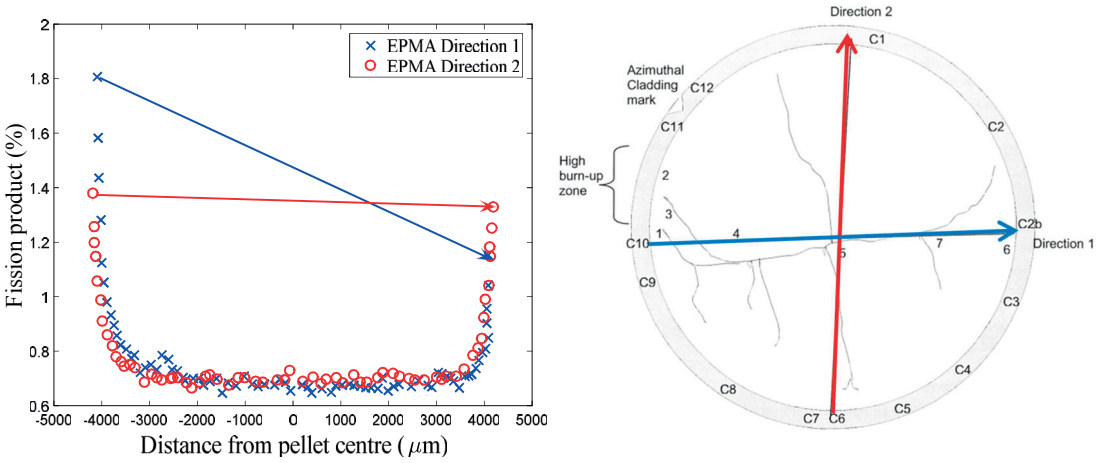

Figure 40: On the left: Distribution of Neodymium across the diameter of BWR fuel sample at 72 MWd/kg derived from EPMA [101] of rod AEB072-E4 taken along two directions. On the right: reference scheme of the EPMA analysis, indicating the location of the "high" burnup side.

The asymmetry in fission product distribution, and therefore burnup, in this BWR fuel rod is evident from the EPMA in direction 1. This is the direction starting from the side oriented towards the water channel. The left figure on Figure 41 demonstrates strong bonding between fuel and cladding. The right figure shows partial bonding and open gap. Voids/pockets located at the pellet-cladding interface, as well as the specific HBS porosity, are potential sites for local fission gas trapping. The rod-average burnup of this rod was about 65 MWd/kgU where the high burnup side reached about 100 MWd/kgU.

The high burnup side shows an intact bonding layer whereas the lower burnup side shows an open gap. Experimental evidence of strong asymmetrical pellet-cladding bonding layers was observed in BWR fuel rods at high burnup, which demonstrates the principal possibility of pellet-cladding bonding layer impact on local fission gas trapping or release.

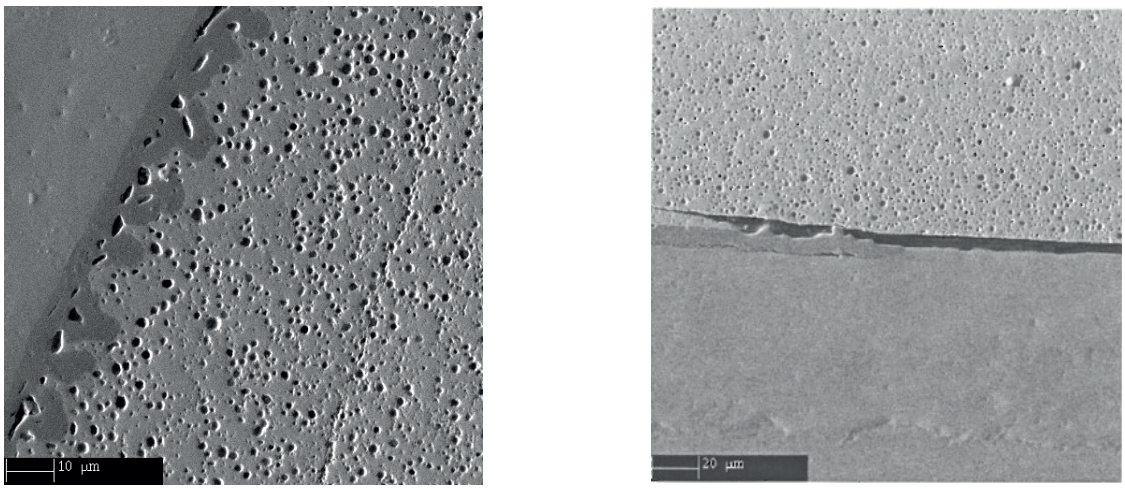

Figure 41: On the left: SEM images at the high burnup side (approximately position C11/C12 on Figure 40). On the right: SEM image at a lower burnup side (position C6/C7 on Figure 40). The data comes from the analysis of the 7-cycle BWR fuel rod AEB072-E4, which is also listed in Table 8 and reported in full in [101] and to some degree in [102].

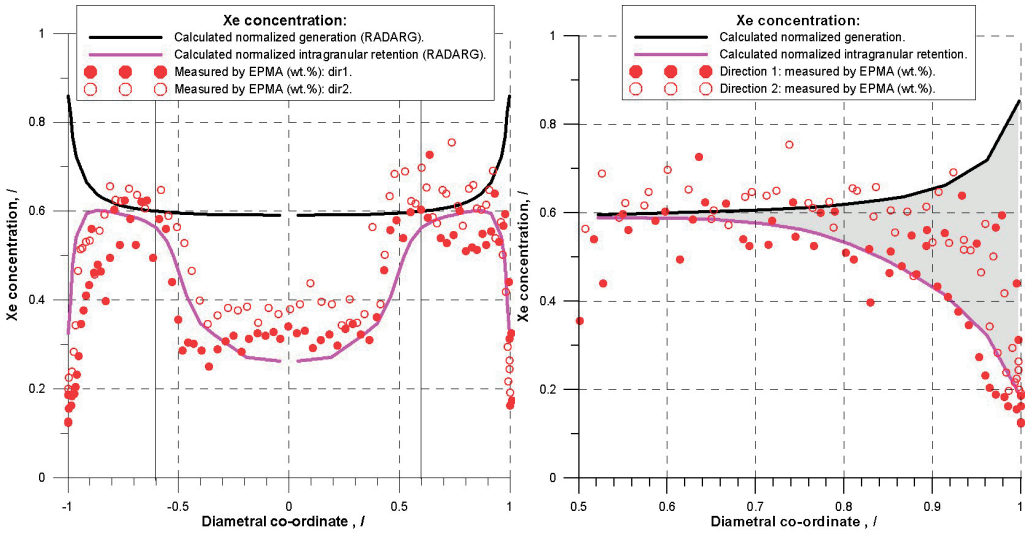

Figure 42: Measured EPMA- concentration of Xe in segment AEB072-E4-GF compared to calculation with FALCON/GRSW-A across the whole pellet diameter (left) and for the pellet periphery (right). The grey field qualitatively shows the potential amount of fission gases that could be trapped due to the effect of bonding.

It is to be noted that the calculation of the GRSW-A model, integrated into the FALCON code [9], covers a wide range of mechanisms of the fission gas kinetics, including both thermal- and a-thermal (HBS assisted) ones. For the fuel rods discussed in section 4.1, an extensive use of EPMA data for intra-granular xenon distribution across the pellet radius was first made in [103] to ensure the general adequacy of the integral analysis of the coupled codes, and in particular that the radial distribution of Xenon at end-of-life is evaluated by FALCON coupled with GRSW-A compares well with the experimental data as shown in Figure 42. As evident, the characteristic depletion of Xenon at high burnup from the pellet centre towards the periphery is captured well. Despite all of this, FALCON modelling with R-Z geometry precludes any discussion about azimuthal heterogeneities like the ones discussed above.

The unavailability of similar PIE for all fuel rods of the discussed database motivated the use of a simple 2-D model with Serpent Monte Carlo code with which to approximate the burnup asymmetry for all the rods. This is the topic of discussion in the next section.

4.4 Serpent Monte Carlo model for approximation of the burnup asymmetry

Some of the rods from Table 9 were subject to extensive post-irradiation examination, including an EPMA analysis [101] which can be used to quantify the burnup asymmetry, for example by taking the ratio of a fission product concentration on the high burnup and the low burnup side of the fuel pellet. In particular, there is EPMA data for the rod in position E4, but no data for any of the rods at the periphery (red region in Figure 35) or the interior (green region) of the fuel assembly. Hence, the degree of asymmetry for these rods in comparison with the rest is unknown. For this reason, a two-dimensional calculation with the Serpent 2 Monte Carlo Code [64] was performed on the reference BWR fuel assembly design. The rod enrichments used in the calculation are taken from the fuel assembly design and a reference void fraction of 0.4 is used, which roughly corresponds to the middle of the core. The Serpent input geometry is shown on Figure 43.

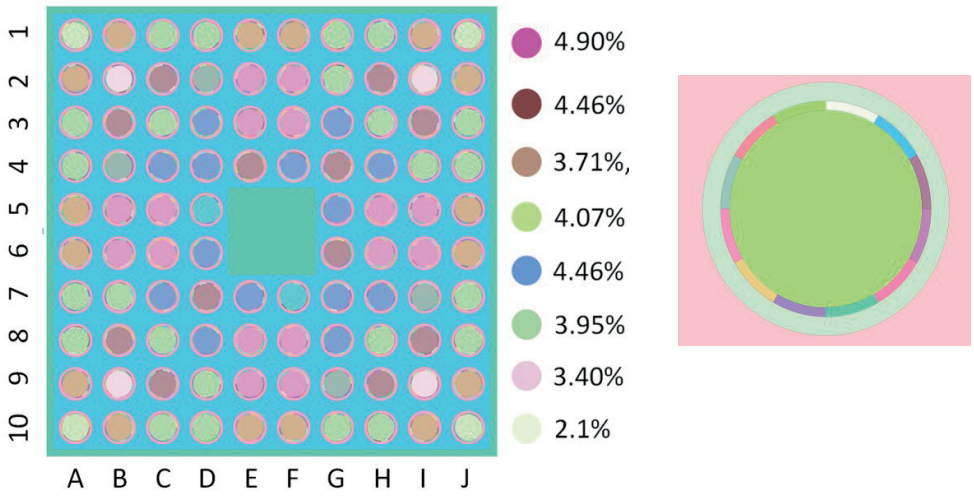

Figure 43: On the left: Serpent MC Model of a reference 10x10 BWR FA with the rod enrichment reported in the colour legend. On the right: modelled geometry of the fuel pin.

In order to capture the burnup asymmetry in the pellet periphery, the fuel pin was modelled by two regions: periphery and bulk. The periphery is represented by 12 sectors, each of which spans 30 degrees and has a thickness of 200 microns as illustrated in the right image on Figure 43. The bulk is represented by a solid circle. Each sector of each fuel pin is depleted individually, which allows evaluating the burnup asymmetries shown on the left pane of Figure 44. The figure is generated by plotting concentrations of Nd-144 from all 12 sectors for all fuel pins.

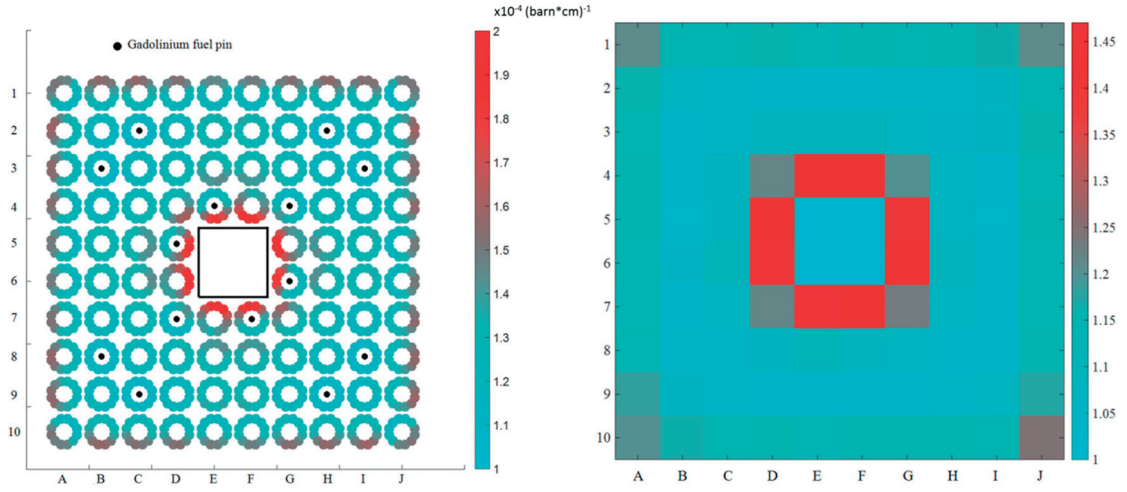

Figure 44: Output of the Serpent simulation on the reference BWR FA design. On the left: map of the Nd-144 circumferential concentration of all fuel pins. On the right: representation of the degree of burnup asymmetry.

The burnup asymmetry was quantified by taking the ratio of the maximum and the minimum concentration. This is visually represented by the right pane of Figure 44. The largest asymmetry is about 1.55 which is comparable to the value obtained from the left pane of Figure 40, and it applies for the rods around the moderator channel. The asymmetry in the interior is about 1.05 and at the periphery around 1.25. It should be kept in mind that the Serpent model ignored some design features such as water wings which undoubtedly have an impact. In addition, in a BWR the void fraction changes axially, which also has an impact on the thermal flux and therefore on the burnup asymmetry. However, for the purposes of this study, the modelling is deemed sufficiently adequate according to the EPMA data on Figure 40, which shows the burnup asymmetry of about 1.5 between the higher and lower burnup sides of the fuel pellet. Still, it should be kept in mind that the burnup azimuthal asymmetry likely varies axially.

The next sections discuss a simple post-processing model whose aim is to optimize the calculation and measurement of FGR in the rod plenum by considering the pellet-cladding interface as a possible trap for fission gases.

4.5 Fission gas trapping model

The hypothesis for fission gas trapping presented in section 4.3, the analysis of the burnup asymmetry with the Serpent code in section 4.4 and the calculated and measured fission gas release from Table 9 are used to formulate a model for fission gas trapping. Firstly, it is worth to see how the calculated and measured FGR, without consideration of fission gas trapping, compare with each other and this is shown on Figure 45.

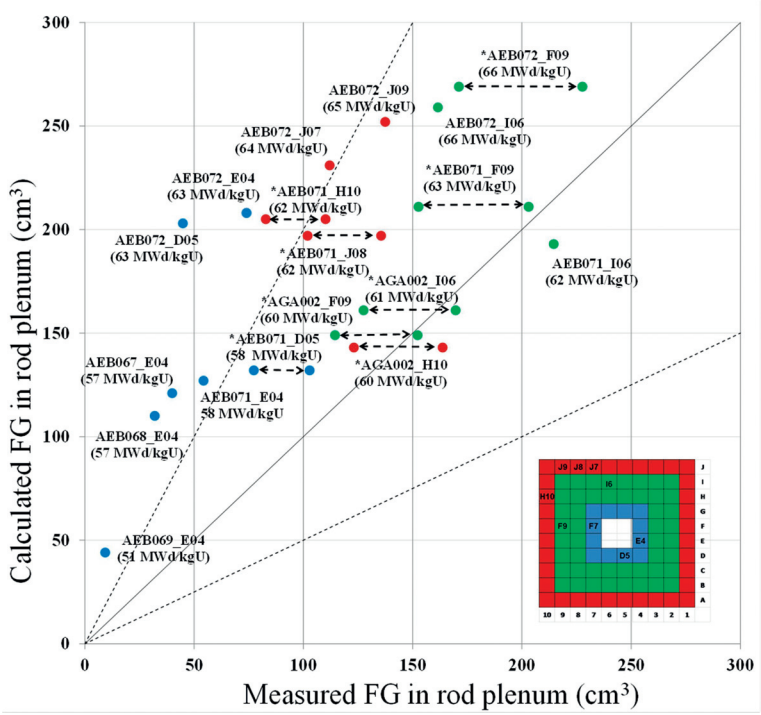

*Figure 45: Calculated versus measured fission gas release into the plenum. Data points with * indicate measurements whose uncertainty is represented by the width of the dashed lines.*

The discrepancy in the measured FGR, expressed in units of volume at standard temperature and pressure, from rod puncture shown on the figure can be explained by a retention mechanism. The measured FGR changes from higher values (green region in Figure 35) to middle (red region in Figure 35) to lower values (blue region in Figure 35) in accordance with the increasing degree of burnup asymmetry evaluated in the previous section. In the context of fission gas release to the plenum, the presence of a bonding layer will act as an obstacle and may trap fission gases locally. The cladding lift-off experiment IFA-610.10 [104] executed at Halden showed a non-zero hydraulic diameter (or open fuel-cladding gap), which could contradict the claim of strong bonding layer, unless the bonding non-symmetry was properly considered. Indeed, the claim made here is that only a fraction of the circumference is closed (as seen on Figure 41) due to a fuel-cladding bonding layer and not the whole circumference, and it is not necessarily in contradiction with the lift-off experiment. It is hypothesized that the degree of burnup asymmetry in BWR fuel is a strong (perhaps a necessary) factor for the development of a permanent partial bonding layer. This notion of partial fuel-cladding bonding may give some explanation for the low quantity of fission gas measured in the rod plenum from puncture in some BWR rods as already reported in Table 9. As demonstrated in the previous sections, experimental evidence shows the presence of tight bonding layers at the time of examination (e.g. Figure 41).

The base irradiation simulations of the rods shown in Table 8 performed with FALCON/GRSW-A resulted in over-prediction of the calculated fission gas release (Figure 45). The calculations were done in R-Z geometry, which by definition assumes azimuthal symmetry. Notions such as permanent partial fuel-cladding bonding and retention of fission gas are not considered. Following the formulation of the evaluation of fuel-cladding bonding in [97], a simple post-processing model is developed to reconcile some of the difference between predicted ($FGR_{calculated}$) and measured (FGR_{plenum}) fission gas release. The necessary parameters, namely contact pressure and time, are extracted from the output of the FALCON/GRSW-A calculation, and the burnup asymmetry is provided by the Serpent simulation. The proposed model is shown in Eq. 1.

Eq. 1: Calculation of the fission gas in the plenum taking into account trapping.

$$FGR_{plenum} = FGR_{calculated}(1 - \Phi_B \Phi_{TR})$$

The term Φ_B is shown on Eq. 2 and characterizes a fuel volume fraction affected by the pellet-cladding bonding.

Eq. 2: Evaluation of the bonding factor.

$$\Phi_B = 1 - exp\left\{-\frac{ICP}{X}\right\},\ ICP = \int_{t_{start}}^{t_{end}} CP(t)dt$$

The ICP is the time integral of contact pressure (CP) from beginning of base irradiation (t_{start}) up to the current time of analysis (t_{end}). The constant parameter *X* has dimensions of MPa·hours and affects the speed of bonding formation. The parameter Φ_B symbolizes the fact that fission gas trapping requires pellet-cladding bonding, which in turn is established through the contact pressure between the fuel and the cladding. The following properties are satisfied by the parameter Φ_B:

a) Until contact pressure between fuel and cladding is established, ICP = 0 and Φ_B is zero.
b) After the onset of contact pressure, the ICP grows continuously and Φ_B approaches the asymptotic value of 1, which can be interpreted as fully developed bonding layer.

The capability of the fuel to retain the released fission gases will be limited by the inevitable gap re-opening and fuel cracking around the bonding layer at each power shutdown (e.g. during refuelling), due to the difference between thermal expansion of the pellet and cladding. Φ_{TR} is the fraction of the pellet-cladding bonding assumed to be broken during any power shutdown. This fraction is deemed to be a function of the asymmetry in radial distribution of burnup (e.g. Figure 40), and expressed in Eq. 3.

Eq. 3: Evaluation of the fraction of irreversible fuel-cladding bonding.

$$\Phi_{TR} = 1 - exp\{-a(k-1)^b\}$$

The parameter Φ_{TR} includes the influence of the burnup asymmetry and characterizes the fraction of the circumference which has a permanent bonding layer, i.e. independent on power shutdown. The larger Φ_{TR} is, the larger the trapping of fission gas (for example, rods around the moderator channel have the highest burnup asymmetry, as seen on Figure 44, and the lowest measured FGR from rod puncture as presented on Table 9). The degree of asymmetry is labelled by *k* and it is calculated as the ratio of the Nd-144 concentration on the high and low burnup sides estimated with the Serpent analysis (Figure 44). The parameters a, b and k are dimensionless. The parameter Φ_{TR} has the following properties:

a) If there is no burnup asymmetry, then $k = 1$, Φ_{TR} is zero (no fission gas trapping according to the mechanism discussed in this chapter).

b) If $k > 1$, then $\Phi_{TR} > 0$ and there is some trapping of fission gas. The asymptotic value of Φ_{TR} is 1 which would require unphysically large burnup asymmetry and therefore it has no meaning.

The product of the two fractions, as described by Eq. 2 and Eq. 3, yields the fraction of fuel volume that will possess the property of trapping of the released fission gases in the sense described in section 4.3. In other words, in order to have trapping of fission gas, both pellet-clad bonding and some degree of bonding asymmetry are needed.

4.6 Best fit of calculated and measured fission gas release

The best fit between calculation and measurement, according to Eq. 1 is done by searching for optimal values of a and b in Eq. 3, as well as X in Eq. 2 such that the difference between measured and calculated FGR (see Table 9) is smallest by minimizing the root square mean error. The best fit values are 4.02 for a, 0.98 for b and $5.1 \cdot 10^6$ for X. The calculated and measured FGR without consideration of fission gas trapping was shown on Table 9. The calculated FGR without accounting for FG trapping was generally well over-predicted for the rods at the periphery and around the moderator channel. On the other hand, when fission gas trapping is calculated with Eq. 1 - Eq. 3 to best fit calculations and measurements produces an improved agreement between measurement and calculation as shown on Figure 46. It should be emphasized that the best fit coefficients (a, b, and X) for the fission gas trapping model are derived for post-processing correction, because no feedback of FG trapping on FGR are assumed. In addition, burnup asymmetry parameter (k) and integral of contact pressure (ICP) are time-dependent parameters. It is reasonable to conclude that a part of the scatter in the measured FGR can be explained by fission gas trapping in permanent partial fuel-cladding bonding layer as described in section 4.3. Furthermore, the degree of fission gas trapping is correlated with the burnup asymmetry which in turn is depended on the rod position within the fuel assembly.

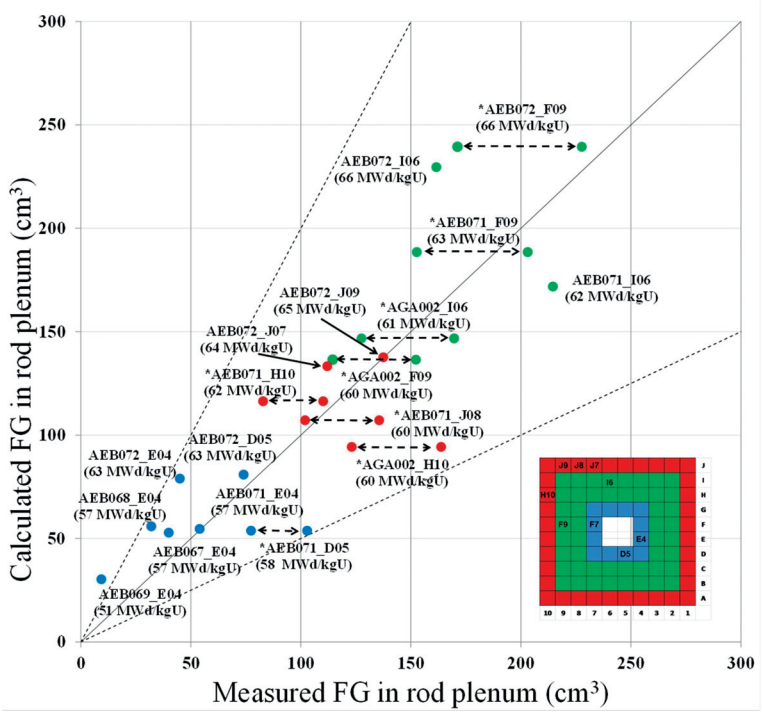

Figure 46: Calculated versus measured fission gas release into the plenum with consideration of fission gas trapping based on the model presented in section 4.5. The data points are shown as blue, green and red in order to emphasize the rod position within the fuel assembly as presented on Figure 35.

It is worth noting that there is a very small change in the green data points with respect to Figure 45 as it should be, considering the lowest burnup asymmetry, which is directly impacting the fraction of trapped fission gas as implied by Eq. 1 almost for all the other data points, there is noticeable improvement.

In conclusion, the conditions of base irradiation in a power reactor, such as e.g. contact pressure between fuel and cladding as function of irradiation time and the azimuthal non-uniformity in burnup are deemed important parameters facilitating the creation of locally trapped fission gas, which provides a reasonable explanation for the observed scatter in FGR rod puncture measurements shown in Table 9 and Figure 46. Although, the trapped fission gas may have limited impact during base irradiation, it should be considered during LOCA where significant cladding deformation and fuel fragmentation take place.

4.7 Trapped fission gas release during the LOCA

A hypothesis for fission gas trapping during base irradiation which reconciles the difference in the FGR measurements of high burnup BWR fuel rods was just presented. Its impact on the base irradiation modelling should be investigated but this trapped gas is of particular interest during LOCA. During the 12th LOCA test of the Halden LOCA test program, unexpectedly high inner rod pressure was measured. The analysis presented in [60] explained the high pressure with large burst FGR occurring during the transient. In particular, the post-test analysis suggests that 13.3% of burst FGR was needed in order to result in such high inner rod pressure.

The first explanation of this high FGR could be fuel fragmentation, especially fuel pulverization, i.e. when fuel fragments to size less than 0.1 mm. The fuel fragment size distributions for tests 12, 13 and 14 (see Table 1) showed less than 1 % of pulverized fuel. Given that the two tests were prepared from the same mother rod and experienced nearly the same transient conditions and fragmentation pattern the conclusion on the fragment size distribution could be extrapolated to test 12. This suggests that such large release of fission gas due to fragmentation could be excluded.

The hypothesis for fission gas trapping at the pellet-cladding bonding layer just discussed could be second explanation. Until the bonding layer is intact, there is no reason for the trapped gas to be released, but once it is broken, the trapped gas in the pockets at the interface will be liberated. Post irradiation examination of test 12 revealed complete pellet-cladding debonding even in a section of the rod with a low cladding strain as shown on Figure 47.

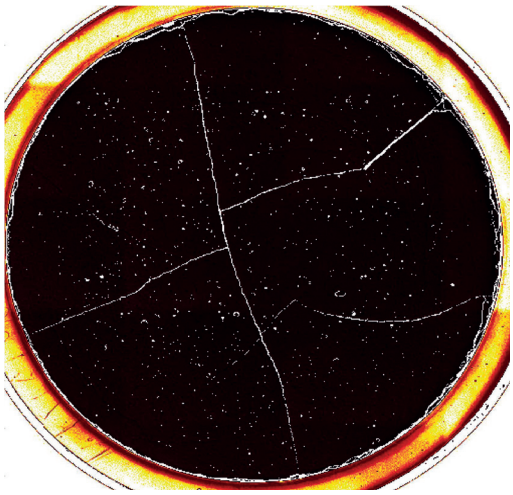

Figure 47: Macrograph of a fuel cross section (cladding outer diameter is 9.62 mm) of Halden LOCA test 12 after the test at low cladding strain. This image is post-processed from the original found in [32] in order to emphasize the fuel-cladding gap.

The fuel rod for the 12th Halden test was prepared from the rod AEB072-E4. Existence of a strong bonding layer before the test was shown on Figure 41. The digitally enhanced image on Figure 47 shows complete debonding and cracking of the bonding layer after the test.

The locally trapped fission gas is an important parameter to be considered in the modelling of a LOCA for high burnup BWR fuel. This gas will stay trapped, or at least its transport to the plenum will be strongly delayed, as long as the bonding layer is intact. Likely the release of this trapped gas happens earlier into the transient because debonding evidently occurred at low cladding strain. This can be explained by a relative displacement of fuel and cladding in the vertical direction all over the rod height, caused by the ballooning onset. Debonding of the fuel and cladding is also supported by the fast rod depressurization of Halden LOCA tests 12 and 13 (see Figure 28). It is hypothesized that any trapped fission gases are released to the rod free volume and increase the inner gas pressure. Based on the experimental data, it is anticipated that the potential for fission gas trapping due to the phenomena in question increases with burnup. It is logical to assume that the trapped fission gas may have non-negligible impact on the time to cladding rupture during the LOCA, as already elaborated in [60], and it should be considered in the modelling.

4.8 Calculation of the trapped gas in the fuel rod segments used in Halden LOCA tests 12, 13 and 14

As already mentioned, the test rods used in Halden tests 12, 13 and 14 were prepared from full-length high burnup fuel rods irradiated at KKL. In particular, rod AEB072-E4 was the mother rod for tests 12 and 13 while test 14 was prepared from rod AEB072-J09. Base irradiation calculation with FALCON/GRSW-A was done on both rods and they are also used in the database (Table 9) used for the calibration of the fission gas trapping model (Chapter 4 section 4.5). The calculated generated fission gas by the end of the base irradiation with FALCON/GRSW-A for the two rods is reported on Figure 48.

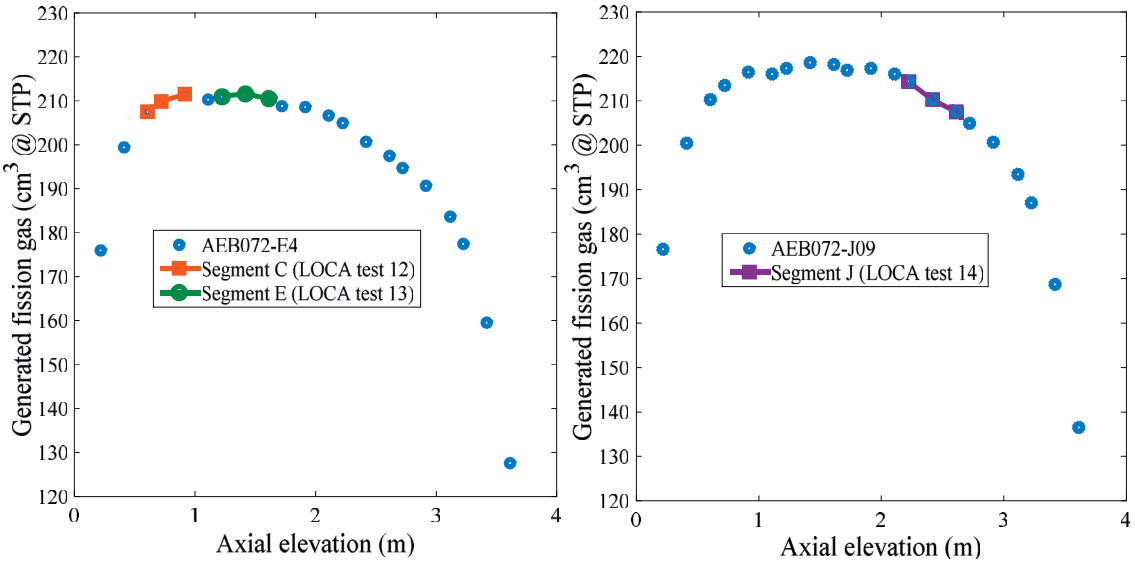

Figure 48: Calculated generated fission gas with FALCON/GRSW-A at the end of BI for rods AEB072-E4 (left) and AEB072-J09 (right).

The calculated generated fission gas for the axial segments that were used in tests 12, 13 and 14 are emphasized on the figure. The FGR model GRSW-A also evaluates the FGR for each individual axial station. A summary of those values are shown on Table 10 and illustrated on Figure 49 for test rod 12.

Table 10: Summary of the GRSW-A output concerning the rod segments used in Halden tests 12, 13 and 14 and parameters for the fission gas trapping model.

Segment ID	Generated fission gas (cm^3)	Released fission gas to plenum (cm^3)	Burnup asymmetry (k)	Φ_B	Φ_{TR}
Segment C	419	37	1.4	1	0.565
Segment E	422	39	1.4	1	0.565
Segment J	421	40	1.15	1	0.530

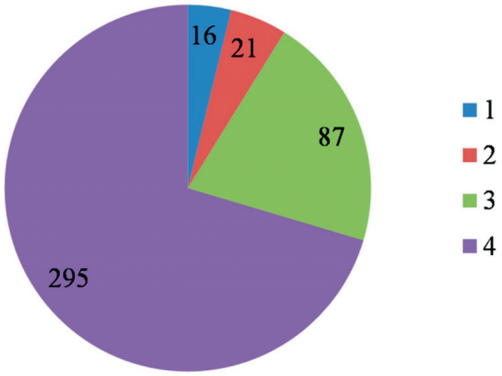

Figure 49: Decomposition of the calculated fission gas amount for test rod 12:
1+2+3+4:Generated fission gas in segment C during base irradiation (419 cm^3)
1+2: Fission gas release during base irradiation according to GRSW-A (37 cm^3)
2: Trapped fission gas in the bonding layer according to the fission gas trapping model (21 cm^3)
3: Retained fission gas in the high burnup structure according to GRSW-A (87 cm^3)
2+3: Available fission gas for the a-thermal fission gas release during LOCA (108 cm^3)

The burnup asymmetry, together with the model parameters *a* and *b* are plugged into Eq. 3 to calculate the reported values for Φ_{TR}. The bonding is fully developed and the values for Φ_B are equal to 1. Finally, using the corresponding values from Table 10 and Eq. 1, the fission gas release to the plenum from these rod segments, taking into account trapping, is presented in Eq. 4:

Eq. 4: Calculation of the trapped fission gases at the pellet-cladding bonding layers of test rods 12, 13 and 14.

$$\mathrm{FGR_{ple}}\ (\mathrm{Segment\ C}) = \mathrm{FGR_{calculated}}(\mathrm{Segment\ C}) * (1 - \Phi_B \Phi_{TR}) = 37 * (1 - 0.565) = 16\ cm^3$$

$$\mathrm{FGR_{plenum}}(\mathrm{Segment\ E}) = \mathrm{FGR_{calculated}}(\mathrm{Segment\ E}) * (1 - \Phi_B \Phi_{TR}) = 39 * (1 - 0.565) = 17\ cm^3$$

$$\mathrm{FGR_{plenum}}(\mathrm{Segment\ J}) = \mathrm{FGR_{calculated}}(\mathrm{Segment\ J}) * (1 - \Phi_B \Phi_{TR}) = 40 * (1 - 0.530) = 19\ cm^3$$

$$\mathrm{FG_{trapped}} = \mathrm{FGR_{calculated}} - \mathrm{FGR_{plenum}}$$

The calculation shows that the trapped fission gas at the pellet-cladding bonding layers of tests 12, 13 and 14 are 21, 22 and 21 cm^3 respectively. A summary of the calculated/measured fission gas release and the estimates for trapped fission gas is shown on Table 11 (see Figure 49 for test rod 12).

Table 11: Comparison of the volume of trapped fission gases at the pellet-cladding interface with the calculation and measurement of burst fission gas release during Halden LOCA tests 12, 13 and 14.

Test number	Measured/estimated FGR (cm^3)	Trapped fission gas (cm^3)
Test 12 [83]	60	21
Test 13*	60	22
Test 14 [105]	70	21

* The transient FGR in test 13 is assumed equal to the one in test 12.

The pressure measurement of test 12 (see Figure 28) allow for the estimate of the transient FGR. Unfortunately, an estimate could not be done for test 13. However, considering the close proximity of the two rod segments within the mother rod (Figure 48) and similar fuel fragmentation pattern as seen on the neutron radiography images shown in [32], it is reasonable to assume that the transient FGR in test 13 is likely similar to the one in test 12. The total FGR is about three times larger than the

estimated trapped gas. As argued in Chapter 4 section 4.7, during LOCA all of the trapped fission gases are released. This suggests that the rest of the burst fission gas release must be coming from fuel fragmentation. For the sake of discussion, let it be assumed that it came from the fuel periphery. From the base irradiation calculation with FALCON/GRSW-A, the amount of Xenon, at the end of base irradiation at the high burnup structure is 87 cm^3, 86 cm^3 and 88 cm^3 for tests 12, 13 and 14 respectively. Considering the limited fuel fragmentation in all three tests, it is logical that not all of the gas stored at the periphery was released. With reference to the above calculations, it means that 30 cm^3, 38 cm^3 and 49 cm^3 of fission gases, respectively for tests 12, 13 and 14, are coming from the periphery and therefore there is no contradiction (see Figure 49 for test rod 12). Therefore, the proposed gas trapping model provides predictions consistent both with measurements after base irradiation and during LOCA.

4.9 Conclusion

The striking scatter in fission gas release measurements, at the end of base irradiation, of high burnup (above 50 MWd/kgU) UO_2 BWR fuel rods motivated the formulation of a hypothesis for fission gas trapping in high burnup BWR fuel during base irradiation. In particular, a pair of rods at the same level of burnup coming from the same fuel assembly showed a difference in fission gas release measurement by a factor of 5. The generated fission gases per MWd are about 31cm^3 (at standard temperature and pressure), which means rods at the same level of burnup and design will have generated the same quantity of fission gas. Any difference in measured FGR, especially when it is too large, should be explained. Larger retention in high burnup structure, last cycle power, fuel type and other factors can impact the released fission gas.

Post-irradiation examination on high burnup BWR fuel showed the presence of strong pellet-cladding bonding layer including some voids/pockets. Its existence presents a potential mechanism for local fission gas trapping, and it may explain the low FGR in some of the rod-puncture measurements on high-burn fuel rods from the KKL BWR.

A model for fission gas trapping due to pellet-cladding bonding was proposed as an attempt to explain the experimental observations of FGR after BI and during LOCA experiments. The main assumption behind the model is that partial bonding between the fuel and the cladding is possible in particular for BWR fuel due to the azimuthal dependence of fuel burnup.

It must be noted that the experimental results show that such an assumption is only valid for fuel having a burnup above a threshold, the value of which needs to be determined and it may not be entirely burnup related (e.g. also rod position-dependent). A qualitative consideration can be put forward that the gas trapping must be highest for the rods around the moderator channel (a typical feature of all BWR fuel assembly designs), lower for rods at the periphery and lowest for the fuel rods in the fuel assembly interior – in line with the degree of azimuthal non-symmetry in burnup distribution as demonstrated with a Serpent Monte Carlo code calculation. An attempt to quantify the amount of trapped fission gas products in the cladding inner oxide layer may help to verify or reject this hypothesis. In the upcoming LOCA simulation phase of the work, the estimated trapped gas will be used to study its effect on the progression of cladding deformation and failure.

5
Chapter 5:
Models for fuel fragmentation, relocation and dispersal

This chapter presents all the modelling work related to fuel fragmentation, relocation and dispersal (FFRD). The contents are presented in the order that the FFRD phenomena occurs. Firstly, the modelling of fuel fragmentation is discussed with the focus being on fuel pulverization – a specific mode of fuel fragmentation in high burnup fuel during LOCA. After the fuel has fragmented and the cladding has ballooned, the necessary conditions for fuel relocation are reached. The new relocation model is presented with all of its assumptions and briefly compared with the FRELAX relocation model. In order to evaluate the effect of the fuel relocation on the cladding temperature (e.g. the hot-spot effect), a simple TRACE thermal-hydraulic model is coupled with the fuel relocation model and FALCON. Finally, the fuel dispersal model is presented together with calibration using experimental data from Halden and Studsvik's LOCA tests. The chapter is concluded with an example of fuel dispersal calculation following a simulated LOCA with a full-length fuel rod. The necessary input parameters are taken from the FALCON calculation and a prediction for the dispersed fuel and the effect of fuel relocation on the local cladding oxidation is briefly presented.

5.1 Fuel fragmentation model

Many countries operating Pressurized or Boiling Water Reactors are using as part of their licensing process the U.S.NRC Loss of Coolant Accident (LOCA) Safety Criteria (NRC Regulations 10 CFR, section 50.46). They were formulated in the 1970's based on studies with fresh or low burnup fuel. Since then, the burnup limit at discharge has been continuously increasing and this fact may require for the review of these criteria. It has been recognized that the UO_2 fuel matrix undergoes significant changes with burnup. Recent LOCA tests with high burnup fuel, such as Halden's LOCA test 9 summarized in [26] or Studsvik's test 193 described in [27], clearly demonstrated the fuel's susceptibility to fragment, easily relocate and be dispersed through the cladding rupture. Efforts to better understand the fuel fragmentation, relocation and dispersal phenomena are on-going within the nuclear fuel community.

It appears that fuel fragmentation during normal operation is already well-modelled. The papers [106] and [107] discuss models for radial and axial cracking during power ramping. The implications are on fuel-cladding gap closure, reduction of fuel thermal conductivity and increase of heat transfer due to PCMI. Yet, these models do not address fragmentation during LOCA and to the student's knowledge such models do not yet exist at least in the open literature.

Strictly speaking, it is necessary to consider the model for fuel fragmentation during LOCA as being made up of two separate models, because two different mechanisms are responsible for the fragmentation. On the one hand, fragmentation in the pellet interior is caused by thermal stress relief when the temperature profile flattens during a LOCA which can lead to rather large fragments (> 1mm) and on the other hand over-pressured bubbles cause grain decohesion at the high burnup structure (HBS) when the back pressure provided by the cladding wall is lost due to ballooning and the

fuel 'pulverizes' to fragments smaller than 0.1 mm. From the point of view of fuel relocation and dispersal, the small fuel fragments (e.g. pulverized fuel) are more interesting, because they are highly mobile and could in principle fit through all cladding rupture openings. It follows that fuel pulverization is considered much more relevant for the present study. On the other hand, fuel fragmentation due to thermal stresses would be important for the heat transfer from the rod to the outside, because cracking deteriorates the heat conduction. Such effects cannot be evaluated in a post-processing manner, but rather should be implemented into the fuel behaviour code as it is done in [108]. The paper by Walton and Husser [109] discusses the crack patterns on more than 60 fuel samples up to burnup of 35 MWd/kgU. They correlated the number of radial cracks as function of power and burnup, where they appear to saturate around the value of 12. Correlations for radial, axial and circumferential cracks can be derived, and when combined, the fragmentation of the pellet interior can be simulated (combination of all three cracks do define individual fragments), but this does not add much to the relocation or dispersal models, nor does it actually address the reasons behind the fragmentation. Nevertheless, this fragmentation does have negative effect on the heat transfer through the fuel.

5.1.1 Fuel pulverization model

The model presented here is fully adopted from the work presented in [31], which were already used in a similar manner in section 2.2 of the paper [108]. The conditions for fuel pulverization are local burnup greater than 71MWd/kgU and local fuel temperature larger than 645°C. Local burnup across the fuel pellet radius is calculated by FALCON with the TUBRNP [56] model. In order to automate the procedure, a Gaussian fit to the calculated radial power distribution is applied as shown on Figure 50 and the equation is solved numerically for $R_{INTERSECT}$ – the distance from the pellet centre at which the local burnup becomes higher than 71 MWd/kgU.

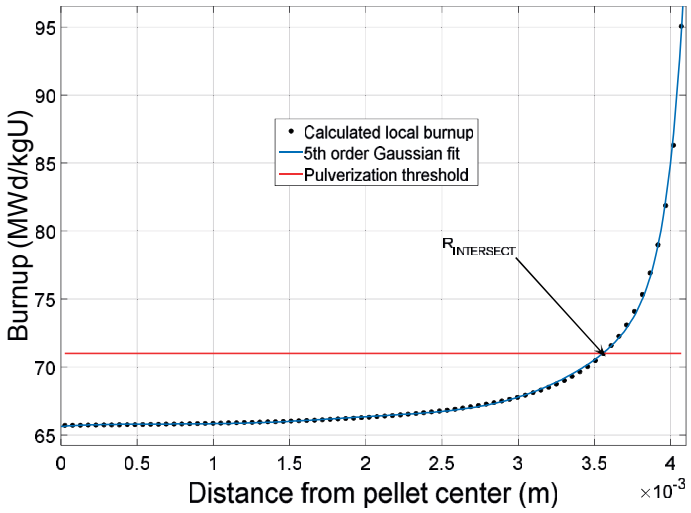

Figure 50: Methodology to obtain the fraction of pulverized fuel from the input of radial burnup distribution in the fuel pellet.

The fraction of pulverized fuel can then be determined according to Eq. 5, where R_{FUEL} is the fuel pellet radius.

Eq. 5: Calculation of the fraction of pulverized fuel.

$$Pulverized\ fuel\ fraction = \frac{R_{Fuel}^2 - R_{Intersect}^2}{R_{Fuel}^2}$$

To give quantitative predictions, it is necessary to know the mass of pulverized fuel not simply the fraction. If the axial burnup distribution is constant, then mass is simply equal to the fraction multiplied by the total mass of the fuel. Although in short fuel rods, such as the Halden LOCA tests, the axial burnup can be assumed constant, for full-length fuel rods (reactor-case) this is not correct (see Figure 36 right in Chapter 4). For this reason, the mass of pulverized fuel must be evaluated for every axial elevation and then the total can be used to calculate the fraction of movable fuel for the fuel dispersal model (see section 5.3).

During the transient analysis, the local temperature is continuously monitored, and as soon as it increases above the threshold of 645°C the time of fuel pulverization is recorded and from that time onwards, pulverized fuel is available for relocation. The two conditions for pulverization are checked for all axial levels and since axial burnup can vary significantly, such as in BWR fuel, some parts may not be subject to pulverization at all. In the case of Halden LOCA tests 12 and 13, the fuel rods are roughly 40 cm long and therefore the burnup can be assumed uniform. In full length rods this will not be the case. In summary, the fuel pulverization model calculates the volume of pulverized fuel for all axial stations and assuming spherical shape of diameter 100μm the number of fuel fragments can be calculated.

Since fragmentation reduces density, the assumption is that the pulverized fuel, which is assumed to be made up of the same particle size, arranges in the densest possible packing – which is the hexagonal close packing of spheres with a packing factor of 0.74048 – a value that can be easily derived. It follows that the volume of pulverized fuel expands by factor of 1/0.74048 = 1.35. This means that pulverization occurs after some cladding deformation occurs. If cladding does not deform, then pulverized fuel is not evaluated even if the temperature and local burnup conditions are reached. This goes in line with the observation that extent of fuel fragmentation is dependent on cladding strain as observed in the post-irradiation examination of Halden LOCA test 5 [26]. Also [70] demonstrated that hydrostatic restraint pressure suppresses fission gas release and fragmentation when high burnup fuel samples are heated up. Therefore, in a LOCA, fuel pulverization will not occur before the hydrostatic restraint pressure supplied by the cladding or the inner rod pressure (in case of open gap) is sufficiently low. This suggests that loss of contact between the fuel and cladding does not necessarily immediately cause pulverization.

5.2 Fuel relocation model

5.2.1 Introduction

Fuel relocation during simulated Loss-of-Coolant Accident has been investigated already more than 30 years ago in the KfK BR-2 program [110] and the PBF LOCA Test Series [111]. Back then, tests were performed with fresh or medium burnup fuel by today's standards (35 MWd/kgU at maximum) and a coarse fuel fragmentation was observed. The packing factors in the balloon were very low – about 35 % according to the data analysis done by Siefken in [88]. Furthermore, he concluded that due to the low packing factor in the balloon and the increased cladding surface area there is no risk of increased local linear heat generation (no hot-spot effect). Nowadays, the situation has changed and a fresh look into the fuel relocation phenomena is necessary. For example, Halden LOCA test 4 [26] demonstrated significant fuel fragmentation, relocation and dispersal (see Chapter 3 section 3.4.2) . The main parameter that has changed is the level of burnup. Formation of the so-called High Burnup Structure (HBS) is characterized by very small fuel grain sizes and larger gas-filled pores. The HBS has been shown to fragment to pieces below 0.1 mm – which is also referred to as "fuel pulverization" (see section 5.1.1). This is a game changer in the discussion regarding axial fuel

relocation during LOCA, because these powder-like fragments can easily relocate and fill up the voids between larger pieces of fuel fragments – thereby increasing the local packing factor and challenging the earlier conclusion by Siefken, that fuel relocation does not create cladding hot-spots.

Fuel relocation can be segregated into three modes: relocation during normal operation, gravity-driven relocation during cladding ballooning in LOCA and fuel relocation driven by the gas outflow after the cladding burst. The first occurs during normal operation when the UO_2 ceramic fuel pellet cracks under the thermal stresses induced by the non-uniform temperature across the fuel. The cracking makes the fuel pellet move radially outward towards the inner cladding wall. The eventual closure of the fuel-cladding gap improves pellet-clad heat transfer, but the cracks also degrade the thermal conductivity [107].This movement of fuel fragments is termed fuel relocation and it is modelled in fuel performance codes such as FALCON [50] by reducing the smeared fuel density. The consequence of cracking and fuel relocation is partial closure of the initial pellet-cladding gap. The effect of it can be significant, because the cracking may even challenge the integrity of the fuel cladding (PCI failure) – the first barrier against release of radioactive materials in the defence-in-depth concept.

In LWR the fuel pellet is designed as a solid cylinder. During reactor operation it was recognized that the phenomena of hour-glassing, depicted on Figure 51, may occur and cause very large localized mechanical stresses of the cladding.

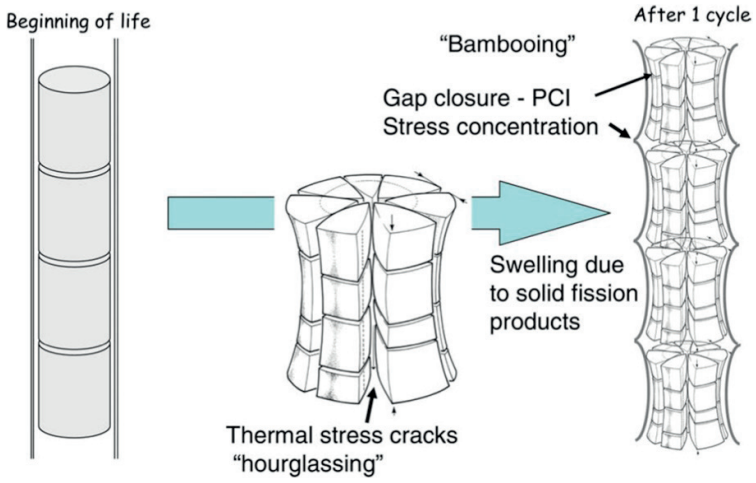

Figure 51: The process of hour-glassing [112].

At the beginning of life, all fuel pellets are arranged in a "perfect" stack and everything looks normal. During power ramp, the fuel cracks according to the shown pattern and this creates the "spots" of stress and local strains of the cladding, referred to as 'ridges'. To mitigate this effect, chamfers were introduced to the fuel pellet design which basically smooths the edges of the fuel pellet.

All in all, the radial fuel relocation affects the effective pellet-gap size thus affecting PCMI. Furthermore, a single crack in the pellet may cause a concentration of local stress in the adjacent cladding and provide the paths for iodine, which is deemed to play a key role in Iodine-Induced Stress Corrosion Cracking PCI failure [113, 114].

During LOCA transient, additional mechanism is unlocked which is driven by gravity. Additional fuel fragmentation does occur during a LOCA and this is an experimentally established fact. Typically, a fragment size distribution which includes both very small and large pieces describes the fragmented fuel. In particular, the small fragments are very mobile and the ballooned cladding provides the necessary condition for axial fuel relocation driven by gravity. Fuel fragmentation is correlated with

the level of burnup: it has been observed that the higher the burnup the smaller the fuel fragments, but this is not general, because it is not the only parameter. For example, Studsvik's LOCA tests 191, 192 and 193 had approximately the same average burnup as Halden tests 12, 13 and 14 but the former fragmented to much smaller fragments. Extent of cladding ballooning and therefore the available room for fuel relocation is very dependent on the transient and mechanical state of the cladding. A "slow" transient in which the internal pressure and cladding temperature increases at a lower rate may allow for more plastic deformation and therefore larger volume and promote more axial fuel relocation.

The third mode of relocation involves the solid-gas interaction after fuel rod rupture. As soon as the cladding fails, the interfacial friction between the gas and the fragmented fuel may set loose fuel fragments in motion. These can be either expelled from the rod or simply relocated downwards.

In the modelling of fuel dispersal discussed in this dissertation, explicit relocation of additional fuel promoted by the gas outflow is neglected. This is not to say, that this mechanism is not important. For example, even after fuel rod failure the cladding continues to oxidize which is driven by the decay heat which in turn is proportional to the local quantity of fuel. Additionally, it may happen that the gas outflow pushes a larger fragment that cannot fit through the cladding rupture opening but it may in fact prevent more fuel to be dispersed. Accurate modelling of such scenario is at the moment impossible and it is subject to large uncertainties because neither cladding ballooning nor fuel fragmentation and relocation can be modelled exactly.

5.2.2 Model parameters and assumptions

Assuming the axial and radial fragment size distribution and the axial cladding hoop strain are precisely known, modelling of axial fuel relocation is mainly a geometrical problem. Some assumptions, such as spherical fragment shape, however, are necessary. Another assumption in the model is that outermost fuel fragments relocate first. Since cladding deforms radially outward, the first fuel fragments which will be freed to relocate are those at the periphery. As they relocate downwards, they will enable the next set of fragments to follow provided there is available room below. The implication of this assumption is that those fragments with highest decay heat power density will be relocated in the balloon. As a consequence, the heat load at the balloon may be seriously modified and create the conditions for a stronger "hot-spot" effect. The effect of this will be increased local cladding oxidation which should be evaluated.

The model for fuel relocation takes as input the cladding deformation evaluated by FALCON, axial distribution of fuel fragmentation, either calculated by the fuel fragmentation model or given by the user and some geometrical parameters. At each time step and axial level, the cladding hoop strain, $\varepsilon_{\theta\theta}\,(t_i, Z)$, is checked against the threshold for relocation ϵ_{TH}. This value is debatable and it certainly depends on the fuel fragment size – which is influenced by burnup. A value of 5% for ϵ_{TH} is derived based on Halden LOCA tests [26] with high burnup fuel and it is used in this model. Relocation cannot occur until sufficient cladding hoop strain is present. If the strain is larger, then fuel can relocate, otherwise not and the model moves to the next calculation step. This condition is expressed by Eq. 6.

Eq. 6: Condition on the cladding hoop strain to allow fuel relocation.

$$\varepsilon_{\theta\theta}\,(t_i, Z) > \epsilon_{TH}$$

Given the hoop strain is larger than the threshold for relocation, then the current axial station, Z, of the fuel rod can relocate fuel and consequently can also accept fuel fragments coming from the station

above. This means that condition in Eq. 6 must be checked for the axial station Z+1 leading to the formulation of Eq. 7.

Eq. 7: Necessary condition for axial fuel relocation from axial station Z+1 to axial station Z.

$$if(\varepsilon_{\theta\theta}\,(t_i, Z) > \epsilon_{TH} \quad \&\& \quad \varepsilon_{\theta\theta}\,(t_i, Z+1) > \epsilon_{TH})$$

Now that it has been verified that fuel relocation between axial stations Z and Z+1 can take place, the code moves onto determining the fragment size class which will be relocated. At each axial station there is a unique fragment size distribution which can either be set by the user or provided as input by a fuel fragmentation model. The assumption is that fuel relocation starts with the outermost fuel fragments and ends with those closest to the pellet centre. This is a logical assumption, because under a ballooned cladding the outermost fragments will become movable first and if fuel fragmentation is driven by loss of contact between the fuel and cladding, then this occurs first at the periphery when the cladding balloons. As a first step, the relocation model finds which the outermost fuel fragment size is. Then, it calculates the available volume for relocation based on the formulas expressed in Eq. 8. In reality, the available volume cannot be fully filled, and this fact is accounted for by multiplying the available volume with a maximum packing factor for relocated fuel, φ_{MAX}, which in this model is set equal to the theoretical maximum packing factor of 0.74 for equal-sized spheres. In the event where much smaller spheres are mixed with large ones the packing factor of the mixture may even exceed 0.74. All in all, this parameter is subject to large uncertainty, because it depends on the fuel fragment sizes and their shapes.

Eq. 8: Calculation of the available volume for fuel relocation into axial station Z.

$$availableVolume(t_i, Z) = total\ avaliable\ volume - volume\ occupied\ by\ the\ fuel$$

$$total\ avaliable\ volume = V_B(t_i, Z) = \pi\left(\left(R_f(1 + \varepsilon_{\theta\theta}(t_i, Z)\right)^2\right) H(Z) \cdot \varphi_{MAX}$$

$$volume\ occupied\ by\ the\ fuel = V_F(t_i, Z) = \frac{\sum N_{J,Z}(t_i) V_{J,Z}}{\varphi_{MAX}}$$

The total available volume is multiplied with the maximum packing factor to obtain the volume that could potentially be filled with fragments. Similarly, when calculating the volume occupied by the fuel, the maximum packing factor needs to be included. The fuel relocation model must deal with two different cases: when the volume of the fragments exceeds the available volume and when it is smaller. In the first case, only part of the fragments is relocated and in the second – all of them, which requires the code to seek the relocation of other fragments. This, also, gives rise to two possibilities. Under the assumption that the outermost fuel fragments relocate first, the code looks into the axial station Z+1 and checks for presence of the outermost fragments. They may have been relocated already, or it may be that they are ready to be relocated. Without going further into the details, the code either relocates fuel from axial station Z+1 down to Z or relocates from Z+2 or even from upper stations. Realistically, if the outermost fragments from axial station Z+1 relocate, then there is no reason for the outermost fragments in axial station Z+2 to stay motionless if the threshold for relocation is reached. Instead, they will also relocate. The code assumes that such is the case. As a final detail, the model keeps track of the axial position of every individual fragment size. As an example, a given fragment size has 10'000 fragments. They can be distributed unevenly among different axial stations. This information is absolutely needed for the model to function as described. All of the input parameters for the fuel relocation models are shown in Table 12.

Table 12: Description of fuel relocation model parameters.

Parameter	Description	Units
t_i	The ith time step	-
R_f	Original fuel radius	m
$\varepsilon_{\theta\theta}(t_i, Z)$	Cladding hoop strain at time t and axial elevation Z	-
$V_B(t_i, Z)$	Volume created from ballooning at time t and axial station Z (m^3)	m^3
$V_F(t_i, Z)$	Volume of the fuel fragments present at axial station Z (m^3)	m^3
$H(Z)$	Height of the axial station Z	m
$N_{J,Z}$	Number of fuel fragments of size class J originating from axial station Z	-
$V_{J,Z}$	Volume of the fuel fragment size class J originating from axial station Z	m^3
$BU_WF(J, Z)$	Burnup weight factor for fragment size class J originating from axial station Z	-
$W(J, Z)$	Decay heat power of fragment class J originating from axial station Z	W/m^3
$W(t_i, Z)$	Decay heat power at time step t_i and axial station Z	W/m^3
$A_{PF}(t_i, Z)$	Axial power factor at time step t_i and axial station Z	-
ϵ_{TH}	Threshold for axial fuel relocation	-
φ_{MAX}	Maximum packing factor for the relocated fuel	-

5.2.3 Calculation of relative change in LHGR

During the axial fuel relocation, there is essentially transfer of decay heat source from one axial elevation to another. This means that the local linear heat generation rate is changed. Consideration of this phenomenon is greatly simplified here but nonetheless it is being considered. It is a fact that the level of burnup across the fuel pellet radius is not the same. Instead, it is highest at the periphery and lowest at the centre. Considering that burnup is directly related to the amount of fissions, which in turn produces radioactive fission products, it follows that a fuel fragment originating at the pellet periphery must have higher decay heat source density than a fragment with the same size originating near the fuel pellet centre. In order to address this fact, the model extracts the radial burnup profile, divides it into sections, each of which is corresponding to the location of each fragment size (Figure 52), extracts the burnup level and finally divides it with the burnup of the fragment size class with lowest burnup to obtain the burnup weight factors.

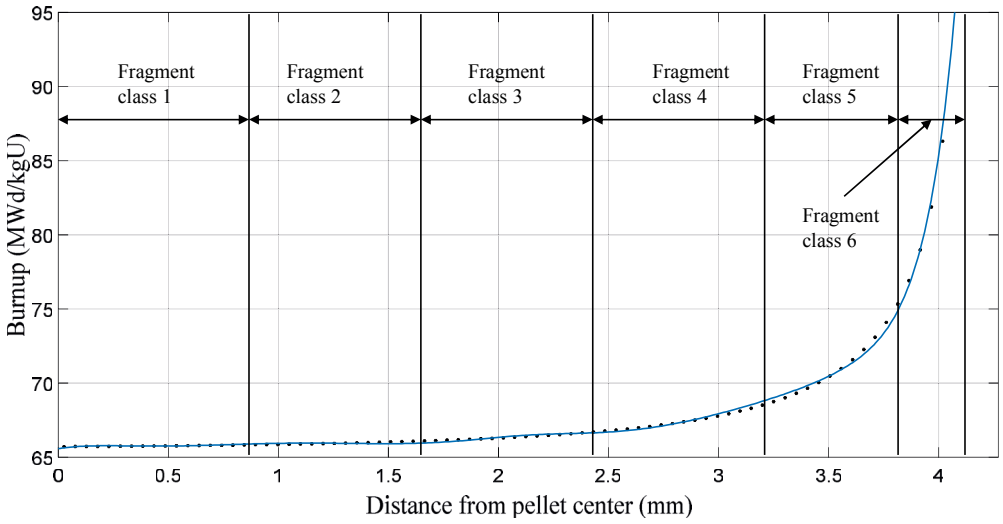

Figure 52: Division of the fuel stack axial station Z into regions corresponding to the location of the different fragment size classes.

The burnup weight factors are collected in the matrix denoted by $BU_WF(J, Z)$. These factors are used in the calculation of the relative change in the axial power shape. It follows that the assumption that

the outermost fragments relocate first becomes important because the balloon will be filled with the "hottest" fuel fragments – those originating from the pellet periphery. The heat power density of each individual fragment is an unknown parameter. An assumption is made that the true heat power density for each fuel fragment is equal to an unknown but averaged parameter W_{Decay} , which has units of W/m^3, and which is multiplied by the burnup weight factor $BU_WF(J,Z)$. It follows that the decay heat power density of fragment class J and axial location Z can be expressed with Eq. 9.

Eq. 9: Evaluation of the decay heat power density.

$$W(J,Z) = W_{Decay} BU_WF(J,Z)$$

It follows that the decay heat power density at time step t_i and axial station Z can be evaluated by considering all fuel fragments at axial station Z and their corresponding decay heat power densities according to Eq. 10.

Eq. 10: Calculation of the decay heat power density at axial station Z.

$$W(t_i,Z) = \sum_J N_{J,Z}\, W(J,Z)$$

Given these assumptions, a relative change in the axial power shape, taking into account axial fuel relocation, can be evaluated for each time point with Eq. 11.

Eq. 11: Calculation of the relative change in axial power shape.

$$A_{PF}(t_i,Z) = \frac{\sum_J N_{J,Z}(t_i)\, W(J,Z)}{\sum_J N_{J,Z}(t_0)\, W(J,Z)} = \frac{\sum_J N_{J,Z}(t_i)\, W_{Decay} BU_WF(J,Z)}{\sum_J N_{J,Z}(t_0)\, W_{Decay} BU_WF(J,Z)} = \frac{\sum_J N_{J,Z}(t_i)\, BU_WF(J,Z)}{\sum_J N_{J,Z}(t_0)\, BU_WF(J,Z)}$$

Finally, a table with the time-dependent axial power shape is output which is prepared for input into the TRACE model discussed in section 5.2.6.

5.2.4 Preparing fuel fragment size input for the relocation model

This section describes the necessary input data for the fuel relocation model. In principle, once a full fuel fragmentation model is implemented, the effort from the user will be reduced, but at this stage for purpose of testing the model the input is provided manually. The model is programmed to allow the user to specify unique fragment size distribution for each axial station and the description begins with supplying the fuel fragments.

There are three pieces of input that need to be prepared: the number of fragments for each fuel fragment size at every axial station, their volumes (assuming spheres) and their position with respect to the fuel pellet centre. The last information is needed in order for the code to extract the burnup weight factors $BU_WF(J,Z)$ according to Figure 52. The radial position is the average of the radial coordinates of the boundaries for each fragment size. The input is arranged in 2-dimensional arrays. Table 13 below shows an example when all axial stations have the same number of different fragment size classes.

Table 13: Example for the input matrix with the number of fuel fragments for each fragment size class assuming all axial stations have equal number of fuel fragment classes.

Axial station	$N_{1,Z}$	$N_{2,Z}$	$N_{3,Z}$	$N_{4,Z}$	$N_{5,Z}$	$N_{6,Z}$
$N-2$	$N_{1,N-2}$	$N_{2,N-2}$	$N_{3,N-2}$	$N_{4,N-2}$	$N_{5,N-2}$	$N_{6,N-2}$
$N-1$	$N_{1,N-1}$	$N_{2,N-1}$	$N_{3,N-1}$	$N_{4,N-1}$	$N_{5,N-1}$	$N_{6,N-1}$
N	$N_{1,N}$	$N_{2,N}$	$N_{3,N}$	$N_{4,N}$	$N_{5,N}$	$N_{6,N}$
$N+1$	$N_{1,N+1}$	$N_{2,N+1}$	$N_{3,N+1}$	$N_{4,N+1}$	$N_{5,N+1}$	$N_{6,N+1}$
$N+2$	$N_{1,N+2}$	$N_{2,N+2}$	$N_{3,N+2}$	$N_{4,N+2}$	$N_{5,N+2}$	$N_{6,N+2}$

It can also happen that the axial stations do not have the same number of fuel fragment size classes. In this case, the input is prepared according to the example shown on Table 14. Basically, the width of the matrix is determined from the axial stations with the largest number of fuel fragment classes and in this example it is 6. For those stations with less than 6 fragment size classes, zeros are used as placeholders. The input matrices for the volume look identical. The code still relocates the outer-most fuel fragments.

Table 14: Example for the input matrix with the numbers of fuel fragments for each fragment size class assuming axial stations have different number of fuel fragment classes.

Axial station	$N_{1,Z}$	$N_{2,Z}$	$N_{3,Z}$	$N_{4,Z}$	$N_{5,Z}$	$N_{6,Z}$
$N-2$	0	$N_{2,N-2}$	$N_{3,N-2}$	$N_{4,N-2}$	$N_{5,N-2}$	$N_{6,N-2}$
$N-1$	0	0	$N_{3,N-1}$	$N_{4,N-1}$	$N_{5,N-1}$	$N_{6,N-1}$
N	0	0	0	$N_{4,N}$	$N_{5,N}$	$N_{6,N}$
$N+1$	0	0	0	0	$N_{5,N+1}$	$N_{6,N+1}$
$N+2$	$N_{1,N+2}$	$N_{2,N+2}$	$N_{3,N+2}$	$N_{4,N+2}$	$N_{5,N+2}$	$N_{6,N+2}$

Although the input can be arranged in simple 2-dimensional matrices, in order to keep track of the relocated fuel fragments a more complicated data structure is needed. In this case, the MATLAB cell array was found suitable. A cell array is an array which can store as elements single numbers, multidimensional arrays of numbers or even other cell arrays. The advantage is that a 1-dimensional cell array can be used to represent the axial stations with the relocated fuel fragments. Therefore, within each cell of the array a 2-dimensional matrix can be stored. All matrices have different number of rows equal to their axial station number. For example, axial station 20 needs to have a 2-dimensional array with 20 rows, because it can happen that the fuel fragments initially located at axial station 20 are now relocated potentially among all other axial stations. Following this logic, axial station 1 has one row, axial station 5 has 5 rows and axial station N has N rows. Therefore, the initial simple 2-dimensional array with the initial number of fragments is automatically converted into cell arrays by the relocation model.

One certain advantage for providing the fragment size distribution in this way is the fact, that it is not necessary to run base irradiation followed by LOCA simulation to get the pulverized fuel. This can be calculated from the BI state using the radial burnup distribution (e.g. Figure 50).

5.2.5 Comparison with the fuel relocation model of FRELAX

Fuel relocation model has been already incorporated into FRELAX [61] – a Halden LOCA test's specific model for axial gas transport and fuel relocation. There are differences between FRELAX's model and the fuel relocation model considered in this thesis and the purpose of this section is to discuss them.

The first difference is that FRELAX considers uniform fuel stack slumping. This means that there is no preferential relocation of fuel fragments either from the periphery or the pellet interior, the relocated fuel is treated as well-mixed. The mechanism behind is that the cladding deformation results first in radial displacement of the fuel fragments. This forms open spaces inside the pellets into which the fragments from above may fall down, causing the axial relocation. Overall, such mechanism is feasible for both high and low burnup fuel, but the resulting effect will essentially depend on the fragment size-distribution and fill ratio. An average fragment size is assumed, but it is actually used in the calculation of the resistance to axial gas flow and not in the fuel relocation itself. However, the increasing amount of pulverized fuel at the pellet periphery with high susceptibility to relocation may cause an additional mechanism.

The model proposed here, on the other hand, considers a fragment size distribution, assumes preferential relocation from the periphery into the balloon and treats the fuel fragments as spheres of different sizes.

In order to compare the two fuel relocation models, the new relocation model was added as an option to FRELAX. The relative increase in local LHGR, compared with the initial state, shown on Figure 53, is able to highlight the differences.

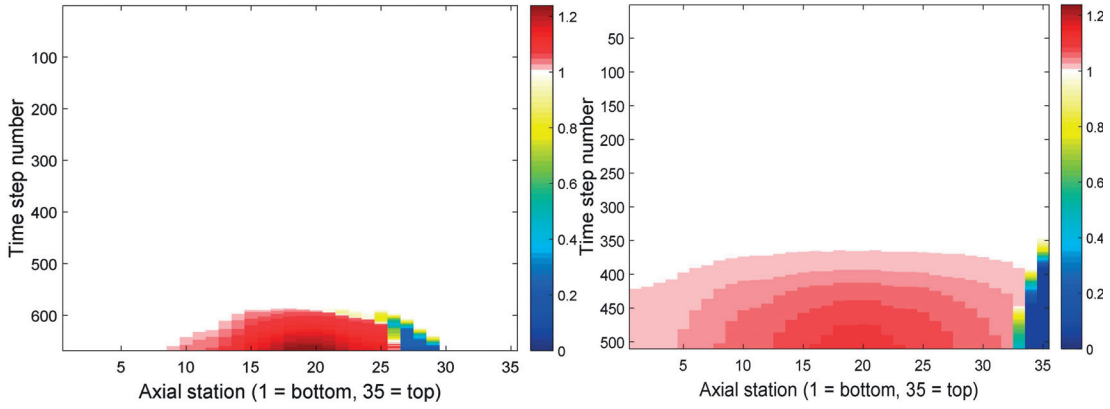

Figure 53: Axial distribution of relative increase in decay heat power during LOCA simulation of Halden test 12 evaluated with the new (left) and original (right) model for fuel relocation in FRELAX.

Few things can be said between the two models. The new relocation model evaluates fuel relocation only if the cladding hoop strain is larger than some threshold as it is evidenced by the fact that the top and bottom of the rod, for the case calculated with the new model, have no change in the relative LHGR. The blue colour on the colour-maps indicates reduction in local LHGR, the red colour – an increase and the white colour – no changes. Furthermore, higher local decay heat power is concentrated at the balloon (around axial station 18) for the reason that the relocated fuel is not re-distributed over the whole length of the rod and also due to the preferential relocation of "hotter" fuel into the balloon.

Relative increase in LHGR is expected to result in larger local cladding temperature and this will have an impact on the local cladding oxidation as it is shown in section 5.4.4. At this time it remains unclear

whether fuel relocation can reduce the time to cladding failure, because the ballooning is a process which occurs within some tens of seconds. With this in mind, the relocation model described in [34], does show reduction in the time to cladding failure when fuel relocation is considered. On the other hand, in [37] it is demonstrated that delayed axial gas redistribution does have an impact on the time to cladding failure. Additionally, Haste T.J. [115] showed that there is a delay in the mixing of the fission gases with the rest of the gas (mixture of Helium and FGR prior to the transient) which has an effect on the gas conductivity. Therefore, under the presence of blockage and the inability of the transient fission gas release to mix with the rest, there will be further temperature amplification due to the much lower thermal conductivity of the gas in the balloon. The effect of the plenum size was discussed in [116].

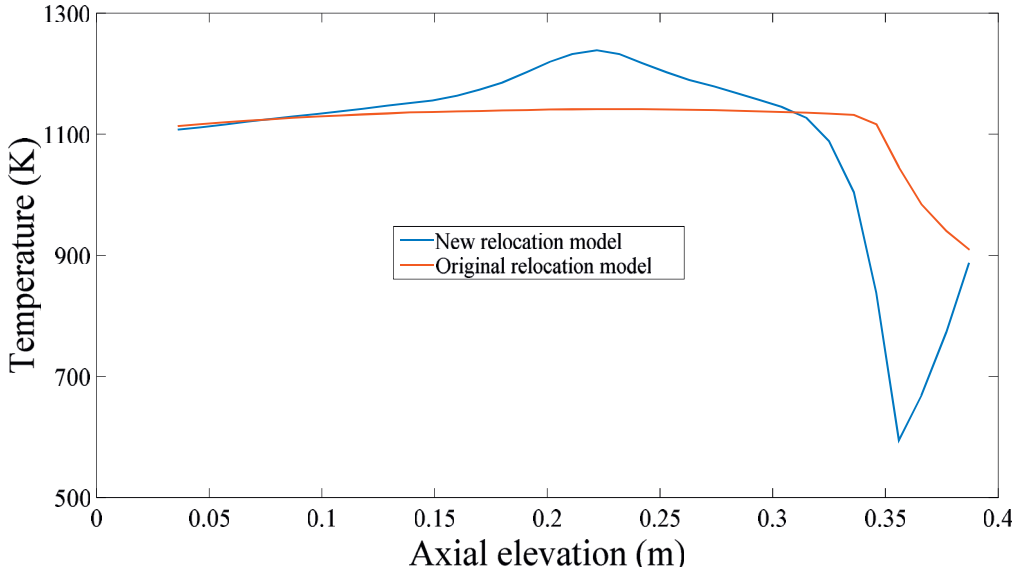

Figure 54: Calculated cladding temperatures by FRELAX with the original and updated models for fuel relocation.

The axial profile of cladding temperature calculated by FRELAX at the moment of clad burst in LOCA test 12 with both models is shown on Figure 54. The temperature at the top of the rod on the blue curve is because the relocation threshold was not reached. A significant difference around the balloon in the calculated cladding temperature profile is evident. There is a well-defined peak coming from the relocation model discussed here. It is caused by the amplification of the LHGR at the balloon. On the other hand, the cladding temperature evaluated with FRELAX's own model does not appear to have a strong peak. This could be explained with the fact that the relocated fuel is more spread-out along the length of the rod as it was shown on Figure 53 and also it does not reflect the preferential relocation of fuel fragments from the fuel periphery which have higher decay heat density.

In conclusion, the purpose of this sub-section was to discuss the differences between the two models. The comparison shows that a predominant relocation of the pulverized fuel from the pellet periphery may have a significant effect on the local cladding temperature (e.g. hot-spot effect). However, the analysis of the Halden data from gamma scanning (see Appendix A) does not give a clear evidence of such relocation, although this cannot be said with certainty because of the high uncertainty in the gamma scan data. All in all, the further experimental investigation can be recommended for more precise parameterization of models. Some proposals are given in section 6.3.5 of Chapter 6.

5.2.6 TRACE model for sub-channel LOCA simulation

A typical large break LOCA is represented as a guillotine break of a main circulation line. Due to the large rupture, the reactor depressurizes quickly and the water level drops leaving part of the core fully uncovered. After the actuation of the emergency core cooling systems (ECCS), the water level in the core begins to rise again and if the LOCA is successfully terminated the core will be re-flooded and none of the LOCA fuel safety criteria (see section 1.9) will be violated. In the introduction of FALCON in section 2.1 it was mentioned that LOCA boundary conditions (outer cladding temperatures) can be given as input from an external thermal-hydraulic code calculation.

A simple TRACE model kindly provided by K. Mikityuk, illustrated on Figure 55, is proposed which captures the main events in a LOCA – the depressurization, actuation of ECCS and core re-flood. The calculated outer cladding temperatures are input to FALCON to evaluate the fuel rod behaviour.

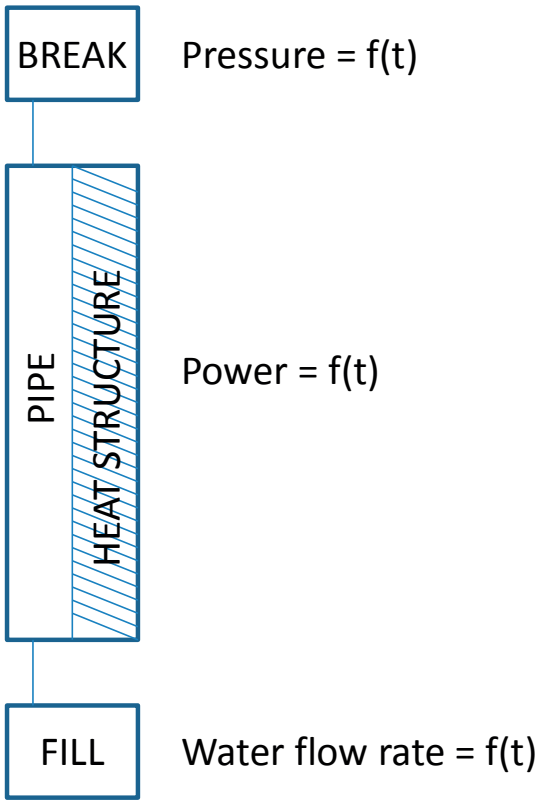

Figure 55: TRACE model for simulating the cladding outer surface temperature conditions during LOCA.

Simulation of a reactor-case LOCA will be as complicated as the TRACE model. In this case, the simplest approach is taken. The model consists of four components: Break, Pipe, Fill and Heat structure. The break essentially simulates the pressure evolution in the core (see Figure 56 left). The Fill component controls the flow rate of liquid water into the system (see Figure 56 right). In particular, it represents the time of actuation of the ECCS. Even with this simple model, by varying the input of the Break and Fill components different LOCA conditions can be simulated. If the mass flow of coolant is too low (e.g. due to partial failure of the ECCS), or the actuation of the ECCS is delayed, then the core may remain uncovered long enough to cause problems for the fuel rod integrity. On the other hand, if the mass flow of the coolant is large and it is injected shortly after the simulation of the LOCA starts, then the calculated cladding temperatures may not become high enough to cause fuel rod failure. The input via the Fill component indirectly determines the size of the balloon (if any). If the input mass flow is too low, or the actuation is delayed, then cladding temperatures will remain high

enough to cause rod ballooning, for example. Clearly the input via the Fill component can generate boundary conditions that will impact the fuel cladding deformation calculated by FALCON. Finally, Heat Structure component is used to represent the fuel rod. For the purpose of a LOCA simulation, only the decay heat power following the reactor SCRAM is given as input (see Figure 56 middle).

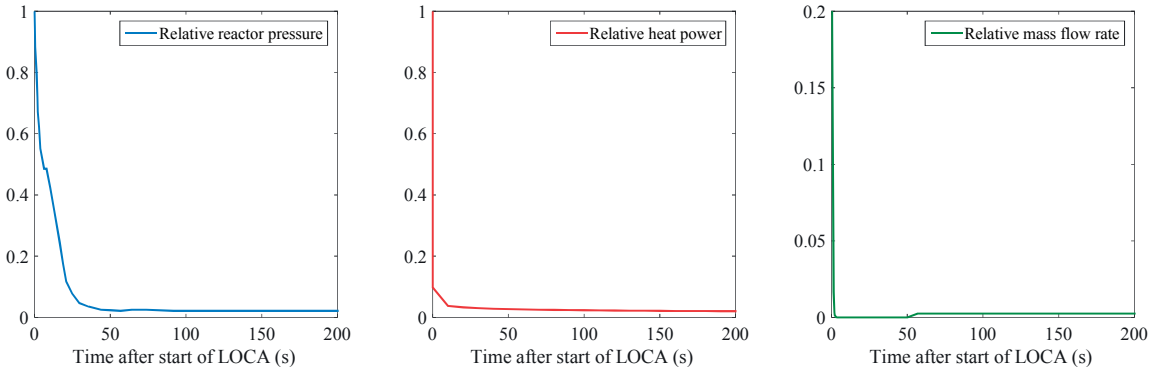

Figure 56: Reactor pressure, fuel rod power and channel mass flow rate evolutions used to simulate LOCA.

In conclusion, this simple model is sufficient for the purposes of providing adequate boundary conditions to evaluate the FFRD phenomena with FALCON and to apply the developed models on a full-length fuel rod (see section 5.4). Yet, the model is flexible enough to obtain conditions for different sized balloon and at different axial elevations and in principle it can be used to provide sensitivity study data for the fuel dispersal model.

5.2.7 Coupling between TRACE – FALCON – MATLAB

TRACE does not have explicit provisions to take into account fuel relocation in the calculation of cladding temperature. A workaround is proposed in which the fuel relocation model evaluates the changes in the axial power profile of the fuel rod, whose shape in a LOCA accident without fuel relocation can be considered constant in time, but in the event of fuel relocation, this is no-longer valid. Considering fuel relocation, input with time-dependent axial power profile is prepared for TRACE, which then evaluates the cladding temperature. The suitability of this approach to capture the effects of fuel relocation can be questioned, because fuel relocation results not only in the local change of LHGR but also in the fuel mass which is not taken into account in the current approach. This simplification can have an impact on the transient evolution of clad temperature. The proposed coupling is logical, because the fuel relocation model is developed in MATLAB, TRACE provides the boundary conditions and FALCON evaluates the ballooning. This is visualized with the flow chart shown on Figure 57.

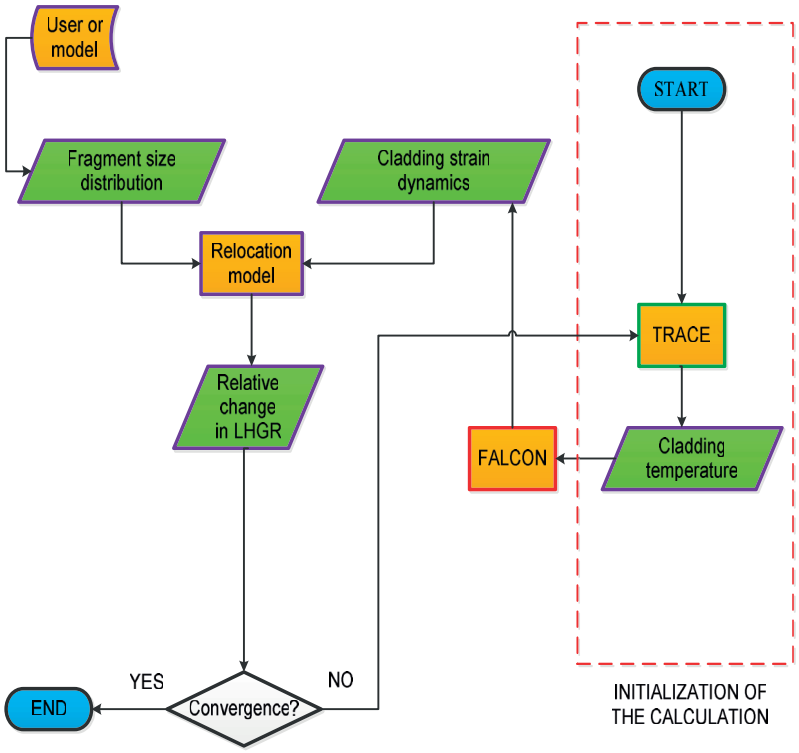

Figure 57: Flow chart of the coupling between TRACE-FALCON-MATLAB.

In order to evaluate the effect of the fuel relocation on the cladding temperature, two cases are evaluated with TRACE and FALCON, in the first case, no fuel relocation is simulated and in the second, the fuel relocation model is used to generate time-dependent axial power profile that reflect the changes in axial distribution of linear heat generation rate. The comparison is shown on Figure 58.

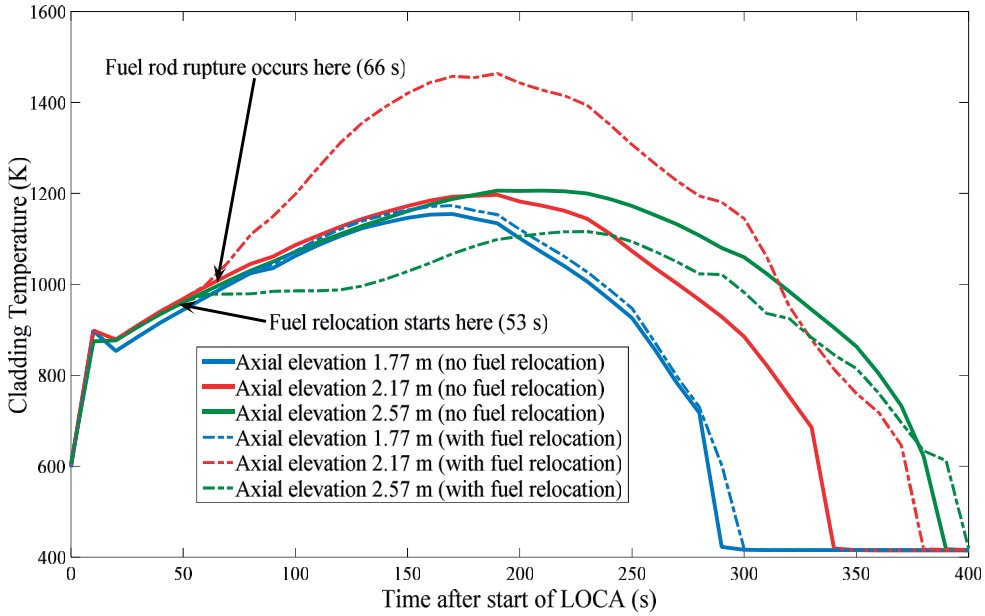

Figure 58: Calculated cladding temperature with the TRACE-FALCON-MATLAB coupling at different elevations with and without the effect of fuel relocation.

The selected axial elevations correspond to locations below the balloon (1.77 m) at the highest cladding strain (2.17 m) and above the balloon (2.57 m). The calculated temperature below the balloon is almost identical for the two cases, because very little fuel relocation took place. Noticeable difference is seen at the location of peak cladding strain where the temperature difference exceeds 200°C and quenching is delayed by about 50 seconds. The region above the balloon shows a reduction in the calculated cladding temperature. This is as expected, because fuel relocated from that region downwards. These results also suggest that fuel relocation does not play a role in the time to cladding failure which developed within 13 seconds after ballooning started. Noticeable effect on the cladding temperature is seen after the cladding failed. Whether or not fuel relocation can impact cladding failure cannot be confirmed with this calculation because the proposed methodology may not be fully representative. Yet, this can be confirmed with specially designed tests without the necessity to use nuclear fuel (section 6.3.5). Such tests can be made with pre-manufactured cladding geometry and the heat source can be simulated with specially designed heaters that will deliver locally more heat at the balloon.

5.3 Fuel dispersal modelling approach

Fuel dispersal may occur during LOCA when the cladding ruptures. There are many factors which influence this phenomenon. Clearly, the size of the rupture opening determines the largest fuel fragment size that can be dispersed. Fuel dispersal is driven by the gas outflow, which in turn is driven by the pressure difference between the inside and outside of the fuel rod which could be a few MPa. Moreover, the gas quantity and pressure in the rod can increase due to a transient fission gas release (FGR) during the LOCA [60, 89]. After the cladding burst, the gas has to go through the fragmented fuel stack to escape from the rod. This results in an interfacial friction which sets in motion fuel fragments. Local pressure losses due to friction of the gas with the irregularly-shaped fuel fragments are essentially stochastic. All in all, a lot of uncertainty comes with the fuel dispersal. Fuel fragmentation and relocation are stochastic processes, and predicting cladding rupture shape and size, as well as modelling the gas-solid outflow, is a separate challenge.

In reality, a fuel fragment may get stuck at the rupture opening and block further fuel from dispersing. The shape of the cladding rupture opening depends on cladding material properties such as ductility as well as on temperature and pressure difference across the cladding wall. Earlier work on cladding rupture is reported in [117] where a correlation is done between the temperature at cladding burst, hoop stress and heating rates. Yet, this applied to particular cladding alloy (Zircaloy 4) and not necessarily with representative oxide layers of today's high burnup fuel rods. To the PhD candidate's knowledge, comprehensive cladding rupture models that will predict the rupture shape and size do not yet exist. Yet, a model was developed [118] that correlated temperature, strain rate and oxidation with the failure of Zircaloy cladding. A conservative assessment of fuel dispersal, which also ignores the discussion on cladding rupture opening size, assumes at least that the smallest fuel fragments can escape through the cladding rupture. Such was the approach adopted in [119] for the estimation of fuel dispersal during a full-core LOCA simulation. Another factor that must influence fuel dispersal is the location of the rupture opening. Unlike in test rods such as in Halden LOCA tests (40-50 cm in length), in full-length rods the location of rupture opening becomes important because it determines the axial distance that the gas must travel [37] and the quantity of fragmented fuel that can interact with the gas outflow. A break near the top of the rod, where the fission gas plenum is located, is expected to result in faster gas outflow, whereas a break near the bottom end may result in slower depressurization. The impact on fuel dispersal in these two different possibilities is unclear.

The first attempt to formulate the fuel dispersal model was to adopt equations for gas-solid outflow from a fluidized bed discussed in [120], but the suitability of the equations was questioned when

applied to the case of a fuel rod after cladding ballooning and rupture. In particular, the equations describe steady-state outflow from a pipe into which particles and gas are continuously added in order to keep the inner pressure constant and reach a state of equilibrium in the gas and solid outflow. In a fuel rod with ruptured cladding, the phenomenon involves the gas-solid interaction of a finite quantity of gas and solids.

A mechanistic modelling approach to fuel dispersion from the rod after the cladding ballooning and rupture is proposed and discussed in this chapter. Calibration against experimental data from Halden's and Studsvik's LOCA test programs is achieved through the tuning of a few parameters which could not be modelled at this time. Pressure measurements of some LOCA tests clearly showed resistance to gas outflow. The reason could rather be attributed to fuel-cladding bonding and small local cladding strain as opposed to the size of the rupture opening as tests with large openings, such as Halden LOCA test 9 and Studsvik's tests 189, 191,192 and 193, showed slow depressurization. A tuning parameter was introduced to simulate the resistance to gas outflow until the model is further developed.

5.3.1 Model outline

A simplified geometry is assumed in which the fuel rod is divided into three regions: (1) plenum, (2) fuel stack between the plenum and balloon, and (3) the balloon with its cladding rupture opening. A schematic is shown on Figure 59. The cooling channel is indicated as (4).

Conservation equations for the mass, momentum and energy of the gas and movable fuel are written for control volumes labelled 1, 2 and 3 together with closure relations for interfacial heat transfer and friction. The plenum, labelled as 1, is a finite cylindrical volume filled with gas. The fuel stack is represented by a cylinder, whose diameter is equal to the average cladding diameter which can be obtained from experimental data or from fuel performance code calculation. Similarly, the balloon is represented by a shorter cylinder whose height can be determined by choosing a suitable cladding cut-off strain. Locating the balloon is easy, but determining where it begins and ends is open for interpretation. The region below the rupture opening is not modelled because the amount of gas there is significantly less compared with the gas stored in the plenum. More precise geometrical representation will have to subdivide the fuel stack and balloon into additional volumes and provide the corresponding mass, momentum and energy conservation equations.

The model starts working at the moment of cladding rupture. The gas flow from the plenum through the fuel stack will contribute most to the quantity of dispersed fuel. The fuel stack, labelled as 2, contains movable and immovable fuel. The immovable fuel determines the cross-sectional area through which the gas and movable fuel can travel. The balloon contains gas, movable and immovable fuel. In the context of this model, the term "immovable fuel" refers to the fuel fragments which are too large to be relocated and dispersed. Similarly, "movable fuel" refers to the fraction of the fuel which can easily relocate – such as the pulverized fuel. An illustrative example is the fragmentation pattern in Halden LOCA test 12 [26] where the fuel stack was more or less preserved. On the other hand, all of the fuel above the rupture in Halden LOCA test 4 is considered "movable" because the fragments were very small. During the initialization process, the pressure, temperature and geometry must be specified. For the calibration, these parameters will come from experimental data such as the OECD Halden LOCA test series or Studsvik's LOCA test series [27]. The transient FGR during the LOCA test before cladding rupture [60] should be accounted by specifying the initial gas pressure.

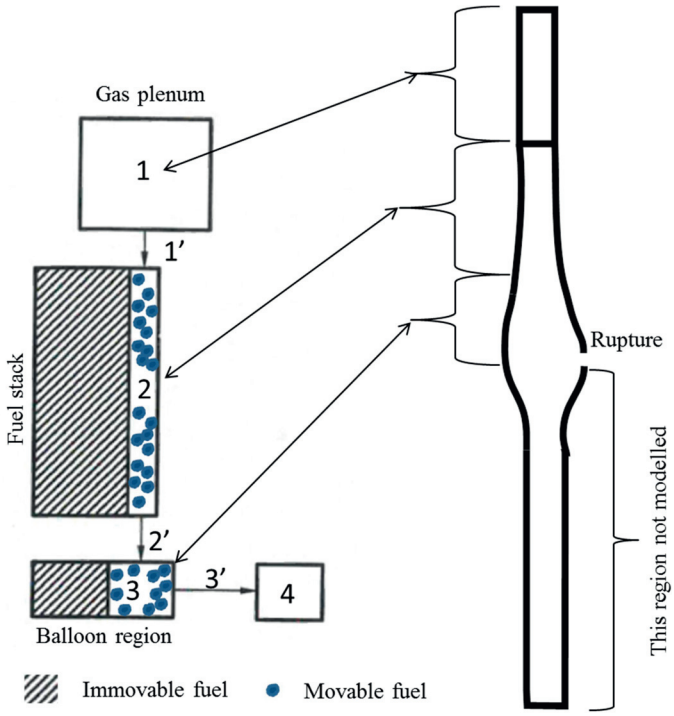

Figure 59: Scheme of the model for fuel dispersal.

By varying the geometry, different conditions can be easily tested. For example, a balloon and rupture occurring far from the plenum can be modelled by increasing the length of the fuel stack between the plenum and balloon. If cladding strain is low, then the flow area and hydraulic diameter are small and there will be higher resistance to axial gas flow. This can be modelled by increasing the fraction of immovable fuel or lowering the cladding inner diameter in the fuel stack and thereby decreasing the flow area and hydraulic diameter.

The quantity of movable fuel can be supplied by a fuel fragmentation model, or specified with the help of post-irradiation examination data as it is done in section 5.3.3 with the available data from Halden and Studsvik LOCA tests. Ultimately, the quantity of movable fuel represents that part of the fuel which is free to relocate and could potentially be dispersed. This is certainly not an easy parameter to predict. Pulverized fuel, described in [31], fits precisely the definition of movable fuel used here.

5.3.2 Model equations

The model consists of mass, energy and momentum conservation equations for gas (g) and movable fuel (s) for the three control volumes: plenum, fuel stack and balloon. While the mass and energy conservation equations are written for the volumes (1, 2, and 3), the momentum conservation equations are written for the junctions (1', 2' and 3') between the volumes. A full description of the variables is shown in Table 16. The system of mass conservation for the movable fuel and the gas is expressed by Eq. 12.

Eq. 12: Gas and movable fuel mass conservation equations.

$$\frac{dm_{g1}}{dt} = -G_{1'}; \quad \frac{dm_{g2}}{dt} = G_{1'} - G_{2'}; \quad \frac{dm_{g3}}{dt} = G_{2'} - G_{3'} \quad \frac{dm_{s2}}{dt} = -S_{2'} \quad \frac{dm_{s3}}{dt} = S_{2'} - S_{3'}$$

The mass is always transferred in the direction from inside to outside. The plenum continuously loses gas to the fuel stack. The rate of change of mass in the fuel stack is equal to the difference between the

mass flow rate coming from the plenum and the mass flow rate going to the balloon. Similarly, the balloon receives mass from the fuel stack and loses mass through the cladding rupture.

The Ideal Gas Law (Eq. 13) is used to calculate the gas pressures, P_1, P_2 and P_3 in the different parts of the model.

Eq. 13: Algebraic equations for evaluating the pressure in the plenum, fuel stack and balloon.

$$P_1 = m_{g1}\frac{RT_{g1}}{M_{gas}A_1L_1}; \quad P_2 = m_{g2}\frac{RT_{g2}}{M_{gas}\left(A_2L_2 - \frac{m_{s2}}{\rho_s}\right)}; \quad P_3 = m_{g3}\frac{RT_{g3}}{M_{gas}\left(A_3L_3 - \frac{m_{s3}}{\rho_s}\right)}$$

The energy conservation equations consider the thermal energy balance for all the components of the modelled system as described in Eq. 14. At this stage of the model development, mechanical energy (kinetic and potential) is assumed negligible.

Eq. 14: Gas energy conservation equations.

$$\frac{dE_{g1}}{dt} = -\frac{G_{1'}E_{g1}}{m_{g1}}$$

$$\frac{dE_{g2}}{dt} = \frac{G_{1'}E_{g1}}{m_{g1}} - \frac{G_{2'}E_{g2}}{m_{g2}} + \left(q_{s\to g}A_{js}\right)_2 + \left(q_{w\to g}A_{wg}\right)_2$$

$$\frac{dE_{g3}}{dt} = \frac{G_{2'}E_{g2}}{m_{g2}} - \frac{G_{3'}E_{g3}}{m_{g3}} + \left(q_{s\to g}A_{js}\right)_3 + \left(q_{w\to g}A_{wg}\right)_3$$

The plenum only loses energy due to the gas mass transfer to the fuel stack region (Eq. 14). The heat exchange with the coolant is neglected. The gas in the fuel stack receives energy via mass convection from the plenum and the heat exchange with the movable fuel, immovable fuel and the cladding wall and loses energy due to mass convection to the balloon. Same approach is adopted in the balloon where in particular the gas energy loss term is determined by the convective gas mass transfer through the rupture opening. The heat flux from the movable fuel to gas, $q_{s\to g}$, as well as from the cladding wall and immovable fuel surface to the gas, $q_{w\to g}$, is calculated according to the Dittus-Boelter correlation shown in Eq. 18a and Eq. 18b respectively. The immovable fuel and cladding temperatures are assumed unchanged due to their relatively large mass.

The thermal energy conservation equations for the movable fuel (Eq. 15) are similar to the ones for the gas, with the exception that the interfacial energy transfer has the opposite sign. The thermal power added to the gas is subtracted from the thermal power of the movable fuel. Heat transfer between the movable and immovable fuel and cladding wall is assumed negligible.

Eq. 15: Movable fuel energy conservation equations.

$$\frac{dE_{s2}}{dt} = -\frac{S_{2'}E_{s2}}{m_{s2}} - \left(q_{s\to g}A_{js}\right)_2$$

$$\frac{dE_{s3}}{dt} = \frac{S_{2'}E_{s2}}{m_{s2}} - \frac{S_{3'}E_{s3}}{m_{s3}} - \left(q_{s\to g}A_{js}\right)_3$$

The change in the gas momentum is driven by the pressure difference between the different regions of the model (plenum, fuel stack, balloon and outside), by the convection of the momentum and by the pressure loss terms ΔP_{gj} which describes the interaction of the moving gas with the movable fuel and

sets it in motion, and the friction with the cladding wall and immovable fuel (Eq. 16). The interfacial friction factor between the gas and the movable fuel, f_j, is computed according to the Blasius correlation (Eq. 18c). The same model is used for the friction factor between the gas and the immovable fuel and the cladding wall, f_{wgj}, (Eq. 18d). An additional term $\Delta P_3{}'$ is added (Eq. 16) which simulates local resistance to gas outflow through the rupture opening.

Eq. 16: Gas momentum conservation equations.

$$\left(\frac{L_1}{2A_1}+\frac{L_2}{2A_{g2}}\right)\frac{dG_{1\prime}}{dt}=P_1-P_2+\rho_{g1}\left(\vartheta_{g1}\right)^2-\rho_{g2}\left(\vartheta_{g2}\right)^2+\left(\frac{\Delta P_{g1}+\Delta P_{g2}}{2}\right)$$

$$\left(\frac{L_2}{2A_{g2}}+\frac{L_3}{2A_{g3}}\right)\frac{dG_{2\prime}}{dt}=P_2-P_3+\rho_{g2}\left(\vartheta_{g2}\right)^2-\rho_{g3}\left(\vartheta_{g3}\right)^2+\left(\frac{\Delta P_{g2}+\Delta P_{g3}}{2}\right)$$

$$\frac{L_3'}{2A_{g3}'}\frac{dG_{3\prime}}{dt}=P_3-P_4+\left(\frac{\Delta P_{g3}}{2}\right)+\Delta P_3{}'$$

$$\Delta P_{gj}=-a_j f_j\frac{\rho_{gj}\vartheta_{ij}\left|\vartheta_{ij}\right|}{2}L_j-f_{wgj}\frac{\rho_{gj}\vartheta_{gj}\left|\vartheta_{gj}\right|}{2}\frac{L_j}{D_{hj}},\qquad j=1,2,3$$

$$\Delta P_3{}'=-f_{og}\frac{\rho_{gj}\vartheta_{gj}\left|\vartheta_{gj}\right|}{2}$$

The movable fuel momentum conservation equations (Eq. 17) also consider the interfacial friction with the gas and friction with the immovable fuel. The friction factor f_{wsj} is calculated with the assumption that Reynolds numbers of the gas and movable fuel are equal.

Eq. 17: Movable fuel momentum conservation equations.

$$\left(\frac{L_2}{2A_{s2}}+\frac{L_3}{2A_{s3}}\right)\frac{dG_{s2\prime}}{dt}=\left(\frac{\Delta P_{s2}+\Delta P_{s3}}{2}\right)$$

$$\frac{L_3{}'}{2A_{s3}'}\frac{dG_{s3\prime}}{dt}=\left(\frac{\Delta P_{s3}}{2}\right)$$

$$\Delta P_{sj}=+a_j f_j\frac{\rho_s\vartheta_{ij}\left|\vartheta_{ij}\right|}{2}L_j-f_{wsj}\frac{\rho_s\vartheta_{sj}\left|\vartheta_{sj}\right|}{2}\frac{L_j}{D_{hj}},\qquad j=2,3$$

Eq. 18: Closure relations.

a) Dittus-Boelter correlation for interfacial heat transfer between the movable fuel and gas

$$\left(Nu_{s\to g}\right)_j=0.023Re_{jg}^{0.8}Pr_g^{0.4},\qquad Pr_g=\frac{c_g\mu}{k_g}$$

$$\left(\alpha_{s\to g}\right)_j=\frac{\left(Nu_{s\to g}\right)_j k_g}{D_{ave}},\quad \left(q_{s\to g}\right)_j=\left(\alpha_{s\to g}\right)_j(T_{sj}-T_{gj})$$

b) Dittus-Boelter correlation for heat transfer between the immovable fuel/cladding wall and gas

$$\left(Nu_{w\to g}\right)_j=0.023Re_{jg}^{0.8}Pr_g^{0.4},\qquad Pr_g=\frac{c_g\mu}{k_g}$$

$$\left(\alpha_{w\to g}\right)_j = \frac{\left(Nu_{w\to g}\right)_j k_g}{D_{hj}}, \quad \left(q_{w\to g}\right)_j = \left(\alpha_{w\to g}\right)_j (T_w - T_{gj})$$

c) Blasius correlation for the friction factor between the gas and movable fuel

$$f_j = \frac{0.316}{Re_{jg}^{0.25}}, \qquad where \qquad Re_{jg} = \frac{D_{ave}\vartheta_{ij}\rho_{gj}}{\mu}$$

d) Blasius correlation for interfacial friction factor between the gas and immovable fuel

$$f_{wgj} = \frac{0.316}{Re_{wgj}^{0.25}}, \qquad where \qquad Re_{wgj} = \frac{D_{hj}\vartheta_{gj}\rho_{gj}}{\mu}$$

Before running the fuel dispersal model it must first be initialized. The required user input is tabulated in Table 15.

Concerning the input parameters, fuel performance codes, such as FALCON [50], can calculate the gas pressure, gas and fuel temperatures at rupture, average cladding strain in the fuel stack and balloon regions. The average fuel fragment size should come from a model on fuel fragmentation (see section 5.1). As a first approximation, the fraction of movable fuel can be calculated according to the criteria for fuel pulverization described in section 5.1.1 using the fuel performance code's calculation for local burnup and fuel temperature. For the time being, it can be assumed that only pulverized fuel can escape. The paper by Raynaud et.al [119] discusses core-wide estimates for fuel dispersal during LOCA and it is assumed that only fine fuel fragments (< 1 mm) can be dispersed.

The present model is applied to existing LOCA experiments from Halden and Studsvik. The initial parameters are obtained from online measurement signals (pressure, temperature) and post-irradiation examinations (fraction of movable fuel, size of rupture opening, average fragment size distribution, cladding deformation). Once the required input parameters are provided, the model uses them to calculate the internal parameters tabulated in Table 16 as functions of time.

Table 15: Table of input parameters necessary to initialize the fuel dispersal model at time = 0 s.

Parameter	Parameter description
$P_1 = P_2 = P_3 = P$	Pressure in the fuel rod at the moment of rupture (Pa)
P_4	Outside pressure (Pa)
T_w	Temperature of the immovable fuel and cladding wall (K)
D_{ave}	Average fuel fragment size (mm)
D_{clad}	As-manufactured cladding inner diameter (mm)
$\overline{D}_{clad}$	Average cladding diameter in the fuel stack (mm)
L_1	Length of the plenum (mm)
L_2	Length of the fuel stack (mm)
L_3	Length of the fuel balloon (mm)
$L_3{}'$	Width of the balloon (mm)
$D_{balloon}$	Average cladding diameter in balloon (mm)
$A_{rupture}$	Area of cladding rupture opening (mm^2)
D_{fuel}	Fuel pellet diameter (mm)
F_{fuel}	Fraction of movable fuel
M_{gas}	Molar mass of gas mixture (He, Xe + Kr) (kg / mol)
ρ_s	Fuel density (kg/m^3)
μ	Gas dynamic viscosity (Pa·s)
k_g	Gas thermal conductivity ($W \cdot m^{-1} \cdot K^{-1}$)
c_g	Gas specific heat capacity ($J \cdot kg^{-1} \cdot K^{-1}$)

Table 16: Description of internally calculated model variables as function of time.

Parameter	Parameter description
P_1	Gas pressure in the plenum (Pa)
P_2	Gas pressure in the fuel stack cladding region (Pa)
P_3	Gas pressure in the balloon (Pa)
T_{g1}	Temperature of gas in the plenum (K)
T_{g2}	Temperature of gas in the fuel stack (K)
T_{g3}	Temperature of gas in the balloon (K)
m_{g1}	Mass of gas in the plenum (kg)
m_{g2}	Mass of gas in the fuel stack (kg)
m_{g3}	Mass of gas in the balloon (kg)
m_{s2}	Mass of movable fuel in the fuel stack region (kg)
m_{s3}	Mass of movable fuel in the fuel balloon (kg)
$G_{1'}$	Gas flow rate from plenum to fuel stack (kg / s)
$G_{2'}$	Gas flow rate from fuel stack to balloon (kg / s)
$G_{3'}$	Gas flow rate from balloon to outside (kg / s)
$S_{2'}$	Movable fuel flow rate from fuel stack to balloon (kg / s)
$S_{3'}$	Movable fuel flow rate from balloon to outside (kg / s)
ϑ_{ij}	Slip velocity between the gas and the movable fuel (m/s)
ϑ_{gj}	Gas velocity at j^{th} junction (m/s), j = 1, 2, 3
ϑ_{sj}	Movable fuel velocity at j^{th} junction (m/s), j = 2, 3
A_{g2}	Flow area in the fuel stack occupied only by the gas (m^2)
A_{g3}	Vertical flow area in the balloon occupied by the gas (m^2)
A'_{g3}	Horizontal flow area in the balloon occupied only by the gas (m^2)
A_{s2}	Flow area in the fuel stack occupied only by the movable fuel (m^2)
A_{s3}	Vertical flow area in the balloon occupied only by the movable fuel (m^2)
A'_{s3}	Horizontal flow area in the balloon occupied only by the movable fuel (m^2)
A_1	Flow area in the plenum (m^2)
A_2=$A_{g2} + A_{s2}$	Total flow area locked between the immovable fuel and the cladding wall (m^2)
A_3=$A_{g3} + A_{s3}$	Total flow area in the balloon (m^2)
ΔP_{gj}	Pressure drop of the gas due to friction with the movable and immovable fuel and cladding wall (Pa)
ΔP_{sj}	Pressure drop due to friction of the movable fuel with the gas and the immovable fuel and cladding wall (Pa)
$\Delta P'_3$	Pressure drop due to resistance at the rupture opening (Pa)
D_{hj}	Hydraulic diameter (m), j = 1, 2, 3
E_{g1}	Thermal energy of the gas in the plenum (J)
E_{g2}	Thermal energy of the gas in the fuel stack (J)
E_{g3}	Thermal energy of the gas in the balloon (J)
E_{s2}	Thermal energy of the movable fuel in the fuel stack (J)
E_{s3}	Thermal energy of the movable fuel in the balloon (J)
ρ_{gj}	Calculated gas density in different parts of the model (kg / m^3)
A_{js}	Interfacial area density of the movable fuel (m^{-1})
$(q_{w\to g})_j$	Heat flux going from the cladding wall and immovable fuel to the gas (W / m^2)
$(q_{s\to g})_j$	Heat flux going from the movable fuel to the gas (W / m^2)
A_{wgj}	Heat transfer area of the immovable fuel and cladding wall in contact with the gas phase (m^2)
f_j	Friction factor between the movable fuel and gas according to Blasius correlation
f_{wgj}	Friction factor between the gas and the immovable fuel and cladding wall according to Blasius correlation
f_{wsj}	Friction factor between the movable and the immovable fuel and cladding wall according to Blasius correlation
a_j	Movable fuel interfacial area density (m^{-1}), j = 2, 3

$(\alpha_{w\to g})_j$	Immovable fuel and cladding wall to gas convective heat transfer coefficient (W/m^{2}K)
Re_{jg}	Reynolds number of the gas in different parts of the model (j = 1,2,3)
$(Nu_{w\to g})_j$ $(Nu_{s\to g})_j$	Nusselt number (j = 2,3)
Pr_g	Prandtl number
f_{og}	Local friction factor at the rupture opening (further discussed below)

For example, using the input for pressure, temperature, plenum length, plenum diameter and gas molar mass, the mass of the gas in the plenum m_{g1}can be determined with the Ideal Gas Law. Using the balloon and fuel stack lengths, fuel density, fuel diameter and the fraction of movable fuel the values for m_{s2} and m_{s3} are initialized.

The parameter f_{og} can be considered as a magnitude of the resistance to the gas outflow through the rupture opening. The term $\Delta P_3'$ is introduced to help the convergence of the differential equations solver. At the moment of cladding rupture there is suddenly a large pressure drop and this causes numerical instabilities in the ODE solver. Without this extra resistance, convergence could not be obtained and for the moment it must be used. Further improvement of the model should consider the conditions of chocked flow and the interaction of gas and movable fuel at the rupture opening.

5.3.3 Calibration using Studsvik LOCA tests with high burnup fuel

5.3.3.1 Studsvik's tests 189, 191, 192 and 193

Together with the LOCA tests executed in the Halden reactor, Studsvik's LOCA tests are the only ones performed with high burnup fuel. Of the six tests reported by Flanagan in [27], only tests 189, 191, 192 and 193 showed fuel dispersal. These tests are a good choice to check the capability and calibrate the fuel dispersal model, because most of the initial conditions can be set with little or no uncertainty: fuel dispersal is precisely measured, while temperature and pressure of the gas in the plenum at cladding rupture, cladding deformation, size of rupture opening and average fragment size are all published in [27]. This section presents the output of the fuel dispersal model for each of the selected Studsvik's LOCA tests.

The adopted strategy in this section is to reproduce as close as possible the pressure measurement after the rupture, which is accomplished by calibrating the resistance to axial gas flow. This is necessary, because Studsvik's LOCA tests clearly demonstrated slow depressurization and the reason for this is some mechanisms of resistance to gas flow. The model is not able to capture this stochastic effect of blockage; therefore a calibration (tuning) parameter (restriction of the hydraulic diameter) was introduced. The fraction of movable fuel is specified using the knowledge of the measured dispersed and remaining fuel after the test reported in Table 17. The comparison of the calculation (C) with the measurement (M) is done by comparing the pressure measurement as well as the dispersed and remaining movable fuel mass for tests 189, 191, 192 and 193 shown in Figure 60 to Figure 63 respectively.

The dispersed and remaining movable fuel mass for all four tests is tabulated in Table 17 together with the dispersed fuel mass in percentage of the total movable fuel mass. The large difference between the first three tests and the last is the fraction of movable fuel. Movable fuel mass is calculated from the published data in the NUREG-2160 by Flanagan [27] which reports the weight of dispersed fuel during the LOCA test and the additional fuel fragments collected during the rod shake-down. The sum of the measured dispersed and remaining fuel masses reported in Table 17 is the quantity of movable

fuel. For example, according to the published data, fuel dispersal during the LOCA test S193 amounts to 105 g and additionally 41 g were removed during the shake-down of the test rod which brings the total amount of movable fuel to 146 g. The model predicted 120 g of dispersed fuel during the S193 LOCA test while 26 g remained in the rod. The dispersal model also gives good prediction for the other three tests, but it should be kept in mind that initial conditions, such as cladding geometry, size of rupture opening and initial pressure did not differ much. The large difference is in the fraction of movable fuel.

The left-hand panes on Figure 60 through Figure 63 show the calculated gas pressure evolution based on the amount of gas and input geometry. A sharp drop in gas pressure of the balloon (P3) corresponds to fast depressurization which cannot be compensated by the incoming gas from the plenum because of high resistance to axial gas flow and large rupture opening. The right-hand panes include the plots for evaluation of dispersed fuel mass. The fuel which is readily available for dispersal is defined by the fraction of movable fuel. For example, if the fraction is 0.5, then half of the fuel mass, located above the rupture opening, is considered movable and therefore could potentially be dispersed. In the context of Studsvik's tests 189, 191, 192 and 193, the movable fuel is made up of the fuel which is dispersed during the LOCA test and the fuel removed during the shake-down of the fuel rod. Some of the movable fuel part is dispersed as indicated by the dispersed fuel mass, and the rest remains in the rod – indicated by the "remaining mass" curve. The rest of the fuel is considered immovable due to fuel-cladding bonding or other reasons and is responsible for the resistance to axial gas flow which controls the rate of gas depressurization. The post-irradiation examination of the Studsvik tests determined that the upper active part of the rod could not be defueled. Considering the small cladding deformation in the upper part during the test and the high burnup level, it cannot be ruled out that the fuel was in tight contact with the cladding and the flow area for the gap was quite small thereby controlling the rate of gas outflow. Therefore, the tuning parameter that is introduced in the dispersal model to control the rod depressurization has a physical meaning – it represents small hydraulic diameter due to fuel-cladding bonding, for example.

In tests 189, 191 and 192 the pressure measurement shows a change in concavity, i.e. a reduction in the rate of depressurization followed by an increase. Clearly, resistance to axial gas flow is temporarily increased which could be due to a restriction at the cladding rupture caused by the fuel fragments outflow. According to the paper by Masimilla et. al. [120], filtration was observed during experiments with solid and gas outflow through an orifice located in the side wall of a pressurized cylinder filled with gas and solid particles. They postulated that outside some critical distance from the orifice the gas-solid mixture acts as a fluid, but close enough to the rupture - the two phases separate. This implies accumulation of solids near the opening, resulting in partial blockage. Such stochastic mechanisms cannot be modelled with the presented fuel dispersal model, but a similar effect could be obtained by assuming temporary blockage and collection of fuel in the balloon and then sudden release. An attempt to re-produce such behaviour with the fuel dispersal model is shown on Figure 64. This example is artificial, because an if-statement controls when the dispersal begins. Until the 23rd second, the fuel amount is increasing in the balloon and after that dispersal is "switched on".

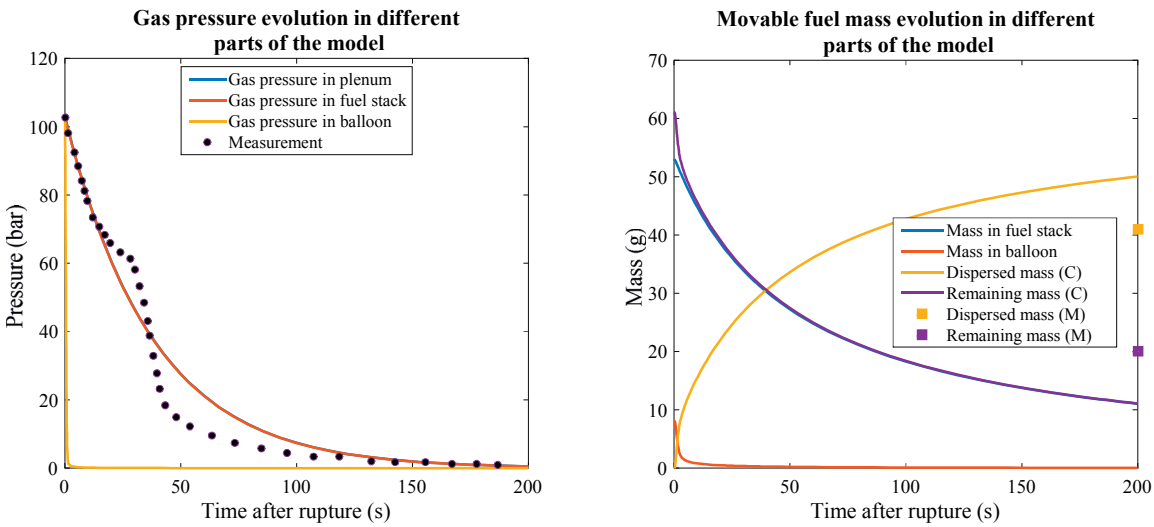

Figure 60: Fuel dispersal calculation with initial parameters of Studsvik's LOCA test S189.

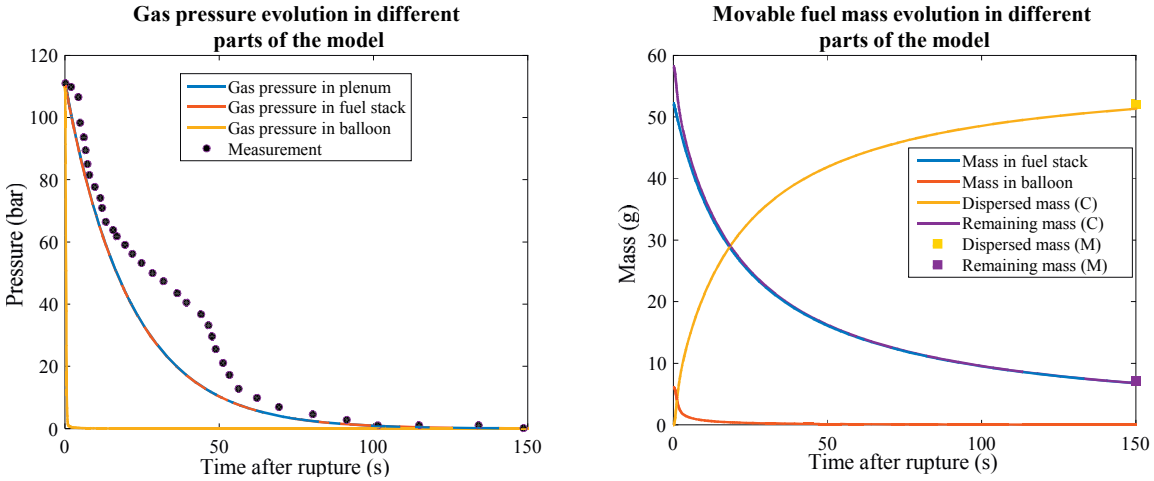

Figure 61: Fuel dispersal calculation with initial parameters of Studsvik's LOCA test S191.

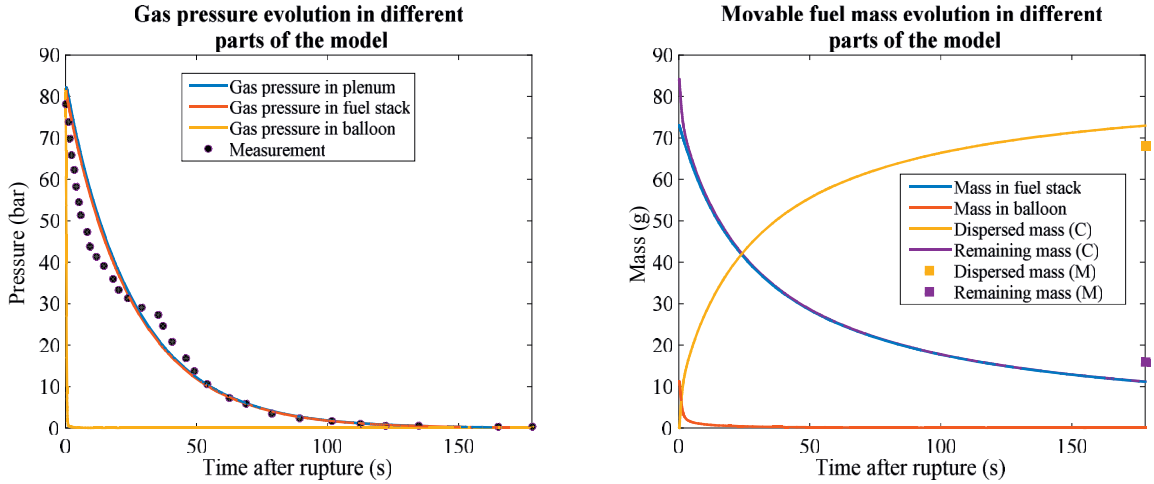

Figure 62: Fuel dispersal calculation with initial parameters of Studsvik's LOCA test S192.

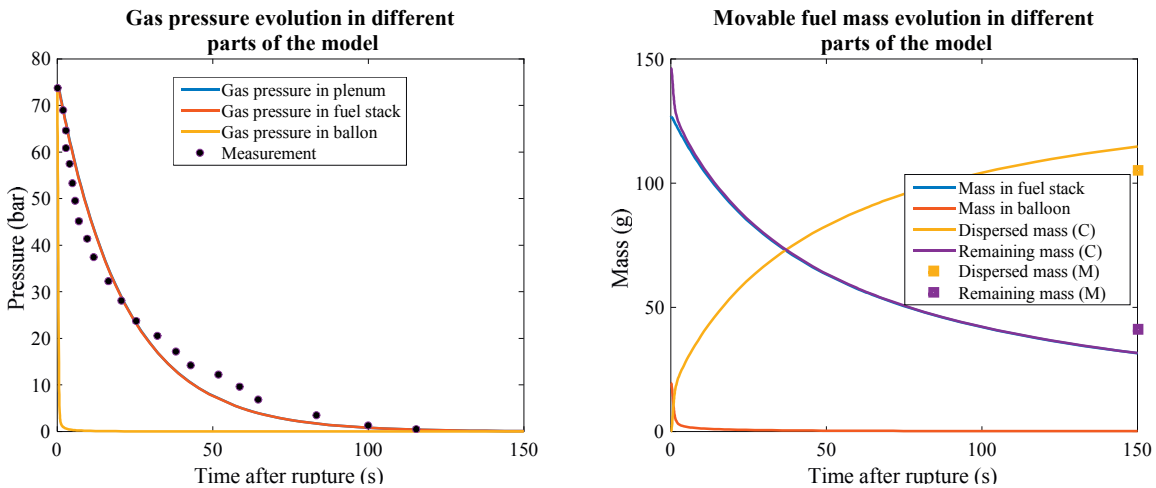

Figure 63: Fuel dispersal calculation with initial parameters of Studsvik's LOCA test S193.

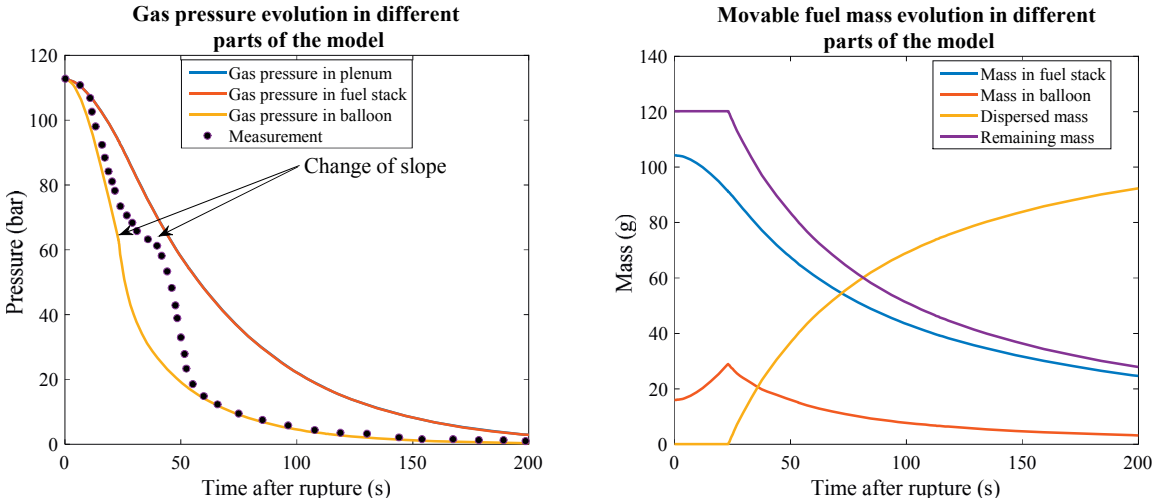

Figure 64: Simulation of temporary fuel blockage.

Table 17: Measured (M) and calculated (C) dispersed and remaining movable fuel for each of the selected Studsvik's LOCA tests.

Test ID	Dispersed (M)	Dispersed (C)	Remaining (M)	Remaining (C)	Dispersed (%) of total (M)	Dispersed (%) of total (C)
S189	41	50	20	11	67	81
S191	52	51	7	8	88	86
S192	68	73	16	11	81	87
S193	105	120	41	26	72	82

The cusp shown by the pressure measurement could be slightly re-produced with the model. It is hypothesized that until the change of slope indicated by the arrows, fuel fragments accumulate somewhere and consequently cause higher resistance to the gas flow, which in turn slows down the pressure decrease. At some point, the obstruction is removed and the rod apparently depressurizes more gradually.

5.3.3.2 Studsvik's test 196

Rupture opening has effect on the rate of gas and solid outflow. Pin-hole rupture will allow only the pulverized fuel to escape and it may even be blocked by a larger fuel fragment and prevent further dispersal. Until now, only tests with large rupture openings and small average fuel fragment sizes were presented. In the case of Studsvik's test 196, the rupture opening was very small, the average fuel fragment size was large and there was no fuel dispersal which is contradicting the claim that the pulverized fuel should escape. Yet, the rupture opening could have been blocked by a larger piece of fuel thereby preventing any release. In such a case, the model should only compute mass transfer from the fuel stack to the balloon and the gas outflow. The fuel dispersal model output considering such initial conditions is shown on Figure 65.

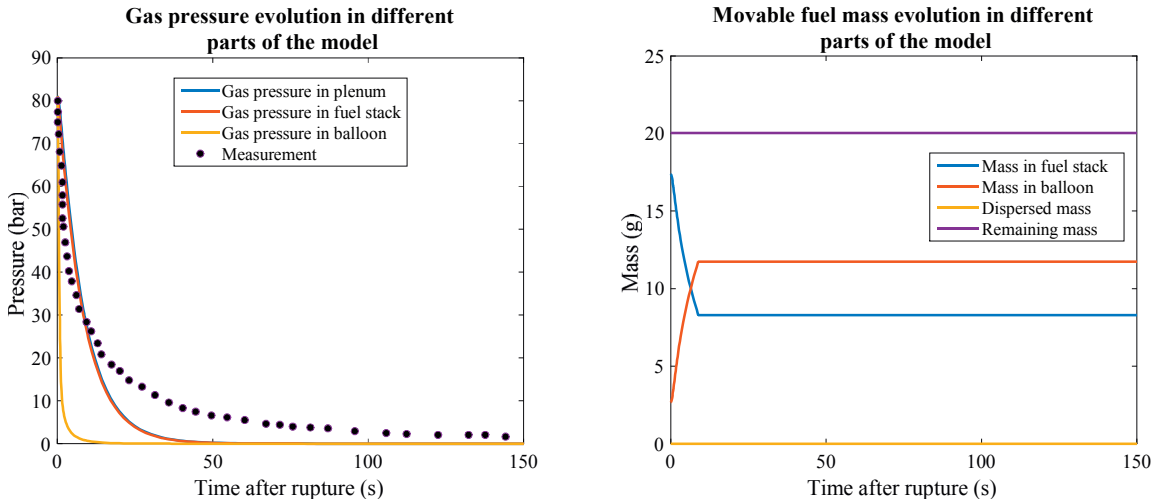

Figure 65: Fuel blockage in test S196 due to smaller cladding the rupture opening size than the average fuel fragment size.

The fuel mass in the balloon keeps increasing due to relocation from the fuel stack until there is no more available room. This reduces the local void fraction, which plays a role in the system of differential equations describing the model. In reality, void fraction in the balloon can never reach zero, and there will always be some empty space for the gas to pass through. Hexagonal close packing (hcp) of equal-sized spheres, with a packing fraction of 0.74, is assumed as the upper limit to the maximum packing factor in the balloon. Although this test shows no dispersed fuel, it is interesting because the fuel relocation into the balloon may have an impact on local cladding oxidation and the Equivalent Cladding Reacted (ECR) due to a hot-spot effect. The resistance to gas outflow is also evident in this test, but it appears more gradual.

5.3.4 Application to Halden LOCA tests

The capabilities and limitations of the proposed modelling approach to the fuel dispersal were demonstrated in the previous section. While the considered Studsvik LOCA tests had rather similar outcome, Halden tests cover a wider range of initial conditions. For example, LOCA tests 5 and 9 demonstrate slow depressurization due to high resistance to axial gas flow, which could be attributed, for example, to the low cladding deformation and large distance to the balloon in test 5 and to the stuck fuel pellets at the very top of test 9. On the other hand, tests 4, 6, 11, 12 and 13 had little resistance to axial gas flow which led to fast depressurization and fuel dispersal. Tests 4 and 9 demonstrated significant amount of dispersed fuel while tests 6, 7, 10, 11 and 12 had none or very little [26]. Furthermore, measurement of the dispersed fuel was not done which requires at least rough estimation from available post-irradiation examination data such as from gamma scanning (see Appendix A) and/or neutron radiography. Having identified the main parameters of influence in the proposed model – namely fraction of movable fuel, cladding rupture opening size, cladding geometry and the tuning parameter (hydraulic diameter) for resistance to axial gas flow, an attempt is made to estimate the amount of dispersed fuel for the Halden LOCA tests. The trapped fission gas in high burnup BWR fuel that was discussed in section 4.3 and its release during LOCA in section 4.7 is relevant for tests 12 and 13. During the initialization of the dispersal model, this source of FG is implicitly taken into account via the pressure measurement at cladding rupture.

Table 18 summarizes all relevant initial conditions for the Halden LOCA tests. Most of the data are obtained from the Halden reports HPR-380 [26] and HPR-383 [32], and the remaining is referenced additionally. Whenever necessary, the hydraulic diameter was tuned in order to obtain agreement with the measured pressure evolution in the plenum.

Table 18: Initial parameters for the fuel dispersal model for all Halden LOCA tests and five Studsvik LOCA tests.

	Halden LOCA tests									Studsvik LOCA tests				
Test ID	4	5	6	7	9	10	11	12	13	S189	S191	S192	S193	S196
Inner pressure (bar)	51	65	58	10	55	72	52	34	34	100	110	82	83	81
Outer pressure (bar)	8	3	9	2.5	2	11	2	4.2	3.3	1	1	1	1	1
Fuel temperature (K)	1070	1073	1070	1320	850	1033	1073	1070	1093	1073	1053	1073	1100	1060
Plenum height (cm)	32	22	36	26	26	30	34	3.3	39	15.30	15.30	15.30	15.30	15.30
Cladding inner diameter (mm)	9.30	9.30	7.77	8.36	9.30	8.36	7.77	8.36	8.36	9.30	9.30	9.30	9.30	9.30
Average cladding inner diameter in fuel stack (mm)	11.55	9.96	8.84	9	11	8.66	8.14	10.8	11	11	10.50	11	11.50	10.5
Average cladding inner diameter in balloon (mm)	18	11	10.6	10.5	17	10.5	9.64	12	13	14	15	14	15	11
Length of fuel stack (cm)	19	37	30	20	20	18	28	12	14	26	27	26	26	28
Balloon length (cm)	10	2	1	3	6	2	2	4	6	4	3	4	4	2
Area of rupture opening (cm^2)	2.1	0.07	0.02	0.09	1.30	0.39	0.02	0.01	0.08	1.42	2.69	1.12	1.71	0
Fraction of movable fuel	1	0.10	0.01	0.01	0.50	0.15	0.01	0.10	0.15	0.30	0.29	0.42	0.73	0.1

5.3.4.1 Halden LOCA test 4

The 4th Halden LOCA test demonstrated that significant fuel fragmentation and dispersal can also happen during a LOCA test. Until recently it was considered a reactivity-initiated accident (RIA) issue. The gamma scanning revealed that the top half of the fuel rod is completely voided of fuel. Post-irradiation examination revealed that cladding deformation in the balloon reached the inner wall of the heater and that significant fraction of the fuel pulverized. The fraction of movable fuel is assumed equal to 1. The fuel dispersal model output is shown on Figure 66.

According to the pressure measurement, there is no evidence of resistance to axial gas flow. The calculated dispersed fuel is 113 g. The lower bound of the dispersed fuel estimate is done by evaluating the fraction of gamma counts below the rod to the total gamma counts and then multiplying by the initial mass. The upper bound is obtained by assuming that all of the missing fuel in the upper half of the fuel rod is dispersed, which is approximately 40%.

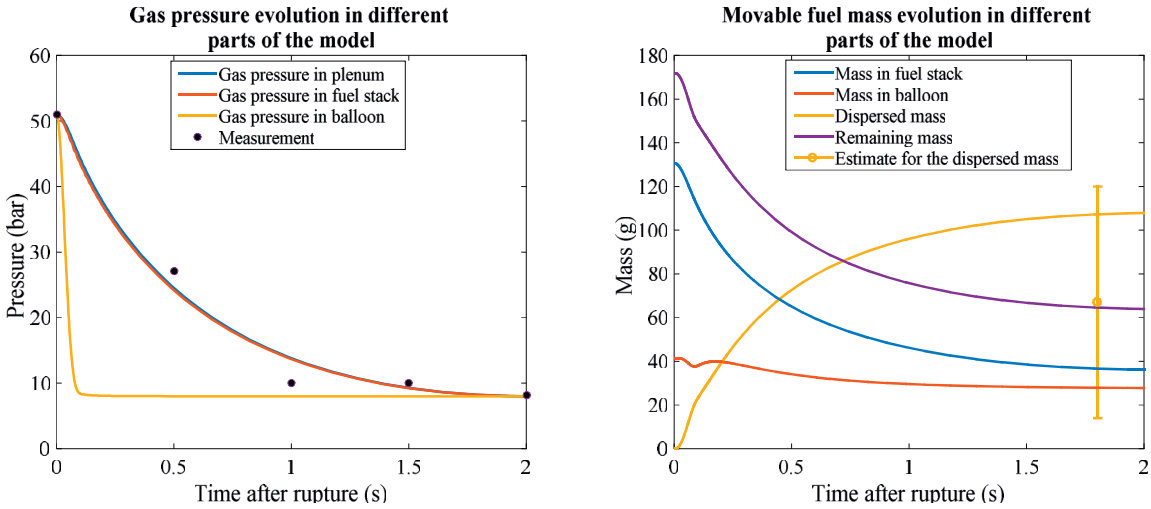

Figure 66: Pressure drop and dispersed fuel calculation for Halden LOCA test 4.

5.3.4.2 Halden LOCA test 5

The fifth LOCA test presented the conditions of a balloon far from the plenum and rather limited cladding deformation, fuel fragmentation and relocation. Some dispersed fuel was evident from the gamma count intensity plot (Figure 17). The pressure measurement shown on Figure 67 is evidence for a strong resistance to axial gas flow. By optimizing the hydraulic diameter in the fuel stack, the fuel dispersal model could roughly reproduce the pressure.

Fragment size distribution for this test was not performed and the fraction of movable fuel has to be taken from elsewhere. Since there is no available data on fragment size distribution, the lower estimation for pulverized fuel in [31] of 10% is used and the calculation predicts 18.7 g of dispersed fuel. An estimate of the dispersed fuel based on gamma scanning count intensity plot is about 13 g. This is likely an upper estimate, because 13 g is equal to approximately 2 whole fuel pellets. The neutron radiography showed a void region whose height equals to about half a fuel pellet, but the packing factor in the vicinity of the balloon seemed also low. All of this information can be referenced to [26].

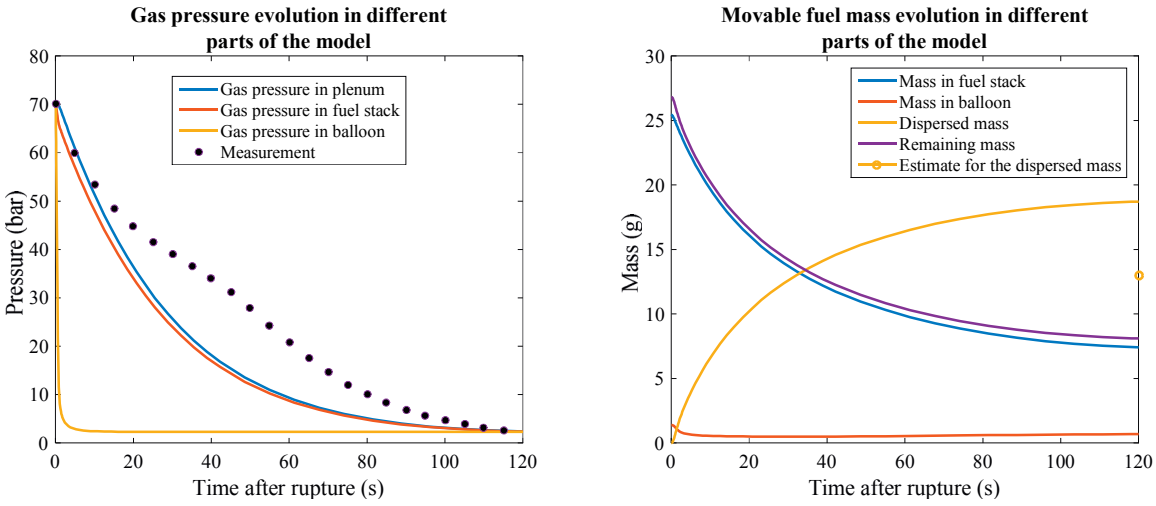

Figure 67: Pressure drop and dispersed fuel calculation for Halden LOCA test 5.

5.3.4.3 Halden LOCA tests 6 and 11

There were two VVER tests within the Halden LOCA test program. The fuel design with central hole virtually eliminates the possibility for some sort of blockage to the axial gas flow. Fuel fragmentation and relocation did occur, as revealed by the neutron radiography [26], but there was weak evidence of dispersal according to the gamma scanning and the average fuel fragment size was likely around 4 mm. The pulverized fuel fraction used in [31] for these tests is about 0.01 and this value was used to initialize the fuel dispersal model. Considering the cladding rupture openings were very small, it is reasonable to expect that only small fragments such as pulverized fuel could escape. Fuel dispersal calculations for tests 6 and 11 are shown on Figure 68 and Figure 69 respectively. The pressure measurements show no evidence of resistance to the gas outflow.

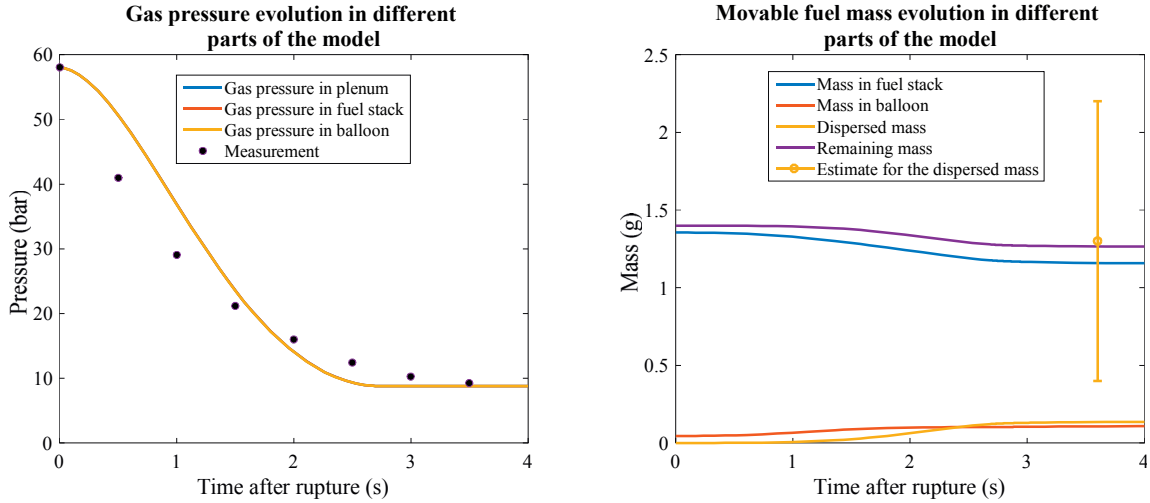

Figure 68: Pressure drop and dispersed fuel calculation for Halden LOCA test 6.

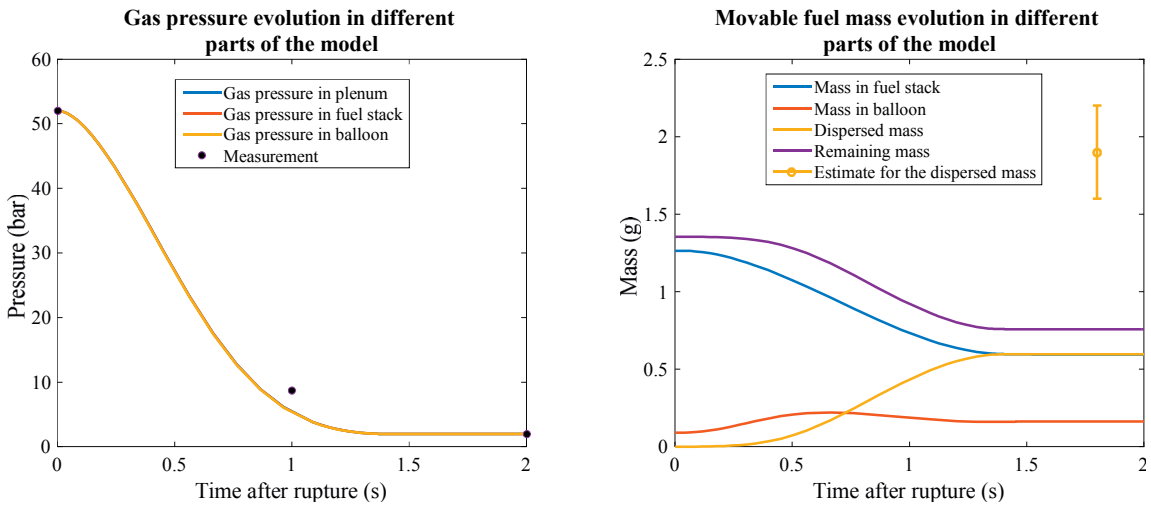

Figure 69: Pressure drop and dispersed fuel calculation for Halden LOCA test 11.

Estimation of the dispersed fuel for these tests is done based on the gamma scan data in two ways:

1) Taking the ratio of the gamma counts of ^{137}Cs below the rod to the total number of gamma counts as a lower bound gives 0.4g and 1.6g for test 6 and 11 respectively.
2) The gamma scanning for both tests [26] shows one axial level voided of fuel due to relocation. The active fuel stack length is 480 mm which means a fraction equal to 5/480 = 0.0104 of the total fuel mass is assumed dispersed. Using the provided geometrical data, the fuel mass is approximately 216 g which means the estimate for dispersed fuel is 2.25 g. This value is chosen as the upper estimate for both tests.

The pressure evolution was reproduced by the model quite well only with the input parameters in Table 18. Fuel pulverization according to the criteria found in [31] is evaluated at about 1% and under this assumption the calculated fuel dispersal is 0.1g and 0.6g for tests 6 and 11 respectively. This is probably not far from reality considering the weak evidence of fuel dispersal from the gamma scanning.

5.3.4.4 Halden LOCA test 7

This was the first LOCA test with BWR fuel. From the point of view of fuel dispersal this test is not very interesting because at average burnup of 44.3 MWd/kgU [26] the fuel fragments were very large with little potential for relocation and dispersal despite the relatively large opening of 10 mm by 2 mm. The fuel dispersal model was initialized with the relevant parameters and the output is shown on Figure 70.

The pressure measurement shows a gradual outflow which means there was little resistance to axial gas flow. Conditions for fuel pulverization were not reached for this fuel because of its lower burnup. Despite this, a fraction of movable fuel equal to 0.01 was used in the calculation.

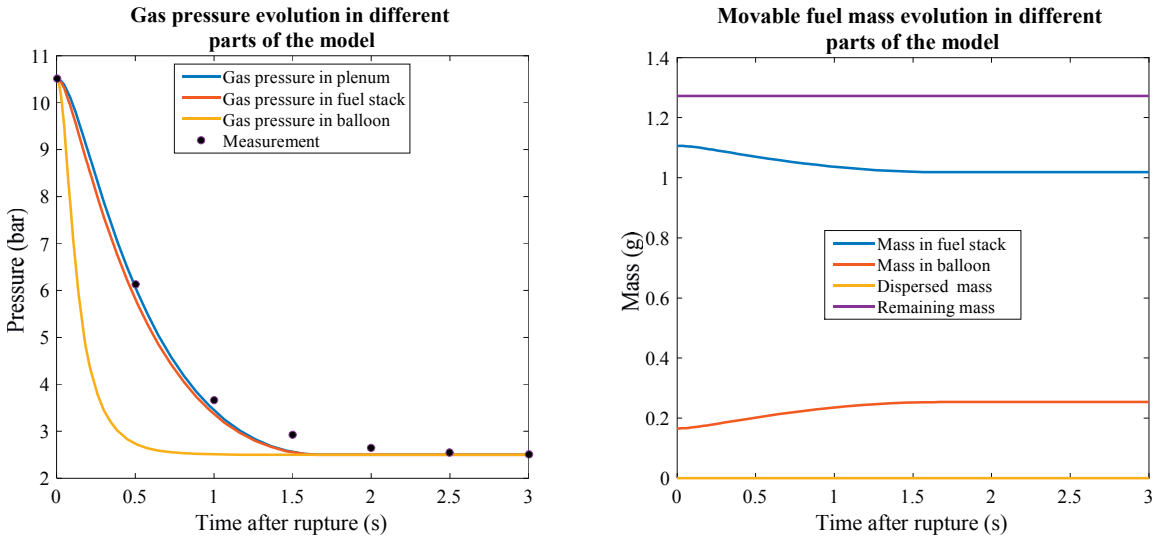

Figure 70: Pressure drop and dispersed fuel calculation for Halden LOCA test 7.

5.3.4.5 Halden LOCA test 9

The 9th test was very similar to the 4th test. The test rod was cut from the same mother rod, had the same geometry and the fuel was at the same burnup level. The fuel fragmented to small pieces including a large fraction of pulverized fuel. The fragmented fuel was highly mobile and from what it appears from the gamma count intensity plot (Figure 21), conditions for hot-spot effect were reached. The slow rod depressurization appears to have been influenced by the fuel which remained stuck to the cladding and possibly to fuel fragments build up in the balloon and rupture region leading to partial blockage. The measured and calculated pressures are shown on Figure 71 . In the time interval of ~50 s to 200 s the rate of pressure decrease is very small which could be due to inability of the gas to push through the accumulated fuel near the rupture region and instead it simply filters through it.

Under these conditions, the model calculates 107 g of dispersed fuel. The initial fuel was about 300 g and the gamma scanning [26] revealed about 25% of the cladding tube to be empty. This means, that maximum of 0.25x300 = 75 g could have been dispersed. This is the upper bound on the estimate of dispersed mass. The lower bound is equal to 6 g and it was estimated in [121]. Without any doubt, the calculated amount of dispersed fuel is an overestimation. The fact that the cladding ballooned up to the heater suggests that the distance between the rupture opening and the heater was very small, and this may have acted as an obstacle to fuel dispersal. Certainly, this is not taken into account with the dispersal model. It is important to make a comparison with the Studsvik's test 193 where even larger quantity of fuel was dispersed, the cladding rupture opening was comparable in size, fuel was also high burnup and fragmented to very small pieces, but there the heater could not have played a role. In reactor case, the role of the heater as potential obstacle to fuel dispersal is taken by the neighbouring rods. With that in mind, if a fuel rod balloons enough to come in contact with a neighbour rod and then ruptures, fuel dispersal may be reduced but also the heat source will be moved right next to another fuel rod and may impact its integrity.

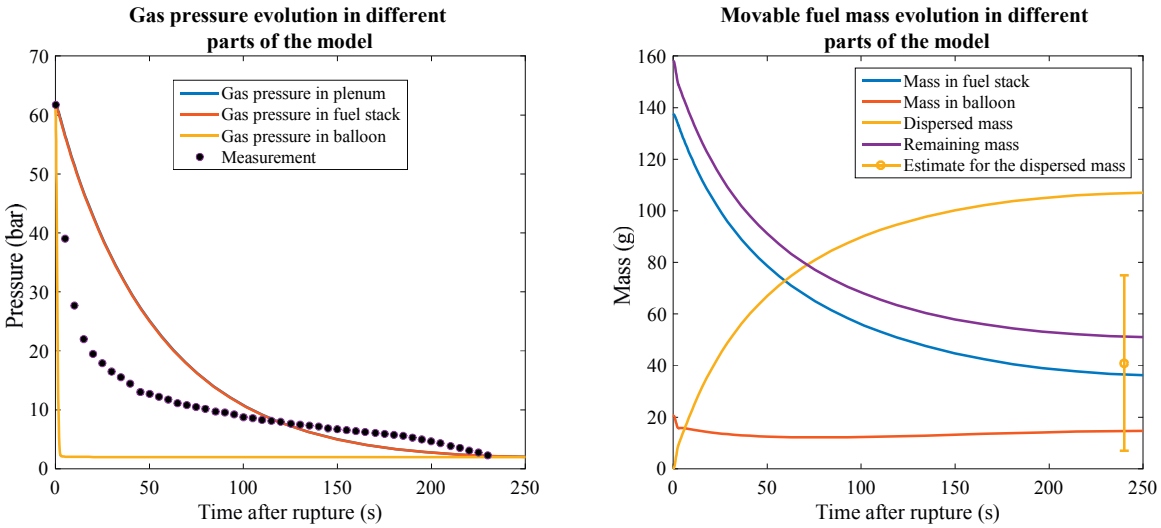

Figure 71: Pressure drop and dispersed fuel calculation for Halden LOCA test 9.

5.3.4.6 Halden LOCA test 10

Fragment size distribution was not measured after this LOCA test and as such it is not known what fraction of the fuel fragments were smaller than the rupture opening. With reference to the paper by Turnbull et.al. [31], the fraction of pulverized fuel in the 10th Halden LOCA test is between 0.01 and 0.1. For this reason, the fuel dispersal model is initialized with a fraction of movable fuel equal to 0.05. The fuel dispersal model calculation initialized with parameters pertaining to the 10th LOCA test is shown on Figure 72.

The model calculates about 5.2 g of dispersed fuel, which is over 90% of the total amount available for dispersal. An estimation based on gamma scanning data predicts fuel dispersal to be between 0.8 - 5 g. This particular analysis is shown in [121].

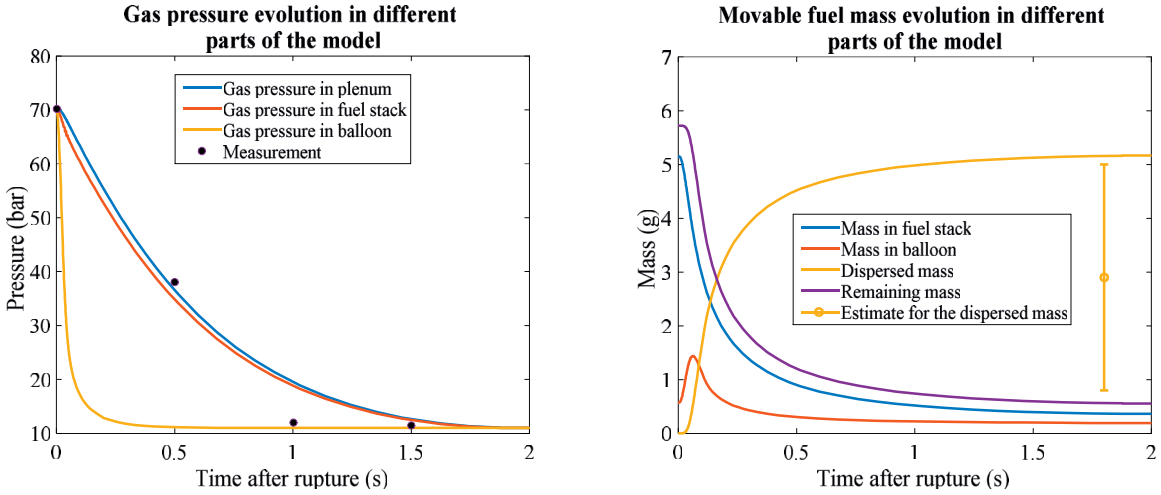

Figure 72: Pressure drop and dispersed fuel calculation for Halden LOCA test 10.

5.3.4.7 Halden LOCA test 12

The neutron radiography done on the rod after the LOCA test revealed large fuel fragmentation but overall preservation of the fuel column. This means the fraction of movable fuel was rather low. The cladding rupture opening (4 mm long and 1 mm wide) is smaller than the average fragment size judging by the neutron radiography and to calculate fuel dispersal, the average fuel fragment size must be lowered. The fuel dispersal model is not very sensitive to the fragment size. For this reason, average fragment size is set equal to 1 mm. The paper by Turnbull et. al. [31], indicates that the fuel in Halden LOCA test 12 reached the conditions of up-to 10% fuel pulverization, which is not evident on the available post-irradiation examinations. Nevertheless, for lack of a better prediction, the fraction of movable fuel is set to 0.1 and the fuel dispersal model output is shown on Figure 73.

The calculated dispersed fuel mass is about 1.5 g, which is 17% of the total amount of assumed available fuel for dispersal (in LOCA test 10, the dispersed mass was 90%). The estimate of the dispersed fuel is based on taking the ratio of ^{137}Cs counts to the total number of counts using the gamma scanning data and is equal to 2 g.

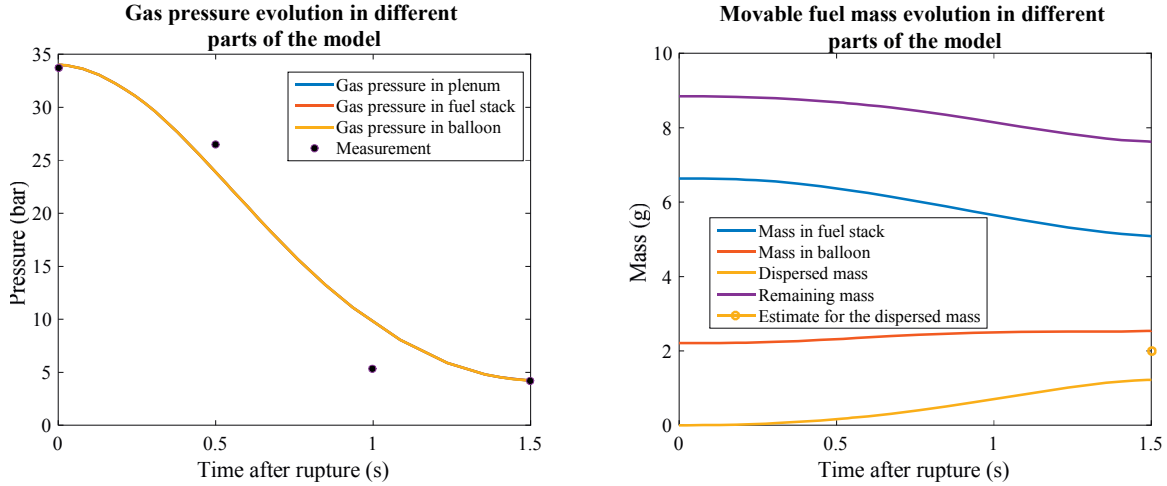

Figure 73: Pressure drop and dispersed fuel calculation for Halden LOCA test 12.

5.3.4.8 Halden LOCA test 13

The 13th LOCA test was cut from the same mother rod as the 12th. Furthermore, maximum cladding temperature, fuel fragmentation (as revealed by neutron radiography) and cladding deformation were very similar. Unlike test 12, fragment size distribution of test 13 indicates that 0.7% of all fuel fragments have sizes less than 2 mm [122]. But the fragment size distribution excludes the already dispersed fuel which needs to be approximated, because only the fuel that was inside the cladding was subjected to fragment size analysis. There is no reason to assume different value for the fraction of movable fuel than test 12 and therefore the dispersal model is initialized with the same fraction of 0.1. The model output is shown on Figure 74.

Gamma scanning revealed some dispersed fuel and the cladding rupture opening was considerably larger than the one of the previous test. The calculation shows 4 g of dispersed fuel, which is 36% of the total amount of assumed available fuel for dispersal. The estimated dispersed mass is based on the gamma scanning data of test 13 and is equal to 3 g.

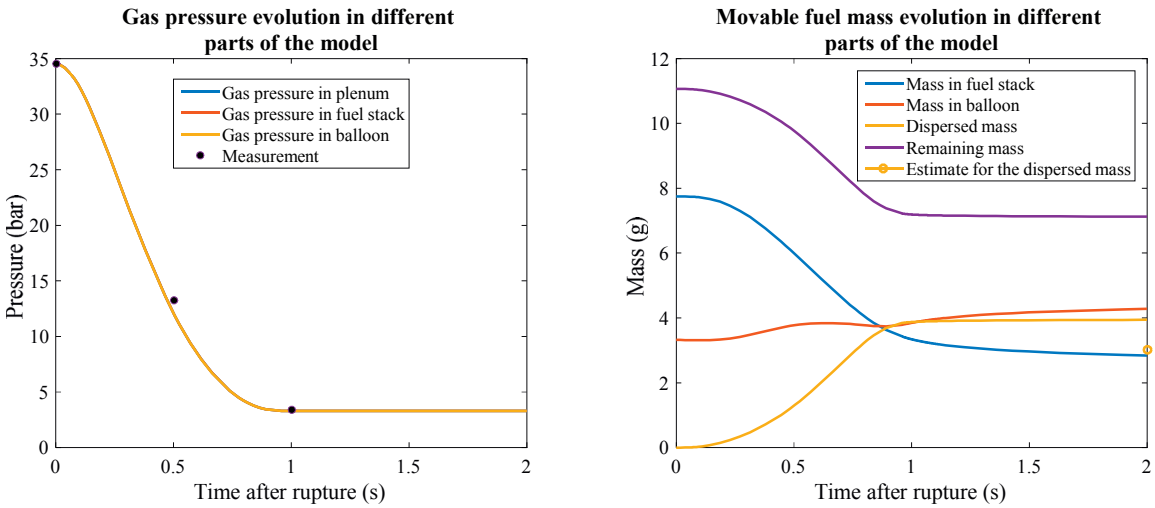

Figure 74: Pressure drop and dispersed fuel calculation for Halden LOCA test 13.

5.4 Application of fuel relocation and dispersal to full-length fuel rod

The end goal of the model development for fuel fragmentation, relocation and dispersal is to be able to evaluate the FFRD phenomena on a full-length fuel rod under realistic LOCA conditions. The aim of this section is to show how the link from the base irradiation to initialization of the transient calculation and simulation of FFRD can be established. In particular, the calculated fission gas release from the base irradiation calculations with FALCON/GRSW-A is used in the initialization of the transient. The necessary parameters to calculate fuel pulverization are taken from the last time step of the base irradiation simulation. The fraction of pulverized fuel is then used in the fuel dispersal model.

5.4.1 Initialization of the transient calculation

The BWR fuel rod AEB072-E4, from which the Halden tests 12 and 13 were made from, is used for the reactor-case application of the models for FFRD. This section describes the input preparation for the transient calculation. To prepare the input, few things are necessary. The FGR evaluated during BI must be included. This can be done via the GAP card in the FALCON input file, where the fraction of Helium and fission gases (Xenon and Krypton) in the free volume and the initial rod pressure are specified. Considering the plenum volume and assuming that half of the original fuel-cladding gap remains open, the rod inner pressure is recalculated using the initial quantity of helium and the quantity of FGR at the end of base irradiation. The FGR during BI for the selected rod can be referenced to Table 9 in Chapter 4. This is important to be included, because it has an impact on the rod pressure which is an important parameter during LOCA simulation. Besides the initialization of the gas pressure in the rod, the other input is the coolant pressure, decay heat power and cladding outer surface temperatures – all of which are taken from the TRACE LOCA simulation (see section 5.2.6).

5.4.2 Evaluation of the fraction of pulverized fuel

To calculate the axial distribution of the pulverized fuel using the fuel pulverization model (section 5.1.1), the radial burnup distribution for all axial stations of the fuel stack at the last time step at the end of base irradiation is needed. The base-irradiation calculation included 9 axial stations where the first and last had natural uranium fuel but the rest had 4.46% enriched UO_2. Figure 75 shows the calculated radial burnup profile at the end of base irradiation simulation with FALCON.

The first and last axial stations have very low burnup, because the fuel was natural uranium. Axial station 2 barely crosses the burnup threshold for fuel pulverization while all other stations show larger fractions of the fuel pellet whose burnup is higher than the pulverization threshold. Two other conditions for fuel pulverization is the loss of the fuel cladding contact pressure and the fuel temperature > 645 °C, both of which can be assumed during a LOCA with rod ballooning. Using the fuel radius of 4.095 mm and the parameters shown in Table 19, the pulverized fuel mass can be calculated for each axial station. This information is needed in order to evaluate the fraction of movable fuel necessary for the fuel dispersal model.

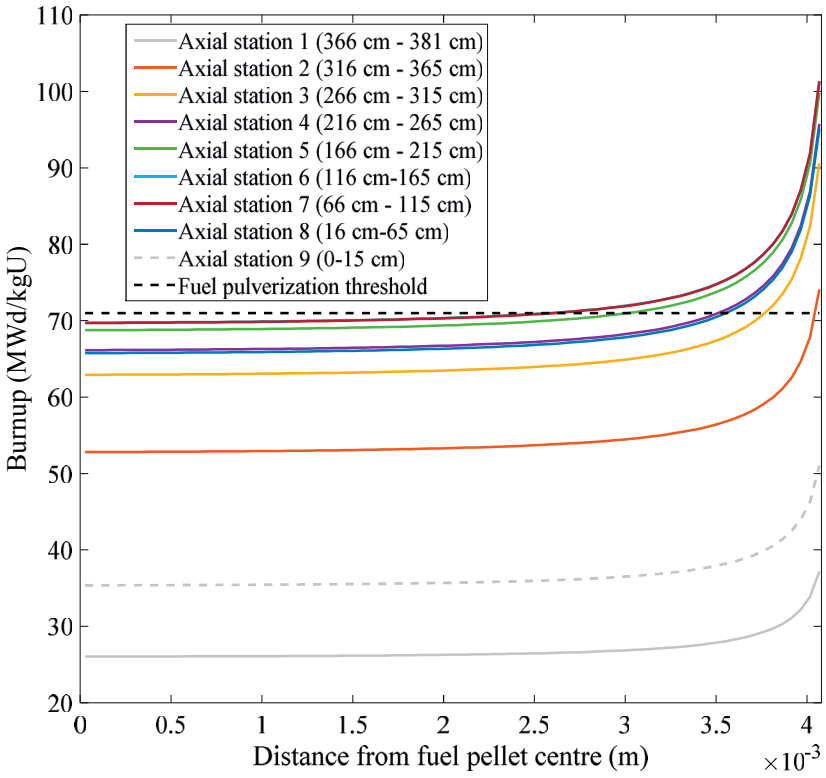

Figure 75: Calculated radial burnup distribution at the end of Base Irradiation at different elevations.

Table 19: Required parameters for the evaluation of the fraction of movable fuel.

Station #	$R_{Intersect}$ (mm)	Pulverized fraction	Station height (cm)	Pulverized fuel mass (g)
2	4.0	0.024	50.1	6.95
3	3.8	0.150	50.1	43.47
4	3.5	0.267	50.1	77.37
5	3.0	0.466	50.1	135.0
6	2.6	0.594	50.1	172.14
7	2.6	0.593	50.1	171.85
8	3.6	0.231	50.4	67.34

Fuel relocation calculated for the full-length fuel rod simulation via the FALCON-TRACE coupling scheme (see section 5.2.7) was already shown on Figure 58.

5.4.3 *Input parameters to the fuel dispersal model*

This section discusses the necessary input parameters to the fuel dispersal model. Perhaps the most important parameter is the inner gas pressure at cladding rupture, because the pressure difference provides the driving force for the gas outflow and the solid-gas interaction and it should, at least in principle, have an impact on the quantity of dispersed fuel. The rod inner pressure, maximum cladding temperature and gap temperature are shown on Figure 76. The values at the moment of rupture are necessary for the initialization of the fuel dispersal model.

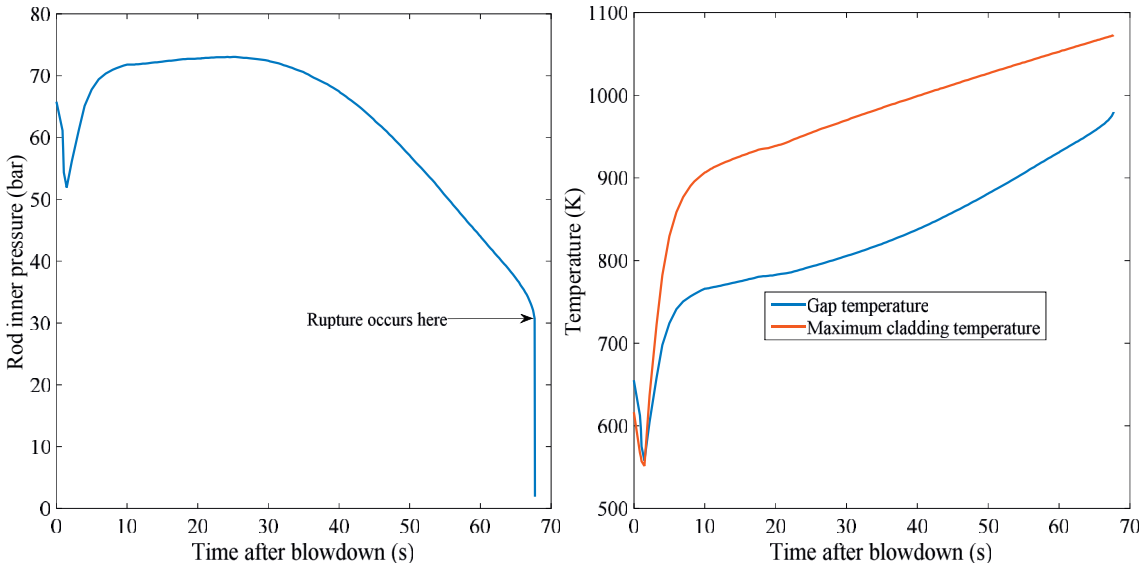

Figure 76: Rod inner pressure evolution (left), maximum cladding temperature and gap temperature (right).

The pressure drop immediately after start of blowdown (Figure 76 left) is due to the drop in temperature, which in turn is caused by the flashing of the coolant which temporary increases the heat removal from the rod. After this, the temperature steadily increases. The pressure begins to decrease about 25 seconds after start of blowdown, which means that the rod started to balloon a second (or two) earlier. The peak pressure was about 72 bars and the rupture pressure about 30 bars.

Most of the required input parameters to the fuel dispersal model are geometrical and are approximated from the axial cladding hoop strain profile calculated by FALCON at the moment of rupture shown on Figure 77.

The location where the ballooning starts and ends is somewhat arbitrary, but here it is assumed that cladding strain above 5% belongs to the balloon and this region is located between the intersection points of the cladding strain profile and the red line shown on Figure 77. In this LOCA simulation, the threshold for fuel relocation is also set equal to 5% cladding hoop strain. The rupture location occurs at axial elevation of 2.16 m. Cladding deformation (and therefore reduction of internal pressure) appears to start around 3 m, but to simplify the discussion let it begin at 3.15 m (the upper bound of axial station 3 on Figure 75). With reference to Table 19, the total mass of pulverized fuel for the region 2.16 m – 3.15 m is 121g. The total fuel mass in the fuel rod is:

$$M = \pi \cdot \mathrm{R}_{Fuel}^2 \cdot H \cdot \rho_{Fuel} = \pi \cdot (4.095 \cdot 10^{-3})^2 \cdot (3.81) \cdot 10980 = 2200\ g$$

which means, the fraction of movable fuel is equal to 121 / 2200 = 0.055. Table 20 summarizes the necessary information for executing the fuel dispersal model.

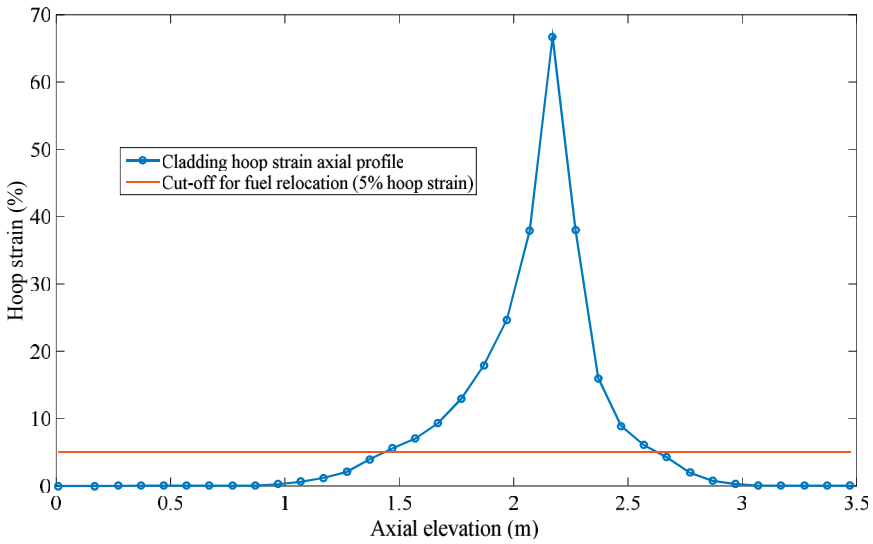

Figure 77: Axial cladding hoop strain at rupture for the simulated LOCA test.

Table 20: Reactor-case input parameters for the fuel dispersal model.

Parameter	Parameter description	Value
$P_1 = P_2 = P_3 = P$	Pressure in the fuel rod at the moment of rupture (bar)	30.4
P_4	Outside pressure (bar)	1.9
T_w	Temperature of the immovable fuel and cladding wall (K)	980
D_{ave}	Average fuel fragment size (mm)	1*
D_{clad}	As-manufactured cladding inner diameter (mm)	8.36
$\overline{D}_{clad}$	Average cladding inner diameter in the fuel stack (mm)	8.93
L_1	Length of the plenum (mm)	259
L_2	Length of the fuel stack (mm)	1190
L_3	Length of the cladding balloon (mm)	450
$L_3{}'$	Width of the balloon (mm)	13.8
$D_{balloon}$	Average cladding diameter in balloon (mm)	11.3
$A_{rupture}$	Area of cladding rupture opening (mm^2)	1*
D_{fuel}	Fuel pellet diameter (mm)	8.19
F_{fuel}	Fraction of movable fuel	0.055
M_{gas}	Molar mass of gas mixture (Helium+Xenon) (kg / mol)	0.076
ρ_s	Fuel density (kg/m^3)	10980
k_g [a]	Gas thermal conductivity ($W \cdot m^{-1} \cdot K^{-1}$)	$6.94 \cdot 10^{-2}$
c_g [b]	Gas specific heat capacity ($J \cdot kg^{-1} \cdot K^{-1}$)	2330
μ [c]	Gas dynamic viscosity ($Pa \cdot s$)	$5.13 \cdot 10^{-5}$
R	The universal gas constant ($J \cdot mol^{-1} K^{-1}$)	8.314
D_H	Hydraulic diameter just below the plenum	30 μm

*assumed values

[a] Combined gas thermal conductivity of the Xenon and Helium

[b] Combined heat capacity of the Xenon and Helium

[c] Combined dynamic viscosity of the Xenon and Helium

Before executing the fuel dispersal model, it remains to find an adequate value for the resistance to axial gas flow (necessary parameter in the modelling of Halden tests 3, 5 and 9 and all Studsvik tests), because as it is evident from the hoop strain profile (Figure 77), there is 0% near the plenum and

considering fuel swelling and possible partial fuel-cladding bonding (e.g. Figure 41) the hydraulic diameter can be quite small which will impact the axial gas flow. Although the modelled fuel rod has been extensively analysed, the hydraulic diameter was not measured. A value of 30 μm is used, which comes from measurement of hydraulic diameters during cladding lift-off studies on PWR fuel reported in [123]. Similar hydraulic diameter is reported in the post-test analysis of Halden LOCA test 5 [124]. The fuel dispersal model is now ready to be executed and the output is shown on Figure 78.

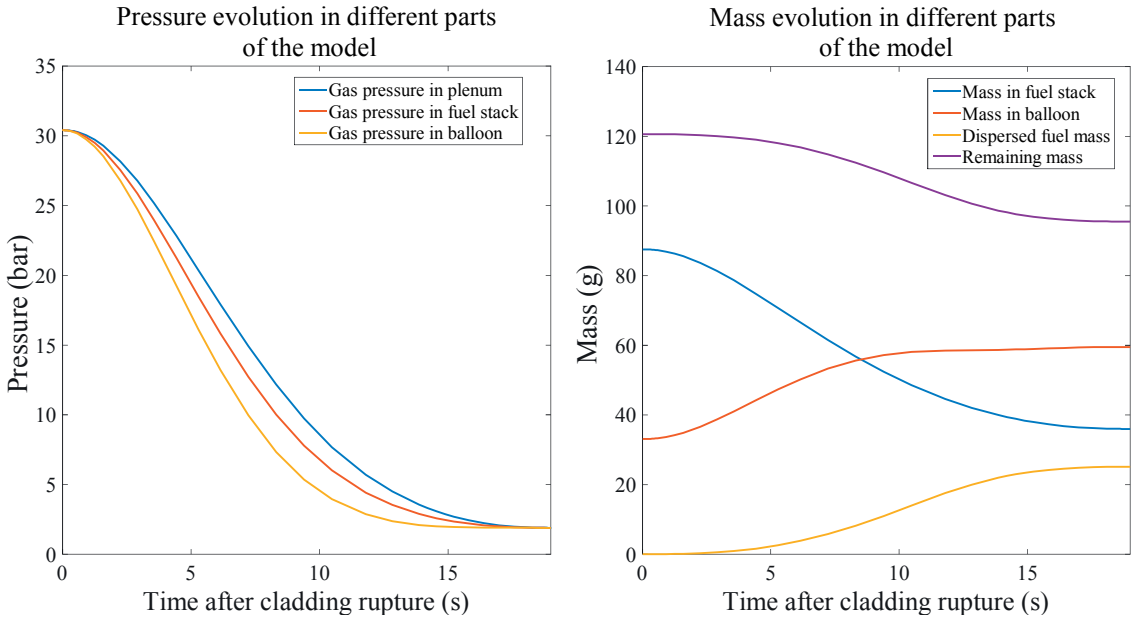

Figure 78: Fuel dispersal model output for the reactor case using initial parameters in Table 20.

The initial value of the "remaining mass" is equal to the mass of the movable fuel. It is distributed between the fuel stack and balloon proportionally to the length of both (e.g. ratio of L_2 and L_3 is equal to the ratio of the mass in the fuel stack and mass in the balloon). The total amount of dispersed fuel is 25 g out of the 121 g available. The dynamics of the dispersed fuel mass is correlated with the dynamics of the gas pressure in the plenum which makes intuitive sense, because driving force will exist until the rod has fully depressurized. According to the fuel dispersal model, the location of the balloon will have a large impact on the calculated dispersed fuel, because the fraction of movable fuel will increase. It is difficult to make predictions on how realistic this is, but with the help of specially designed mock-up tests (see Chapter 6 section 6.3.5.1); the influence of the distance between the rupture and the plenum on the dispersed fuel and other parameters can be investigated.

5.4.4 Calculation of the Equivalent-Cladding Reacted (ECR)

Cladding ballooning is a process which starts and ends (at the moment of rupture) within few tens of seconds. Because of thermal inertia, the feedback from the increased LHGR (due to fuel relocation into the balloon) may not play an important role. During ballooning, the increasing volume locally leads to a pressure reduction and it was shown by Khvostov [83] that in the event of fuel bonding gas re-distribution from the plenum to the balloon may be delayed and actually impact the time to rod rupture (rupture takes longer time). Since relocation is a gravity-driven phenomenon, it can be anticipated that under conditions of bonding and delayed gas re-distribution the thermal feedback on the cladding may in fact play a role, but this has not been investigated in this dissertation. The effect of fuel relocation on the cladding temperature is considered from the point of view of creation of hot-spot and oxidation.

This section presents the same LOCA calculation that was used in the previous section but an additional FALCON simulation is executed that does not reflect the effect of fuel relocation on the cladding temperature. In essence, the fuel relocation model was switched off during the TRACE calculation that supplied the boundary conditions. The goal is to compare the inner and outer oxidation for the two simulations and it is reported on Figure 79.

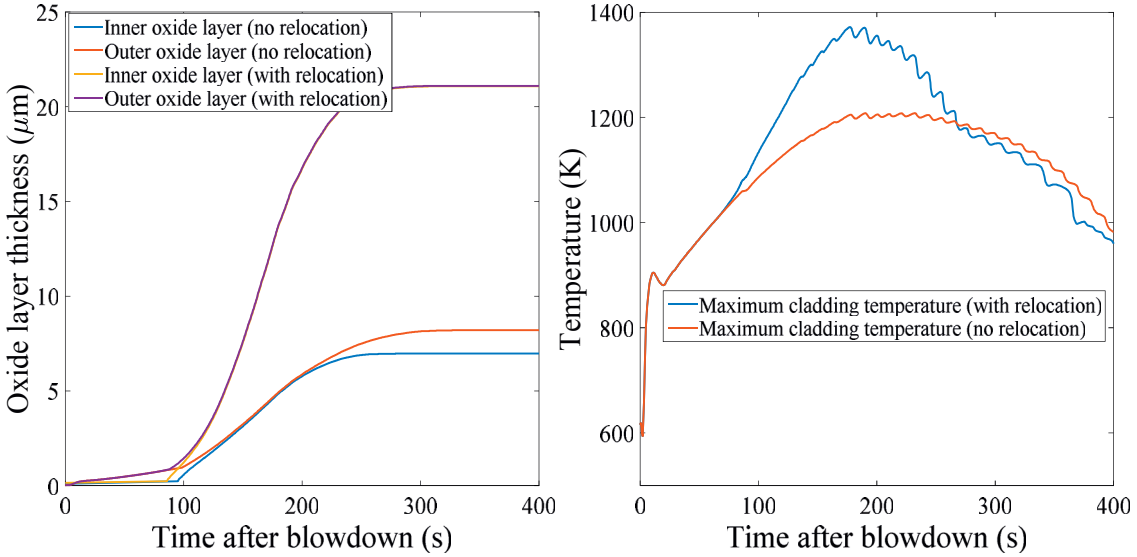

Figure 79: On the left: Calculated maximum inner and outer oxide layer thickness with FALCON and the high-temperature oxidation model Baker-Just[54] for two cases: with and without the effect of fuel relocation on the cladding temperature. On the right: Evolution of the maximum cladding temperature where the case with relocation is the one reported in Figure 58.

In the event of cladding rupture, both inner and outer oxidation must be included in the evaluation of the ECR [84]. Evidently, the case with simulation of fuel relocation resulted in more than double the oxide layer thickness (inner + outer) compared to the case without relocation (about 42 μm against 15 μm respectively).

The motivation behind a limit on cladding oxidation (expressed as ECR) is to ensure mechanical integrity of the fuel cladding in the event of a LOCA. It follows that a conservative assessment of the ECR should also include the fact that at the balloon and rupture the cladding wall is in fact – thinner [125]. The calculation of the ECR taking into account the thinning of the cladding is expressed by Eq. 19

Eq. 19: Calculation of the Equivalent-Cladding Reacted (ECR).

$$ECR = \frac{\delta_{oxide} \cdot (1 + \varepsilon_{max})}{w_t}$$

The parameter δ_{oxide} is the double oxide layer thickness at the end of the transient simulation, ε_{max} is the maximum cladding hoop strain and w_t is the cladding thickness at the start of LOCA transient with the oxide layer thickness at the end of Base Irradiation subtracted. Using the oxide layer thicknesses from Figure 79, the maximum cladding strain of 68% from Figure 77, the as-manufactured cladding wall thickness of 630 μm, the base irradiation oxide thickness of 40 μm and Eq. 19, the ECR for the two cases is 12% and 4.3% for the simulation with and without fuel relocation respectively. The calculated ECR with the effect of relocation is getting close to the LOCA safety criterion of 17%.

5.5 Conclusion

Many countries operating Pressurized or Boiling Water Reactors are using as part of their licensing process the U.S.NRC Loss of Coolant Accident (LOCA) Safety Criteria (NRC Regulations 10 CFR, section 50.46). They were formulated in the 1970's based on studies with fresh or low burnup fuel. Since then, the burnup limit at discharge has been continuously increasing and this fact may require for the review of these criteria. It has been recognized that the UO_2 fuel matrix undergoes significant changes with burnup. Recent LOCA tests with high burnup fuel, such as Halden's LOCA test 9 summarized in [26] or Studsvik's test 193 described in [27], clearly demonstrated the fuel's susceptibility to fragment, easily relocate and be dispersed through the cladding rupture. Efforts to better understand the fuel fragmentation, relocation and dispersal phenomena are on-going within the nuclear fuel community.

Fuel fragmentation is a complicated phenomenon which is influenced by many parameters, such as the back pressure supplied by the cladding wall in case of pellet-cladding mechanical interaction or the inner rod pressure in case of open pellet-cladding gap, burnup, last power cycle and temperature. It is not yet fully understood and there are no comprehensive models describing it. Two modes of fragmentation exist, one for the fuel interior which creates large fuel fragments and one at the periphery, leading to the so-called fuel pulverization. From the point of view of fuel relocation, the pulverized fuel presents particular interest because it can easily relocate and it can be dispersed after cladding failure. Because the fuel fragments can be smaller than 100 μm, it can be assumed that they can fit through all cladding rupture openings. The conditions for fuel pulverization are established during special tests [30, 31] and this allows more accurate modelling of this phenomena. With regards to the fragmentation of the pellet interior where thermal and mechanical stresses play leading role, there are some correlations presented in [34, 109] from which the number of fuel fragments can be calculated. In any case, no model can predict all the different shapes and sizes of the fuel fragments following a LOCA and the focus should be on whether those fragments can be relocated and dispersed. In the case of pulverized fuel both conditions are applicable.

Fuel relocation is treated as mostly a geometrical problem. Assuming the fuel has fragmented, extent of relocation will depend on the fragments shape and size and the cladding hoop strain. Fuel relocation is gravity driven until cladding rupture and afterwards under the influence of the gas outflow additional fuel can be relocated downwards. The presented fuel relocation model assumes that outermost fragments relocate first and this gives weight to the pulverized fuel which also has highest decay heat density and as such it should have the largest effect on the cladding temperature in the conditions of a hot-spot. In reality, relocation likely occurs more chaotically and in experiments [110] stack slumping have been observed. The FRELAX original relocation model operates under the assumption of uniform stack slumping and therefore the model discussed in this dissertation simply provides another approach with focus on the pulverized fuel.

The proposed approach to modelling fuel dispersal during LOCA seems to be adequate although it uses much simplified geometry. According to the model, there are only few parameters having significant impact on the quantity of dispersed fuel, such as the fraction of movable fuel, and the rest require only rough approximations. At the moment, the model takes as input only an average fuel fragment size which could be a serious limitation. Modelling of fuel dispersal for fuel rods whose cladding rupture opening is smaller than the average fuel fragment size will predict no dispersal, although pulverized fuel is small enough to fit through the rupture opening. This limitation, however, can be circumvented by setting the average fragment size smaller than the rupture opening and reducing the fraction of movable fuel. In essence, we are giving as input the fraction of fuel fragments whose sizes are smaller than the rupture opening. The current formulation of the model is also not very

sensitive to the average fuel fragment size, except when it is larger than the cladding rupture opening. There is little difference in the dispersed fuel for 0.05, 0.5 and 5 mm average fuel fragment sizes. This is a limitation of the model, because the smaller the fuel fragment sizes, the larger the area of the solid interacting with the gas and this must have an impact on the dispersed fuel.

The described modelling approach is capable of representing well the pressure measurements in Halden and Studsvik LOCA tests but it requires the tuning of the available area for gas flow within the fuel stack. Prediction of this parameter will be a challenging task and it could not be done in the context of this work. Parameters which can influence it are pellet-cladding bonding and cladding strain – both of which are not necessarily axis-symmetric. Additionally, the model cannot predict stochastic behaviour such as temporary increase in the resistance to gas flow observed in Studsvik's tests 189, 191 and 192.

The model provides a comprehensive framework for further extension, having incorporated the three fundamental conservation laws. An advantage is that it has been shown to be applicable to nearly all the available data from LOCA testing carried out in Halden and Studsvik. It has been shown that after a tuning of a few input parameters the amount of dispersed fuel can be reproduced by calculation with a reasonable precision. Clearly the model can be further improved. For example, the fuel stack can be represented more accurately by sub-dividing it into smaller parts which will require additional differential equations for the conservation of mass, energy and momentum. Frictional forces between the solid particles can be considered, which will make the average fuel fragment size more important and adding the possibility to input a fragment size distribution. In order to validate such model, additional experimental data is required which is specifically designed for this purpose. Fortunately it is not necessary to use real high burnup fuel, because the interaction between the different fragment sizes and the gas can be investigated with substitute particles. The trapped fission gases were implicitly included in the fuel dispersal modelling of Halden tests 12 and 13 via the pressure measurements. When performing LOCA simulation of high burnup BWR fuel, the calculated trapped fission gases need to be explicitly released during the LOCA and added to the rest of the gas and recalculate the pressure. The model for fission gas trapping is now integrated into FALCON and it can evaluate the quantity of trapped fission gas that can be assumed released during a LOCA.

6
Chapter 6:
Conclusions and recommendations

6.1 Executive summary

The main goal in this PhD project was the developing of models for fuel fragmentation, relocation and dispersal during Loss-of-Coolant Accidents in Light Water Reactors. Although fuel fragmentation and relocation has been studied long ago, interest on the subject was recently renewed and it is quite relevant because there appears to be strong correlation between burnup and the extent of fuel fragmentation which in turn directly influences relocation and dispersal. Since today's reactors operate fuel to ever higher burnup, the FFRD phenomena is very relevant and in fact a revision of the LOCA safety criteria is underway. This is necessary, because conclusions made on experiments with fresh or low burnup fuel (at the time of writing the current LOCA safety criteria) cannot be extrapolated to high burnup fuel. Today's computing power led to the development of sophisticated software tools with 3-dimensional capabilities such as INL's BISON and CEA's ALCYONE. Yet, experimental data is scarce and the phenomena surrounding the fuel fragmentation are not yet fully understood. Additionally, there are uncertainties with the modelling of cladding deformation and no comprehensive models on cladding rupture.

Main source of experimental data for the present work was the OECD Halden Reactor Project LOCA test program. For this reason, a three-month technical visit at the Halden Reactor Project was organized in order to learn more about the experiments and collect relevant experimental data. Particular attention was paid to the gamma scanning data – a standard Post-Irradiation Examination procedure conducted for all LOCA tests with the primary aim to provide visual image of the fuel rod state and confirm whether the test objectives were met. The gamma scanning data could in fact reveal other valuable insight, which led to the formulation of a gamma transport model (see Appendix A) that was published in the journal Nuclear Engineering and Design. Its aim was to investigate the origin of the relocated fuel (e.g. from periphery or from the pellet interior, or mixture) into the balloon. This is important question, because owing to the much higher burnup, fuel at the periphery has higher decay heat density and therefore it may lead to higher local cladding temperatures in the event of a hot-spot. The data analysis, however, could not show preferential fuel relocation from the periphery which is in-line with the assumption in FRELAX, a Halden LOCA-specific model for axial gas flow and fuel relocation, that the relocated fuel in the balloon is mixed. Yet, the quality of the gamma scanning data was not sufficient to conclusively prove this. Although it is not clear whether this work had anything to do with the effort to enhance the gamma scanning procedure, researchers at the Halden Reactor Project used a gamma tomography in order to get a 3-dimensional image of the relocated fuel in LOCA test 15 (see section 3.6.5). With this procedure, individual fuel fragments are now visible and more insight into the fuel relocation can be obtained. The technical visit at the Halden Reactor Project was concluded with observation of the successful test execution of the non-burst LOCA test 14.

Over the course of the Halden LOCA test program, Switzerland was active participant thanks to the high burnup PWR and BWR fuel irradiated in KKG and KKL and the pre-test calculations and post-test analysis done at PSI and in particular by Grigori Khvostov. Tests 4 (prepared from fuel irradiated at KKG), in fact, surprised the community with the large quantity of dispersed fuel and fine fuel

fragmentation and the FFRD phenomena attracted the attention of many institutions. Significant fuel fragmentation, relocation and dispersal were demonstrated also in Halden's test 9 and in Studsvik's tests 189, 191, 192 and 193 (see Figure 21 and Table 17).

During the execution of Halden's test 12, the inner rod pressure reached unexpectedly high values and that was attributed to an additional a-thermal mechanism of fission gas release that is unlocked during the LOCA transient. The mother rods for tests 12, 13 and 14 came from KKL and in particular from selection of high burnup BWR fuel rods that were part of a KKL-Westinghouse-PSI fuel performance program, which among other things included measurements of the fission gas release in the rod plenum at the end of base irradiation. Those measurements showed significant scatter that could not be immediately explained, because the burnup level, fuel enrichment and operating history were very similar. Other post-irradiation examination data on the mother rod of Halden tests 12 and 13 (AEB072-E4) revealed intact fuel pellet-cladding bonding. The fact that the fuel was bonded only on one side (e.g. Figure 41) was explained with the azimuthal burnup asymmetry which was confirmed from Electron-Probe Microanalysis measurements (see Figure 40). This asymmetry was particularly pronounced for a fuel rod located next to the moderator channel, because of the exposure to higher thermal neutron flux at the side oriented towards the moderator channel (see Figure 35). This led likely to asymmetrical fuel-cladding bonding that could remain intact during power dips – thereby creating the conditions of a permanent fuel-cladding bonding layer. Scanning electron microscopy images at the bonding layer revealed presence of large voids and 'pockets' (as seen on Figure 41). It is hypothesized that they are examples of potential local trapping sites for fission gases. Base irradiation was simulated with FALCON coupled with the GRSW-A model for all rods and in all cases the calculated fission gas release was overestimated, yet for some rods much more than other in relative sense. A two-dimensional Serpent Monte Carlo model was used to evaluate the burnup azimuthal asymmetry as function of rod position. It was established that the rods near the moderator channel have the highest asymmetry, the rods in the interior – the lowest and those at the periphery – somewhat in-between. The creation of a bonding layer requires time and it was assumed that the burnup azimuthal asymmetry is also important. Fuel-cladding contact pressure was calculated with FALCON and together with the calculated degree of burnup asymmetry by Serpent, a model for fission gas trapping (see section 4.5) was formulated. After this, fission gas trapping was calculated and the comparison between the calculated and measured fission gas release was improved. The culmination of this work is integration of the model for trapping with FALCON/GRSW-A by Grigori Khvostov. One may wonder what the interest in the trapped fission gas release is. For one, it could have been the cause for the rod burst in test 12 which was designed as a non-burst LOCA test. In the pre-test calculations of test 14 (repetition of test 12) extra burst fission gas release was accounted for and the test was successful. In reality, it is very possible that burst FGR plays an important role for the LOCA transient; it raises the gas pressure and it may impact the time to cladding failure. The former will cause larger internal gas pressure drop that may amplify the fuel dispersal. This hypothesis can actually be studied with specially designed mock-up tests as presented in section 6.3.5.1.

The work continued with the formulation of a model for fuel fragmentation (see section 5.1). It is actually based on the conditions for fuel pulverization published by J.A. Turnbull et.al. based on a research work in the framework of the Nuclear Fuel Industry Research (NFIR) program led by EPRI. The necessary parameters, namely local fuel temperature and burnup, could be extracted from the FALCON output. Unfortunately, further development for the fragmentation model was not made. Still, from the point of view of fuel relocation and dispersal, addressing the pulverized fuel is deemed to be more important, because it can be assumed that the pulverized fuel can easily relocate and be dispersed during a LOCA transient. Such assumptions were adopted by the US.NRC when evaluating

fuel dispersal during full-core LOCA simulations [119]. Nevertheless, the fragmentation model remains incomplete.

The fuel relocation model (presented in section 5.2) was started independently, and it requires only two inputs from modelling: the cladding hoop strain as a function of time calculated by FALCON (or any other fuel behaviour code) and input for the fragment size distribution. The model is flexible and allows the user to input any fragment size distribution. It provides individual fragment size tracking, which can be used to visualize how a given fragment size is distributed along the length of the rod. When a more comprehensive fuel fragmentation model is developed, it should be a separate task to connect it to the fuel relocation model.

Modelling of the fuel dispersal (see section 5.3) is currently highly simplified, but it manages to capture the underlying reason behind the dispersal – the interfacial friction between the gas and the solid. The rate of pressure decrease calculated by the model compared well to experimental data after the introduction of a resistance parameter to the axial gas flow. This parameter reduces the hydraulic diameter which is shown via lift-off tests to be very small in high burnup fuel. All of the LOCA tests in Halden and Studsvik that showed resistance to the axial gas flow experienced some sort of restriction in the parts of the cladding that had low hoop strain. Therefore, the physical interpretation of this parameter is partial gap closure due to the combined effect of fuel swelling and low cladding hoop strain.

Modelling of fuel fragmentation, relocation and dispersal is complicated and there is still much more to be done. Ideally, the developments in this PhD project will be used as basis for further development within this topic.

6.2 Main achievements

During the course of the PhD project on fuel fragmentation, relocation and dispersal, three conference papers were presented, two journal papers are published and one have been submitted and is still under journal review. A contribution has been made to Chapter 5 of the NEA report on Fuel fragmentation, Relocation and Dispersal (NEA/CSNI/R (2016)16).

The potential to use the gamma scanning data at Halden for more than just visual image of the post LOCA state of the test rod has been demonstrated and the results reported in a journal paper. Gamma scanning has the potential to reveal more details about the relocated and dispersed fuel, including origin and packing factors.

A hypothesis for fission gas trapping and a model were formulated that explain, at least partly, the scatter in the fission gas measurements of high burnup BWR fuel. The analysis is published in a journal paper and the model for fission gas trapping has been integrated into the FALCON code by Grigori Khvostov.

The model for fuel relocation is very quick, it allows the user to input any fragment size distribution and provides individual fragment tracking. Furthermore, it considers the origin of the fuel fragments in the calculation of the change in LHGR in the axial direction. It can be further improved, but it already provides reasonable modelling of this phenomenon.

The presented modelling approach to fuel dispersal can be used as the basis for a more sophisticated model. It appears that the calculated gas outflow compares well with experimental data after

adjustments of the hydraulic diameter. At the time of writing this section, there are no comprehensive models published on this topic.

6.3 Recommendations for future work

This section discusses possible changes and additions to the developed models and it concludes with brief discussion of possible non-nuclear tests for gathering validation data for selected phenomena.

6.3.1 Fuel fragmentation model

The fuel fragmentation model currently only considers fuel pulverization occurring at the fuel periphery, which is driven specifically by the loss of hydrostatic pressure and the over-pressure of the fission gas bubbles. This process seems to be already well understood in the community. But, the fuel interior also fragments and there the cause is completely different. Indeed, good progress for this model was not made during the PhD study, but fuel fragmentation in the pellet interior is very complicated phenomenon which is not yet fully understood and requires much more time and validation data for the creation of a comprehensive model which is recommended to be done in the future.

6.3.2 Fuel relocation model

Fuel relocation before cladding failure is driven by gravity and after rupture it can be influenced by the gas outflow. The current version of the model only covers the first part. Clearly, after cladding rupture, fuel may be further relocated under the action of the gas outflow and this may change the quantity of fuel in the balloon and either amplify or reduce the hot-spot effect. A link between the relocation and dispersal models should be established, but this cannot be done until the latter can take the same fragment size input as the former. An assumption of the relocation model is that the outermost fragments relocate first. Although this makes intuitive sense, a situation of stack slumping cannot be adequately modelled. This may occur, for example, when all the fuel from axial station 20 has relocated, but the fuel at axial station 21 was held in place due to low cladding hoop strain, but if the threshold is reached then there is no reason for the fuel at axial station 21 simply not to fall down as one.

Additionally, influence of the fragment shape is not taken into account and it is currently assumed that the relocated fuel packs as close as possible – thereby achieving the maximum packing factor. There is a stochastic effect associated with the packing of the fragments and it could be somehow incorporated into an updated value for the maximum packing factor. Furthermore, in the presence of say two different fragment sizes with one much smaller than the other, even higher packing factors can be achieved, because the voids that exist between the large fragments can be filled with the smaller fragments. The current formulation of the model assumes that the different fragment sizes do not mix at all. It is recommended that relocation after cladding rupture is added to the model. Additionally, once the average fuel fragment size, currently used in the relocation model, is replaced with a fragment size distribution, it will be necessary to update the calculation of the relocated fuel packing factor.

6.3.3 Fission gas trapping model

The model of fission gas trapping currently considers an integral value for the fuel bonding along the whole length of the fuel rod. This is a very rough approximation, because bonding is time and burnup-dependent process and as such the lower half of the fuel rod (in case of BWR) may develop bonding layer much sooner than the upper half (if it ever develops one, because as it was shown from the modelling in Chapter 4, the upper cladding gap may not even close). Therefore, it makes sense that trapping is calculated individually for each axial station of the finite element mesh. If the model mechanics is kept the same, this will require obtaining the burnup asymmetry calculated with different moderator void and therefore the Serpent model (section 4.4), that is used to calculate the burnup asymmetry, needs to be extended in the axial direction. It is recommended that the fission gas trapping model is updated to evaluate bonding at each axial station of the finite element mesh. To obtain the burnup asymmetry, the Serpent model must be evaluated with the void fraction corresponding to each axial station. As a first approximation, the void fraction can be taken from the FALCON base irradiation simulation.

6.3.4 Fuel dispersal model

There are many uncertainties associated with the fuel dispersal. Perhaps the most important parameter in the end is the size of rupture opening because it determines the maximum fragment size that can potentially be dispersed from the fuel rod. At present, a model that can make predictions on the cladding rupture size does not exist and in general, validating such model will be a daunting task. A good assumption is that the pulverized fuel, which is known to exist under certain conditions, can escape regardless of the cladding rupture opening size. Fuel fragment shape is another parameter that cannot be modelled. The further away a fragment's shape is from spherical, the higher the friction will be between such particles and this will likely reduce the quantity of dispersed fuel and even lead to some sort of blockage. Non-nuclear mock-up tests can perhaps shed some light on this (see next section).

At the moment, the plenum, fuel stack and balloon are treated as single control volumes (see Chapter 5 Figure 59). This may be valid for the plenum, but certainly not for the fuel stack, which may be over 1 meter long, or the balloon, where cladding deformation may change significantly over the length of the balloon. It makes sense that the fuel stack and balloon are further divided into smaller control volumes and the system of ODEs is expanded to reflect this.

As Halden (e.g. tests 3, 5 and 9) and Studsvik (e.g. tests 191, 192 and 193) LOCA tests demonstrated, that obstruction to the gas outflow may exist whether due to bonding or other effects and this is currently not modelled. Instead, the user must provide some reasonable value (such as measurement of the hydraulic diameter in high burnup fuel) otherwise the ODE solver may even not converge.

At the moment, this issue can be addressed by using the cladding hoop strain value near the plenum and the fuel swelling calculated by FALCON-GRSW-A in order to derive an approximation to the effective hydraulic diameter. If the fuel-clad bonding can be simulated in the future, it can also be incorporated into the fuel dispersal model.

Another problem from using an average fuel fragment size is the fact that the model will calculate no dispersal if the fragment size is smaller than the rupture opening. If all of the fuel is pulverized, then there is no problem, but if the average fragment size, is taken from the post-irradiation examination of Halden LOCA test 13 (e.g. 4 mm), then no dispersal will be calculated (width of the rupture was 2 mm). This limitation will be eliminated once the model is able to handle fragment size distribution as input but then a mechanism for "filtration" at the cladding rupture will need to be introduced as well.

Under the assumption of fluidized solid phase, the solid-solid interaction is ignored. In reality this is unrealistic, because cladding geometry and rupture size opening guarantee solid-solid interactions and as such the momentum equation for the solid phase may need to be updated.

6.3.5 Non-nuclear tests for gathering validation data

The most sophisticated fuel modelling software can be written but in the end the models still need to be validated. It is a fact that there is only limited amount of experimental data and for a good reason. High burnup nuclear fuel is highly radioactive and it requires great effort and resources to move it from the reactor core to the test site (e.g. Halden Reactor or Studsvik). After testing, it must be analysed in a hot-cell which requires additional resources and time. In addition, many parameters are typically associated with a given phenomenon. For example, fuel fragmentation is impacted by the burnup, last cycle power, temperature, compressive forces exerted by the cladding tube or the inner rod pressure and other factors. Furthermore, tests should be repeated under the same conditions to check and see whether the outcome is similar (repeatability). If it is, then this is good news. If not, then there may be other mechanisms at play that need to be investigated (or the process is purely stochastic). In the end, to gather the necessary validation data, many different tests need to designed and executed. Fortunately, some phenomena can be studied without the need of nuclear fuel.

6.3.5.1 Mock-up tests to simulate fuel dispersal

Fuel dispersal is impacted by the cladding rupture size opening, fuel fragments' shape and size, inner gas pressure and possibly cladding deformation. The dispersal has nothing to do with the presence of the radioactive fission products. This means, that mock-up tests can be designed to gather validation data for a fuel dispersal model. A substitute material for the UO_2 can be lead, because it has almost the same density. Furthermore, lead spheres can be manufactured down to a size of 100μm to represent the pulverized fuel. Using some grinding and pressing, the spherical shapes can be changed in order to reflect the fact that fragmented fuel is not spherical. It is expected that the non-spherical shape should actually reduce the dispersal, because of the larger friction and possibility of local blockages. The cladding balloon and rupture can be pre-manufactured – thereby removing any uncertainty in these parameters. Serious technical obstacles for such mock-up tests do not appear to exist.

In order to keep the representativeness, the fuel geometry needs to be kept the same. This means that the cladding tube should have inner diameter of about 1 cm and this may lead to practical issues, such as filling the cladding tube with the different size fragments. This can be helped by using specially designed cylindrical sleeves as shown on Figure 80.

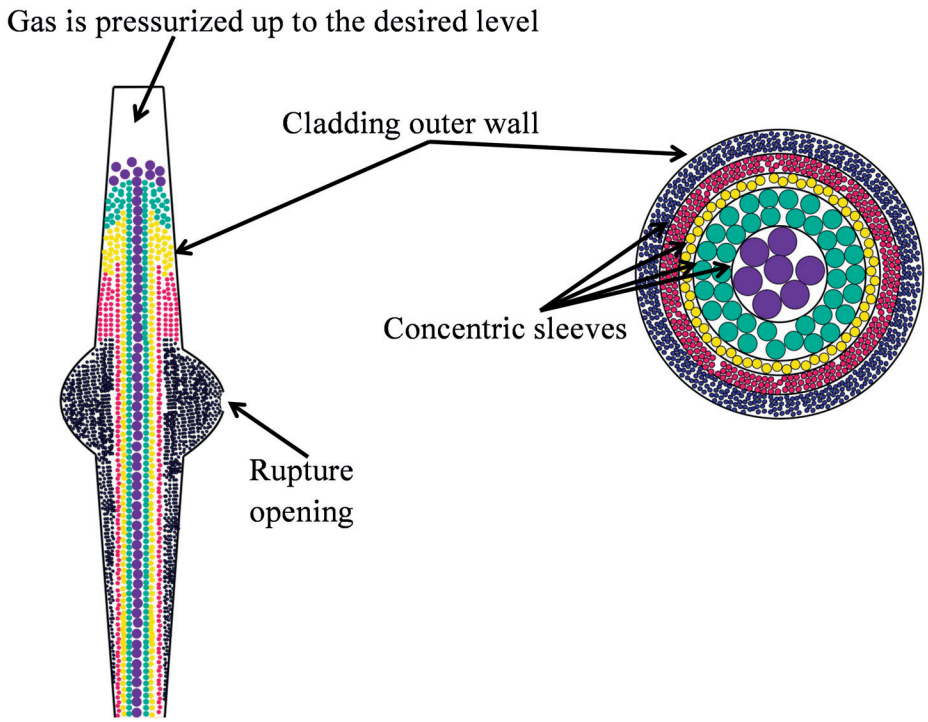

Figure 80: Sketch of the fuel dispersal mock-up test.

The sleeves will need to be mechanically stable, so that they do not easily buckle and at the same time should be manufactured as thin as possible. When they are positioned inside the cladding, the fragments can be inserted in between the sleeves with the help of funnels. When the filling is done, the sleeves will be withdrawn one by one and this should preserve the original loading pattern at least near the balloon. As it is shown in Figure 80, the top of the fragment column will likely relocate to fill up the balloon.

In chapter 3 section 3.4.4 it was hypothesized that the central hole in VVER fuel pellets may play an important role during fuel dispersal. If the central sleeve is perforated and left free of fuel fragments – thereby roughly simulating the presence of the central void, this hypothesis can be tested.

Next, the cladding tube will be filled with Helium (or other gas) and pressurized to the desired pressure while keeping the rupture opening blocked. Finally, the rupture blockage will be removed and the dispersal will run its course. After the test, the fragments can be collected and subjected to fragment size distribution.

Evidently, such tests can generate large quantity of validation data relatively quickly. Uncertainties with some parameters, such as cladding balloon size and rupture opening, can be eliminated. The aim of this section was just to present a simple idea and some important details may have been overlooked. If such tests are executed, the adopted procedures can be quite different.

6.3.5.2 Simulation of the hot-spot effect

In the past, when fuel relocation was studied with low to medium burnup fuel, appearance of a hot-spot on the cladding was ruled out, because the large fragments when relocating left a lot of void volume and overall the local linear heat generation rate could even be reduced. This can no-longer be assumed for high burnup fuel, because the fragmentation of the pellet periphery creates very small and very mobile fragments which can potentially fill the voids between larger ones and thereby lead to the creation of a hot-spot effect. The importance in this phenomenon is that it could cause high localized cladding oxidation and possibly challenge the 17% ECR LOCA safety criteria. As with fuel dispersal, the presence of nuclear fuel is not required. The decay heat can be simulated with electrical heaters and to create the conditions of a hot-spot effect, the electrical heater can be designed in such a way that it delivers more heat at the level of balloon. To create mock-up tests to study the hot-spot, unirradiated cladding tubes with pre-manufactured balloon, electrical heater and steam environment are needed.

Acknowledgements

There are many people that have contributed to my success and well-being at PSI over the past four years.

- I would like to express my gratitude to swiss***nuclear*** and PSI for the financial and technical support.

- I would like to thank Grigori Khvostov, Dr. Konstantin Mikityuk and Prof. Andreas Pautz for their support, patience and effort. No question or problem was left unaddressed. Without their help I will not be writing this page.

- I would like to thank Dr. Terttaliisa Lind for accepting my application to do internship in her group. I consider it as my starting point for my professional development. More importantly, I am grateful for her friendship, all the Christmas parties and barbecues and for trying to keep up during bike-to-work.

- To (now Dr.) Torsten Betschart and (hopefully soon Dr., but still Mr.) Filip Janasz, my fellow officemates during my time at the Severe Accident Group, I'd like to say thank you for the out-of-the-ordinary work environment.

- To Petros Papadopoulos, I hope your dedication to the cause of having affordable, clean and reliable energy source – in other words nuclear energy, will result one day in a new build in Switzerland.

- To Damar, Petra, Boris and Dionysios I say thanks for the discussions on various topics, the hikes, weddings, barbecues and beers. I do look forward to crossing paths again in the future. Boris, I am looking forward to reading news about you and the Molten Salt Reactor advancements.

- To Philippe Jacquemoud – thank you for being such a nice guy and always ready to resolve IT issues of any sort even when I should have sent a trouble ticket.

- To Ruth Ringele, thank you for your help with all the administration and organizational work.

- To Cedric Cozzo - now you are a FALCON master. With such power, comes great responsibility!

- My gratitude also goes to Urs and Teresa Stiefel for hosting me at their home in Mellingen all those years and for providing excellent living conditions.

In general, I'd like to thank all my colleagues at NES for the pleasant work environment and I wish them all the best.

References

1. Patterson, J.F. and K.P. Galbraith, *Mixing vane grid spacer*. 1978, Google Patents.
2. Fuel, M.N. *Scheme of a PWR fuel assembly*. Available from: http://www.mnf.co.jp/en/business/process.html.
3. AREVA, *GAIA Fuel Assembly. Maximum Fuel Robustness, Performance and Reliability*. 2014, Areva.
4. Spino, J., D. Baron, M. Coquerelle, and A.D. Stalios, *High burn-up rim structure: evidences that xenon-depletion, pore formation and grain subdivision start at different local burn-ups.* Journal of Nuclear Materials, 1998. **256**(2–3): p. 189-196.
5. Koo, Y.H., B.H. Lee, J.Y. Oh, and K.W. Song, *Conservative width of high-burnup structure in light water reactor UO2 fuel as a function of pellet average burnup.* Nuclear Technology, 2008. **164**(3): p. 337-347.
6. Une, K., M. Hirai, K. Nogita, T. Hosokawa, Y. Suzawa, S. Shimizu, and Y. Etoh, *Rim structure formation and high burnup fuel behavior of large-grained UO2 fuels.* Journal of Nuclear Materials, 2000. **278**(1): p. 54-63.
7. Rondinella, V.V. and T. Wiss, *The high burn-up structure in nuclear fuel.* Materials Today, 2010. **13**(12): p. 24-32.
8. Serna, J.J., P. Tolonen, S. Abeta, S. Watanabe, Y. Kosaka, T. Sendo, and P. Gonzalez, *Experimental observations on fuel pellet performance at high burnup.* Journal of Nuclear Science and Technology, 2006. **43**(9): p. 1045-1053.
9. Khvostov, G., K. Mikityuk, and M.A. Zimmermann, *A model for fission gas release and gaseous swelling of the uranium dioxide fuel coupled with the FALCON code.* Nuclear Engineering and Design, 2011. **241**(8): p. 2983-3007.
10. Nogita, K. and K. Une, *Irradiation-induced recrystallization in high burnup UO2 fuel.* Journal of Nuclear Materials, 1995. **226**(3): p. 302-310.
11. Matzke, H., A. Turos, and G. Linker, *Polygonization of single crystals of the fluorite-type oxide UO2 due to high dose ion implantation +.* Nuclear Instruments and Methods in Physics Research Section B: Beam Interactions with Materials and Atoms, 1994. **91**(1): p. 294-300.
12. Kinoshita, M., T. Sonoda, S. Kitajima, A. Sasahara, T. Kameyama, T. Matsumura, E. Kolstad, V.V. Rondinella, C. Ronchi, J.P. Hiernaut, T. Wiss, F. Kinnart, J. Ejton, D. Papaioannou, and H. Matzke. *High Burnup Rim Project: (III) properties of rim-structured fuel*. in *Proceedings of the 2004 International Meeting on LWR Fuel Performance*. 2004.
13. Romano, A., M.I. Horvath, and R. Restani, *Evolution of porosity in the high-burnup fuel structure.* Journal of Nuclear Materials, 2007. **361**(1): p. 62-68.
14. Kulacsy, K., *Mechanistic model for the fragmentation of the high-burnup structure during LOCA*. Journal of Nuclear Materials, 2015. **466**: p. 409-416.
15. Matzke, H. and J. Spino, *Formation of the rim structure in high burnup fuel.* Journal of Nuclear Materials, 1997. **248**: p. 170-179.
16. Matzke, H., *On the rim effect in high burnup UO2LWR fuels.* Journal of Nuclear Materials, 1992. **189**(1): p. 141-148.
17. OECD/NEA, *Thermal Performance of High Burn-up LWR Fuel*. 1998, OECD Nuclear Energy Agency.
18. Pastore, G., L. Luzzi, V. Di Marcello, and P. Van Uffelen, *Physics-based modelling of fission gas swelling and release in UO2 applied to integral fuel rod analysis.* Nuclear Engineering and Design, 2013. **256**(0): p. 75-86.
19. Zwicky, H.U., J. Low, M. Granfors, C. Alejano, J.M. Conde, C. Casado, J. Sabater, M. Lloret, M. Quecedo, and J.A. Gago, *Nuclide analysis in high burnup fuel samples irradiated in Vandellós 2.* Journal of Nuclear Materials, 2010. **402**(1): p. 60-73.
20. Lemoine, F., O. Serot, P. Leconte, and D. Bernard, *The Isotopic Composition of Fission Gas Release from MOX and High Burnup UO2 Fuel to Check the Fission Yield Database*, in *Water Reactor Fuel Performance Meeting*. 2014: Sendai, Japan.
21. OECD/NEA, *Fission Gas Behaviour in Water Reactor Fuels*. OECD Publishing.

22. Vitanza, C., E. Kolstad, and G. Gracioni. *Fission Gas Release from UO2 Pellet Fuel at High Burnup*. in *Am. Nucl. Soc., Topical Meeting on Light Water Reactors Fuel Performance*. 1979. Porland, Oregon.
23. Turnbull, J.A., P. Menut, and E. Sartori, *A review of fission gas release data within the Nea/IAEA IFPE database*. 2002, Nuclear Energy Agency of the OECD (NEA): Organisation for Economic Co-Operation and Development - Nuclear Energy Agency.
24. Oberländer, B.C. and H.K. Jenssen, *PIE on the Rod from the LOCA Test IFA-650.14 on High Burn-up BWR Fuel*. 2014, OECD Halden Reactor Project.
25. Raynaud, P., *Fuel Fragmentation, Relocation and Dispersal During the Loss-of-Coolant Accident (NUREG-2121)*. 2012, U.S.NRC.
26. Wiesenack, W., *Summary of the Halden Reactor Project LOCA Test Series IFA-650*. 2013, OECD HRP.
27. Flanagan, M., *NUREG-2160: Post-test examination results from integral, high-burnup, fueled LOCA tests at Studsvik Nuclear Laboratory*. 2013, US NRC.
28. Bianco, A., C. Vitanza, M. Seidl, A. Wensauer, W. Faber, and R. Macián-Juan, *Experimental investigation on the causes for pellet fragmentation under LOCA conditions.* Journal of Nuclear Materials, 2015. **465**: p. 260-267.
29. Raynaud, P., *Fuel Fragmentation, Relocation and Dispersal During the Loss-of-Coolant Accident*. 2012, Nuclear Regulatory Commission.
30. Yueh, K., N. Snis, D. Mitchell, and C. Munoz-Reja, *Fuel Fragmentation Data Review and Separate Effects Testing*, in *TopFuel*. 2014: Sendai, Japan.
31. Turnbull, J.A., S.K. Yagnik, M. Hirai, D.M. Staicu, and C.T. Walkert, *An assessment of the fuel pulverization threshold during LOCA-type temperature transients.* Nuclear Science and Engineering, 2015. **179**(4): p. 477-485.
32. Wiesenack, W., *Summary and Comparison of LOCA Tests with BWR Fuel in the Halden Reactor Project Test Series IFA-650*. 2015, Institutt for Energiteknikk, Halden, Norway.
33. Khvostov, G., *TM-41-13-15: Parameter optimization for the Halden LOCA test IFA-650.14 using the FALCON fuel behaviour code.* . 2013, Paul Scherrer Institute: Villigen, Switzerland.
34. Jernkvist, L.O. and A.R. Massih, *Models for axial relocation of fragmented and pulverized fuel pellets in distending fuel rods and its effects on fuel rod heat load*. 2015, Swedish Radiation Safety Authority.
35. Nagase, F., *2.23 - Behavior of LWR Fuel During Loss-of-Coolant Accidents A2 - Konings, Rudy J.M*, in *Comprehensive Nuclear Materials*. 2012, Elsevier: Oxford. p. 595-608.
36. Ammirabile, L. and S.P. Walker, *Dynamic ballooning analysis of a generic PWR fuel assembly using the multi-rod coupled MATARE code.* Nuclear Engineering and Design, 2014. **268**: p. 24-34.
37. Khvostov, G., W. Wiesenack, M.A. Zimmermann, and G. Ledergerber, *Some insights into the role of axial gas flow in fuel rod behaviour during the LOCA based on Halden tests and calculations with the FALCON-PSI code.* Nuclear Engineering and Design, 2011. **241**(5): p. 1500-1507.
38. Garlick, A., P. Hindmarch, and A. McKee, *Fuel stack relocation associated with initial stages of cladding deformation during internal pressurisation tests on irradiated PWR fuel*. UKAEA Report ND-R-970(W), May 1984.
39. Garlick, A., P. Hindmarch, A. McKee, and M.A. Brearley, *Influence of vibrations, simulating reflood conditions, on the fuel stack mechanical stability after internal pressurisation tests on irradiated PWR fuel*. UKAEA Report ND-R-950(W), May 1984.
40. Govers, K. and M. Verwerft, *Discrete element method study of fuel relocation and dispersal during loss-of-coolant accidents.* Journal of Nuclear Materials, 2016. **478**: p. 322-332.
41. Flanagan, M., *Observation of fuel fragmentation, mobility and loss in integral high burnup fueled LOCA tests.*
42. Raynaud, P. *Core-wide estimates of fuel dispersal during a LOCA*. in *TopFuel 2013*. 2013. Charlotte, North Carolina.
43. Wiesenack, W., *Summary of the HRP-WGFS workshop on fuel fragmentation, relocation and dispersal.* 2015.
44. OECD/NEA, *Nuclear Fuel Behaviour in Loss-of-Coolant Accident (LOCA) Conditions. State-of-the-art report. NEA 6846*. 2009.

45. U.S.NRC, *"Acceptance Criteria for Emergency Core Cooling Systems for Light-Water Nuclear Power Reactors", U.S. Code of Federal Regulations, Title 10, Part 50, Section 46*. 1974.
46. Billone, M., Y. Yan, T. Burtseva, and R. Daum, *Cladding Embrittlement during postulated Loss-of-Coolant Accidents. NUREG/CR-6967*. 2008, US NRC: United States.
47. Zimmermann, M.A. and G. Bart, *Review of the Licensing Basis for RIA and LOCA Transients in Light of New Evidence on High Burnup Fuel Behavior.* CHIMIA International Journal for Chemistry, 2005. **59**(12): p. 950-956.
48. Kok, K.D., *Nuclear engineering handbook*. Mechanical engineering series. 2009: Boca Raton : CRC Press. 768 S.
49. Various, *Very High Burn-ups in Light Water Reactors*. 2006, OECD Nuclear Energy Agency.
50. Rashid, R.Y., R.S. Dunham, and R.O. Montgomery, *FALCON MOD01: Fuel Analysis and Licensing Code*. 2004, EPRI.
51. Khvostov, G., W. Lyon, and M.A. Zimmermann, *Application of the FALCON code to PCI induced cladding failure and the effects of missing pellet surface.* Annals of Nuclear Energy, 2013. **62**: p. 398-412.
52. Khvostov, G., *Improvement and Verification of the START-3 Code as a constituent of the IAEA CRP "Improvement of Models Used for Fuel Behavior Simulation (CRP FUMEX II)*. 2012.
53. Allison, C.M., G.A. Berna, R. Chambers, and E.W. Coryell, *MATPRO -- A Library of Materials. Properties for Light-Water-Reactor Accident Analysis*, in *SCDAP/RELAP5/MOD3.1 Code Manual Volume IV*, D.T. Hagrman, Editor. 1993, Idaho National Engineering Laboratory: Idaho Falls, USA.
54. Baker, L. and L. Just, *Studies of Metal-Water Reactions at High Temperatures -III. Experimental and Theoretical Studies of the Zirconium-Water Reaction*. 1962.
55. Cathcart, J.V., *"Quarterly Progress Report on Zirconium Metal-Water Oxidation". Kinetics Program sponsored by the NRC, Division of Reactor Safety Research*. 1976, Oak Ridge National Laboratory.
56. Lassmann, K., C. O'Carroll, J. van de Laar, and C.T. Walker, *The radial distribution of plutonium in high burnup UO2 fuels.* Journal of Nuclear Materials, 1994. **208**(3): p. 223-231.
57. Spino, J., J. Rest, W. Goll, and C.T. Walker, *Matrix swelling rate and cavity volume balance of UO2 fuels at high burn-up.* Journal of Nuclear Materials, 2005. **346**(2–3): p. 131-144.
58. Ribeiro, F. and G. Khvostov, *Multi-scale approach to advanced fuel modelling for enhanced safety.* Progress in Nuclear Energy, 2015. **84**: p. 24-35.
59. Herranz, L.E., I. Vallejo, G. Khvostov, J. Sercombe, and G. Zhou, *Assessment of fuel rod performance codes under ramp scenarios investigated within the SCIP project.* Nuclear Engineering and Design, 2011. **241**(3): p. 815-825.
60. Khvostov, G., A. Pautz, E. Kolstad, and G. Ledergerber, *Analysis of a Halden LOCA Test with the BWR High Burnup Fuel*, in *LWR Fuel Performance Meeting /TopFuel 2013*. 2013: Charlotte, NC, USA.
61. Khvostov, G., A. Romano, and M.A. Zimmermann, *Modeling the effects of axial fuel relocation in the IFA-650.4 LOCA test*, in *Enlarged Halden Programme Group Meeting*. 2007: Storefjell Hotel, Gol, Norway.
62. Khvostov, G., *Parameter optimization for the Halden LOCA test in IFA-650.14 using the FALCON fuel behaviour code.* 2013, Paul Scherrer Institute (PSI), Switzerland.
63. Leppänen, J., M. Pusa, T. Viitanen, V. Valtavirta, and T. Kaltiaisenaho, *The Serpent Monte Carlo code: Status, development and applications in 2013.* Annals of Nuclear Energy, 2015. **82**: p. 142-150.
64. Leppänen, J., *Serpent - a Continuous Monte Carlo Reactor Physics Burnup Calculation Code. VTT Technical Research Centre of Finland.* . 2015: VTT Research Center of Finland.
65. Reocreux, M., *Safety Analysis and Best Estimate Codes*, in *4th Regional Meeting Nuclear Energy in Central Europe*. 1997: Bled, Slovenia.
66. Khvostov, G. and M.A. Zimmermann, *Parameters of fuel rod design and test conditions for the high temperature LOCA experiment IFA-650.7. Pre-calculation with the FALCON fuel behavior code. TM-41-07-11*. 2007, Paul Scherrer Institute: Villigen, Switzerland.

67. Khvostov, G., *Parameters of fuel rod design and test-conditions for the two-run Halden LOCA test using KKL BWR high-burnup fuel: Pre-calculation with the FALCON fuel behavior code. TM-41-10-26*. 2011, Paul Scherrer Institute: Villigen, Switzerland.
68. Lestinen, V., *LOCA Testing at Halden, First Experiment IFA-650.1: HWR-762*. 2004, OECD Halden Reactor Project.
69. Ek, M., *HWR-785: LOCA TESTING AT HALDEN, THE THIRD EXPERIMENT IFA-650.3*. 2005, OECD HRP: Halden, Norway.
70. Yagnik, S., J. Turnbull, J. Noirot, C.T. Walker, L. Hallstadius, N. Waeckel, and P. Blanpain, *An Investigation into Fuel Pulverization with Specific Reference to High Burn-up LOCA*, in *WRFPM 2014*. 2014: Sendai, Japan. p. 6.
71. Kekkonen, L., *HWR-838: LOCA TESTING AT HALDEN, THE FOURTH EXPERIMENT IFA-650.4*. 2007, OECD HRP: Halden, Norway.
72. Erbacher, F.J. *LWR fuel cladding deformation in a LOCA and its interaction with the emergency core cooling*. in *ANS/ENS Topical Meeting on Reactor Safety Aspects of Fuel Behaviour*. 1981. Sun Valley, USA.
73. Kekkonen, L., *HWR-839: LOCA TESTING AT HALDEN, THE PWR EXPERIMENT IFA-650.5*. 2007, OECD HRP: Halden, Norway.
74. Kekkonen, L., *HWR-870: LOCA TESTING AT HALDEN, THE VVER EXPERIMENT IFA-650.6*. 2007, OECD HRP: Halden, Norway.
75. Jošek, R., *HWR-906: LOCA TESTING AT HALDEN, THE BWR EXPERIMENT IFA 650.7*. 2008, OECD HRP: Halden, Norway.
76. Chomont, F.B.d., *HWR-916: LOCA TESTING AT HALDEN, THE EIGHTH EXPERIMENT IFA-650.8*. 2009, OECD HRP: Halden, Norway.
77. Eitrheim, K.K.R., *HWR-967: IODINE AND CESIUM RELEASED FROM THE LOCA EXPERIMENT IFA-650.9*. 2010, OECD HRP: Halden, Norway.
78. Lavoil, A., *HWR-974: LOCA TESTING AT HALDEN, THE TENTH EXPERIMENT IFA-650.10*. 2010, OECD HRP: Halden, Norway.
79. Lavoil, A., *HWR-976: LOCA TESTING AT HALDEN, THE VVER FUEL EXPERIMENT IFA-650.11*. 2010, OECD HRP: Halden, Norway.
80. Bremond, O., *HWR-1009: LOCA TESTING AT HALDEN, THE BWR FUEL EXPERIMENT IFA-650.12*. 2011, OECD HRP: Halden, Norway.
81. Khattout, F., *HWR-1042: The BWR LOCA test IFA-650.13: in-pile measurements*. 2013, OECD HRP: Halden, Norway.
82. Tradotti, R., *HWR-1084: LOCA TESTING AT HALDEN, THE BWR FUEL EXPERIMENT IFA-650.14*. 2014, OECD HRP: Halden, Norway.
83. Khvostov, G., *Post-test Analysis of the IFA-650.12 Halden LOCA Experiment using the FALCON Code coupled to FRELAX Model. TM-41-13-04*. 2013, Paul Scherrer Institute.
84. Furuta, T., H. Uetsuka, and S. Kawasaki, *Ductility loss of zircaloy cladding by inner-surface oxidation during high temperature transient.* Journal of Nuclear Science and Technology, 1981. **18**(10): p. 802-810.
85. Matsson, I. and B. Grapengiesser, *Developments in gamma scanning irradiated nuclear fuel.* Applied Radiation and Isotopes, 1997. **48**(10–12): p. 1289-1298.
86. Andersson, P., S. Holcombe, and T. Tverberg, *Inspection of LOCA Test Rod IFA-650.15 Using Gamma Emission Tomography*. 2016, Institutt for Energiteknikk: OECD Halden Reactor Project.
87. Brankov, V., G. Khvostov, K. Mikityuk, A. Pautz, and K. Eitrheim. *Analysis of Axial Fuel Relocation Based on Gamma Scan Data from OECD HRP LOCA Tests*. in *WRFPM/TopFuel 2014*. 2014. Sendai, Japan.
88. Siefken, L.J., *Fuel axial relocation in ballooning fuel rods*. 1983: Idaho Falls,United States.
89. Brankov, V., G. Khvostov, K. Mikityuk, A. Pautz, R. Restani, S. Abolhassani, G. Ledergerber, and W. Wiesenack, *Analysis of effects of pellet-cladding bonding on trapping of the released fission gases in high burnup KKL BWR fuels.* Nuclear Engineering and Design, 2016. **305**: p. 559-568.
90. Ledergerber, G., *Fuel Performance Beyond Design - Exploring the Limits*, in *WRFPM 2010*. 2010: Orlando, Florida, USA. p. 12.

91. Ledergerber, G., S. Abolhassani, M. Limbäck, R.J. Lundmark, and K.Å. Magnusson, *Characterization of high burnup fuel for safety related fuel testing.* Journal of Nuclear Science and Technology, 2006. **43**(9): p. 1006-1014.
92. Causey, A.R., R.A. Holt, N. Christodoulou, and E.T.C. Ho. *Irradiation-enhanced deformation of Zr-2.5Nb tubes at high neutron fluences*. in *ASTM Special Technical Publication*. 2000.
93. Bang, J.-G., *Modelling of Zircaloy-4 cladding behaviour at high burnup*, in *Nuclear fuel behaviour modelling at high burnup and its experimental support*. 2001, Korea Atomic Energy Research Institute. p. 407-416.
94. Adamson, R., F. Garzarolli, and C. Patterson, *In-Reactor Creep of Zirconium Alloys*. 2009, Advanced Nuclear Technology International.
95. Loberg, J., M. Österlund, and J. Blomgren, *Neutron Detection-Based Void Monitoring in Boiling Water Reactors.* Nuclear Science and Engineering, 2010. **164**.
96. Suzuki, M. and H. Saitou, *Light Water Reactor Fuel Analysis Code FEMAXI-6 (Ver. 1).* 2005(JAEA-Data/Code 2005-003).
97. Suzuki, M., H. Uetsuka, and H. Saitou, *Analysis of mechanical load on cladding induced by fuel swelling during power ramp in high burn-up rod by fuel performance code FEMAXI-6.* Nuclear Engineering and Design, 2004. **229**(1): p. 1-14.
98. Yagnik, S.K., A.J. Machiels, and R.L. Yang, *Characterization of UO2 irradiated in the BR-3 reactor1*. Journal of Nuclear Materials, 1999. **270**(1–2): p. 65-73.
99. Nogita, K., K. Une, and Y. Korei, *TEM analysis of pellet-cladding bonding layer in high burnup BWR fuel.* Nuclear Instruments and Methods in Physics Research Section B: Beam Interactions with Materials and Atoms, 1996. **116**(1–4): p. 521-526.
100. Berghe, S.V.d., A. Leenaers, B.Vos, L. Sannen, and M. Verwerft. *Observation of a Pellet-Cladding Bonding Layer in High Power Fuel*. in *Seminar proceedings on Pellet-clad Interaction in LWR Fuels*. 2004. Aix-en-Provence.
101. Restani, R. and A. Wälchli, *WA-KKL-PSI Fuel Performance Programme: Electron Probe Microanalyses on Rod AEB072-E4*. 2004, Paul Scherrer Institute (Internal Document TM-43-04-10).
102. Ledergerber, G., *Characterisation of KKL BWR Fuel for Test Series in IFA-610, IFA-629 and IFA-650*, in *HWR-1033*. 2013, Kernkraftwerk Leibstadt AG.
103. Khvostov, G., W. Wiesenack, B.C. Oberländer, E. Kolstad, G. Ledergerber, M.A. Zimmermann, and O. Bremond, *Pre-calculation using the FALCON fuel behaviour code of the fuel rod design parameters and the test-conditions for a two-run Halden LOCA test with KKL BWR high-burnup fuel*, in *Enlarged Halden Programme Group Meeting (EHPGM)*. 2011: Norway.
104. Masaki, A., *The Lift-off Experiment IFA-610.10 with a High Burn-up BWR UO2 Fuel Rod: In-pile Results during the First Irradiation Cycle, HWR-877*. 2008: Institutt for Energiteknikk OECD Halden Reactor Project.
105. Oberländer, B.C. and H.K. Jenssen, *HWR-1096: PIE ON THE ROD FROM THE LOCA TEST IFA-650.14 ON HIGH BURN-UP BWR FUEL*. 2014, IFE/OECD HRP: Halden, Norway.
106. Huang, H., B. Spencer, and J. Hales, *Discrete element method for simulation of early-life thermal fracturing behavior in ceramic nuclear fuel pellets.* Nuclear Engineering and Design, 2014. **278**: p. 515-528.
107. Jernkvist, L.O., *A continuum model for cracked UO2 fuel.* Nuclear Engineering and Design, 1997. **176**(3): p. 273-284.
108. Jernkvist, L.O. and A.R. Massih, *Axial Relocation of Fragmented and Pulverized Fuel and its Effects on Fuel Rod Heat Load during LOCAS*, in *Topfuel 2015*. 2015: Zurich, Switzerland.
109. L.A.Walton and D.L.Husser, *Fuel fracture and relocation.* Water reactor fuel element computer modelling, 1983.
110. Karb, E.H., M. Pruessmann, L. Sepold, P. Hofmann, and G. Schanz, *LWR fuel rod behavior in the FR2 in-pile tests simulating the heatup phase of a LOCA. Report KFK 3346*. 1983, KIT.
111. Waterman, M.E. and T.R. Yackle, *PBF-LOCA Test Series: Test LOC-5 experiment predictions, TFBP-TR--332*. 1979: United States. p. 58.
112. Olander, D., *Nuclear Fuels: Present and Future.* EJ: Engineering Journal, 2009. **13**(1).

113. Yagnik, S.K., D.J. Sunderland, and B.C. Cheng. *Effect of PWR restart ramp rate on pellet-cladding interactions*. in *OECD Seminar on Pellet-Clad Interaction in Light Water Reactor Fuels*. 2004. Aix-en-Provence.
114. Hofmann, P. and J. Spino, *Can we expect a low ductility failure of Zircaloy tubing due to iodine-induced stress corrosion cracking in a LOCA transient*, in *ANS/ENS Topical Meeting on Reactor Safety Aspects of Fuel Behaviour*. 1981: Sun Valley, USA.
115. Haste, T.J. *A Review of Axial Gas Communication in Oxide Fuel Rods*. in *Enlarged Halden Programme Group Meeting on Fuel Performance Experiments and Analysis*. 8-13 May 1988. Loen, Norway.
116. Haste, T.J., J. T., C. Vitanza, C. R.J.P., and H. B.J., *Design and Feasibility Studies for the Proposed Cladding Deformation Experiments (IFA-541), Halden HWR-11*. May 1981.
117. Powers, D.A., *Cladding swelling and rupture models for LOCA analysis*, R.O. Meyer, Editor. 1980, Division of Systems Safety, Office of Nuclear Reactor Regulation, U.S. Nuclear Regulatory Commission :: Washington, D.C. :.
118. Raff, S. and R. Meyder. *NORA-2: A model for creep deformation and rupture of Zircaloy at high temperatures*. in *Specialists' meeting on fuel element performance computer modelling*. 15-19 March 1982. Preston, United Kingdom.
119. Raynaud, P. and I. Porter. *Predictions of Fuel Dispersal During a LOCA*. in *WRFPM 2014*. 2014. Sendai, Japan.
120. Massimilla, L., V. Betta, and C.D. Rocca, *A study of streams of solids flowing from solid-gas fluidized beds.* AIChE Journal, 1961. **7**(3): p. 502-508.
121. Brankov, V., G. Khvostov, K. Mikityuk, A. Pautz, and W. Wiesenack, *Characterization of the relocated and dispersed fuel in the Halden reactor project LOCA tests based on gamma scan data.* Nuclear Engineering and Design, 2016. **300**: p. 97-106.
122. Oberländer, B.C. and H.K. Jensen, *PIE ON THE ROD FROM THE LOCA TEST IFA-650.13 ON HIGH BURN-UP BWR FUEL*. 2014(HWR-1095).
123. Wiesenack, W., T. Tverberg, M. McGrath, E. Kolstad, and S. Béguin, *Rod Overpressure/Lift-off Testing at Halden In-pile Data and Analysis.* Journal of Nuclear Science and Technology, 2006. **43**(9): p. 1037-1044.
124. Wiesenack, W., L. Kekkonen, and B.C. Oberländer, *Axial gas transport and loss of pressure after ballooning rupture of high burnup fuel rods subjected to LOCA conditions*, in *International Conference on the Physics of Reactors "Nuclear Power: A Sustainable Resource"*. 2008: Interlaken, Switzerland.
125. Khvostov, G., *Evaluation of KKG STAV7/TU-WSE Licensing Application: Follow-up to STARS On-Call 2015 on Code Review (AN-41-16-06)*. 2016, Paul Scherrer Institute.
126. Mathworks. *Simulink Helps PNNL Create Vibration-Free Robotic Control System*. 2010; Available from: http://ch.mathworks.com/company/user_stories/simulink-helps-pnnl-create-vibration-free-robotic-control-system.html.
127. Mathworks. *ABB Accelerates Application Control Software Development for a Power Electronic Controller*. Available from: http://ch.mathworks.com/company/user_stories/abb-accelerates-application-control-software-development-for-a-power-electronic-controller.html.
128. Mathworks. *Transpower Ensures Reliability of New Zealand National Grid with Reserve Management Tool*. 2012; Available from: http://www.mathworks.com/tagteam/74273_92070v00_Transpower_UserStory_final.pdf.

Appendix A:
Other uses of the gamma scan data

This Appendix shows the manuscript of a journal paper [121] describing other uses of the gamma scan data from Halden LOCA tests. In particular, it discusses methodology to analyse the origin of relocated and dispersed fuel by using different isotopes from the gamma spectrum.

Nuclear Engineering and Design 300 (2016) 97–106

Contents lists available at ScienceDirect

Nuclear Engineering and Design

journal homepage: www.elsevier.com/locate/nucengdes

Characterization of the relocated and dispersed fuel in the Halden reactor project LOCA tests based on gamma scan data

Vladimir Brankov[a,b,*], Grigori Khvostov[a], Konstantin Mikityuk[a], Andreas Pautz[a,b], Wolfgang Wiesenack[c]

[a] Paul Scherrer Institut, 5232 Villigen PSI, Switzerland
[b] École Polytechnique Fédérale de Lausanne, CH-1015 Lausanne, Switzerland
[c] Institutt For Energiteknikk OECD Halden Reactor Project, P.O. Box 173, Halden 1751, Norway

HIGHLIGHTS

- We propose method to estimate dispersed fuel based on gamma scan data.
- Analysis to determine the origin of relocated and dispersed fuel in Halden LOCA tests.
- Useful data is gathered for code validation.
- Suggestions are discussed to improve the quality of gamma scan data at Halden.
- Dispersed and relocated material is a mixture of fuel from pellet periphery and bulk.

ARTICLE INFO

Article history:
Received 17 June 2015
Received in revised form 27 October 2015
Accepted 12 November 2015
Available online 5 February 2016

ABSTRACT

The on-going Loss-of-Coolant Accident (LOCA) test program at the OECD Halden Reactor Project (HRP) conducts in-house gamma scanning as standard post-irradiation examination (PIE) procedure on Light Water Reactor (LWR) fuel rods. One of the primary objectives of the program is to investigate fuel relocation into the balloon region and fuel dispersal through the cladding rupture opening after burst. A simple model called Gamma Transport Model was formulated for the purpose of interpretation of fuel relocation based on the gamma scan data. Fuel relocation may have a strong effect on the linear heat generation rate at the balloon due to, firstly, increase in linear fuel density, and secondly due to differences in burn-up and local heat generation rate at the periphery and bulk of the pellet. For this analysis, a pair of short-lived isotopes with very different fission product yields for ^{235}U and ^{239}Pu is selected from the gamma scan spectrum. The intention is to use the difference in the ratio of their concentrations in the balloon region to qualitatively make conclusion on the fuel relocation. As a separate outcome, the same analysis can be applied to the dispersed fuel region and to draw conclusion on its origin (pellet rim or bulk). The Gamma Transport Model is validated against a special (non-destructive) case from the Halden LOCA test program and then applied for the analysis of selected tests. In addition, a methodology is presented for estimation of the amount of dispersed fuel from the LOCA tests based on the gamma scan data. Currently, at Halden there is no possibility to measure the dispersed fuel and hence an alternative is needed. Such information can be used for code validation and for inferring additional information based on other test parameters such as cladding rupture opening.

© 2015 Elsevier B.V. All rights reserved.

1. Introduction

The LOCA test program at OECD HRP was established in 2003 and to this day 14 tests have been conducted. The primary objectives of the LOCA program at Halden are (Wiesenack and Oberländer, 2014):

(1) Measure the extent of fuel (fragment) relocation into the ballooned region and evaluate its possible effect on cladding temperature and oxidation;
(2) Investigate the extent (if any) of "secondary transient hydriding" on the inner side of the cladding and above and below the burst region;

* Corresponding author at: Paul Scherrer Institut, Vladimir Brankov, OHSA/D06 CH-5232, Villigen PSI, Switzerland. Tel.: +41 56 310 5327.
E-mail address: vladimir.brankov@psi.ch (V. Brankov).

http://dx.doi.org/10.1016/j.nucengdes.2015.11.023
0029-5493/© 2015 Elsevier B.V. All rights reserved.

(3) Measure iodine and cesium release from failed fuel (Kolstad et al., 2011).

With respect to the test program objectives, this paper focuses on the first. In the first part of the paper, an attempt is made to draw qualitative conclusions on the fuel relocation state within the ballooned region with the aim to distinguish between fuel fragments from different origins. Fuel relocation is a complex phenomenon that depends on parameters such as fuel fragment size and cladding deformation. The fuel relocation into the balloon may give rise to so-called 'hot-spot' effect, which is increased local heat generation that may impact the peak cladding temperature and, therefore, the time to cladding rupture and the equivalent cladding reacted (ECR). This effect is not only caused by the amount of relocated fuel but also by the heat source density of the fuel. Burn-up at LWR pellet rim is significantly higher than at pellet bulk. The higher local fission product concentration induces larger decay heat generation during the LOCA. Thus, the fuel pellet can be divided into two regions: pellet bulk and pellet rim. The distinction between the two may be done on the level of ^{239}Pu concentration which sharply increases towards the rim. The reason for this is neutron captures by ^{238}U which transforms to ^{239}Np and quickly decays to ^{239}Pu. The rim region is characterized by very high levels of burn-up, small grain sizes, reduced concentration of the fission gases in the fuel matrix (i.e., intra-granular gas) and increase in fuel porosity (Khvostov et al., 2005).

As a standard non-destructive PIE procedure, available at Halden, gamma scanning is performed on the test rod shortly after the test. It is a valuable PIE, especially for the Halden LOCA tests, because it takes a snapshot of the fuel relocation state as it was induced by the LOCA. The gamma scan data used in the analyses presented in this paper was not generated for this purpose. The data belongs to the standard set of PIE performed, within the Halden LOCA Test Program, before this paper was conceived. Care is taken not to induce fuel relocation during the transportation from the reactor to the scanning facility (Wiesenack and Oberländer, 2014). Clearly visible features of the gamma scan are the rod deformation, regions voided of fuel and dispersal through the clad rupture. The gamma scanning produces as output a two-dimensional matrix of gamma spectra, where each matrix element represents spectrum gathered from the local projection through the fuel rod. As such, characteristics of fuel bulk and rim are mixed together. The only location that has a chance to demonstrate features of the pellet rim is at the peripheral scans on the left and right of the fuel rod.

The second part of the paper discusses a method for estimating the quantity of dispersed fuel based on the gamma scan data. Such knowledge can be useful in the validation of fuel dispersal models.

2. Background

2.1. On-going project on fuel fragmentation, relocation and dispersal (FFRD)

The work presented in this paper is a part of a research project at the Paul Scherrer Institute, whose main goal is model development for fuel fragmentation, relocation and dispersal. Computations are performed with the fuel performance code FALCON (Rashid et al., 2004) coupled with advanced fission Gas Release and SWelling model GRSW (Khvostov et al., 2011a). The work on relocation is closely linked with existing efforts for interpreting FFRD and in particular a Halden-specific model for fuel relocation FRELAX (Khvostov et al., 2011b). The model for relocation in the context of the research project will be an extension of FRELAX. In this paper an assumption regarding the fuel relocation into the balloon, which is presently used in FRELAX, is challenged. An estimation of the quantity of dispersed fuel from Halden's LOCA test program is necessary for the future validation of the fuel dispersal model. Presently, the only option is to use the gamma scanning data.

2.2. Challenging an assumption used in FRELAX

One of the main assumptions of FRELAX is the homogeneous mixing of fuel in the balloon. This means, that fuel fragments from the periphery are well mixed with those from the pellet bulk. In other words, there is no preferential relocation of fuel from the periphery into the balloon. The implication of such a scenario is non-negligible. The periphery is at much higher burn-up than the bulk which means it has higher fission product concentration and therefore higher decay heat potential. Application of the FRELAX model to a Halden LOCA test with severe fuel relocation is discussed in Khvostov et al. (2007) and Khvostov et al. (2011b). In FRELAX, the rate of enthalpy change due to axial fuel relocation in a calculation slice is formulated as follows:

$$\Delta\dot{h} = w\kappa K_y - F - \mathrm{div}(\vec{v}\,\Delta h). \quad (1)$$

In Eq. (1), K_y is the relative fuel mass linear density (ratio of the current mass density that may or may not have been affected by relocation and the density prior to the LOCA test), F is the linear heat power leaving the fuel through the cladding, w is the local linear heat generation rate, $\vec{v}$ is the axial drift velocity of the fuel, κ is a weighting factor which characterizes the degree of relocation of fuel from the periphery into the balloon. Qualitatively, the range of κ can be defined as follows:

(1) Case 1: $\kappa \equiv 1$
In this case, relocated fuel is considered a homogeneous mixture of fuel from the pellet rim and pellet bulk that is relocated in the balloon.
(2) Case 2: $\kappa < 1$
This case implies, that the lower decay heat source (fuel from the bulk) prevails over the higher decay heat source (fuel from the pellet periphery/rim). In other words, there is preferential relocation of fuel from the bulk into the balloon.
(3) Case 3: $\kappa > 1$
This case considers the notion of preferential relocation of fuel from periphery into the balloon.

The Gamma Transport Model, presented in Section 3.3, challenges the assumption in FRELAX for homogeneous mixing ($\kappa \equiv 1$) in the balloon. If there is evidence for preferential fuel relocation into the balloon, then the FRELAX model may need to be updated.

2.3. Data for validation of model for fuel dispersal

The second part of the paper discusses a method for estimating dispersed fuel, which is important for the validation of the model for fuel dispersal to be developed in the next phase of the research project on FFRD. Halden's LOCA test program is highly relevant because it uses high burn-up fuel specimens and addresses the concern of fuel dispersal during LOCA. At present, there is no capacity to measure the quantity of dispersed fuel at Halden. Estimates can be attempted based on PIE data such as the gamma scanning. A straight-forward approach is to estimate the fraction of voided regions within the fuel rod as is visible on the gamma count intensity plot of the 9th Halden LOCA test shown on Fig. 1. Another approach is to use the gamma counts of selected isotopes and estimate the dispersed fuel mass based on the ratio of gamma counts outside the rod over the total gamma counts. The second approach is described in Section 3.4, and results are reported in Section 4. In order to reduce the overall uncertainty, the energy of

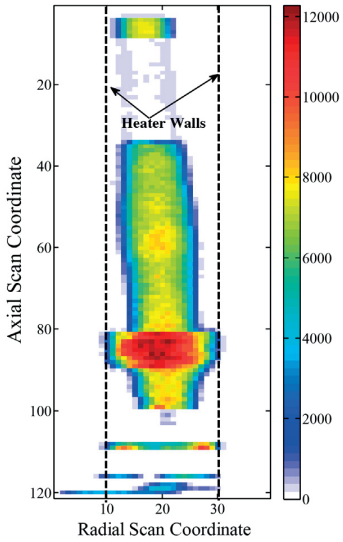

Fig. 1. Gamma count intensity plot of the 9th Halden LOCA test based on the 1596 keV gamma peak of ^{140}La.

the selected gamma ray should be as high as possible (to reduce the effect of attenuation).

3. Analysis methods

Firstly, the Halden LOCA test program is briefly introduced then followed by description of the gamma facility and the format of the gamma scan data and finally the suggested methods for interpretation of the experimental data are presented. In particular, determining the origin of relocated fuel and method for estimation of the quantity of dispersed fuel are the main topics of this paper.

3.1. OECD HRP LOCA test program

The test fuel rods for LOCA testing in the Halden experimental facility come from light-water reactors. Low level of nuclear power generation, provided by the Halden Boiling Water Reactor (HBWR), is used to simulate decay heat, whereas an electrical heater surrounding the rod simulates heat from neighboring rods in a fuel assembly. The pellet-averaged burn-up at discharge for the tested rods ranges from 40 to 90 MW d/kg U. The tests in the upper burn-up range may be somewhat higher than the current operating limits, but analysis of the results may lead to conservative estimates during a LOCA transient and as such they are of relevance. In addition, a good reproducibility between tests was demonstrated in the 12th, 13th and 14th Halden LOCA tests in particular with respect to fuel fragmentation pattern and relocation, as well as the 4th and 9th tests with respect to fuel fragmentation and dispersal (Kolstad et al., 2011). A number of signals are measured online during LOCA tests, such as fuel rod pressure, cladding temperature at different elevations, axial cladding elongation and others. Furthermore, a number of non-destructive PIEs are performed, including gamma scanning, visual inspection, cladding diameter profilometry, and destructive PIEs such as measurements of fuel fragment size distribution and fission gas release due to the LOCA for a non-burst test (Halden LOCA test 14).

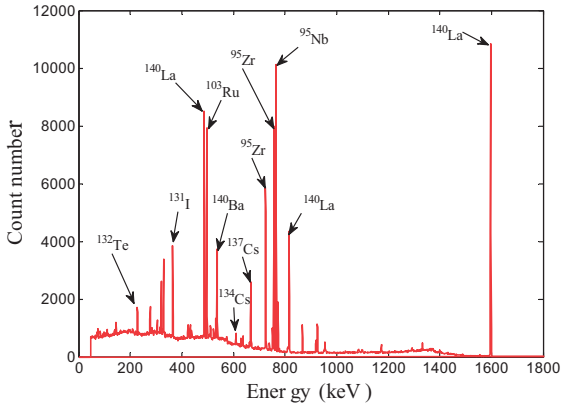

Fig. 2. Typical gamma spectrum shortly after the end of the LOCA test. Here, data from LOCA test 8 is shown.

3.2. Gamma scanning at Halden and format of the data

Gamma scanning is the first PIE after the LOCA test and reveals features such as cladding deformation, fuel relocation and dispersal. The scanning facility at Halden uses a high-purity germanium detector (HPGe) which has very good energy resolution. As such, gamma peaks even in close proximity can be clearly distinguished and assigned to their source. The typical gamma scanning is sampling the rod every 5 mm in the vertical and 1 mm in the horizontal direction where a collimator typically 1.5 mm in diameter is used. This means, that vertically there are portions of the fuel rod which are not scanned, but horizontally everything is scanned. The typical distance from detector to fuel is about 1 m which suggests, that only gammas which leave the fuel surface at an angle of $\sim 90^{\circ}$ are reaching the detector. In other words, gamma rays coming from outside the projection of the collimator through the fuel rod can be neglected. The scanning procedure is fully automatic and takes about 3 days to complete. Scanning is done at two rod orientations that are 90° apart. Considering the short half-lives of most isotopes and the time necessary for full rod scan, the experimental data must be decay corrected, for adequate interpretation, against the time stamp of the first scanned point. In cases where the gamma scan is conducted shortly after the LOCA test, a number of isotopes can be identified in the gamma spectrum like the one shown on Fig. 2. The gamma spectrum, with the exception of longer lived fission products such as ^{134}Cs and ^{137}Cs comes from accumulation of fission products during a short irradiation time prior to the LOCA test. In the case of LOCA test 8, which was prepared with fresh fuel, the entire gamma spectrum is generated during short irradiation in the Halden BWR before the test. The gamma peaks which are used in the analyses later in the paper are ^{103}Ru, ^{140}Ba and its decay product—^{140}La. The format of the gamma scan data is a two-dimensional matrix where each matrix element is a gamma spectrum collected from a projection through the fuel rod. The selection of a particular energy range from the gamma spectrum yields a two-dimensional matrix of counts. A straightforward plot of this matrix produces an image of the fuel rod where the color intensity is proportional to the gamma source. An example is shown in Fig. 1. Clearly visible features are:

- Cladding balloon in the lower part of the active fuel stack.
- Fuel fallen down to the bottom of the pressure flask (scan coordinate 110) and also driven into the blow-down line (scan coordinate 115–120) after the fuel dispersal.

Table 1
Fission yields, half-lives and gamma decay energies for selected fission products.

Isotope	Gamma energy (keV)	Half-life (d)	^{235}U yield (%)	^{239}Pu yield (%)
^{132}Te	228	3.2	4.3	3.86
^{131}I	365	8	2.9	3.86
^{103}Ru	496	39.3	3.03	6.95
^{140}Ba	537	12.7	6.2	5.35
^{134}Cs	604, 795	800	6.7	6.9
^{137}Cs	662	10,950	6.19	6.61
^{95}Zr	724, 756	64	6.5	4.82
^{95}Nb	766	50.9	6.50	4.94
^{140}La	486, 815, 1596	1.7	6.21	5.36

- Relocated fuel from the upper part of the rod (indicated by the empty cladding tube).
- Stuck fuel above the empty tube section.

This plot is generated from the gamma counts of ^{140}La at 1596 keV because from the available isotopes in the spectrum the attenuation will be lowest and as such better contrast between regions of different fuel density is anticipated. A short table of selected properties is compiled for several isotopes in the spectrum and shown in Table 1. The use of ^{140}La for determination of the axial power distribution in a fuel rod is discussed in (Matsson and Grapengiesser, 1997). In the present paper, that isotope is used together with ^{103}Ru to capture the increase in concentration of ^{239}Pu at the pellet periphery and to estimate the quantity of dispersed fuel. The fission product yields of ^{103}Ru and ^{140}La suggest, that an increase in fission of ^{239}Pu will increase the production of Ruthenium and reduce that of Lanthanum. This fact can be utilized by considering the ratio of the concentrations of the isotopes, or in this case—the ratio of the gamma counts. It is a well-known observation that ^{239}Pu concentration sharply increases towards the fuel periphery due to neutron captures by ^{238}U. Therefore, the ratio of the gamma counts of the selected pair should be lowest at the pellet center and highest at the periphery. The intention is to use this information together with the gamma scan data to analyze the relocated fuel in the ballooned region. There are three gamma decay energies of ^{140}La that are recorded in the spectrum. For relocation analysis, the 486 keV is selected because its energy is almost identical to that of ^{103}Ru (496 keV) and therefore differences in detector efficiency and attenuation can be neglected.

Table 1 shows suitable choices of isotope pairs such as Ru/Zr and Ru/Nb that will yield larger difference in the ratio of the gamma counts, but the larger difference in gamma energy (~200 keV) will require corrections for attenuation and detector efficiency, where the former may prove to be too difficult.

Due to the two-dimensional nature of the gamma scanning, it is not reasonable to expect identification of the pellet rim at locations other than the fuel rod periphery. Fig. 3 shows a sketch of the fuel pellet horizontal and vertical cross-sections and two possible projections by the detector collimator at the periphery. The grey region represents the rim, which is about 5% of the pellet radius in high burn-up fuel. The collimator window is drawn to scale with the pellet dimensions. Two possibilities for scanning the periphery are shown: "full scanning" (at the left-hand side) and "partial scanning" (at the right). The projection through the fuel rod on the left shows that in the first case, the majority of gammas will originate in the bulk region while in the latter—in the periphery.

A non-negligible source of uncertainty is associated with the scanning of the fuel periphery. It is not possible to optically align the detector collimator with the fuel rod periphery because the fuel is encased in a steel flask. In addition, fuel rod deformation during the LOCA test complicates matters further. Improving the scanning resolution by reducing the collimator size should reduce this uncertainty. In high burn-up fuel, the high-burn-up structure (HBS) is, for the sake of an example, 200 μm. Collimator sizes down to 100 μm are available, which means that the pellet rim could be scanned very accurately. In any case, higher resolution scanning will require longer time, which means, that compromises must be made elsewhere (for example, selective scanning only for regions of interest, such as the balloon or ejected fuel). It is without question that visually the gamma scan data carries important information with regard to the fuel state. In spite of the discussed uncertainties in the gamma scan data, the next sections present ideas on how to use it.

3.3. Gamma transport model

A model to interpret the gamma-scanning measurements considers the geometry shown in Fig. 4. The output of the model is the radial distribution of the ratio of gamma counts of the two selected isotopes (^{103}Ru and ^{140}La), which will serve as reference for the interpretation of fuel relocation and dispersal.

The two gray rings represent the zirconium alloy cladding and steel flask which surround the fuel rod. The governing equation assuming gamma attenuation only in the fuel pellet is shown below.

$$N(a,b) = \int_{a-b}^{a+b} dx \int_{-\sqrt{R^2-x^2}}^{\sqrt{R^2-x^2}} dy S(x,y) \times \exp\left(-\sum_a \left(y+\sqrt{R^2-x^2}\right)\right)\left(2\sqrt{b^2-(x-a)^2}\right) \quad (2)$$

The left-hand side represents the number of gammas entering the detector each second from the projection located distance "*a*" from the pellet center and half-width equal to the radius of the collimator window (parameter "*b*"). Solid angle is not taken into account, because the collimator opening is only 1 mm in diameter and it is about 1 m from the fuel rod. In that respect, only gammas

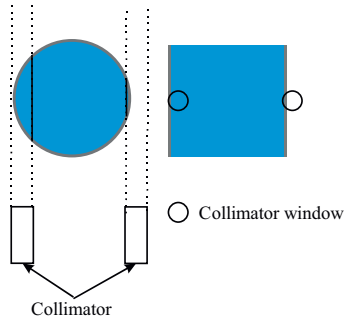

Fig. 3. Superposition of the collimator window and the fuel pellet.

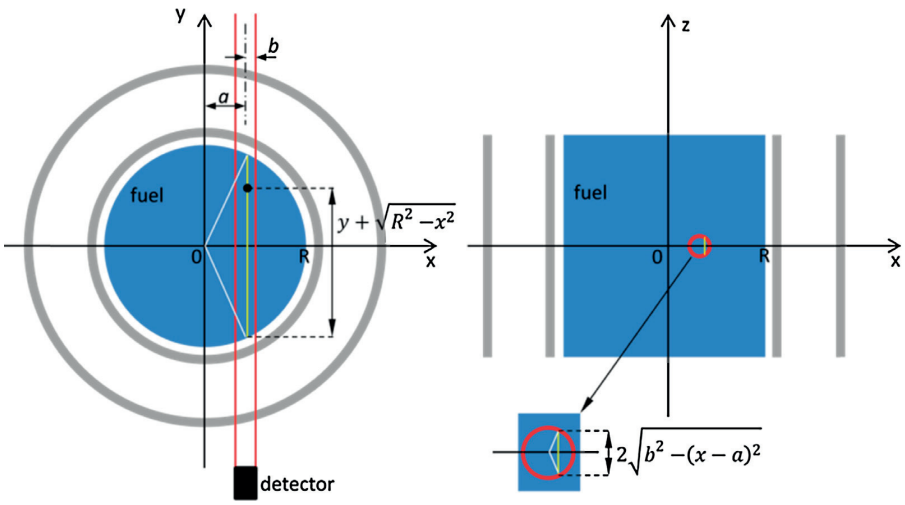

Fig. 4. Schematic representation of the gamma transport model.

coming straight at the collimator are considered. Attenuation by the steel flask and cladding is considered not important for this analysis. The integral is taken over the volume spanned by the projection of the detector window through the fuel rod. The attenuation parameter dependent on the distance travelled by gammas in the fuel is calculated and the attenuation macroscopic cross-section is labeled as Σ_a. The function $S(x,y)$ represents the gamma source density at the given scan coordinates. All parameters in Eq. (2) are known except the source density and as such it needs to be specified. A priori, one fact that is known about this function is that it must be increasing towards the pellet periphery because the fission product concentration is proportional to burn-up which is highest at the periphery and lowest at the pellet center. The shape function is taken from literature (Lassmann et al., 1994) and reported in Eq. (3) below:

$$S(x,y) = 1 + p_1 \exp\left(-p_2\sqrt{R-\left(x^2+y^2\right)}\right) = 1 + p_1 \exp\left(-p_2\sqrt{R-r}\right) \quad (3)$$

The parameter R is the pellet radius and r is the distance from the pellet center while p_1 and p_2 are free parameters. As r approaches the pellet periphery, the exponent becomes less negative and achieves its maximum value when $r \equiv R$. On the other hand, the lowest value occurs at the pellet center. Therefore the proposed function (Eq. (3)) has the desired properties. The governing equation (Eq. (2)) can now be used to calculate the radial distribution of gamma counts. For the next step, by probing the gamma scan data, an axial scan level is selected that is considered representative of the original geometry (i.e., undisturbed by the LOCA test). Using the experimental radial gamma count distribution for the two isotopes, shape functions are calculated by varying parameters p_1 and p_2 until agreement with the distribution calculated with Eq. (2) is satisfactory. Finally, the ratio of the two shape functions is calculated which is used as the reference distribution in the fuel before the LOCA test. The adequacy of the model is checked against gamma scan data from the 8th Halden LOCA test—a special qualification test using un-irradiated fuel rod and ensuring no ballooning during heat-up. Approximating the radial power distribution across the un-irradiated fuel pellet as constant, although in reality it is not, produced good results as shown on Fig. 5.

3.4. Dispersed fuel estimation based on the gamma scan data

The isotope with the least attenuation, namely ^{140}La at 1596 keV, is selected for the analysis. In relocated fuel geometry as it is the case in LOCA tests, it is important that the isotope used for this analysis is as little affected by geometry as possible. Evaluation of the attenuation is not attempted in this paper, because of the significant change in fuel geometry due to relocation. A simple method is proposed to approximate the amount of dispersed fuel based on the gamma scan data:

$$\text{Ejected fuel fraction} = \frac{\text{Sum of gamma counts in the ejected fuel region}}{\text{Sum of all gamma counts inside and outside the rod}} \quad (4)$$

The fact, that the rod is scanned vertically in steps of 5 mm with a collimator of 1.5 mm in diameter means, that about two-thirds of the rod is not scanned at all and this is taken into consideration when approximating the dispersed fuel by making reasonable assumptions about the missing data. In this case, the ejected fuel estimate is reported as a range of values, rather than a particular value. The range itself is determined by making the least and most conservative assumption about the missing data. Prior to using the

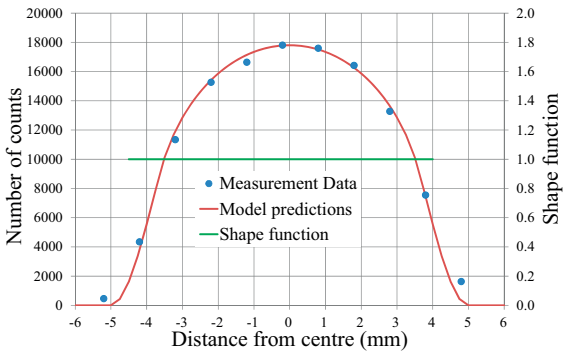

Fig. 5. Comparison of model predictions against gamma scan data from LOCA test 8 assuming flat shape function.

gamma counts, some corrections on the gamma scan data are necessary. The most important is the decay correction, because the isotopes are short-lived and a full scan typically takes between 2 and 3 days to complete. It must be noted, that the ^{140}La (half-life 1.7 d) visible on the gamma spectrum comes entirely from the decay of ^{140}Ba (half-life 12.7 d). The relationship between the two isotopes at the time of gamma scanning is expressed by Eq. (5), and the decay-corrected gamma count intensity of ^{140}La is given by Eq. (6).

$$\dot{N}_{La}(t) = -\lambda_{La}N_{La}(t) + \lambda_{Ba}N_{Ba}(t) \quad (5)$$

$$N_{La,0} = \left(N_{La}(t) - N_{Ba,0}\left(\frac{\lambda_{Ba}}{\lambda_{La}-\lambda_{Ba}}\right)(\exp(-\lambda_{Ba}t) - \exp(-\lambda_{La}t))\right) \times \exp(\lambda_{La}t) \quad (6)$$

The decay constants are labeled with λ_{La} *and* λ_{Ba} and the decay-corrected gamma count distribution is labeled with $N_{La,0}$ and $N_{Ba,0}$ for ^{140}La and ^{140}Ba, respectively. The very large difference in energy between ^{140}Ba (537 keV) and ^{140}La (1596 keV) requires correction for the difference in attenuation (due to fuel matrix and structural materials) as well as correction for the detector efficiency. The correction for attenuation was estimated with the attenuation law, whereas the difference in detector efficiency was estimated in a personal communication with experts at PSI and Halden working with HPGe detectors. The detector efficiency curve was determined with known gamma emitting sources at known activity.

The validity of Eq. (6) was successfully tested against the gamma scanning data of the 8th Halden LOCA test mentioned before. Eq. (6) should yield a uniform count intensity matrix for $N_{La,0}$—which it did.

4. Results and discussion

The gamma transport model is applied to the fuel relocation in the 13th Halden LOCA test, and the fuel dispersal estimation method is applied to the 9th and 10th Halden LOCA tests. In principle, the method can be applied to all tests that have good quality gamma scanning data.

4.1. Origin of relocated fuel in the 13th Halden LOCA test

The 13th LOCA test was executed in October 2012 and it was similar to the 14th test (Khvostov et al., 2013) in the sense that the fuel came from a BWR fuel assembly irradiated in the nuclear power plant Leibstadt in Switzerland with an average burn-up of 72 MW d/kg U. The cladding failed as designed, and the fuel experienced significant fragmentation, relocation and some dispersal. Reference gamma scan count intensity plots can be seen in Fig. 7 (right). The balloon is located between axial levels 30 and 40 and the dispersed fuel is colored in blue below axial level 80. This test was chosen for analysis with the gamma transport model. The axial scan level of 69 was selected as representative of the original geometry, and iterations of the shape function parameters (p_1 and p_2 in Eq. (3)) were done until the best fit was provided by the model to the experimental data for the two isotopes (Fig. 6).

The shape function is a combination of two shape functions, one for each half, which can be explained by non-uniformities in the power distribution in the BWR fuel rod. This particular rod was located next to the fuel assembly's water channel and it was subjected to non-uniform thermal neutron flux. The ratio of the shape functions is presented in Fig. 7 (left) together with the ratio of the gamma counts of ^{103}Ru and ^{140}La for selected scan points in the balloon and dispersed fuel region.

The red and green points shown on Fig. 7 (left) are representative of coordinates ±4 mm and ±5 mm in the balloon, which is shown in the upper left corner of the figure for reference and found between axial levels 30 and 40 on Fig. 7 (right). The ratio of gamma counts from the ejected fuel region (axial coordinate 90 on Fig. 7 (right)) are reported in the upper right corner of Fig. 7 (left) together with their arithmetic average. These results suggest, that there is no evidence of preferential relocation of fuel into the balloon or fuel ejection either from the bulk or periphery. The points which are lying above or below the reference curve can simply be assigned to originate from the periphery or the pellet centre respectively. The derived reference curve is only a qualitative result and not an exact representation of the reality. Furthermore, there is likely some statistical error associated with the gamma counts, which will also affect the calculated ratios of the selected points. Also, the positioning of the collimator with respect to the fuel periphery, as illustrated on Fig. 3, varies vertically because of cladding deformation and fuel relocation and this will also impact the calculated ratios. Several factors play a role in this analysis, but there is no evidence of preferential fuel relocation which would require modification of FRELAX (Section 2.2).

4.2. Estimation of amount of dispersed fuel in selected Halden LOCA tests

The methodology presented in Section 3.4 is applied to selected LOCA tests from Halden's LOCA test program. The selection criterion is based on the availability of sufficient count statistics and the required isotopes. The estimation of the dispersed fuel fraction using the gamma scan data is compared against a straight-forward approach by considering the void regions in the neutron radiography image and the gamma count intensity plots.

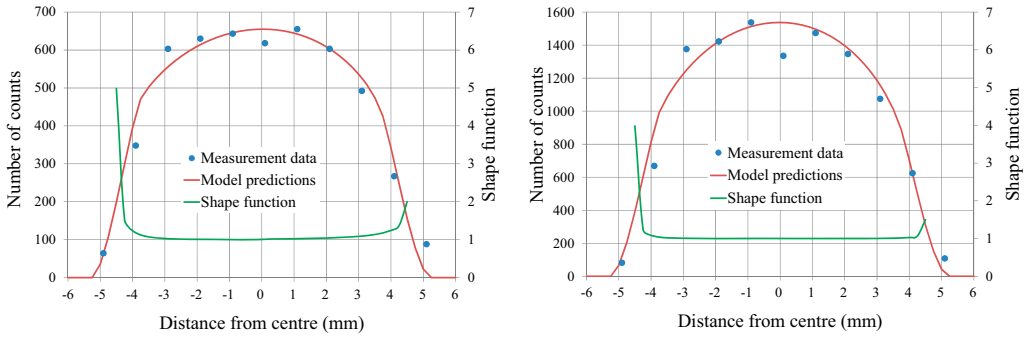

Fig. 6. Model fitting and shape function calculation for ^{103}Ru (left) and ^{140}La (right) gamma count distributions at selected axial elevation with minimal rod deformation.

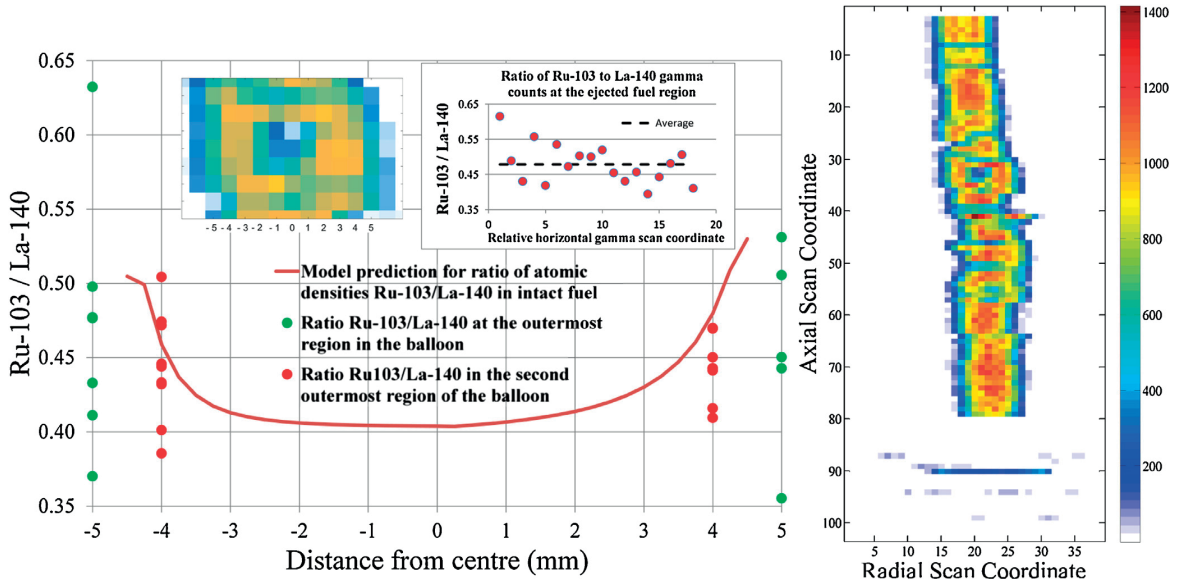

Fig. 7. Reference radial distribution curve for interpretation of balloon and dispersed fuel in the 13th Halden LOCA test (left) and gamma scan intensity plot (right).

4.2.1. Estimation of dispersed fuel in Halden's 9th LOCA test

The 4th and 9th Halden LOCA tests showed severe fuel fragmentation, relocation and dispersal. The dispersed fuel is only estimated for test 9 because the gamma scan data for test 4 is not suitable for the presented methodology. The gamma count intensity plot of the decay-corrected ^{140}La gamma count signal is shown in Fig. 8 for both scanning orientations together with cladding diameter profilometry. A few things are immediately evident. Approximately 26% of the fuel stack is missing at the top of the rod due to fuel relocation and dispersal. The cladding developed a balloon at approximately axial scan level 60 (gamma count intensity is peaking at that region) and ruptured below level 80. The significant cladding deformation, as evident from the cladding profilometry in Fig. 8, combined with the very fine fuel fragmentation enhanced the fuel relocation and dispersal. The high count intensity at the rupture location is due to fuel relocation into the extra space within the rod. Considering the gamma signal of the dispersed fuel found below the rod, the estimation using the procedure in Section 3.4 yields the ranges 1.92%–9.21% and 2.03%–9.56% ejected fuel for 0° and 90° orientations, respectively. Therefore, the ejected fuel in LOCA test 9 is

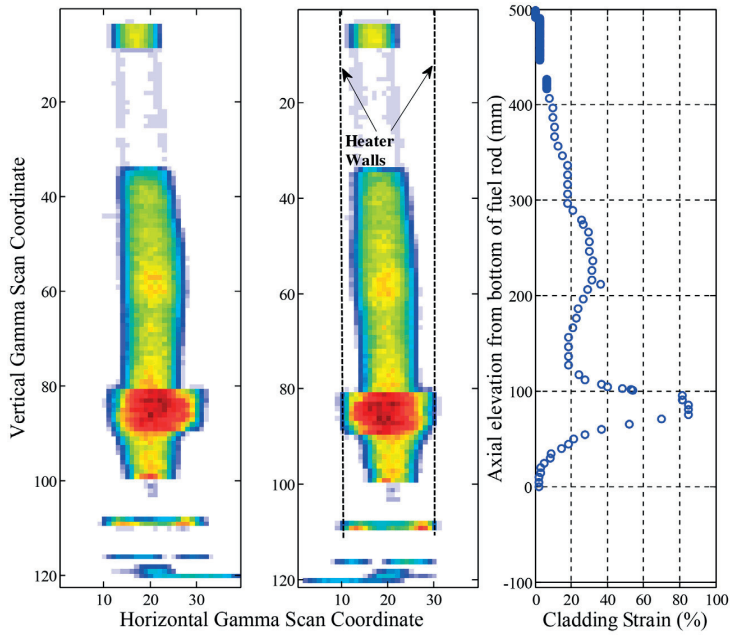

Fig. 8. Gamma count intensity plot for 0° and 90° orientation and cladding diameter profilometry.

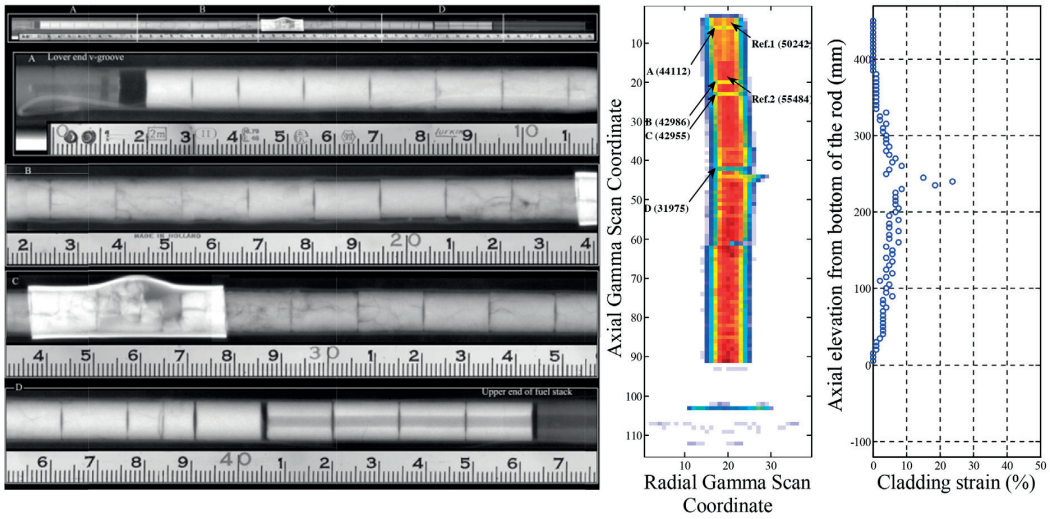

Fig. 9. Neutron radiography of the 10th LOCA test (Raynaud, 2012) (left) and gamma count intensity plot together with the cladding diameter profilometry (right).

between 1.92% and 9.56% of the total fuel. Rough estimate of the created volume inside the rod due to the cladding deformation, based on the cladding strain on Fig. 8, is large enough to accommodate all the fuel which is missing at the top with a packing factor of 0.5.

4.2.2. Estimation of dispersed fuel in Halden's 10th LOCA test

The 10th LOCA test of Halden's program had a burn-up of 61 MW d/kg U. Gamma scanning of the rod suggests less fuel dispersal than in the 9th test, and neutron-radiography (NR) shows that the fuel geometry is more or less preserved (see Fig. 9). This test offers three ways to estimate the quantity of dispersed fuel: using the procedure outlined in Section 3.4, estimating the void regions from the NR image and from the gamma count intensity plot. The gamma count ratio based on ^{140}La at 1596 keV gives an estimated range for the quantity of ejected fuel of 0.34–2%. Unlike the previous test, void regions could be linked with the quantity of dispersed fuel, because cladding deformation was very little and the original fuel stack geometry did not change much. The fuel stack length is 440 mm. The axial void region based on the NR image is about 8 mm (6 mm near the lower end, and 2 mm near the upper end). The ratio of 8/440 ≡ 0.0182 ≡ 1.82% of the stack length. This estimate includes fuel relocation into the balloon which suggests that the actual quantity of dispersed fuel is less than 1.82%. An empirical correlation of 5% cladding strain needed for fuel relocation is exceeded about 10 cm below and 5 cm above the balloon. An alternative estimate can be roughly made from the gamma scan intensity plot (shown in Fig. 9). Four axial levels clearly show reduced gamma count intensity, which means reduced fuel density. They are labeled by A, B, C and D, and the sum of the gamma counts is reported in the brackets. Two axial levels representative of the original geometry are selected (labeled as Ref. 1 and Ref. 2). The necessity of two different regions is the presence of a central hole (not due to fuel design) in the top four pellets (also seen on the NR image on Fig. 9). In fact, this central hole can be vaguely seen on the gamma count intensity plot as a lighter column starting at the top of the rod and going down to level 15. The counts in the region labeled A is 87.8% that of Ref. 1. The corresponding values for B, C and D are 77.48%, 77.42% and 57.63% of the counts of Ref.2, respectively. If the differences can be interpreted as voids, then the sum of the voids at these four locations approximately equals to one fully voided axial level. The fuel rod is 440 mm long, and axial sampling is 5 mm, which translates to 440/5 ≡ 88 axial levels in the gamma scan of which 1 is fully voided, which is equivalent to 1.13% of the fuel stack length. Of course, this estimate is very rough, because as pointed out in Section 3.4 only 1/3 of the rod is actually scanned, but the neutron radiography reveals rather limited relocation which gives more confidence to this estimate.

In summary, the estimated quantity of dispersed fuel as percentage of the total is:

(a) 0.34–2% based on the procedure outlined in Section 3.4.
(b) 1.82% based on the void regions of the neutron radiography image.
(c) 1.13% based on the gamma count intensity plot.

It should be mentioned, that the estimates (a) and (b) do not account for relocated fuel. In this case, the reported values for ejected fuel will be overestimations; therefore, they should be closer to (c) if relocation is taken into account.

5. Discussion

The proposed method for estimation of quantity of dispersed fuel relies on the availability of ^{140}La, preferably two scan orientations and good count statistics. These requirements were present in only two LOCA tests: the 9th and 10th Halden LOCA tests. The estimate of the dispersed fuel in test 9 yielded the range of 1.92%–9.56% due to the significant fuel relocation and clad deformation. In reality, all of the missing fuel at the top could be accommodated within the deformed cladding with a packing factor of 0.5. On the other hand, the estimate from the 10th test is between 0.34% and 2% based on three different approaches. These estimations already provide some means for code validation. Not all Halden LOCA tests can benefit from several ways of estimating quantity of dispersed fuel. Some do not have the necessary quality of gamma scan data. Others, that have severe fuel fragmentation and cladding deformation, are not suitable for estimation based on NR image, or gamma count intensity plot because the geometry had changed too much. The dispersed fuel estimates made for the 10th LOCA test with the NR image and the reduced density regions in the gamma count intensity plot were used to check the validity of the approach outlined in Section 3.4, and it showed good agreement. This can be considered

as validation for the moment and used for the determination of dispersed fuel at least until a more accurate method is developed. Ideally, the dispersed fuel will be collected and measured precisely with a scale; however, such capability does not currently exist. The accuracy of the fuel dispersal estimation depends on many parameters, but the most important is decay correction and complete scanning of the fuel rod. Sufficiently long gamma scanning will reduce the statistical error at the expense of longer scanning time. The neutron flux profile in the Halden Boiling Water Reactor (HBWR) has influence on the fission product concentration but it cannot be corrected in cases of severe fuel relocation and rod deformation. Attenuation in the fuel matrix can be significant, but it cannot be accounted for the same reason as the neutron flux profile and this motivates the use of high energy gammas for the analysis. Detector efficiency is required in the solution of Eq. (5) because ^{140}Ba (537keV) and ^{140}La (1596 keV) have very different energies. On the other side, the gamma transport model does not require correction for attenuation because it uses isotopes with gammas of similar energies, and analysis of fuel dispersal can neglect the effect of attenuation if the 1596 keV gamma of ^{140}La is used. All the uncertainties with detector efficiency, attenuation, and neutron flux profile will also have an impact on the analysis and the data interpretation. Despite all of these shortcomings, estimation of quantity of dispersed fuel in Halden is currently possible via analysis of the gamma scan data.

The analysis with the Gamma Transport Model can benefit from higher resolution at the pellet periphery, better count statistics and reduced delay in scanning time. Increasing the resolution by a factor of 5 is technically possible via choice of smaller collimator size and motion of the fuel rod in smaller steps, but practically it is not possible because the scanning time will increase proportionally. A workaround is to perform a fast scan in order to identify the coordinates of the features of interest, such as the location of balloon(s) and the dispersed fuel. Once known, higher resolution scanning could be performed for selected coordinates. Also, scanning should be done not too long after the LOCA test in order to make use of the higher activity and the useful gamma isotopes such as ^{140}La emitting high-energy gamma rays that are less affected by attenuation. The analysis of the dispersed fuel would also benefit from higher resolution scanning. Non-trivial practical issues need to be resolved in order to facilitate changes to the current gamma scan procedure at Halden.

The analysis of fuel relocation in the 13th Halden LOCA test with the gamma transport model suggested a mixture of fuel from the periphery and pellet bulk. In view of this result, the assumption used in FRELAX (e.g., $k \equiv 1$, see Section 2.2) remains valid. Considering the uncertainty in the gamma scanning at the periphery, it can only be concluded that at the moment there is no evidence of predominant fuel relocation into the balloon either from the bulk or the periphery.

6. Conclusions

The gamma scan data is the most representative post-irradiation examination of the fuel state after the LOCA test carried out at Halden. It reveals information on cladding deformation, fuel relocation and dispersal. Currently, the gamma scan data is primarily used to get a first view of the fuel rod state right after the LOCA test and confirm the success of the test objectives. Two other methods to use the gamma scan data were presented. The first is to interpret fuel relocation and dispersal by distinguishing between fuel belonging to the pellet periphery and the pellet bulk. This is done by considering gammas from fission products that have large difference in the fission product yield of ^{239}Pu. The second is to estimate the amount of dispersed fuel based on the gamma scan data.

The non-uniform radial power distribution in high burn-up fuel results in non-uniform concentration of fission products and consequently on non-uniform decay-heat source density distribution during the LOCA for more adequate prediction of the local heat generation. The latter is highest at the pellet periphery in accordance with the burn-up and lowest at the pellet center. This fact must be considered in the analysis of axial fuel relocation into the ballooned area of the rod during LOCA. The goal of the proposed Gamma Transport Model is to address this question. The predictions by the gamma transport model based on the analysis of the 13th LOCA test's gamma scan data suggest that relocated fuel in the balloon and dispersed fuel from the rod originate from both the pellet bulk and periphery. At least, there is no evidence in the available data points that indicates a dominant origin, e.g., a pellet periphery or center, for the fuel from the balloon area and the dispersed fuel. In that respect, the assumption of homogeneous mixing of fuel from the pellet rim and bulk used in FRELAX—an OECD Halden Reactor Project' LOCA test series specific fuel relocation model—appears to be valid.

The applicability of the gamma scan data for estimation of the dispersed fuel quantity shortly after the simulated LOCA is shown with a few selected tests. The value of this method is amplified by the fact, that it provides a method for quantification of fuel dispersal observed in the Halden LOCA tests which is difficult to achieve more directly due to the utilization of an in-core test facility. The use of the gamma scanning data is subjected to availability of the necessary isotopes, sufficient counting statistics, good measurement resolution and the necessary data corrections such as decay, attenuation and detector efficiency. The largest uncertainty with respect to the application of the gamma transport model is the scanning resolution at the fuel periphery, whereas the dispersed fuel estimates are more influenced by the decay correction, counting statistics and incomplete scanning in the vertical direction.

Acknowledgments

The presented work was motivated by a three month technical visit at the Halden Reactor Project (HRP). This venture was supported by the Swiss Nuclear Safety Inspectorate (ENSI), swiss*nuclear* and the Paul Scherrer Institut in Switzerland and by the OECD HRP in Norway. Special thanks go to Dr. Margaret McGrath for organizing the technical visit at the HRP. Furthermore, gratitude is expressed to Dr. Gregory Perret at PSI, Dr. Scott Holcombe and Knut Eitrheim at HRP for their help on discussion about HPGe detector efficiency curves.

References

Khvostov, G., Mikityuk, K., Zimmermann, M.A., 2011a. A model for fission gas release and gaseous swelling of the uranium dioxide fuel coupled with the FALCON code. Nucl. Eng. Des. 241, 2983–3007.

Khvostov, G., Wiesenack, W., Zimmermann, M.A., Ledergerber, G., 2011b. Some insights into the role of axial gas flow in fuel rod behaviour during the LOCA based on Halden tests and calculations with the FALCON-PSI code. Nucl. Eng. Des. 241, 1500–1507.

Kolstad, E., Wiesenack, W., Oberländer, B.C., Tverberg, T., 2011. High burn-up fuel behavior under LOCA conditions as observed in Halden experiments, IAEA Technical Meeting on Fuel Behavior and Modelling Under Severe Transient and LOCA Conditions, Japan.

Khvostov, G., Novikov, V., Medvedev, A., Bogatyr, S., 2005. Approaches to Modeling of High Burn-up Structure and Analysis of its Effects on the Behaviour of Light Water Reactor Fuels in the START-3 Fuel Performance Code, LWR Fuel Performance Meeting, Kyoto, Japan.

Khvostov, G., Pautz, A., Kolstad, E., Ledergerber, G., 2013. Analysis of a Halden LOCA Test with the BWR High Burnup Fuel, LWR Fuel Performance Meeting/TopFuel 2013, Charlotte, NC, USA.

Khvostov, G., Romano, A., Zimmermann, M.A., Modeling the effects of axial fuel relocation in the IFA-650.4 LOCA test. 2007, Enlarged Halden Programme Group Meeting, Storefjell Hotel, Gol, Norway.

Lassmann, K., O'Carroll, C., van de Laar, J., Walker, C.T., 1994. The radial distribution of plutonium in high burnup UO2 fuels. J. Nucl. Mater. 208, 223–231.
Matsson, I., Grapengiesser, B., 1997. Developments in gamma scanning irradiated nuclear fuel. Appl. Radiat. Isot. 48, 1289–1298.
Rashid, R.Y., Dunham, R.S., Montgomery, R.O., 2004. ANATECH Corp., Palo Alto, USA (Technical Report ANA-04-0666).
Raynaud, P., 2012. Fuel Fragmentation, Relocation and Dispersal During the Loss-of-Coolant Accident. Nuclear Regulatory Commission, Washington DC, USA.
Wiesenack, W., Oberländer, B.C., 2014. Overview of Halden Reactor LOCA Experiments (with Emphasis on Fuel Fragmentation) and Plans. IFE-Kjeller, Kjeller, Norway (IFE/KR/E-2014/001; ISBN: 978-82-7017-874-2).

Appendix B:
Model for fast neutron flux calculation

In FALCON, the default procedure is that the fast flux is calculated as local LHGR multiplied by a coefficient specified in the code input file. In PWR, this ratio can be taken as constant, but in BWR the coolant void fraction may have an impact on this ratio. The purpose of this Appendix is to illustrate how the fast neutron flux was calculated for the analysis of gas trapping in the BWR fuel rods, as discussed in Chapter 4 section 4.3. Firstly, an expression for the thermal flux is needed as function of relevant parameters such as fuel density, fuel pellet diameter, enrichment and Linear Heat Generation Rate.

As a first step, the volume-averaged fission rate is expressed as function of the fuel diameter and LHGR, F_V (fissions / (cm^3·sec)

Eq. 20: Volume-averaged fission rate as function of the Linear Heat Generation Rate and fuel diameter

$$F_V = a \cdot LHGR/(D_F^2)$$

where a is a constant, D_F is the fuel diameter in cm and the LHGR is in kW/cm.

Assuming 158 MeV are released per fission, then the energy released per fission is:

$$158\frac{MeV}{fission} \cdot 10^6 \frac{eV}{MeV} \cdot 1.602 \cdot 10^{-19}\frac{J}{eV} = 2.53 \cdot 10^{-11}\frac{J}{fission}$$

Therefore, in 1 J there are $3.95 \cdot 10^{10}$ fissions. This means that in 1 kJ there are $3.95 \cdot 10^{13}$ fissions. Finally, the volume-averaged fission rate can be expressed by Eq. 21.

Eq. 21: Volume-averaged fission rate as function of the Linear Heat Generation Rate and fuel diameter

$$F_V = \frac{3.95 \cdot 10^{13} LHGR}{D_F^2} \quad \left[\frac{fissions}{cm^3 \cdot sec}\right]$$

The volume-averaged fission rate can also be expressed in terms of the thermal neutron flux with the expression shown on Eq. 22.

Eq. 22: Volume-averaged fission rate as function of number of U-235 atoms, thermal neutron flux and thermal fission cross-section

$$F_V = N_{U235} \cdot \sigma_{thermal} \cdot \varphi_{thermal}$$

where N_{U235} is the number of U-235 atoms per cm^3, $\sigma_{thermal}$ is the thermal neutron cross-sections for fission of U-235 (cm^2) and $\varphi_{thermal}$ is the thermal neutron flux (n/cm^2·sec).

Let us suppose that the enrichment is ε and the fuel density is ρ_{Fuel}. Therefore, the number density N_{U235}, of U-235 atoms, can be expressed with Eq. 23 below.

Eq. 23: Number density of U-235 atoms as function of the enrichment and fuel density

$$N_{U235} = 6.022 \cdot 10^{23} \left[\frac{atoms}{mol}\right] \cdot \frac{1}{270.03} \left[\frac{mol}{g}\right] \cdot \rho_{Fuel} \left[\frac{g}{cm^3}\right] \cdot \varepsilon = 2.23 \cdot 10^{21} \cdot \rho_{Fuel} \cdot \varepsilon \left[\frac{atoms}{cm^3}\right]$$

Substituting Eq. 23 into Eq. 22 and equating with Eq. 21 gives the possibility to solve for the thermal neutron flux. The calculation is shown on Eq. 24.

Eq. 24: Thermal neutron flux as function of LHGR, fuel diameter, fuel density and enrichment

$$\sigma_{thermal} \cdot \varphi_{thermal} \cdot 2.23 \cdot 10^{21} \cdot \rho_{Fuel} \cdot \varepsilon = \frac{3.95 \cdot 10^{13} LHGR}{D_F^2}$$

$$\varphi_{thermal} = \frac{1.77 \cdot 10^{-8} \cdot LHGR}{D_F^2 \cdot \rho_{Fuel} \cdot \varepsilon \cdot \sigma_{thermal}}$$

The thermal flux is now expressed as function of available parameters, such as the LHGR, fuel diameter, density and enrichment. The thermal neutron fission cross-section is assumed equal to 580 barns. Finally, to get the fast flux, the ratio of the fast to thermal neutron flux needs to be evaluated as function of the void fraction and fuel burnup, because both are affecting it. This is, of course, not an easy task and therefore only rough approximation will be used. From the paper by Loberg et.al. [95], an equation relating the ratio of fast to thermal flux as function of the time-dependent burnup $BU(t)$ and coolant void fraction $VF(t)$ can be put together, which is reported in Eq. 25.

Eq. 25: Ratio of fast to thermal neutron flux, R_{FTHF}, as function of the time-dependent void fraction and rod-average burnup

$$R_{FTHF} = \frac{(-0.41 \cdot VF(t) + 0.614)}{\left(2 + (4.37 \cdot 10^{-3} \cdot BU(t) - 0.42)\right)}$$

Finally, the fast flux as function of the thermal flux is calculated with Eq. 26 and then input to FALCON.

Eq. 26: Calculation of the fast neutron flux

$$\varphi_{fast} = \varphi_{thermal} \cdot R_{FTHF}$$

To make the fast flux input more accurate, a core-physics code can be used.

Appendix C:
Brief introduction to MATLAB

MATLAB is perhaps one of the most well-known software tools for numerical analysis in the academic world. This is mainly because of two things: the licensing is much cheaper for non-commercial use and the availability of large selection of tools, manuals, examples and large user community makes it easier to get help with your task. MATLAB is short form of MATrix LABoratory and it was developed over thirty years ago. As with all old programs, MATLAB initially provided a command-line interface and a limited selection of mathematical functions for data manipulation, which was later enhanced with a graphical user interface. MATLAB is optimized to work with matrices, and as such each number is actually a 1x1 matrix. Multiplying two matrices together can be done with a single line command, as opposed to writing loops. Data analysis with MATLAB is optimized for linear algebra operations and as such it finds best uses in matrix data applications, such as image processing and systems of differential equations.

In the industrial world, MATLAB often finds application in the development of control systems via its toolbox called Simulink®. For example, the Pacific Northwest National Laboratory in the U.S. used MATLAB to design control system for a robotic arm used for the manipulation of high radioactive materials [126]. ABB in Switzerland had used MATLAB to develop a Power Electronic Controller for use in "high-power rectifiers, frequency converters for micro turbines, wind turbines, traction drives, battery energy storage systems, and other power electronic applications" [127]. MATLAB-developed management tool is used by New Zealand's National Grid to estimate necessary reserve power in case of generator failure in order to ensure the stability of the electrical grid [128].

There are many toolboxes and features of MATLAB, but a general introduction should focus on the most basic interface - an example of which is reproduced on Figure 81.

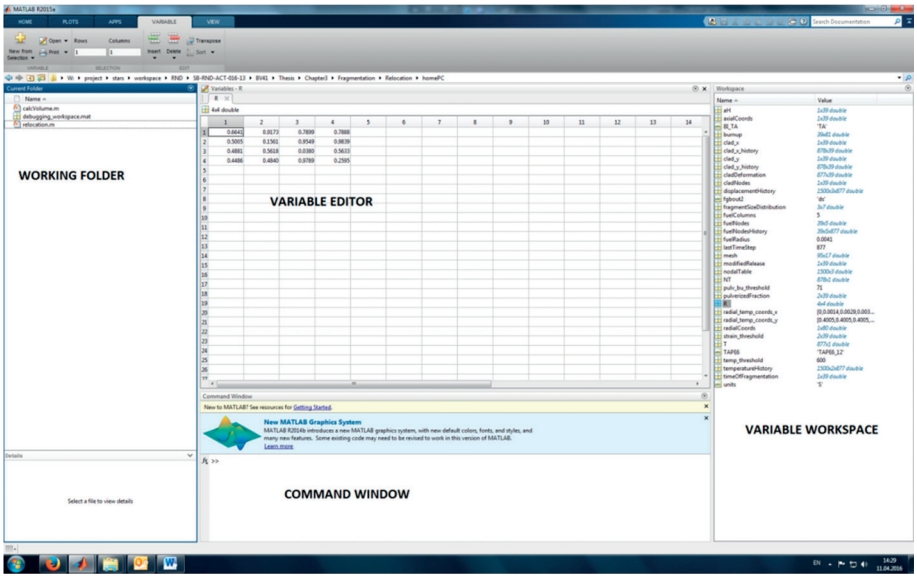

Figure 81: MATLAB main window showing the basic graphical user interface.

With reference to Figure 81, the most basic features of MATLAB are explained. To begin with, the working folder pane shows all existing files and subfolders in the working directory. All instructions

to MATLAB are given in the command window, which provides immediate access to all functions and commands that come with it. Whenever a new variable is created, it will appear in the variable workspace pane. Each variable can be accessed through the variable editor by double mouse click, where it can be simply visualized or modified. For example, in Figure 81 the editor shows the contents of a 4x4 matrix. The variable editor pane closely resembles Microsoft Excel and MATLAB and allows exporting quickly any one and two-dimensional variables to a spreadsheet via the function **xlswrite**. Similarly, Excel-generated tables can be easily imported into MATLAB workspace.

MATLAB comes with its own programming language, which is loosely based on the C/C++ programming language. Numerical data is by default set to **double**, which means there will never be a run-time error by trying to assign a floating point number to an integer variable. Of course, the user is able to specify the numerical type which may be necessary when dealing with very large amounts of data. All data can be conveniently stored in MATLAB's own data structure called the **mat** file. It has the interesting property, that a 100x100x100 double array, which occupies 8 000 000 bytes (about 7 MB) in the memory, actually occupies only 40KB on the disk when saved in a **mat** file, after MATLAB applies compression. This feature allows for large quantity of data to be conveniently stored on the disk and easily retrieved later for further analysis. It is also possible to process data from a **mat** file in a piece-wise manner, thereby reducing the memory load at run-time.

MATLAB's programming language is an interpreter language, which means each line of code is converted into machine language at run-time. If the data analysis relies on many nested loops, then the time to finish the analysis can be substantial. In such cases, the workaround is to convert MATLAB code into a C/C++ code, which can be done very easy with the MATLAB toolbox called Coder. Only basic knowledge of C/C++ is necessary, and the user is guided from start to finish during the conversion process.

MATLAB programs can be structured in two ways: as a script and as a function. Functions can be re-used throughout the code and all variables declared in a function are local variables, unless explicitly declared as global, which means they are deleted when the function call ends. In contrast, all variables declared in a script will appear in the main MATLAB workspace, which can clutter the space with unnecessary data and/or modify existing data, thereby compromising reusability. Furthermore, functions can improve code maintenance and readability by structuring the code into separate modules, which are then combined via a main, or a driver function. Such structure is used throughout the models developed in this dissertation.

The biggest drawback of MATLAB is that it is not free; however, the possibility to develop programs and deploy them on machines that do not have MATLAB exists. Free alternatives to MATLAB are the environments Octave and Scilab that provide similar capabilities; however, their industrial application is rather limited and they are primarily used in education.

In this dissertation, MATLAB is extensively used for data processing (reading, writing, production of figures), model development and code coupling as is the case of FALCON-TRACE coupling. The model development with MATLAB is done under Windows OS; however, batch jobs can be executed under Linux when better stability and speed is required.

Vladimir Brankov Rietschenweg 19 5507 Mellingen
Tel: +41 76 739 81 44 E-Mail:vladbrankov@gmail.com

Lebenslauf

Persönliche Angaben

Name:	Vladimir Brankov
Geburtsdatum:	30.06.1985
Heimatort:	Sofia, Bulgarien
Zivilstand:	ledig
Nationalität:	Bulgarien, Kanada

Ausbildung

06/2013-06/2017 **Doktorand**
Paul Scherrer Institut und ETH Lausanne
Titel der Doktorarbeit:
„Model Development for Fuel Fragmentation, Relocation and Dispersal during Loss-of-Coolant Accident in Light Water Reactors“

09/2010 - 06/2012 **MSc. Kerntechnik**
ETH Zürich und ETH Lausanne

09/2006-06/2010 **BSc. Mathematische Physik**
Universität Waterloo, Ontario, Kanada

Berufserfahrung

07/2012 – 05/2013 **Praktikum, Paul Scherrer Institut**
Software Entwicklung mit Matlab, Big Data Analyse

07/2007 – 06/2010 **Studentenwohnung Rezeptionist, Universität Waterloo, Kanada**
Persönliche Beratung, Verwaltungsaufgaben, Problemlösen

09/2003 – 06/2006 **Küchen Baumeister, Euro-Rite Cabinets, BC, Kanada**
Qualitätsüberwachung, Mitarbeiterschulung, Problemlösen

Vladimir Brankov Rietschenweg 19 5507 Mellingen
Tel: +41 76 739 81 44 E-Mail:vladbrankov@gmail.com

Sprachen

Deutsch	Verhandlungssicher
Englisch	Fliessend
Bulgarisch	Muttersprache
Russisch	Grundkenntnis

EDV Kenntnisse

MATLAB	Sehr gut
MS Office	Sehr gut
FORTRAN	Gut
C/C++	Gut
Python	Gut
FALCON	Gut
R	Gut
Serpent Monte Carlo	Grundkenntnis

Publikationen

[1] Brankov, V., G. Khvostov, K. Mikityuk, A. Pautz, and W. Wiesenack, Characterization of the relocated and dispersed fuel in the Halden reactor project LOCA tests based on gamma scan data. Nuclear Engineering and Design, 2016. 300: p. 97-106.
[2] Brankov, V., G. Khvostov, K. Mikityuk, A. Pautz, R. Restani, S. Abolhassani, G. Ledergerber, and W. Wiesenack, Analysis of effects of pellet-cladding bonding on trapping of the released fission gases in high burnup KKL BWR fuels. Nuclear Engineering and Design, 2016. 305: p. 559-568.
[3] Brankov, V., G. Khvostov, K. Mikityuk, A. Pautz, and K. Eitrheim. Analysis of Axial Fuel Relocation Based on Gamma Scan Data from OECD HRP LOCA Tests. in WRFPM/TopFuel. 2014. Sendai, Japan.
[4] Brankov, V., G. Khvostov, K. Mikityuk, A. Pautz, R. Restani, S. Abolhassani, G. Ledergerber, and W. Wiesenack. Modelling of axial distribution of released fission gas in KKL BWR fuel rods during base irradiation. in WRFPM/Topfuel. 2015. Zürich, Switzerland.
[5] Cozzo, C., A. Epiney, S. Canepa, H. Ferroukhi, O. Zerkak, G. Khvostov, V. Brankov, and A. Gorzel, Full core LOCA analysis for BWR/6 - Methodology and first results Top Fuel 2016: LWR Fuels with Enhanced Safety and Performance. 2016. 1135-1144.
[6] Krepel, J., V. Brankov, and K. Mikityuk. Selection of initial fuel composition for the ESFR core based on the knowledge of its equilibrium closed cycle parameters. in FR13: International Conference on Fast Reactors and Related Fuel Cycles: Safe Technologies and Sustainable Scenarios. 2013. Paris, France.
[7] Betschart, T., D. Suckow, V. Brankov, and H.-M. Prasser, The hydrodynamics of two-phase flow in a tube bundle and a bare channel International Congress on Advances in Nuclear Power Plants, ICAPP 2014. Vol. 2. 2014. 1403-1411.

Freizeit-Aktivitäten

Velofahren, Lesen, Schach spielen, Wandern, Mitglied der SGK und Pro Velo Schweiz